Dynamical Symmetry Breaking in Molecules and Molecular Aggregates

by

Günter Maximilian Schmid
Diplomchemiker, Technische Universität München, 1991

Submitted to the Department of Chemistry
in partial fulfillment of the requirements for the degree of

Doctor of Philosophy

at the

MASSACHUSETTS INSTITUTE OF TECHNOLOGY

September 1994

Author .....
Department of Chemistry
August 12, 1994

Certified by .....
Robert J. Silbey
Professor of Chemistry
Thesis Supervisor

Accepted by .....
Dietmar Seyferth
Chairman, Departmental Committee on Graduate Students

This doctoral thesis has been examined by a Committee of the Department of Chemistry as follows:

Professor Irwin Oppenheim .....

(Chairman)

Professor Robert J. Silbey .....

(Thesis Supervisor)

Professor Robert W. Field .....

Dynamical Symmetry Breaking in Molecules and Molecular Aggregates

by

Günter Maximilian Schmid

Submitted to the Department of Chemistry
on August 12, 1994, in partial fulfillment of the
requirements for the degree of
Doctor of Philosophy

Abstract

In this thesis we explain dynamical symmetry breaking as an important and practically relevant mechanism of localizing excitation in molecules and molecular aggregates. Explicitly treated are the normal to local mode transition in triatomic molecules AB_2 of symmetry C_{2v}, modelled by two harmonically coupled anharmonic oscillators, and the self-trapping transition of an excess charge in a molecular crystal dimer with site exchange symmetry, modelled by Holstein's molecular crystal. At these transitions, localization of excitation occurs in violation of symmetry requirements. The potentials that confine the excitations appear upon excitation and thus are called dynamic potentials. Therefore localization occurs under dynamical symmetry breaking.

We show that all qualitative and quantitative aspects of dynamical symmetry breaking in these systems can be successfully discussed in the language of quasiparticles. For the triatomic molecules, the quasiparticle is referred to as "local mode" and consists of a bare vibrational excitation and an induced distortion of the molecular equilibrium configuration; for the molecular crystal dimer, the quasiparticle is known as "small polaron" and consists of an excess charge and an induced distortion of the crystal equilibrium configuration. On the basis of timescale arguments, we obtain the equations of motion for these quasiparticles, called Duffing's equation, and solve them analytically. In addition, we employ geometrical methods from classical mechanics to discuss various dynamical aspects.

In the discussion of the triatomic molecules we put emphasis on the connection of classical, semiclassical and quantum mechanical modes of description. In particular, we formulate a stability criterion for eigenstates of the quantum system in terms of susceptibilities to symmetry breaking perturbations and show that parametric instability in the classical correspondent can be deduced in the classical limit. We discuss the practical relevance of the susceptibilities for the control of intramolecular dynamics by lasers.

In the discussion of the molecular crystal we focus on the derivation of the equations of motion in two different "adiabatic" limits, which we distinguish as the standard adiabatic limit and the Duffing limit. We establish the connection to the commonly employed adiabatic approximation.

Thesis Supervisor: Robert J. Silbey
Title: Professor of Chemistry

Acknowledgments

This thesis was presented in its final form with the help and advice of my mentors, friends and colleagues.

First and foremost I thank my supervisor Bob Silbey for creating, with his unique ability to wittingly intertwine the professional and personal aspects of life, a very pleasant and stimulating working environment. He taught me to be open to ideas from different branches of science and boldness in borrowing from these.

I owe to my teacher Irwin Oppenheim the valuable insight that apparently difficult problems are often "very easy". His early morning pat on the shoulder gave me the momentum to penetrate the sometimes very difficult issues of the day,some of which he presented in his immaculate lectures.

Highly infectious in his incomparable enthusiasm for science is my teacher Bob Field, whose feel for scientific and social issues guided me through graduate student terrain.

With his enormous skill and patience in explaining experimental and theoretical issues, as well as U.S.- American social culture, Steve Coy kept me going at decisive steps of our research.

My friend Sophia Yaliraki read through the entire manuscript and made many valuable suggestions. For this and her good sense of humor in dealing with me over the last two years I thank her very much. My friends and house-mates Mauricio "Maybe" Barahona and Robert "Breyers" Grotzfeld always gave me cultivated company and never shied away from a scientific argument. My friend and office-mate Luis Cruz always had at least one open ear for my worries of the day and played often the "advocatus diaboli" when I couldn't. My "older" friends David Chasman "the Caleian" , David Dab, Bih-Yah Jin, Alex Orsky and Alberto Suarez were always patient with me and my "younger" friends Cliff Liu, Dave Reichmann, Welles Morgado and Joan Shea.

I thank all of them.

Contents

List of Figures

Chapter 1

Introduction

1.1 Motivation

Modern technology has high demands on materials. Often a new technology requires engineering of materials down to the molecular or atomic level. This process of characterization and conversion of materials is referred to as chemistry. The trend is to use materials not only as building blocks constituting a functional unit, but as functional units themselves which respond to excitation. Conspicuous examples that come to mind are micro electronics [1] and fiber optics [2]. Lesser-known to the public, but economically equally important, are ongoing efforts to optimize industrial chemical catalysts [3]. Futuristic and perhaps most challenging appear attempts to tailor bio-compatible or bio-mimicking tissues [4]. If the search for a material with a desired property is not to become the quest for the philosopher's stone of modern Alchemy, it is necessary to gain far-reaching control over the process of engineering. This goal can be achieved only on the basis of the ability to predict the relevant chemical and physical properties. In this thesis we set out to contribute to this endeavor by explaining the little understood mechanism of localization of excitation in molecules and molecular aggregates under dynamical symmetry breaking.

1.2 Basic notions

Technically important physical properties of molecules and molecular aggregates such as dipole moment and polarizability are expected to vary with the locus of excitation. Both localized and delocalized excitations are observed in molecules and molecular aggregates. Typical examples are vibrational excitations in molecules [5] or excess charges of various topologies in molecular aggregates [6].

In the following sections we will introduce some basic notions that will allow us to develop some intuitive insight into possible mechanisms of dynamical symmetry breaking and to state the problems this thesis offers a solution for. At this preliminary stage it will be sometimes unavoidable to speak in somewhat loosely defined terms. Therefore we will carry out the discussion following the two examples that constitute the main part of this thesis: localization of vibrational excitations in molecules and localization of excess charges in molecular crystals. The statements will be considerably refined, quantified, generalized and properly referenced in the later chapters.

1.2.1 Localized and delocalized excitations

The locus of excitation within a system and the point symmetry of a system are intimately related. If the locus of the excitation extends uniformly over the entire system the excitation is called delocalized, localized otherwise. Later on we will use the dynamic equivalent of this definition: if the excitation can be completely transferred between any parts of the system it is called delocalized, otherwise localized.

It is plausible that in the absence of point symmetry any excitation will be localized to some degree. Conversely, if any excitation is delocalized there will be some symmetry.

The degree of localization can be specified in terms of the distribution of the excitation over a partition of the system. If the system has a certain point symmetry a convenient partition is such that the parts are equivalent under the symmetry operations of the corresponding symmetry group. Equidistribution of excitation on these symmetrized parts implies delocalization on the considered scale. Deviation

from equipartition implies localization. If the localization extends over a macroscopic fraction of the system it is usually referred to as *large*, if it extends over a microscopic fraction only it is called *small*.

As a first example consider a vibrational excitation in symmetric molecules. Let us take as a partition the individual bond oscillators. An excitation of a non degenerate normal mode is considered delocalized, since it involves the coherent motion of all bond oscillators with a single frequency (Figure 1-1).

In contrast, an excitation of a local mode is considered localized since it involves coherent motion of only a certain fraction of bond oscillators at the same frequency (Figure 1-2). Note that periodic complete transfer of vibrational excitation between degenerate local modes amounts to coherent motion of the bond oscillators at one frequency and thus constitutes a normal mode (Figure 1-3). If the single bond oscillators are polarized, the dipole moment of the molecule changes upon localization of vibrational excitation.

Let us mention as a brief aside that the notion *normal mode* implies that the vibrational potential be harmonic. In the recent literature this condition was relaxed. Now symmetry adapted linear combinations of the displacement coordinates not obeying Hooke's law are sometimes paraphrased as normal modes. In addition, let us point out that excitation of a normal mode does not necessarily lead to delocalization of vibrational excitation even if it transforms according to the symmetry operations of the molecular point group. As an example consider excitations of normal modes that transform according to the E representations in systems with C_3 axes and higher that are always localized to some extent.

As a second example take an excess charge in a molecular crystal. Choose as a partition molecules located at the crystal sites. Delocalization is indicated by a uniform probability density of the excess charge over the entire crystal (Figure 1-4), and localization by accumulation of probability density of the excess charge at particular molecular sites (Figure 1-5). If the excess charge extends over many molecular sites it is referred to as large, if it is localized at a single molecular site it is called small. If each molecule is polarized, the polarization of the crystal changes upon localization

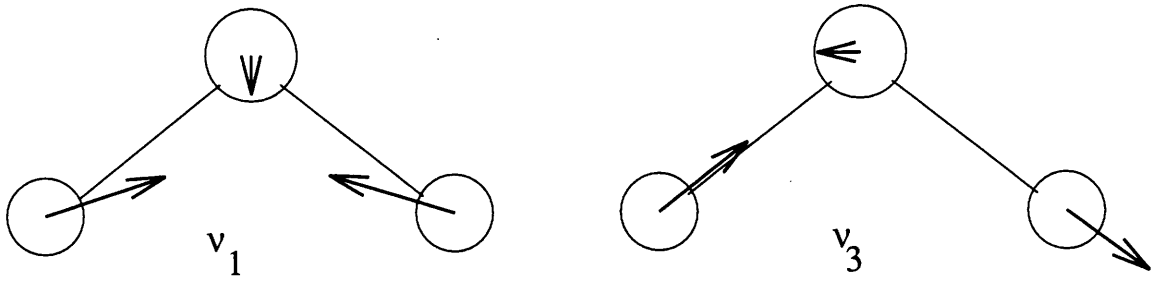

Figure 1-1: Delocalized vibrational excitation in normal modes ν_1 and ν_3 of AB_2 systems.

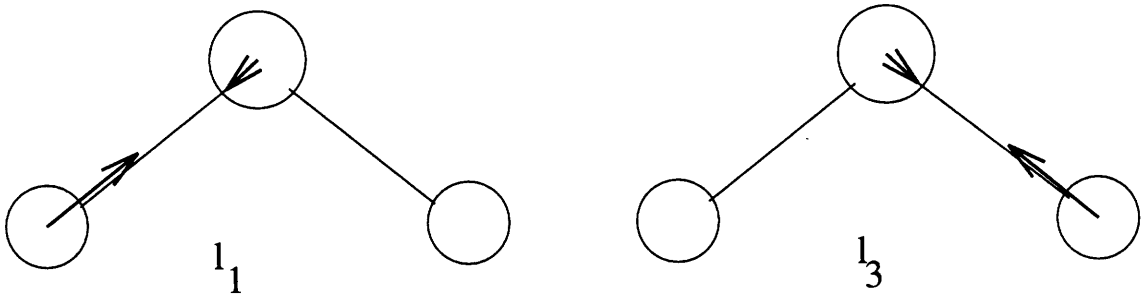

Figure 1-2: Localized vibrational excitation in local modes l_1 and l_2 of AB_2 systems.

of the excess charge.

1.2.2 Transitions from delocalized to localized excitations

The same type of excitation, e.g. a vibrational excitation in a molecule, can be localized or delocalized in the same system, depending on the mechanism or level of excitation.

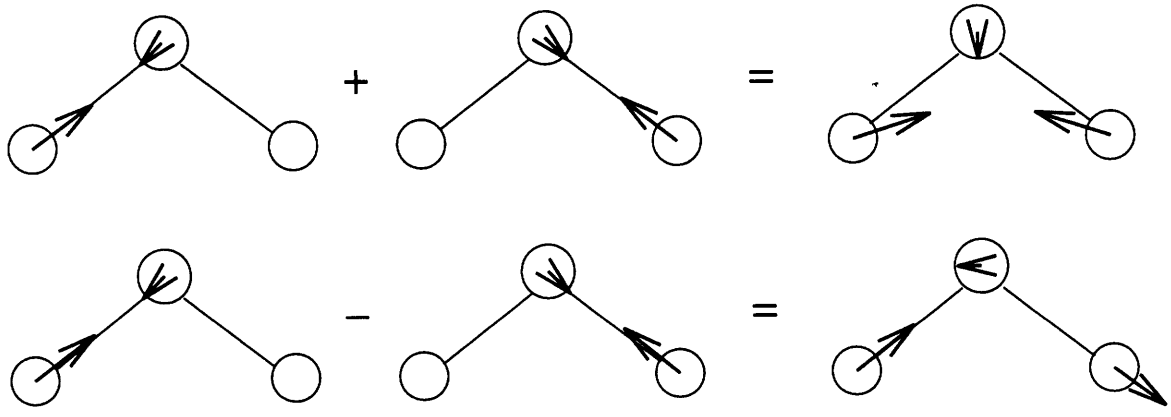

Figure 1-3: Coherent degenerate local modes l_1 and l_2 form normal modes ν_1 and ν_3 of AB_2 systems.

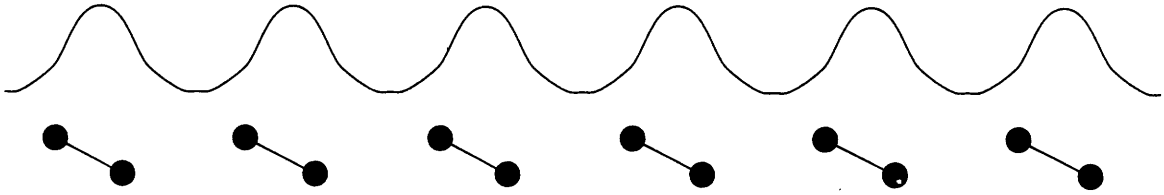

Figure 1-4: Probability density of a delocalized excess charge in a molecular crystal of diatomic monomers. Translational symmetry is conserved.

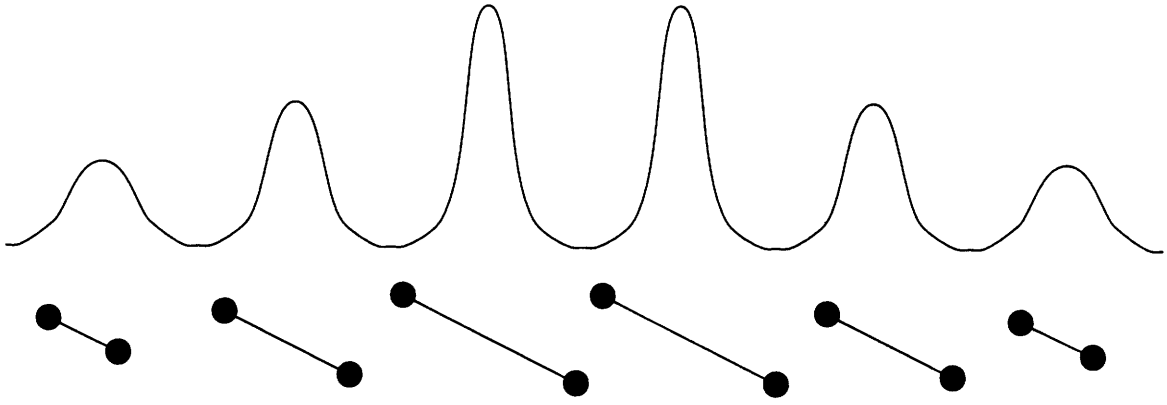

Figure 1-5: Probability density of a localized excess charge in a molecular crystal of diatomic monomers. Translational symmetry is broken due to the induced distortion.

Mechanisms of excitation that favor localization are collisions or other local interactions since they introduce large inhomogeneities into the system. For example, collisions of molecules in the gas phase can lead to large distortions of the molecular geometry. If the collision event lasts longer than a typical period of oscillation ($O(10^{-14}s)$) around the equilibrium geometry, the induced vibrational excitation is "drained away" unsymmetrically.

The *degree* of excitation is equally important, since it influences the instability towards localization. For vibrational excitations, normal modes prevail at low levels of excitation as opposed to local modes that predominate at high levels of excitation. For excess charges delocalization is likely at high values of kinetic energy in contrast to localization at low values of kinetic energy.

Consequently, there is the possibility of transition from a delocalized to a localized excitation of the same type within the same system. For vibrational excitations this transition is called the *normal to local mode transition*, for excess charges in a crystal the *trapping transition*. In the following we state different conditions and mechanisms

of localization.

Conditions of transition

Transitions can occur under different conditions. For isolated systems excitation must be redistributed within the system. For closed or open systems excitation can be additionally interchanged with the surroundings. Which conditions prevail for a given system depends on the relative magnitude of the time scales of the processes involved.

For example, redistribution of vibrational excitation in molecules in the low density gas phase takes place ($O(10^{-10}s)$) before it can be relaxed via a collison or emission of a photon ($O(10^{-8}s)$). Thus the molecules behave effectively like isolated systems during the relaxation of vibrational excitation. Most dramatic is the localization of vibrational excitation into a chemical bond that can lead to dissociation of that bond. In condensed phases, vibrational excitation is rapidly exchanged between molecules ($O(10^{-9}s)$) before it can relax completely within the molecule ($O(10^{-10}s)$). Thus the molecules behave effectively like closed or open systems during the relaxation of vibrational excitation.

As a further example consider an excess charge in a molecular crystal. Its kinetic energy can be dissipated into phonon degrees of freedom until the kinetic energy falls below a certain threshold that allows conservative localization. Then the kinetic energy of the excitation is converted into a local increase of potential energy of the crystal through distortion and thus forces its own confinement.

These examples raise the issue of the mechanisms of transition from a delocalized to a localized excitation.

Mechanisms of transition

Two generic mechanisms of localization can be distinguished by the nature of the potential that confines the excitation.

Localization in a static potential. First, localization in a minimum of a *static* potential occurs under relaxation by some external mechanism. A static potential exclusively depends on the *coordinates* of the system. It is insensitive to initial conditions and does not vary with time.

For molecular vibrations, a static potential that allows localization is usually present in the absence of symmetry. For excess charges in crystals a static potential that permits localization can occur around a defect.

Typical external mechanisms of relaxation are emission of a photon or phonon.

Localization in a dynamic potential. Dynamical symmetry breaking. Second, localization in a minimum of a *dynamic* potential can occur, in contrast to the first case, even in the absence of relaxation by some external mechanism. A dynamic potential depends on the *momenta* and eventually on the coordinates of the system. Thus it is sensitive to initial conditions and varies with time (Figure 1-6). This time dependence can be interpreted as arising from the mutual interaction of the excitation and the medium it is moving in.

Localization in a dynamical potential becomes most evident in the absence of a static potential that could allow localization. This is the case for symmetric molecules where it leads to lowering of the molecular symmetry via increase of the equilibrium bond lengths of the locally excited bonds (Figure 1-7).

A similar situation occurs for molecular crystals with translational symmetry. Here localization leads to lowering of translational symmetry via distortion of the lattice around the localized excess charge.

The process of lowering the symmetry of a system is known as *symmetry breaking.* If it occurs upon localization in a dynamic potential we refer to it as *dynamical symmetry breaking.* Symmetry breaking upon a spontaneously occuring fluctuation within the system is called *spontaneous symmetry breaking.* Finally, symmetry breaking can be induced by the surroundings and is then known as *induced symmetry breaking.*

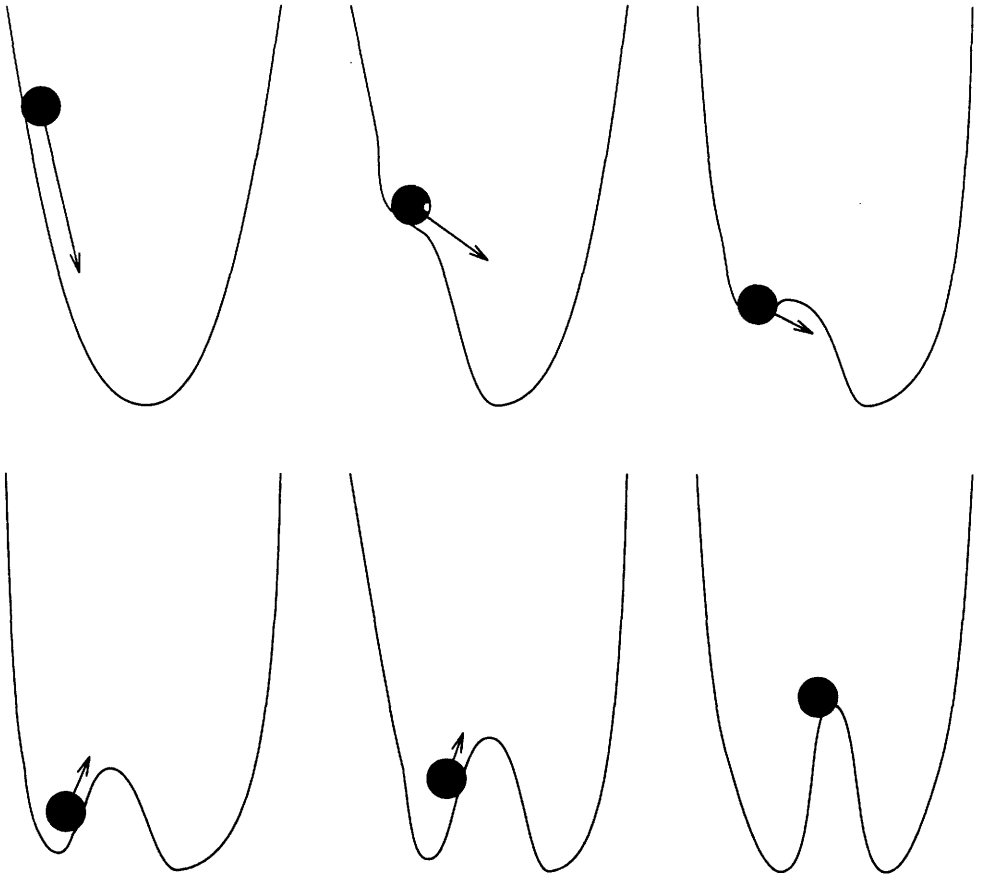

Figure 1-6: Localization in a dynamic potential: Particle moving in gravitational field on a deformable surface under friction.

Localization in a static and dynamic potential We expect that in an actual physical system localization involves both static and dynamic potentials. For example, consider an excess charge around a minor defect in a crystal that is too small to lead to considerable localization all by itself. Simultaneously, far from the defect the induced distortion of the crystal by an excess charge is too weak to allow localization in a dynamic potential well all by itself. Yet in the presence of the excess charge the defect will be amplified through additional distortion of the crystal lattice. Therefore the excess charge will localize in a static potential under support by a dynamic potential, each of which alone is too small to lead to localization. In the case of an immobile defect the excess charge will be localized at a certain locus in the crystal. For a mobile defect it will drag around the induced distortion and the defect.

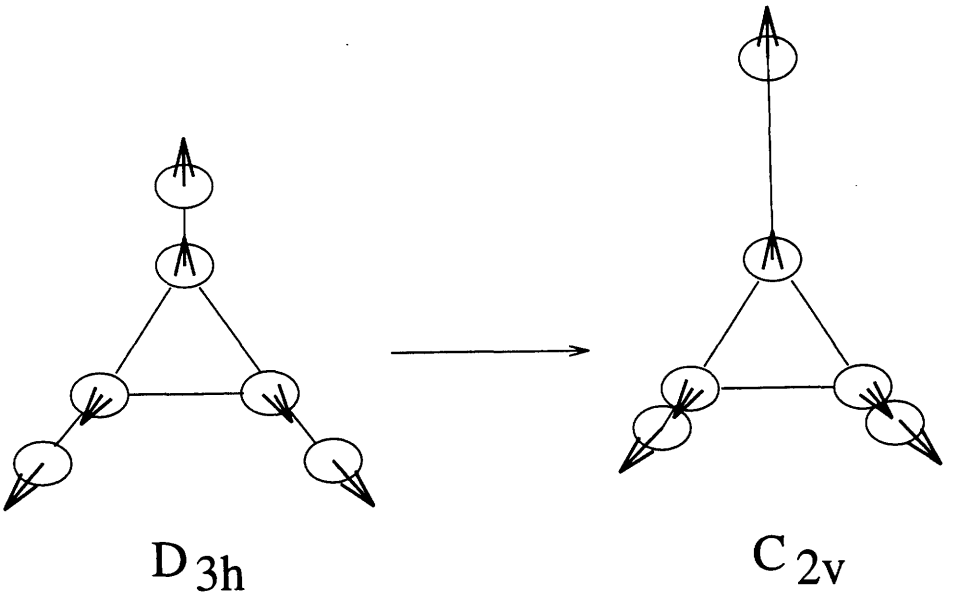

Figure 1-7: Localization of vibrational excitation leads to dynamical symmetry lowering, here from D_{3h} to C_{2v} symmetry.

1.3 Realizations of dynamical symmetry breaking

Realizations of dynamical symmetry breaking are reported from particle physics [7], solid state physics [8] and molecular physics[9].

Dynamical symmetry breaking causes particle like excitations. It arises from the mutual interaction of an excitation and the medium it is moving in.

In the following we will provide intuitive explanations of the physical mechanisms of dynamical symmetry breaking using the examples of a small polaron in a crystal and a local mode in a symmetric molecule. The problems will be stated and explained concisely in the following chapters.

1.3.1 Formation of a polaron

Polarons result from dynamical symmetry breaking. They consist of localized excess charges in a polar crystal that are accompanied by a local distortion of the crystal configuration. Therefore the translational symmetry of the crystal is broken. If the distortion extends over a macroscopic fraction of the crystal the excitation is called

large polaron, small polaron otherwise.

The formation of a polaron follows a feedback mechanism. Consider an excess charge moving through a polar crystal. Through coulomb interaction, the crystal lattice locally relaxes when the excess charge has sufficiently low kinetic energy. Then the excess charge is accompanied by that distortion. Its mass increases by the inertia of the distortion to an effective mass. Consequently it slows down, which allows the crystal lattice to relax further. As a result, the effective mass increases and the velocity drops further until eventually the distortion of the crystal lattice is large enough to considerably confine the excess charge as a bound state. In turn, the bound state potential itself is stabilized by the presence of the excess charge bound in it and *the trapping transition occurs.* The distortion and the excess charge move now as a particle like unit, called the polaron. The polaron was initially proposed by Landau [10] and investigated early on by Pekar [11].

A necessary condition for the formation of the polaron is that the kinetic energy of the electron is initially small enough such that the distortion can develop and follow the excess charge. Furthermore, it must be slowed down enough to allow the formation of a distortion large enough to provide a bound state. If the excess charge is initially completely delocalized the symmetry breaking has to be spontaneous in the form of a fluctuation in the equilibrium geometry of the crystal or induced by external stress. If the excess charge is initially localized to some extent, the polaron can form directly.

The described distortion potential depends on the momentum and the position of the excess charge and therefore is a dynamical potential in the sense discussed above.

The conditions under which the formation occurs can be conservative or non-conservative. In the conservative case the potential energy of the excess charge is lowered by the same amount that the potential energy of the crystal lattice is increased given that the polaron slows down enough to match the kinetic energy of the former nonlocalized excess charge. Conservative formation of the polaron is sometimes called *self-trapping*, the associated transition *self-trapping transition* [12]. In the non-conservative case the formation of the polaron may be supported by emission

of a photon or dissipation into the phonons of the crystal.

1.3.2 Formation of a local mode

Local modes in symmetric molecules result from dynamical symmetry breaking. Let us view a local mode as a localized vibrational excitation in a molecule that is accompanied by a distortion of the molecular equilibrium configuration. Therefore the point symmetry of the molecule in its electronic ground state is reduced.

Similar to the polaron, the formation of a local mode follows a feedback mechanism. Consider a vibrational excitation moving through a symmetric molecule. The molecular equilibrium configuration is relaxing at sufficiently low kinetic energy of the excitation which is then accompanied by that distortion. The distortion is due to the general form of a typical adiabatic bond potential. Now it is important to realize that with increasing localization of the excitation on one bond oscillator, the total potential energy of the system tends to a minimum. Upon transfer to another bond oscillator the excitation has to pass through the state of least distortion that is the state of maximal overall potential energy. As for the polaron, the excitation is slowed down by the distortion that accompanies it and therefore may further develop. Thus it may be the case that the kinetic energy of the excitation vanishes before the state of least distortion is overcome. The *normal to local mode transition* occurs and the excitation is truly localized. The potential which confines the excitation is stabilized by the presence of the excitation. As for the polaron, the symmetry lowering can be induced, spontaneous, conservative or non-conservative.

For both examples the important issue of the relative phase of various excited degrees of freedom of the system was ignored. The relative phase determines the amount of the total energy of the system contained in the couplings and will be explained in detail in the following chapters.

Furthermore, the issue of dissipation was avoided. We will later show that in the two model systems we are about to analyse the process of localization cannot occur without dissipation of energy. The reason is that all degrees of freedom are involved in the confinement of the excitation. Therefore a redistribution of excitation within

the system out of the region of localization into the rest is impossible.

Finally, the outlined pictures are classical and have to be modified for quantum systems by considering additional phenomena like tunneling.

In summary, a localized excitation can develop following a variety of mechanisms under different conditions so that we have to expect that in a real system we won't usually encounter one or the other textbook example. Yet in order to control material properties it is important to distinguish between the different mechanisms and estimate their relative importance under different experimental regimes. Therefore it is necessary to exactly state the extent to which certain conditions favor particular mechanisms.

1.4 Theory of dynamical symmetry breaking

Dynamical symmetry breaking in classical systems is treated in the framework of catastrophe theory [13]. Qualitative features of the dynamics can be predicted from geometrical methods, like phase plane or potential analysis. Analytic prediction of trajectories is possible in different limiting regimes, yet usually unavailable over the complete range of system parameters.

Dynamical symmetry breaking in quantum systems is described in the framework of quantum field theory [14] and formulated in the Lagrangian formalism. It occurs for a system whose Lagrangian is invariant under a particular symmetry transformation yet its ground state is not invariant under that same transformation. Qualitative features can be predicted on the basis of semiclassical methods. However, it is not straightforward to apply the full range of classical methods for quantum systems. The reason is that the notion of classical stability does not have an obvious quantum mechanical counterpart. Semiclassical approaches show some promise and have boomed over the last ten years [15].

In both classical and quantum mechanical cases the study of simple model systems promises some intuitive insight in the process of dynamical symmetry breaking. The nonlinear dimer and the two coupled Morse oscillators are two such models. For both

systems it is possible to reduce the equations of motion under adequate conditions to the discrete nonlinear Schrödinger equation which has been extensively investigated.

1.4.1 Model systems

The nonlinear dimer

For the small polaron such a model system is the nonlinear dimer, which is the simplest model to show localization of an excess charge in a crystal. It is the smallest possible realization of Holstein's molecular crystal [16]. The basic ingredients are: the medium is modelled by two identical diatomic molecules. Their centers of mass occupy two lattice sites and their relative orientation is fixed. A single excess charge can occupy the two sites. The treatment of the electronic properties of the system can be simplified a great deal given a weak electronic overlap between the two molecules. Then the Schrödinger equation can be solved separately for each site and the electronic state assumed to be a linear combination of those solutions. This procedure is called the tight binding approximation. On the basis of numerical evidence the vibrational properties of the molecules are assumed to be sufficiently described by two uncoupled classical harmonic oscillators. Finally, the coupling of the excess charge and the vibrations is assumed to show linear dependence in their coordinates for reasonably low levels of excitation.

Two coupled Morse oscillators

For a local mode in a symmetric molecule, a simple model system that displays dynamical symmetry breaking is given by an AB_2 molecule with C_{2v} symmetry which is the simplest to show localization of vibrational excitation in a molecule [17]. For a given electronic state the AB bond potential is assumed to obey the typical general form of an adiabatic bond potential which is intrinsically anharmonic. A convenient choice for the interatomic potential is the Morse potential. The bond oscillators can exchange vibrational excitation via a coupling that up to moderately high levels of excitation can be assumed to be harmonic. The total amount of excitation is not

restricted to one as for the nonlinear dimer.

1.4.2 The discrete nonlinear Schrödinger equation

The two model systems introduced lead under certain conditions to equations of motion for the excitation that can be transformed into the discrete nonlinear Schrödinger equation which is sometimes also referred to as the discrete self-trapping equation (DSE) [12]. The discrete nonlinear Schrödinger equation has been extensively investigated in the context of solitary excitations in solids and polymers. Possible applications for molecular vibrations were indicated [18].

Without writing it down explicitly for the moment, let us have a look at its structure. It consists of a system of first order partial differential equations for the time evolution of the probability amplitudes of the excitation in different parts of the system, e.g. local bond oscillators. The time evolution of the *probability amplitudes* depends linearly both on the *probability amplitudes* and *probability densities.*

This can be understood in the following way. The linear coupling in the probability amplitudes results in recurrent transfer of the excitation between parts of the system. The linear dependence on the probability densities increases or decreases the tendency of excitation transfer and thus leads to confinement. Therefore the two basic ingredients are given for a system that can display both localization and delocalization and thus the transition between both regimes. Note that the solutions of the discrete nonlinear Schrödinger equation will not obey the principle of superposition that only applies for linear differential equations. A detailed exposition of the topic is given in Appendix C.

1.4.3 Classical and quantum mechanical aspects

So far we have not emphasized conceptual differences in possible mechanisms of localization for classical and quantum systems. A difference that immediately comes to mind is that an excitation in a quantum system can penetrate a classically forbidden region by tunneling. The classical picture of confinement of the excitation in a

potential well can be saved by modifying it to a semiclassical picture that includes this effect.

The true conceptual difficulty arises from the correspondence principle in connection with the notion of classical stability. Let us begin with a brief account of the facets of meaning of classical stability, yet without suffocating the exposition in the exact mathematical definitions.

Stability in classical mechanical systems is distinguished as local and global stability [19].

Local stability characterizes the properties of trajectories contained in a small volume element of phase space, i.e. the immediate change in the dynamics under an instantaneous switch from one trajectory to another nearby trajectory in the same volume element. The volume element contains stable, unstable or neutrally stable trajectories if their tangents at the time of switch intersect after or before the time of switch or their tangents are parallel. The difference in slopes of two tangents of nearby trajectories gives the rate of divergence from a trajectory under a small perturbation. Note that we use "local stability" in the sense of linear stability.

Global stability characterizes the properties of trajectories over a large fraction of the phase space and can be quantified by generalizing the idea of local divergence of trajectories. As before, we start with two trajectories contained in a small volume element of phase space and determine the local rate of divergence. Then we follow each trajectory for a short time and evaluate the new rate of divergence and so on. After repeating this procedure a large number of times we can determine on average the rate of divergence of two initially nearby trajectories, usually referred to as the Lyapunov exponents. Positive Lyapunov exponents imply global instability of a trajectory and negative exponents global stability of a trajectory.

In quantum mechanics the rate of divergence of two states cannot be used to define stability of a particular state upon a small displacement in a certain region of the Hilbert space or the entire Hilbert space. The reason is that the overlap of two states is constant under Hamiltonian time evolution which is unitary [20]. Therefore any state is certain to recur since the quantum equations of motion are linear and

thus at most locally divergent.

However, what can be done is to determine the time dependent overlap of one particular state with itself under propagation by two slightly different Hamiltonians which essentially probes the rate of divergence of a state from its original position under a small perturbation.

Another possibility to characterize stability in a quantum system is to quantify the complexity of the eigenvalue spectrum in terms of the level statistics. This approach has been especially fruitful in molecular and atomic spectroscopy.

Still, the underlying physical property of a quantum system whose classical correspondent has a particular stability property is unclear. This property is fundamental since the stability properties of the classical correspondent can be deduced from the quantum original in the classical limit.

1.5 Posed problems

We conclude our introductory remarks and can set out now to explain the little understood mechanism of localization of excitation in molecules and molecular aggregates under dynamical symmetry breaking. In particular, we wish to address the following issues.

- *Conditions of localization*

  What are the exact conditions under which dynamical symmetry breaking leads to localization of excitation in molecules and molecular aggregates? What are quantitative measures for the tendency to localization of excitation? Which systems meet those conditions? What are the particular mechanisms? What do those mechanisms have in common, how do they differ?

- *Dynamical properties of particle like excitations*

  What are the dynamical properties of excitations? How does the dynamics of the excitation affect the medium it is moving in? How does the dynamics change under damping or driving?

- *Quantum-classical correspondence*

  What properties of a quantum system lead to a classical system with particular stability properties? To what extent can classical pictures account for dynamical symmetry breaking in a quantum mechanical system?

- *Practical implications*

  What are the experimental manifestations of localization under dynamical symmetry breaking? To what extent can localization be controlled?

This thesis is organized as follows. The investigation is carried out in the framework of two model systems and covered in the following three chapters:

- in chapter 2 we give a full account of the normal to local mode transition of vibrational excitation in AB_2 molecules with C_{2v} symmetry.

- In chapter 3 we deal with self-trapping of an excess charge as a small polaron on the nonlinear dimer. Chapter 2 and chapter 3 can be read independently.

On our way to answer the posed questions we encounter a couple of interesting side issues such as

- limitations on the use of Fourier analysis to detect chaotic dynamics (Appendix A),

- stability of eigenvalue problems towards small mistakes and round off errors (Appendix B) and

- various derivations of the nonlinear Schrödinger equation (Appendix C).

Bibliography

[1] J. L. Jewell, J. P. Harbinson and A. Scherer, *Sci. Am.*, 265, 67 (1991); P. F. Fagan and M. D. Ward, *Sci. Am.* , 267 86 (1992)

[2] see special issue of *Physics today*, 47 (1994).

[3] J. F. LePage et al., Applied Heterogeneous Catalysis: Design, Manufacture and Use of Solid Catalysts, Technip (1987).

[4] M. A. Mahowald and C. Mead, Silicon Retina, in: Analog VLSI and Neural Systems, C. Mead ed., Addison-Wesley (1989); E. A. H. Hall, Biosensors, Open Univ. Press (1990).

[5] M. S. Child and L. Halonen, *Adv. Chem. Phys.* 57,1 (1984).

[6] A. S. Ioselevich and E. I. Rashba, Tunnelling in Condensed Media, Yu. Kagan and A. J. Leggett eds., Chapter 7, Elsevier (1992). E. I. Rashba, Excitons, E. I. Rashba and M. D. Sturge eds., North-Holland (1982). Y. Toyozawa, *J. Luminiscence*, 1, 632 (1970).

[7] T. D. Lee, Particle Physics and Introduction to Field Theory, Harwood Academic Publishers (1981).

[8] A. R. Bishop, J. A. Krumhansl and S. E. Trullinger, *Physica D*, 1, 44 (1980).

[9] P. N. Schatz, in: Mixed Valence Compounds, D. B. Brown ed., D. Reidl Publ. Comp. (1980).

[10] L. D. Landau, *Phys. Zs. Sowjet.*, 3, 664 (1933).

[11] S. Pekar, *J. Phys. USSR*, 10, 341 (1946). S. Pekar, *J. Phys. USSR*, 10, 347 (1946).

[12] J. C. Eilbeck, P. S. Lomdahl and A. C. Scott, *Physica D*, 16, 318 (1985).

[13] V. I. Arnold, Catastrophy Theory, Springer (1984).

[14] L. H. Ryder Quantum Field Theory, Cambridge University Press (1985).

[15] E. J. Heller and S. Tomsovic, *Physics Today*, 46, 38 (1993).

[16] T. Holstein, *Ann. Phys.*, 8, 325 (1959). T. Holstein, *Ann. Phys.*, 8, 343 (1959).

[17] P. R. Stannard, M. L. Elert and W. M. Gelbart, *J. Chem. Phys.* 74, 6050 (1981).

[18] A. C. Scott, P. S. Lohmdahl and J. C. Eilbeck, *Chem. Phys. Lett.*, 113, 29 (1985).

[19] J. Guckenheimer and P. Holmes, Nonlinear Oscillations, Dynamical Systems and Bifurcations of Vector Fields, Springer (1983).

[20] F. Haake, Quantum Signatures of Chaos, Springer (1991).

Chapter 2

The local to normal mode transition in polyatomic molecules

2.1 Introduction

The reactivity of a molecular species depends on the distribution of excitation on internal degrees of freedom in the transition state. Therefore, localization of vibrational excitation into specific degrees of freedom will affect the rates of chemical reactions. Usually the degree of freedom responsible for a chemical reaction is associated with a highly excited vibrational state of the molecule, whose population depends on both the inter- and intramolecular dynamics. Thus the efficiency of excitation transfer into the degrees of freedom that support or lead to dissociation affects the rate. In the case of localization of excitation, it may lead to considerable deviation of the actual population from the population predicted from Maxwell-Boltzmann statistics.

In this investigation we shall be exclusively concerned with localization in a dynamic potential. The object of our study will be the class of AB_2 molecules with C_{2v} symmetry [1] for the following reasons.

First, due to symmetry constraints there exists no intramolecular static potential that allows localization of vibrational excitation into a specific AB bond oscillator. Therefore the study of localization in a minimum of a *dynamic* potential becomes important. It results in the reduction of the molecular symmetry, often referred

to as "dynamical symmetry breaking". Obviously the normal mode description of the molecular oscillations becomes then inadequate and local modes provide a more satisfactory picture. The *normal to local mode transition* occurs at the boundary between these two descriptions.

Second, the system is simple enough to be treated analytically in both the classical and quantum mechanical limits and may thus allow generalization of the results. The specific questions we want to address will become apparent after a brief survey of previous investigations on the normal to local mode transition in triatomic molecules AB_2.

The Hamiltonian for the water molecule, the epitome of molecules AB_2 with symmetry C_{2v}, was originally written down by Podolsky [2]. Perturbative analysis of the vibrational contributions led Bonner [3] to an expansion of the vibrational level energies in powers of the vibrational quantum numbers of the normal modes. Inconsistencies of calculated and observed spectra were removed by Darling and Dennison [4] who recognized that, due to the near degeneracy of the symmetric and antisymmetric normal modes, the coupling between these two modes had to be taken into account. The corresponding Hamiltonian correctly generating the spectrum is called the Darling-Dennison Hamiltonian, the introduced resonant term the Darling-Dennison term. The Darling-Dennison Hamiltonian in the second quantized representation is an algebraic form of the raising and lowering operators for the *normal* modes. The discovery by Henry and Siebrand [5] that an algebraic form in the raising and lowering operators of the *local* modes shows at least equally good agreement with the spectra and even excellent agreement with the low energy states within the same overtone manifold opened the discussion as to the *physical nature* of these vibrational states.

From here on there have been a number of efforts on the problem. For a comprehensive review and bibliography on the topic, the reader is referred to [1]. The focus of attention has been on models of two identical harmonically coupled local bond Morse oscillators, both classical and quantum mechanical. These are especially appealing from a physical point of view and lead directly to the local expansion mentioned above.

In the following treatment of the classical aspects, we connect to the hindered rotor model developed by Sibert et al. [6, 7]. Their analysis is carried out in action angle coordinates, where the action of the hindered rotor is given by the action difference, the angle of rotation by the phase difference of the oscillators. The potential of hindrance is periodic in 2π. In the weak coupling limit they identified the regime of *local modes* with *libration* of the rotor and *normal modes* with *hindered rotation.* Using the WKB method they obtained the semiclassical eigenvalues in good agreement with the exact result from the quantum mechanical analogue.

The quantum mechanical aspects were studied by Stannard et al. [8], Mortensen et al. [9] and then in a series of detailed investigations by Child and Lawton [10], who found from numerical calculations an indicator of local and normal character of a state in the spectrum. This indicator is given by the ratio of the coupling between the oscillators and the anharmonicity constant of the oscillators. *Local character* was attributed to states that appear in pairs split by an energy difference small compared to the energy difference to neighboring states in the spectrum, *normal character* to all other states. The splitting between states of local character was attributed to tunneling between degenerate local modes. States of the same total vibrational quantum number n are grouped in the "n^{th} polyad ". States of local character usually appear at low energies within a polyad, states of normal character at high energies. The number of states of local character increases with n. Weak coupling, strong anharmonicity and high excitation favor local character states. These observations can be understood and quantified from the properties of a dynamical double well potential using semiclassical ideas.

Part of the discussion was reconciled by Lehmann [11] and then Kellman [12] who demonstrated the equivalence of the normal Darling-Dennison Hamiltonian and the local algebraic Hamiltonian, which are related by a $SU(2)$ transformation. Kellman also pointed out, that the labeling of states in either normal or local zeroth order basis is both inaccurate and ambiguous. Xiao and Kellman [13] proposed then a classification scheme for the vibrational states in terms of the dynamical properties of the classical Darling-Dennison Hamiltonian. Their contribution is important in two

aspects. First, they showed by numerical integration of the equations of motion that the locality or normality of a classical trajectory is independent of the representation in a local or normal basis. The display of the classical phase space trajectories of states in the same polyad on the "polyad phase sphere" spanned by $SU(2)$ coordinates allowed them to assign *unambiguously* the label of local or normal character. For example, a trajectory corresponding to a state with local character in the spectrum must be inside the nonresonant area in the local representation and inside the resonant area in the normal representation, i.e. two normal classical normal modes exchanging vibrational excitation form a local classical mode. Second, they demonstrated that their model is a legitimate extension of the one treated by Sibert et al [6, 7] beyond the weak coupling limit.

Finally, let us mention that the connection of the dynamics of normal and local modes to the nonlinear Schrödinger equation was first pointed out by Scott et al. [14] and will be commented on in Appendix C.

At this point, the distinction between *local* and *local character* has been made. Classical local modes can be assigned to quantum mechanical states of local character. Yet in contrast to the possibility of localization of excitation in the classical local modes the quantum mechanical modes of local character are characterized by *delocalization* of excitation in *any* basis. The reason is that all eigenstates are invariant under the symmetry operations according to the molecular symmetry, i.e. in the local mode representation they are formed by a superposition of two local states of identical excitation and are thus inherently of non-local nature.

Therefore the question at the heart of the issue remains unanswered: can we intuitively understand the physical content of the normal to local mode transition?

On our way to an answer we face several obstacles.

Is the proper theoretical framework classical, semiclassical or quantum mechanical? What are the assets and drawbacks in each mode of description? What are the proper quantitative measures that support an intuitive picture?

What are the exact conditions for the normal to local mode transition to occur under dynamical symmetry breaking? Can we predict this transition for particu-

lar systems? For which systems can this transition take place under conservative conditions? Is an exact specification of the particular mechanism that leads to the transition necessary?

What can we say about the dynamics of the excitation in the normal mode and local mode limits? What are the features of the process of localization?

We address these issues in two steps, first, by a head on attack on the classical system and second, by an investigation of the implications of the classical results for the properties of the quantum system.

The dynamics of a vibrational excitation of the classical system is shown to be equivalent to an undamped Duffing oscillator without driving. The dynamical properties of the system are then discussed using phase plane analysis and potential analysis of the Duffing potential. The initial condition dependence of the dynamics and the potential is discussed using a phase diagram that can be extended to a phase surface, known as the Poincaré sphere. Then we evaluate the theoretical results for a variety of molecular systems, to be specific H_2O, O_3, SO_2, C_2H_2 and C_2D_2. In the following, the equations of motion for the excitation are solved analytically and the conditions for the normal to local mode transition formulated. A panoptic view of the analytic tools and results leads us to an intuitive interpretation of the classical normal to local mode transition, which can be understood in terms of the explicit dynamical Duffing potential that changes from single well to double well form upon excitation. Its origin is due to the general form of a typical adiabatic bond potential and it is therefore present in any moderately excited polyatomic molecule. Localization of vibrational excitation into a bond leads to a state of unsymmetric distortion of the equilibrium geometry and minimum overall potential energy. Upon transfer of the excitation to another bond the molecule passes through the state of least distortion and highest overall potential energy. If the kinetic energy of the excitation vanishes at that state the normal to local mode transition occurs. Finally, it turns out that the process of localization cannot occur for the discussed systems under conservative conditions. An extension to damped conditions is qualitatively discussed.

The discussion of the quantum mechanical aspects is opened by an introduction

into the eigenvalue problem of the quantum Darling-Dennison Hamiltonian and the quantum Duffing Hamiltonian. Quantum states can be uniquely labelled as normal or local character states on the basis of the analytical classical results. Yet due to symmetry requirements none of them can display excitation localization. However, the physical relevance of this distinction can be understood in terms of the susceptibility to a symmetry breaking perturbation. This susceptibility quantifies the tendency for localization. Local character states are much more susceptible to a symmetry breaking perturbation than normal character states under the same perturbation. The conditions for the quantum mechanical normal to local mode transition are formulated. The classical physical interpretation is modified due to the possibility of tunneling. The developed concepts are applied to the already classically treated molecular systems.

The susceptibility to almost any symmetry breaking perturbation turns out to be extraordinarily high in some cases. Therefore it is necessary to define a stability criterion for vibrational eigenstates of polyatomic molecules interacting with an inhomogeneous environment. This can be done in terms of random matrix theory. The stability analysis is explicitly carried out for a variety of molecules.

2.2 The classical Darling-Dennison system

2.2.1 Derivation of the classical Darling-Dennison Hamiltonian

The quantum mechanical Darling-Dennison Hamiltonian for two coupled stretch vibrations in its local form can be written to good approximation as [12]

$$\begin{aligned} \hat{H}_{DD} &= \hat{H}_0 + \hat{V}_{1:1}, \\ \hat{H}_0 &= \omega(\hat{n}+1) + \frac{\alpha}{2}[(\hat{n}_1+\frac{1}{2})^2 + (\hat{n}_2+\frac{1}{2})^2] + \alpha_{12}(\hat{n}_1+\frac{1}{2})(\hat{n}_2+\frac{1}{2}), \\ \hat{V}_{1:1} &= \frac{1}{2}[\beta + \frac{\epsilon}{2}(\hat{n}+1)](\hat{a}_1^\dagger \hat{a}_2 + \hat{a}_2^\dagger \hat{a}_1). \end{aligned} \tag{2.1}$$

Here $\hat{a}_i^\dagger$ and $\hat{a}_i$, $i = 1, 2$, are raising and lowering operators defined by their action on the state of the ith *local anharmonic oscillator*

$$\hat{a}_i|n_i> = \sqrt{n_i}|n_i - 1>, \tag{2.2}$$

$$\hat{a}_i^\dagger|n_i> = \sqrt{n_i + 1}|n_i + 1> . \tag{2.3}$$

The number operator $\hat{n}_i$ and total number operator $\hat{n}$ are given by

$$\hat{n}_i = \hat{a}_i^\dagger \hat{a}_i, \tag{2.4}$$

$$\hat{n} = \hat{n}_1 + \hat{n}_2. \tag{2.5}$$

The Hamiltonian parameters $\omega, \alpha, \alpha_{12}, \beta$ and ϵ are obtained by a non-linear least-squares fit to the spectrum and can be interpreted in terms of the physical picture of two harmonically-coupled identical Morse oscillators as follows. ω is the fundamental frequency of the oscillators, α the anharmonicity constant and α_{12} the cross anharmonicity constant. The harmonic coupling $\hat{V}_{1:1}$ increases linearly with the total number of vibrational quanta. The magnitudes and signs of the parameters $\alpha, \alpha_{12}, \beta$ and ϵ can strongly vary from molecular species to molecular species, indicating different causes for anharmonicity and coupling. As will turn out later, these aspects are completely irrelevant for the appearance of the normal mode to local mode transition. For more details on the Hamiltonian and the procedure to obtain the parameters the reader is referred to [12, 13]. Following a suggestion of Kellman we define the SU(2) operators

$$\hat{I}_x = \hat{a}_1^\dagger \hat{a}_2 + \hat{a}_2^\dagger \hat{a}_1, \tag{2.6}$$

$$\hat{I}_y = -i(\hat{a}_1^\dagger \hat{a}_2 - \hat{a}_2^\dagger \hat{a}_1), \tag{2.7}$$

$$\hat{I}_z = \hat{n}_1 - \hat{n}_2, \tag{2.8}$$

$$\hat{I} = \hat{n} + 1, \tag{2.9}$$

$$\hat{\zeta} = \frac{1}{2}[\beta + \frac{\epsilon}{2}(\hat{n} + 1)]. \tag{2.10}$$

They obey the commutation relations

$$[\hat{I}_i, \hat{I}_j] = 2i\epsilon_{ijk}\hat{I}_k, \tag{2.11}$$

where ϵ_{ijk} is the Levi-Civita tensor. Note that

$$\hat{I}^2 = \hat{1} + \hat{I}_x^2 + \hat{I}_y^2 + \hat{I}_z^2. \tag{2.12}$$

We define the constants

$$\xi = \frac{\alpha + \alpha_{12}}{4}, \tag{2.13}$$

$$\chi = \frac{\alpha - \alpha_{12}}{4}. \tag{2.14}$$

The Hamiltonian (2.1) can now be written in compact form

$$\hat{H}_{DD} = (\omega + \xi\hat{I})\hat{I} + \hat{C}, \tag{2.15}$$

$$\hat{C} = \hat{\zeta}\hat{I}_x + \chi\hat{I}_z^2. \tag{2.16}$$

The dynamical invariants are given by the vanishing commutators

$$[\hat{H}_{DD}, \hat{H}_{DD}] = 0, \tag{2.17}$$

$$[\hat{H}_{DD}, \hat{I}] = 0, \tag{2.18}$$

$$[\hat{H}_{DD}, \hat{C}] = 0. \tag{2.19}$$

It may seem artificial for the moment to emphasize the invariant nature of $\hat{H}_{DD}$ under propagation by itself, yet later on we will use an algebraic relation of the three invariants that by construction is an invariant itself.

As a brief aside let us mention the analogy to Schwinger's formulation of the theory of angular momentum in second quantized form which leads in the classical limit to the interpretation of $< \hat{I} > /2, < \hat{I}_x > /2, < \hat{I}_y > /2, < \hat{I}_z > /2$ as actions. As opposed

to Schwinger's construction, the basic constituents of angular momentum here are not harmonic but anharmonic oscillators from which we infer that the phenomenon of localization of excitation will occur in angular momentum problems in the context of hindered rotations.

In particular, $< \hat{I}_z(t) > / < \hat{I} >$ can be interpreted as the probability difference for the total vibrational excitation to be found on either oscillator and thus is the proper tool to diagnose symmetry breaking due to self-trapping. If the time average of this ratio is nonvanishing, we have to conclude, that the vibrational excitation is trapped on one of the oscillators. We will later on obtain the analytical solutions for this quantity in the classical limit.

The time evolution of $\hat{I}_z(t)$ is given by

$$\dot{\hat{I}}_z = i[\hat{I}_z, \hat{H}_{DD}] = -2\hat{\zeta}\hat{I}_y. \tag{2.20}$$

For highly excited vibrational states, i.e. $< \hat{n} >= n \gg 1$, the classical limit of the quantum mechanical Hamiltonian is expected to provide a satisfactory description of the system. The raising and lowering operators $\hat{a}_i^\dagger, \hat{a}_i$ correspond in the classical limit to the complex mode amplitudes a_i^*, a_i, to be specific

$$\hat{a}_i^\dagger \rightarrow a_i^* = \sqrt{n_i + \frac{1}{2}} \exp(i\phi_i), \tag{2.21}$$

$$\hat{a}_i \rightarrow a_i = \sqrt{n_i + \frac{1}{2}} \exp(-i\phi_i). \tag{2.22}$$

The operators $\hat{I}/2, \hat{I}_x/2, \hat{I}_y/2, \hat{I}_z/2$ correspond to the actions $I/2, I_x/2, I_y/2, I_z/2$ and $\hat{\zeta}, \hat{C}$ to the numbers ζ, C. In the classical limit the Hamiltonian (2.15) takes the form

$$H_{DD} = (\omega + \xi I)I + C. \tag{2.23}$$

$$I^2 = I_x^2 + I_y^2 + I_z^2 \tag{2.24}$$

$$C = \zeta I_x + \chi I_z^2. \tag{2.25}$$

Let us denote the associated energy by E_{DD}. Note that $(I/2, \Psi = \phi_1 + \phi_2)$ and

$(I_z/2, \Phi = \phi_1 - \phi_2)$ are pairs of conjugate coordinates, called action angle coordinates for H_{DD}. In particular, Ψ is a cyclic coordinate which implies for its conjugate coordinate $I/2$ that $\dot{I}/2 = 0$.

The dynamic invariants are given by the vanishing Poisson brackets

$$\{H_{DD}, H_{DD}\} = 0, \tag{2.26}$$

$$\{I, H_{DD}\} = 0, \tag{2.27}$$

$$\{C, H_{DD}\} = 0. \tag{2.28}$$

The time evolution of I_z is given the Poisson bracket

$$\dot{I}_z = \{I_z, H_{DD}\} = -2\zeta I_y. \tag{2.29}$$

2.2.2 Equivalency to Duffing's oscillator

It is possible to solve the equation of motion eqn.(2.29) for I_z by numerical integration. Obviously an analytical solution would be of advantage, since it provides expressions for the explicit dependence of the dynamics on the Hamiltonian parameters. In order to simplify the problem of finding that analytical solution and a physical interpretation, we will carry out a canonical transformation on the Hamiltonian H_{DD} such that $(I_z, \dot{I}_z)$ are conjugate coordinates to a new Hamiltonian H.

Naturally the equations of motion are then given by

$$\dot{I}_z = \{I_z, H\} = \partial_{\dot{I}_z} H, \tag{2.30}$$

$$\ddot{I}_z = \{\dot{I}_z, H\} = -\partial_{I_z} H. \tag{2.31}$$

The invariants given in eqn.(2.24,2.25) will be by construction invariants to H, i.e.

$$\{H, H\} = 0, \tag{2.32}$$

$$\{I, H\} = 0, \tag{2.33}$$

$$\{C, H\} = 0, \tag{2.34}$$

and then by construction

$$\{H, H_{DD}\} = 0. \tag{2.35}$$

The transformation can be carried out for both the classical and quantum mechanical system. We focus on the "construction work" of H which makes the physical content of the dynamics intuitively clear. The building blocks are the invariants I and C. We treat the classical case in detail and give the result for the quantum mechanical case.

The idea is to write the new Hamiltonian H as an algebraic form in the invariants I C, i.e.

$$H = X + Yf(I) + Zg(C), \tag{2.36}$$

where X, Y, Z are constants, $f(I)$ is some polynomial in the total action I and g(C) is some polynomial in the invariant C, all of which we are about to determine under the condition that $I_z, \dot{I}_z$ are conjugate coordinates to H.

The Hamiltonian in question has a kinetic and a potential contribution

$$H(I_z, \dot{I}_z) = T(\dot{I}_z) + V(I_z). \tag{2.37}$$

The kinetic contribution $T(\dot{I}_z)$ has to be according to eqn.(2.29)

$$T = \frac{\dot{I}_z^{\,2}}{2} = 2\zeta^2 I_y^2. \tag{2.38}$$

The potential contribution $V(I_z)$ can now be obtained in two steps. Since I and C must be invariants of both H_{DD} and H we can use them to eliminate I_x. First we substitute eqn.(2.38) in the expression for the invariant I given by eqn.(2.24). Second, we eliminate I_x using the invariant C given by eqn.(2.25). The result is

$$X = 0, \tag{2.39}$$

$$Y = 2\zeta^2, \tag{2.40}$$

$$Z = -2, \tag{2.41}$$

$$f(I) = I^2, \tag{2.42}$$

$$g(C) = C^2, \tag{2.43}$$

where we set the constant $X = 0$. Therefore we obtain for the Hamiltonian H

$$\begin{aligned} H &= 2[(\zeta I)^2 - C^2] = T + V = \\ &= 2(\zeta I_y)^2 + \frac{A}{2} I_z^2 + \frac{B}{4} I_z^4. \end{aligned} \tag{2.44}$$

$$A = (2\zeta)^2 - 8\chi C, \tag{2.45}$$

$$B = 8\chi^2. \tag{2.46}$$

Let us denote the associated energy by E. We see that the potential $V(I_z)$ is a linear combination of a quadratic and a quartic term. Thus we can visualize the dynamics of I_z as the motion of a classical particle in a single or double well potential, dependent on the constants A, B. Note, that in the $(I_z, \dot{I}_z)$ representation the potential $V(I_z)$ is static, whereas in the original (a_j, ia_j^*) representation it depends on the momenta and thus is dynamic.

The reason why we could carry out the transformation is that the motion of $I(I_x, I_y, I_z)$ in the original system is restricted by the invariant I onto the surface of a sphere of radius $|I|$. The invariant C determines the trajectory on that surface. Using C we can formulate I_x as a quadratic function of I_z. Therefore we can view the trajectories as arising from motion of a classical particle in a harmonic potential under the restriction that the particle has to move on the surface of a sphere of radius $|I|$ [15]. Thus there is only one time dependent degree of freedom to be solved for which we identified to be the difference in excitation I_z of the two local oscillators.

The quantum mechanical form of the Hamiltonian (2.44) follows in analogy

$$\begin{aligned} \hat{H} &= 2[\hat{\zeta}^2(\hat{I}^2 - \hat{1}) - \hat{C}^2] = \\ &= 2(\hat{\zeta}\hat{I}_y)^2 - 2\chi\{\hat{C}, \hat{I}_z^2\} + 2\zeta^2\hat{I}_z^2 + 2\chi^2\hat{I}_z^4. \end{aligned} \tag{2.47}$$

$$\{\hat{C}, \hat{I}_z^2\} = \hat{C}\hat{I}_z^2 + \hat{I}_z^2\hat{C}. \tag{2.48}$$

Note that

$$[\hat{H}_{DD}, \hat{H}] = 0, \tag{2.49}$$

i.e. $\hat{H}_{DD}$ and $\hat{H}$ have the same eigenstates, which we will take advantage of later.

In the classical limit, $\hat{C}$ and $\hat{I}_z^2$ anticommute and Hamiltonian (2.44) proves to be the correct classical correspondent. The major difference between the classical and quantum mechanical Hamiltonians is that although the symmetry with respect to a sign change in I_z is present in both, only the classical system can display local modes in the double well potential. The reason is that the quantum mechanical system allows tunneling through the well between local states, which is impossible in the classical system.

The Hamiltonian defined in eqn.(2.44) turns out to be identical to the Hamiltonian of an undriven Duffing [1] oscillator without damping [16]. Not only is the Duffing oscillator one of the best studied models in nonlinear dynamics but has also in the form given above an analytic solution to its equation of motion. The equation of motion is called *Duffing's equation* and is given by

$$-\delta_{I_z} V(I_z) = \ddot{I}_z = -AI_z - BI_z^3. \tag{2.50}$$

The solution for I_z allows together with the definition of C in eqn.(2.25) the solution for I_x. Then we can readily solve for I_y from the definition of I in eqn.(2.24). Finally from the definition of I_x, I_y and I_z we can obtain the solution for the complex mode amplitudes a_1 and a_2 and therefore for the trajectories of both bond oscillators.

The advantage of mapping the intramolecular energy transfer of the oscillating molecule onto the Duffing oscillator goes well beyond the benefit of an analytical solution. The visualization of the stability properties of the system by a single or double well potential is established in physics under the notion of the Landau function

[1] Biographic note. Georg Duffing (* 1861 † 1944), full-blooded engineer of the Wilhelminic era in Berlin, Germany, who carried out extensive experiments investigating anharmonic oscillations in mechanical systems. His monograph on the topic, "Erzwungene Schwingungen bei Veränderlicher Eigenfrequenz", remained largely unnoticed until in the 1960's it went through a Renaissance with the "discovery" of chaos in dynamical systems. How little his work is still appreciated can be estimated from the fact that neither of the leading encyclopedias contains his biographic note.

and allows intuitive insight. We will use this insight in the following section to qualitatively discuss the dynamical properties of the molecular vibrational excitation and to obtain the parametric dependence as well as initial condition dependence of the normal to local mode transition. Another advantage is that the extension of the model to damped and driven cases allows the adaption of well known results from the Duffing system.

2.2.3 Geometrical construction of the polyad phase-sphere

Before we will analytically solve the equation of motion eqn.(2.50) let us extract information about the dynamics of the system using geometrical methods from classical mechanics. First, we will investigate the phase plane and the potential associated with the Duffing equation. Second, we will discuss the parametric and initial condition dependence of the solutions to the Duffing equation and display the results in a phase diagram spanned by the initial values of the actions that constitute C. The synthesis of the phase diagram and the phase plane will lead us to a geometric representation of the phase space trajectories on the Poincaré sphere, which in the context of molecular dynamics is referred to as the *polyad phase-sphere.*

Phase plane analysis

The phase plane analysis for the Duffing equation can be carried out in the coordinates $(I_z, \dot{I}_z)$ [17]. Note however, that due to the appearance of the invariant C in the constant A we have to expect that the determination of the stationary points of the system requires a specification of I_x as well.

Let us first introduce the normalized variables

$$\mathcal{I}_{x,y,z} = \frac{I_{x,y,z}}{I}, \tag{2.51}$$

which is the trivial case of a canonical transformation changing the scale of the canonical variables.

Furthermore we introduce the dimensionless parameter κ

$$\kappa = \frac{\zeta}{2\chi I} = \frac{\frac{\epsilon}{2} + \frac{\beta}{I}}{\alpha - \alpha_{12}}. \tag{2.52}$$

The definition for κ is motivated by the idea to relate the antagonistic tendencies of excitation transfer and localization. The transfer tendency is reflected in the magnitude of the coupling parameter ζ that increases linearly with the total vibrational excitation I. The localization tendency manifests itself in the parameter χ which is proportional to the degree of anharmonicity α reduced by the diagonal coupling α_{12} of the oscillators for any given excitation. The normalization by I makes κ dimensionless. Small values of κ indicate a high tendency, large values a low tendency of localization of vibrational excitation. The dependence of κ on I indicates, that with increase of total vibrational excitation the tendency of localization also increases.

Now we will carry out the phase plane analysis in the normalized coordinates $(\mathcal{I}_{z,1}, \mathcal{I}_{z,2})$ defined by

$$\mathcal{I}_{z,1} = \mathcal{I}_z, \tag{2.53}$$

$$\mathcal{I}_{z,2} = \dot{\mathcal{I}}_{z,1}. \tag{2.54}$$

The Duffing equation eqn.(2.50) can be written as a system of two coupled first order differential equations

$$\dot{\mathcal{I}}_{z,1} = \mathcal{I}_{z,2}, \tag{2.55}$$

$$\dot{\mathcal{I}}_{z,2} = -A\mathcal{I}_{z,1} - BI^2\mathcal{I}_{z,1}^3. \tag{2.56}$$

The condition for stationary points $S(\mathcal{I}_x, \mathcal{I}_y, \mathcal{I}_z)$ is that

$$\dot{\mathcal{I}}_{z,1} = 0 \tag{2.57}$$

$$\dot{\mathcal{I}}_{z,2} = 0. \tag{2.58}$$

- For $|\kappa| > 1$ we find two stationary points

$$S^{1,2} = (\pm 1, 0, 0). \tag{2.59}$$

- For $|\kappa| < 1$ we find four stationary points

$$S^{1,2} = (\pm 1, 0, 0), \tag{2.60}$$

$$S^{3,4} = (\kappa, 0, \pm\sqrt{1-\kappa^2}). \tag{2.61}$$

Linear stability analysis of eqn.(2.56) around the stationary points gives the following results.

- For $|\kappa| > 1$, $S^{1,2}$ are center points (neutrally stable).
- For $|\kappa| < 1$ we have to distinguish between $\kappa > 0$ and $\kappa < 0$.
  - For $\kappa > 0$, S^1 is a saddle point (unstable), $S^{2,3,4}$ are center points.
  - For $\kappa < 0$, $S^{1,3,4}$ are center points, S^2 is a saddle point.

We see that number and stability of stationary points changes at $|\kappa| = 1$ and $\kappa = 0$, i.e. three bifurcations occur. The bifurcation diagram is shown in Figure 2-1. It displays a combination of two pitchfork bifurcations that occur at $\kappa = \pm 1$ and a transcritical bifurcation at $\kappa = 0$. Since the picture is somewhat reminiscent of two pitchforks crossed in a fight between farmers in the author's bavarian homeland we will call the bifurcation the "Bauernrauferei" or *farmers fight* bifurcation. This result is consistent with results obtained for the Darling-Dennison Hamiltonian [18].

At this point it is important to notice that apparently only the modulus of the parameter κ is important to detect qualitative changes in the dynamics of the excitation transfer. Therefore the particular mechanisms that lead to the transfer or the localization of the excitation, as reflected in different signs of the Hamiltonian parameters ζ and χ, do not have to be invoked in order to explain the dynamics.

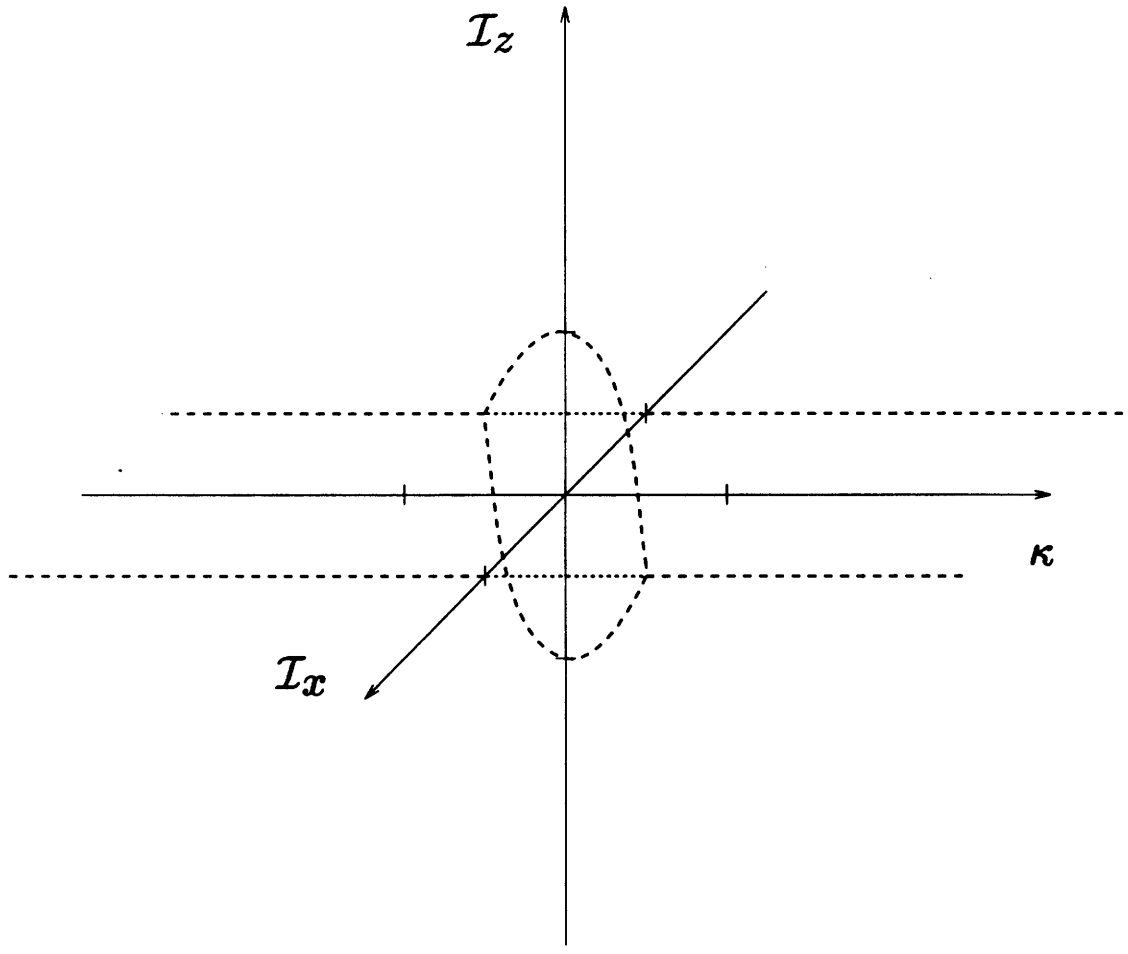

Figure 2-1: Bifurcation diagram for the undamped Duffing oscillator without driving. Dashed lines (- -) indicate neutrally stable branches, dotted lines (...) unstable branches. At $|\kappa| = 1$ there occurs a pitchfork bifurcation and at $\kappa = 0$ there occurs a transcritical bifurcation.

The Duffing Potential $\mathcal{V}(\mathcal{I}_z)$

In order to explore the dynamical properties of the *non stationary* trajectories, let us discuss the properties of the potential $\mathcal{V}(\mathcal{I}_z) = V(I_z)/I^2$.

The potential parameters A, B in $\mathcal{V}$ depend both on the original Hamiltonian parameters, whereas only A depends via C on the initial conditions. Since B is positive semidefinite, $\mathcal{V}$ can either have one minimum or one maximum and two minima, dependent on the sign of A. The transition between these two forms occurs at $A = 0$ and indicates the bifurcation discussed above. In the single well form the $\mathcal{I}_z$ coordinates of the centers coincide with those of the minima of $\mathcal{V}$. In the double well form the $\mathcal{I}_z$ coordinates of saddle and the appearing centers are identical to those of the maximum and the minima, respectively. The following dynamic regimes are possible.

- For all extrema of $\mathcal{V}$, $\mathcal{I}_z$ is stationary.
- For the case of a single well potential, $\mathcal{I}_z$ oscillates around $\mathcal{I}_z = 0$. The vibrational excitation undergoes complete exchange between the two local oscillators within half a period of oscillation.
- For the case of a double well potential we have to distinguish between two situations.
  - First, if $E > 0$, $\mathcal{I}_z$ oscillates around $\mathcal{I}_z = 0$, yet due to the potential well under reduced velocity at the origin.
  - Second, if $E < 0$, $\mathcal{I}_z$ oscillates around one of the minima of $\mathcal{V}$. The vibrational excitation is not completely exchanged between the two local oscillators. The excitation is trapped.

The energies E_{DD} and E at the stationary points $S^{1,2,3,4}$ as calculated from eqn.(2.23,2.44) are

$$E_{DD}^{1,2} = (\omega + \xi I)I \pm \zeta, \tag{2.62}$$

$$E_{DD}^{3,4} = (\omega + \xi I)I + \chi I^2 + \frac{\zeta^2}{4\chi}, \tag{2.63}$$

$$E^{1,2} = 0, \tag{2.64}$$

$$E^{3,4} = -\chi^2(1-\kappa^2)^2 I^4. \tag{2.65}$$

It is worth mentioning that the stationary states are gauge invariant, to be specific, invariant under a change of the coordinates $a_i \to a_i \exp(i\gamma t)$ where the frequency γ can be determined from H_{DD}.

This concludes the discussion of the dependence of the dynamics of the excitation on the Hamiltonian parameters. In the following section we investigate the dependence on the initial conditions.

The phase diagram

The dependence on initial conditions is best displayed in a phase diagram spanned by $(\mathcal{I}_z(t_0), \mathcal{I}_x(t_0))$. First, from the definition of I we conclude that

$$\mathcal{I}_z^2(t_0) + \mathcal{I}_x^2(t_0) \leq 1, \tag{2.66}$$

which restricts the accessible area of the phase diagram to the unit circle. There exist two more lines that separate three different dynamic regimes.

- The regions of single and double well potentials are separated by the *bifurcation parabola*

$$\mathcal{I}_x^b(t_0) = \kappa - \frac{\mathcal{I}_z^2(t_0)}{2\kappa}, \tag{2.67}$$

  which we readily obtain from the condition $A = 0$ in eqn.(2.45).

- The regions for which $E > 0$ and $E < 0$ are separated by the *localization parabola*

$$\mathcal{I}_x^s(t_0) = \pm 1 - \frac{\mathcal{I}_z^2(t_0)}{2\kappa}, \tag{2.68}$$

  which we readily obtain from the condition $E = 0$ in eqn.(2.44). For $\kappa > 0$ the ordinate has to be taken positive, for $\kappa < 0$ the ordinate has to be taken

negative.

- In order to locate a state observed in the spectrum at energy E_{DD} in the phase diagram, we eliminate C from eqn.(2.25,2.23) to obtain the *spectral parabola*

$$\mathcal{I}_x^\lambda(t_0) = \mathcal{C} - \frac{\mathcal{I}_z^2(t_0)}{2\kappa} \tag{2.69}$$

$$\mathcal{C} = \frac{1}{\zeta I}[E_{DD} - (\omega + \xi I)I]. \tag{2.70}$$

- The stationary points lie on the unit circle and have the coordinates $(\pm\sqrt{1-\kappa^2}, \kappa)$.

Figure 2-2 displays several possible states in the phase diagram for given κ. From here on let us assume without loss of generality that $\kappa > 0$, unless stated explicitly otherwise.

We see that the area of the phase diagram within the unit circle is divided into three regions by the localization parabola $\mathcal{I}_x^s(t_0)$ and the bifurcation parabola $\mathcal{I}_x^b(t_0)$ indicated as solid lines. They have the same curvature $-1/\kappa$ but different intercepts with the ordinate. The ordinate of the localization parabola is fixed at $\mathcal{I}_x^s(t_0) = 1$, the ordinate of the bifurcation parabola is variable at $\mathcal{I}_x^b(t_0) = \kappa$. The spectral parabolae $\mathcal{I}_x^\lambda(t_0)$ are indicated as dashed lines and have the same curvature as the localization and bifurcation parabolae.

We can now unambiguously assign dynamical properties to a particular spectral state by drawing the corresponding spectral parabola in the phase diagram. Note that C is a linear function of the energies of the spectral states. There are five possible cases.

- For $\mathcal{C} > 1$ the corresponding spectral parabolae $\mathcal{I}_x^\lambda(t_0)$ lie in the region of trapped motion.

- For $\mathcal{C} = 1$ the corresponding spectral parabolae $\mathcal{I}_x^\lambda(t_0)$ coincides with the localization parabola $\mathcal{I}_x^s(t_0)$.

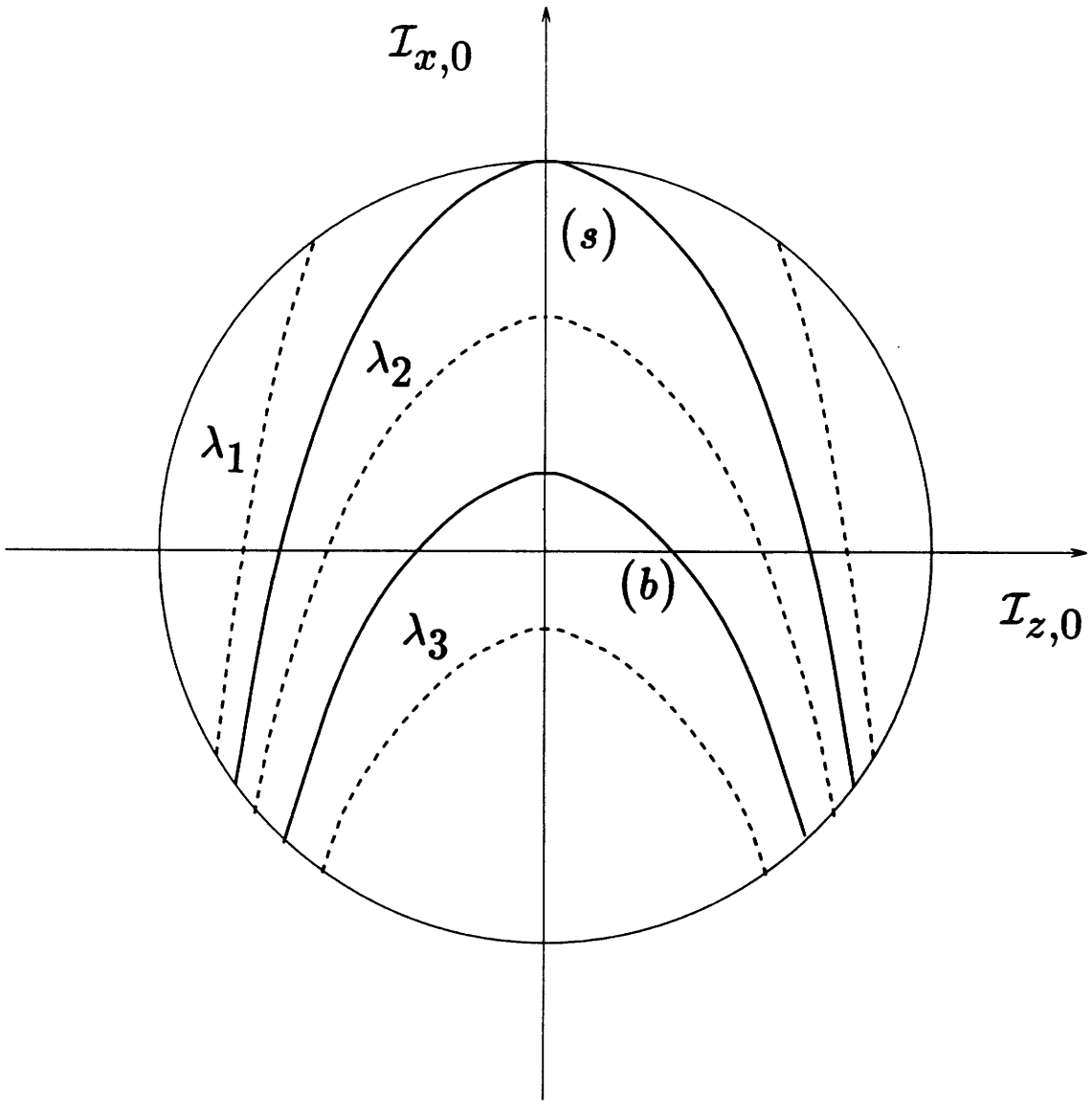

Figure 2-2: Phase diagram for $0 < \kappa < 1$. The solid circle (-) restricts the accessible area of the phase diagram. The solid parabolae (-) are the localization parabola (s) and the bifurcation parabola (b). The dashed parabolae (- -) are in the local mode region (λ_1), in the region of a normal mode in a double well potential (λ_2) and in the region of a normal mode in a single well potential (λ_3).

- For $1 > \mathcal{C} > \kappa$ the corresponding spectral parabolae $\mathcal{I}_x^\lambda(t_0)$ lie in the region of free motion, yet the excitation is subjected to a double well potential.

- For $\mathcal{C} = \kappa$ the corresponding spectral parabolae $\mathcal{I}_x^\lambda(t_0)$ coincides with the bifurcation parabola $\mathcal{I}_x^b(t_0)$

- For $\kappa > \mathcal{C}$ the corresponding $\mathcal{I}_x^\lambda(t_0)$ lies in the region of free motion in a single well potential.

The parametric dependence on κ can be directly read from the phase diagram. Let us consider the limits of small and large absolute values of κ.

- For small absolute values of κ the area of trapped motion is large compared to the area of free motion. Thus there exists a wide range of initial conditions for which the vibrational excitation is trapped.

- For large absolute values of κ the situation is reversed. In agreement with the phase plane analysis we see, that a *necessary condition* for self-trapping is that $|\kappa| < 1$, since for $|\kappa| > 1$ the localization parabola does not include any area with the unit circle. Then localization is impossible for any initial condition.

Note that, due the fact that all parabolae have the same slope, a change in dynamic properties of a spectral state is only possible by shifting the intercept with the ordinate. This amounts to a change in energy E_{DD}. *Therefore the process of localization cannot occur under conservative conditions.*

The polyad phase-sphere

The results of the phase plane analysis displayed in a flow diagram yield information about the flow of the excitation, the results of the potential analysis displayed in the phase diagram yield information about the initial condition dependence of the dynamics. We should explicitly warn here that a standard phase plane picture will display intersecting flow lines due to the initial condition dependence of the Duffing potential and should therefore be used only with caution.

If we insist on displaying the complete dynamic information in a single phase diagram we have to employ a construction called the *Poincaré sphere.* It displays the phase space trajectories and the flow direction for a given value of the dimensionless parameter κ. It is spanned by the normalized actions $\mathcal{I}_x, \mathcal{I}_y$ and $\mathcal{I}_z$. The invariant I gives the radius as $|\mathcal{I}| = 1$. The invariant $\mathcal{C}$ determines the trajectory of corresponding energy on the sphere.

For a particular molecular species the Hamiltonian parameters are fixed, such that the only degree of freedom remaining in κ is the principal action I. Thus the Poincaré sphere consists of several layers of phase portraits, one for each value of I. This suggests, that all states within the same polyad are displayed on the same Poincaré sphere, which is therefore referred to as the *polyad phase-sphere.*

The *phase plane* $(\mathcal{I}_z, \dot{\mathcal{I}}_z)$ can be obtained from the Poincaré sphere as the projection of a trajectory specified by $\mathcal{C}$ and κ onto the $(\mathcal{I}_y, \mathcal{I}_z)$ plane, apart from a scaling factor -2ζ for $\dot{\mathcal{I}}_z$ as can be seen from eqn.(2.29).

The *phase diagram* results as the projection onto the $(\mathcal{I}_z, \mathcal{I}_x)$ plane.

Now, let us have a look at the geography of the Poincaré sphere.

We will call

- the point $(1, 0, 0)$ the north pole and
- the point $(-1, 0, 0)$ the south pole;
- the line $(\mathcal{I}_x = 0, (\mathcal{I}_z)^2 + (\mathcal{I}_y)^2 = 1)$ the equator, separating the northern and southern hemispheres and
- the line $(\mathcal{I}_z = 0, (\mathcal{I}_x)^2 + (\mathcal{I}_y)^2 = 1)$ the zeroth meridian, separating the western and eastern hemispheres.

For further discussion we have to distinguish between $\kappa < 1$ and $\kappa > 1$.

- Figure 2-3 shows the Poincaré sphere for $\kappa < 1$. The north pole is occupied by a saddle, the south pole by a center as stationary points. Two additional centers as stationary points specified by the coordinates $(\kappa, 0, \pm\sqrt{1-\kappa^2})$ lie on the stationary meridian in the northern hemisphere parametrized by $(\mathcal{I}_y = 0, \mathcal{I}_x \leq$

$0, (\mathcal{I}_z)^2 + (\mathcal{I}_x)^2 = 1)$. The localization parabola appears as a separatrix on the sphere, originating at the north pole, embracing regions of local excitation on the western and eastern hemispheres, largely extended over the northern hemisphere. Around the south pole we find the region of normal excitation. The bifurcation line appears as a bifurcation loop south from the separatrix. The self-trapping line and the bifurcation line are indicated as solid lines.

- For $\kappa > 1$ we find centers on the poles as stationary points. The area of normal excitation extends over the complete Poincaré sphere.

Let us establish the connection to the phase plane and the phase diagram. For a given trajectory in the phase diagram, we can identify the points of intersection of the spectral parabola $\mathcal{I}_x^{\lambda}(t_0)$ and the unit circle with the turning points of the motion on the Poincaré sphere. The points of intersection with the $\mathcal{I}_z$ axis constitute foci of the motion in the phase plane. At these points the trajectory on the sphere arrives at the maximum value of $\mathcal{I}_y$.

Let us have a look at the trajectories on the Poincaré sphere for $\kappa < 1$, as displayed in Figure 2-4. The trajectories are indicated as dashed lines. It is straightforward to show, that trajectories in the areas of free motion circulate counterclockwise around the I_x axis and trajectories in the trapped region for positive I_z counterclockwise, for negative I_z clockwise around the stationary points on the northern hemisphere.

In summary, we were able to determine the dynamical properties of the system by exploring the geometry of the associated phase space. The invariants were the key to the successful analysis. The parametric dependence of the qualitative change from normal to local excitation has been condensed in the bifurcation parameter κ. Particular trajectories can be assigned 1:1 to spectral states via their dependence on $\mathcal{C}$.

Two main results could be established so far.

- First, the particular physical mechanism of confining a localized excitation is unimportant, since only the modulus of the dimensionless parameter κ is relevant. We will see several examples in the next section.

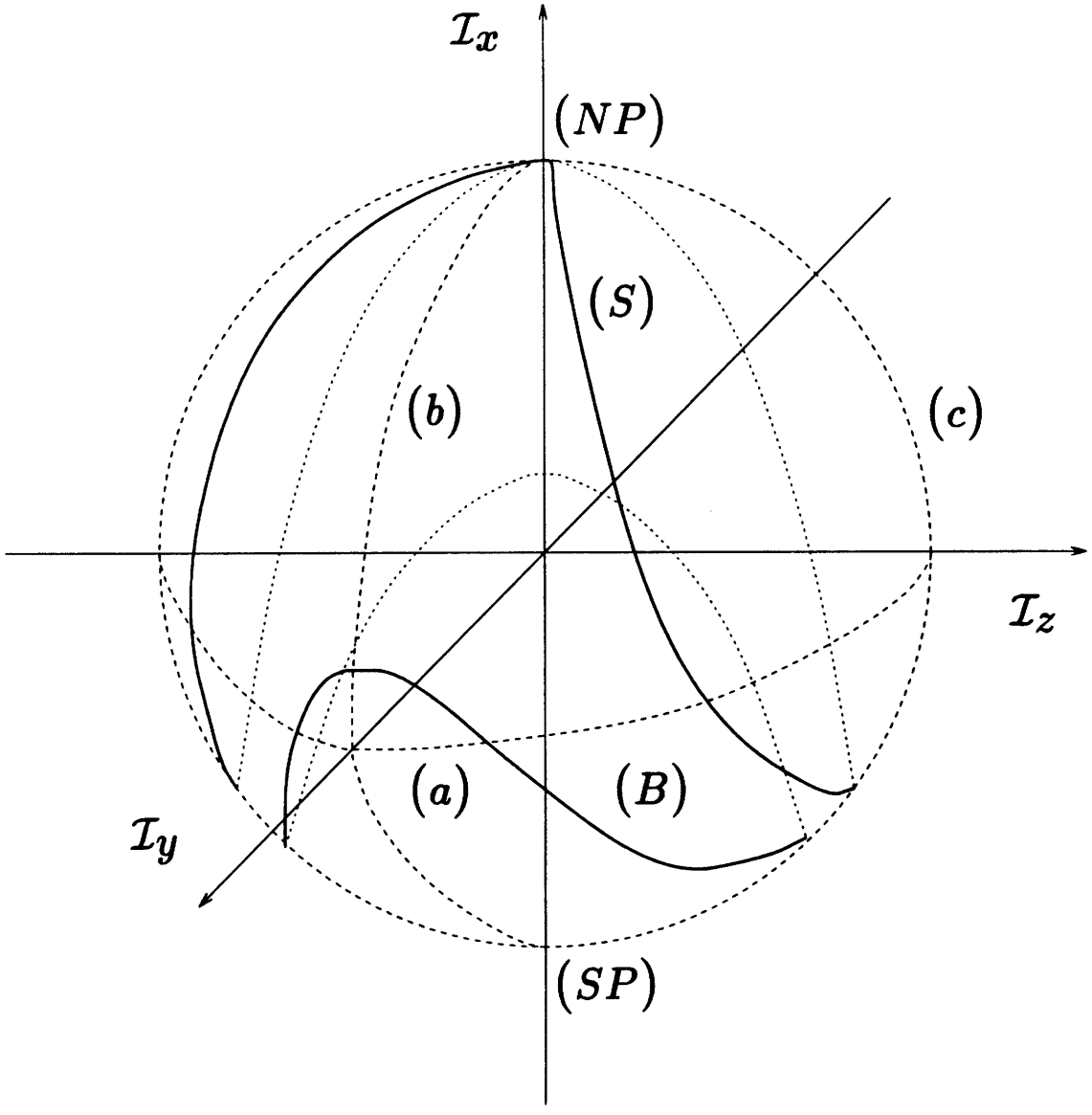

Figure 2-3: Poincaré sphere for the undamped Duffing oscillator without driving, $0 < \kappa < 1$. The dashed circles (- -) indicate the equator (a), the 0th meridian (b) and the 90th meridian (c) which intersect at the north pole (NP) and the south pole (SP). The dotted parabolae (...) are the localization parabola and the bifurcation parabola from the phase diagram. The solid loops (-) on the sphere indicate the localization loop (S) and the bifurcation loop (B).

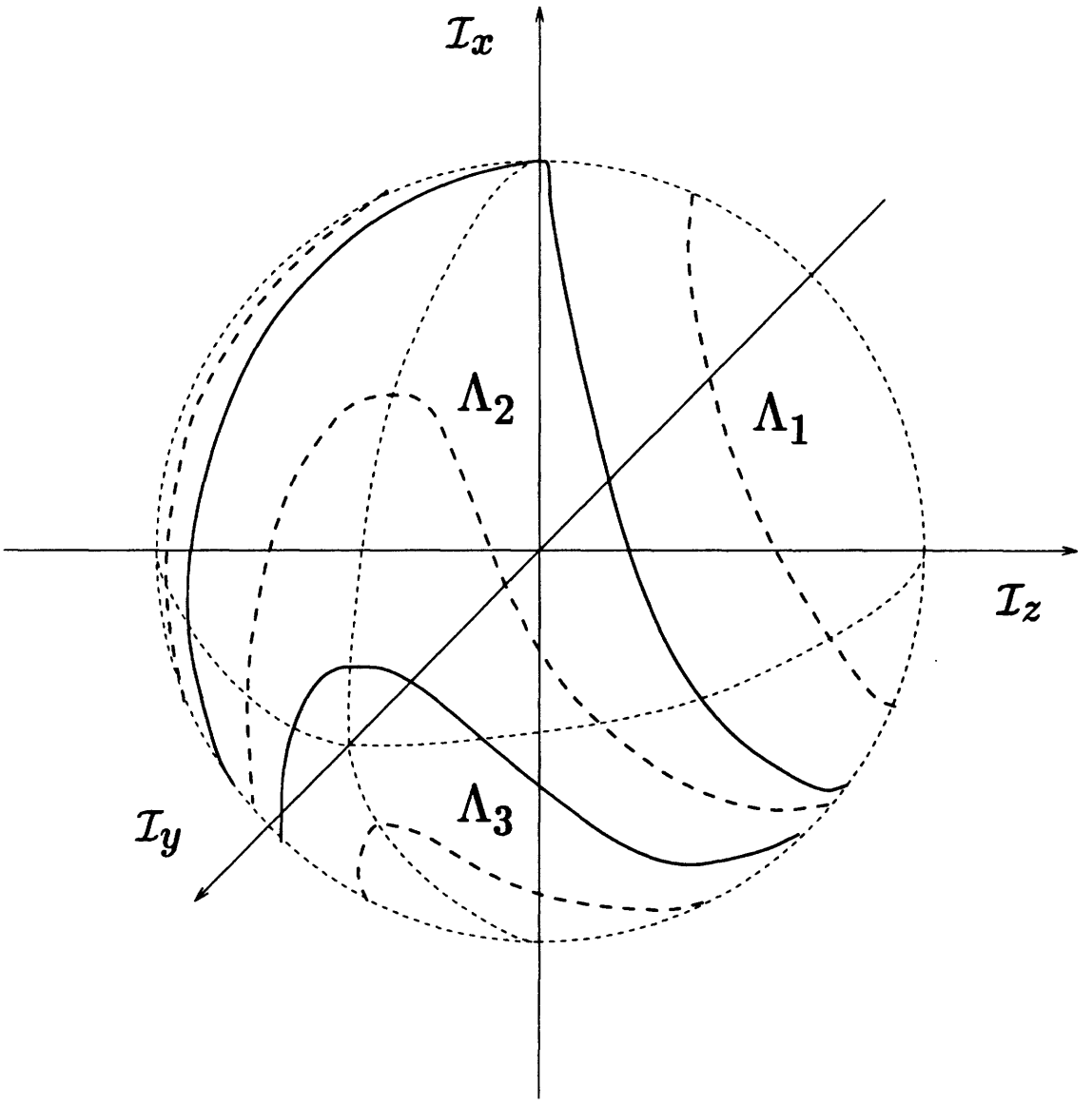

Figure 2-4: Trajectories on the Poincaré sphere. The dashed lines (- -) indicate trajectories of a local mode (Λ_1), a normal mode in a double well potential (Λ_2) and a normal mode in a single well potential (Λ_3).

- Second, the process of localization cannot be conservative, since a crossing of the localization parabola by a spectral parabola can only be achieved by dissipation of energy.

Furthermore, we want to mention that the same type of analysis can be carried out for any coupling $V_{k:l}$. The cases $k = l = 1, 2$, which constitute the Hamiltonian for degenerate local and normal modes can both be solved analytically in terms of Jacobian elliptic functions. We will give that solution for the case $k = l = 1$.

Before we proceed in that direction it will be instructive to apply the theoretical results to some experimental data.

2.2.4 Adaptation to experimental data

In this section we evaluate the phase diagram for H_2O, O_3, SO_2, C_2H_2 and C_2D_2. The data for the Hamiltonian parameters are taken from [12] and were obtained by a nonlinear least-square fit of experimental data to $\hat{H}_{DD}$ for the molecular species in the gas phase. [2]

The phase diagrams are organized as follows. The unit circle, the localization parabola and the bifurcation parabola are indicated as solid lines. The spectral parabolae are represented by dashed lines, the calculated energy E_{DD} of lines in the absorption spectra is given in wavenumbers above the corresponding spectral parabola.

Phase diagrams for water

First, let us compare the phase diagrams for the same molecular species for different values of I. Figure 2-5, Figure 2-6 and Figure 2-7 show results for water from $I = 2$ to $I = 6$.

[2]The Hamiltonian in Kellman's investigation contains both $V_{1:1}$ and $V_{2:2}$. Yet the coupling constant associated with this additional term turns out to be $O(10^{-1})$ compared to ζ and thus can be neglected without changing the result qualitatively. Corrections for the dynamics of I_z can be obtained by perturbative techniques.

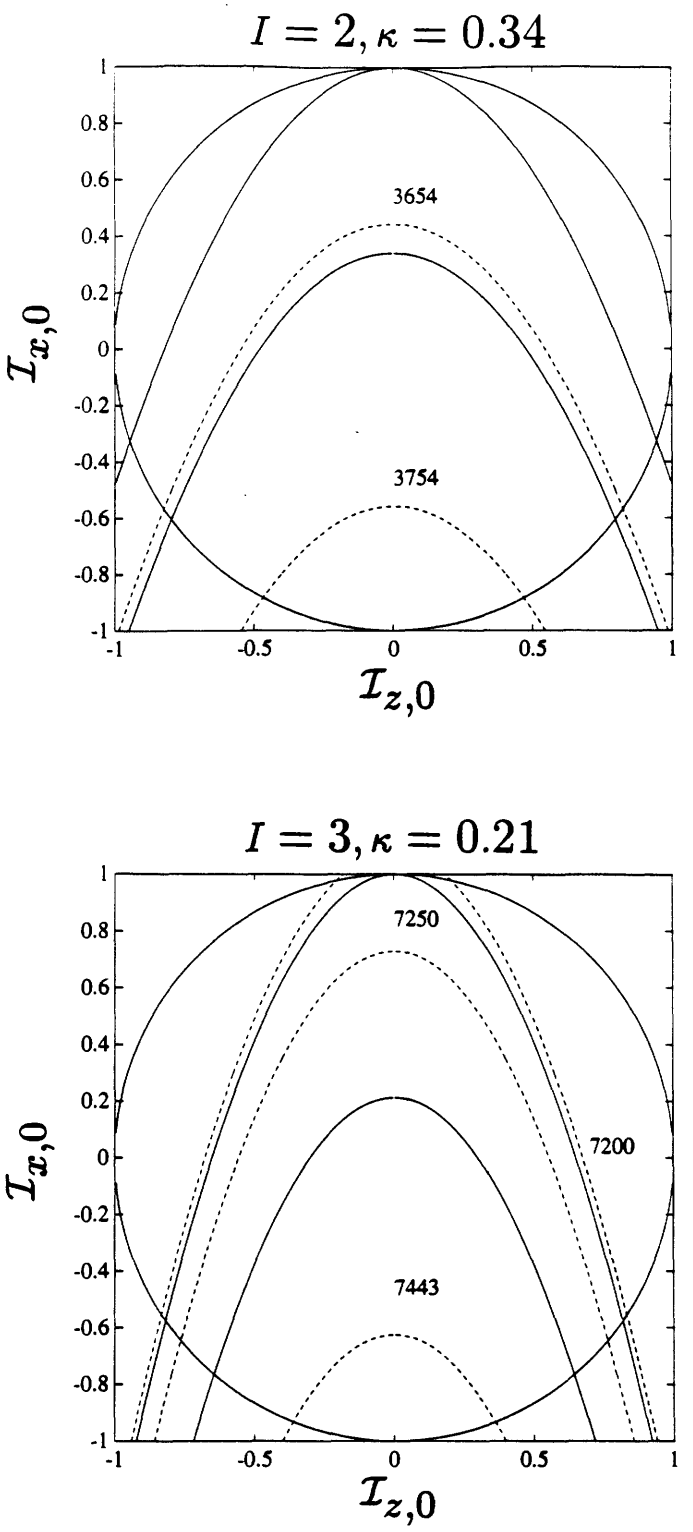

Figure 2-5: Phase diagrams for H_2O, $I = 2$ and $I = 3$. The dashed lines (- -) indicate spectral parabolae, the energies of the corresponding transitions are given in cm^{-1} above the parabolae.

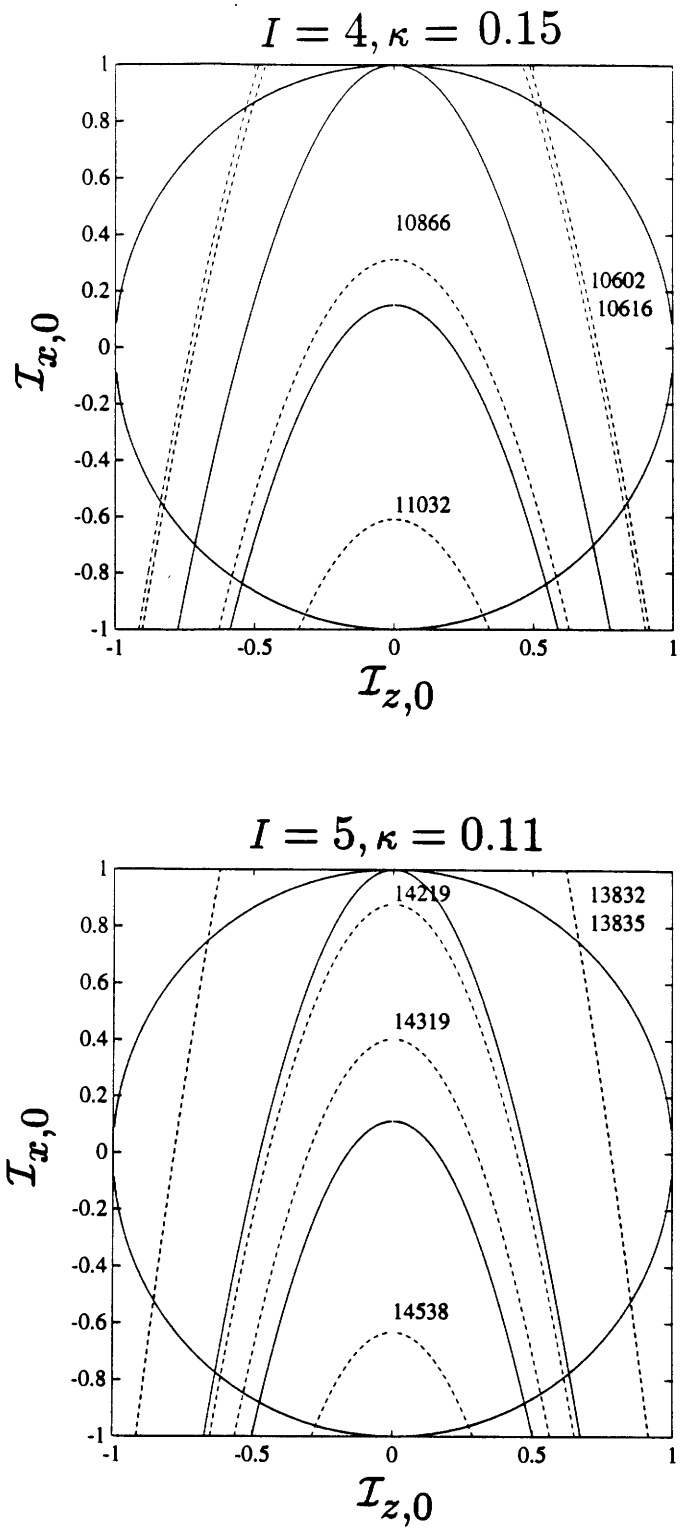

Figure 2-6: Phase diagrams for H_2O, $I = 4$ and $I = 5$. The dashed lines (- -) indicate spectral parabolae, the energies of the corresponding transitions are given in cm^{-1} above the parabolae.

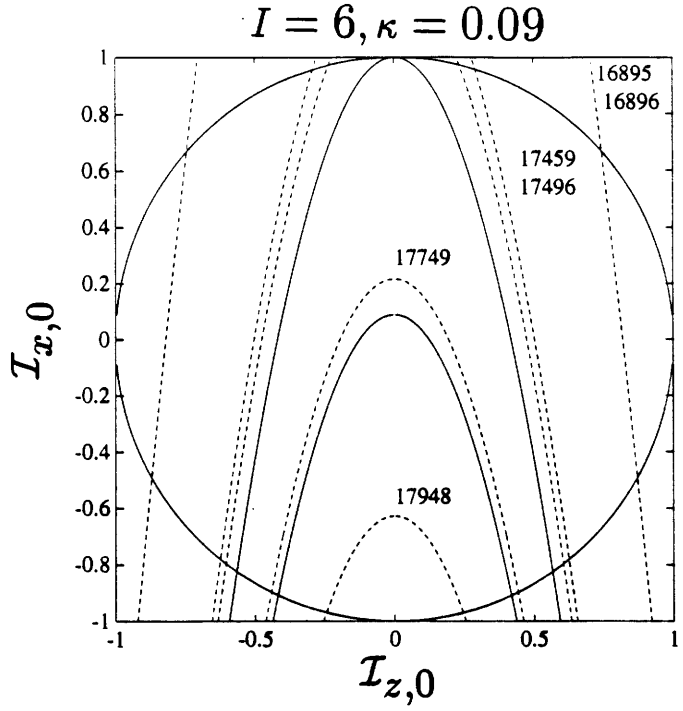

Figure 2-7: Phase diagram for H_2O, $I = 6$. The dashed lines (- -) indicate spectral parabolae, the energies of the corresponding transitions are given in cm^{-1} above the parabolae.

- Already for $I = 2$ we find $\kappa < 1$. Since κ is monotonically decreasing with I, localization is possible in that polyad and for all following polyads. There are two normal spectral parabolae, one in the region south of the bifurcation parabola, the other north of the bifurcation parabola and south from the localization parabola.

- For $I = 3$ we observe two major changes. First, there is one spectral parabola in the local region north of the localization parabola, the other two at higher wavenumbers in the local region south. Second, the energy difference between the two energetically lower lying spectral parabolae is smaller than the one between the two higher lying spectral parabolae.

- For $I = 4$ we can observe already of a pair of two local spectral parabolae split in energy by an amount significantly smaller than the other splittings.

- For $I = 5$ the splitting between the pair of local spectral parabolae is further decreased. The points of intersection with the unit circle, i.e. the turning points of the motion of I_z are shifted to large absolute values of I_z. The two spectral parabolae in the bifurcated region show already a separation from both the two local and the normal spectral parabola.

- For $I = 6$ the two lowest lying spectral parabolae are almost degenerate in energy, followed by a pair of local spectral parabolae split by a larger margin of energy. At some distance there are two normal spectral parabolae.

Note three features of the sequence.

- First, the energetically highest lying normal spectral parabola remains approximately at the same position in the phase diagram. This indicates the universality of the representation, which relies on the dimensionless parameter κ and the normalized actions.

- Second, the local character of local spectral parabolae becomes more pronounced and correlates with the drift of the turning points towards $\mathcal{I}_z = 1$.

- Third, as κ decreases the number of spectral parabolae in the localized region increases and the low lying spectral parabolae develop the structure of split pairs. Note that the difference in $\mathcal{C}$ for two spectral parabolae is a linear function of the energy difference between the corresponding states.

We will give a tentative explanation of these observations in the semiclassical discussion of the normal to local mode transition and a detailed explanation in the quantum mechanical analysis of the problem.

Phase diagrams for different molecular species

Let us continue by comparing the phase diagram corresponding to polyads $I = 6$ for different molecular species shown in Figure 2-8 - Figure 2-12.

- Figure 2-8 shows the phase diagram for ozone.

The first difference we notice is that the diagram is "upside down", as indicated by a negative value of κ. The reason is that $\zeta > 0$, i.e. the coupling between the local oscillators increases E_{DD}, as opposed to water where $\zeta < 0$, i.e the coupling decreases E_{DD}. One can speculate about the physical mechanism that causes $\zeta > 0$. Yet it is important to notice, that no matter what effect turns out to be responsible, the local character of the modes depends only on the absolute value of κ. We arrived at this statement earlier in the phase plane analysis.

In somewhat popular terms the situation can be explained as follows. For water, each bond oscillator finds vibrational excitation "attractive" and there is competition, whereas for ozone, it is considered "unattractive" and the vibrational excitation is "shoveled around like a hot potato" between the bond oscillators. The decisive point is, that for both water and ozone the bond oscillators have the *same type and degree of preference.*

The second difference compared to water is that there are only two spectral parabolae in the local region. This indicates, that for the same degree of vibrational excitation the polyad $I = 6$ shows larger local character for water than for ozone.

- Figure 2-9 shows the phase diagram for sulfur dioxide. The predominant feature here is that all spectral parabolae are equally spaced. Since $\kappa > 1$ we know that all modes must be of normal character. Compared to water and ozone, the polyad $I = 6$ for sulfur dioxide shows strong normal character.

Effects of isotopic substitution

As a brief interlude it is interesting to have a look at the effects of isotopic substitution on the normal to local mode transition. Although acetylene and deuterated acetylene do not belong to the class of triatomic molecules studied here, the local CH and CD stretch vibrations obey the Darling-Dennison Hamiltonian.

- Figure 2-10 shows the result $I = 6$ for acetylene. There are two local spectral parabolae and a pair of spectral parabolae in the bifurcated region. The one

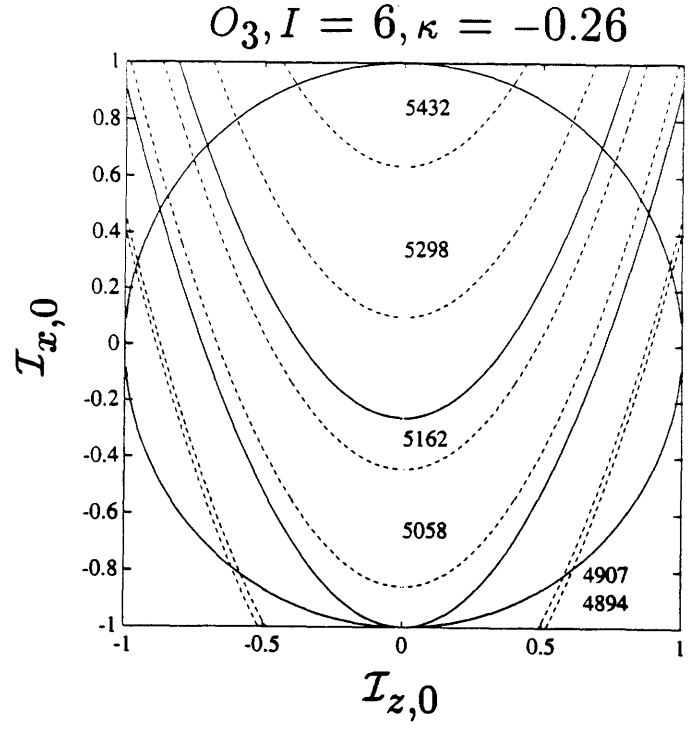

Figure 2-8: Phase diagram for O_3.

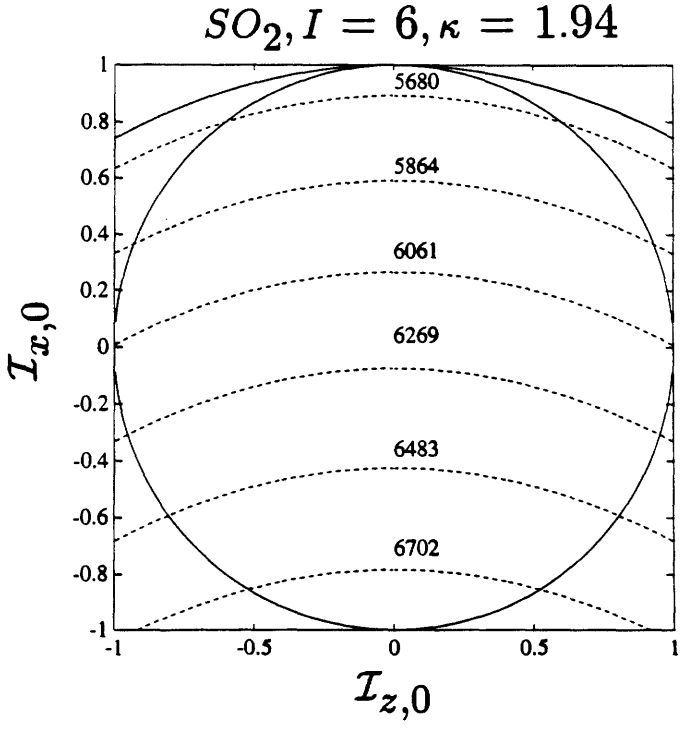

Figure 2-9: Phase diagram for SO_2.

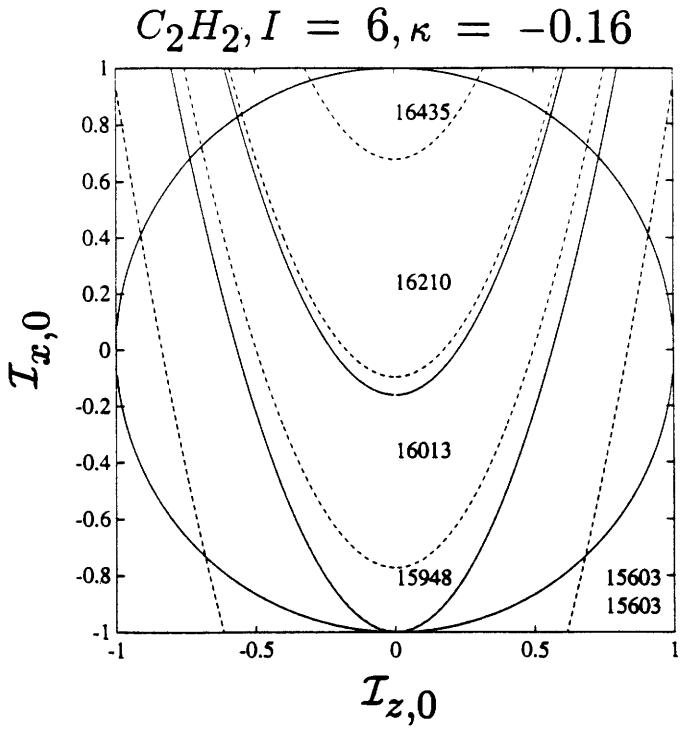

Figure 2-10: Isotope effect: Phase diagram for C_2H_2.

lower in energy coincides with the bifurcation parabola.

- Figure 2-11 shows the phase diagram $I = 6$ for deuterated acetylene. We notice that $|\kappa| \approx 1$ and see accordingly no spectral parabolae in the local region, i.e. the phase diagram exhibits strong normal character.

- The first phase diagram for C_2D_2 to show local spectral parabolae is shown in Figure 2-12 and appear at $I = 21$.

This impressively demonstrates that upon isotope substitution we do not only have to expect quantitative changes in the dynamics, such as shifts in frequency, but also *qualitative changes* regarding the stability of the modes.

In summary, we have seen that the phase diagram turns out to be a convenient tool of discussing the question of local and normal character of different molecular species, their polyads and states within a polyad.

- The functional dependence of κ on the total excitation I for different molecular species can be used to label a particular species as "local type" or "normal

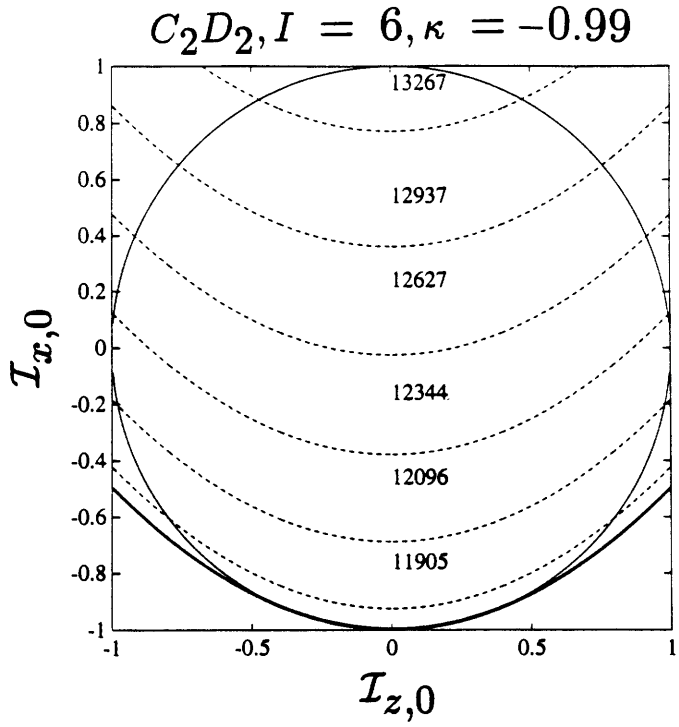

Figure 2-11: Isotope effect: Phase diagram for C_2D_2 at low excitation.

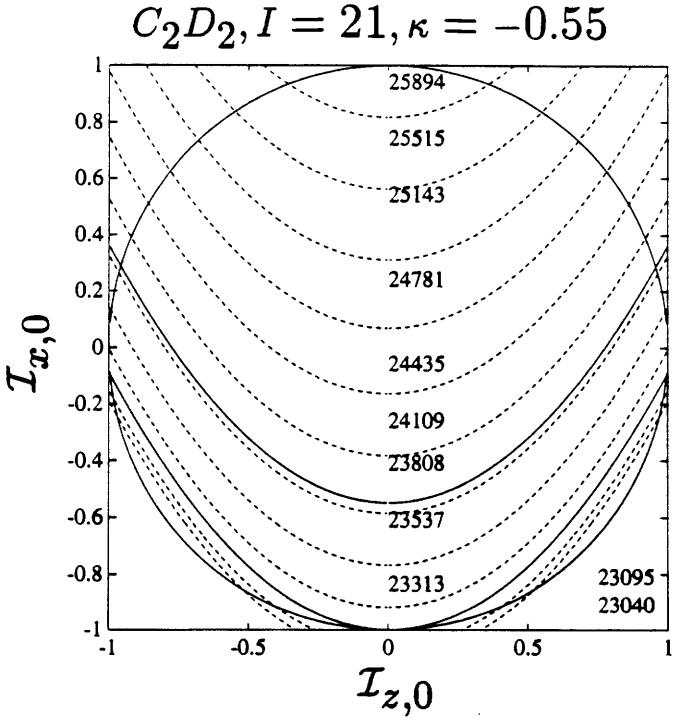

Figure 2-12: Isotope effect: Phase diagram for C_2D_2 at high excitation.

type" according to their overall tendency to localize excitation.

- The values that κ takes for particular polyads I are indicative of how many of the contained states may be labeled as local modes and how large their degree of locality is.

- For a particular state within a polyad these issues can be directly decided by comparing the invariant $\mathcal{C}$ with κ.

In the following section we will solve for the time dependence of I_z and thus complete the the discussion of the classical local to normal transition.

2.2.5 Analytical solution of the equations of motion

The analytical form of $\mathcal{I}(\mathcal{I}_x, \mathcal{I}_y, \mathcal{I}_z)$ is obtained in a straightforward manner. For $\mathcal{I}_z$ we solve in terms of Jacobian elliptic functions. The solutions for $\mathcal{I}_x$ and $\mathcal{I}_y$ follow immediately from eqn.(2.24,2.25). From the definitions of $\mathcal{I}_x, \mathcal{I}_y$ and $\mathcal{I}_z$ in eqn.(2.51) one can then easily solve for complex mode amplitudes a_1 and a_2.

Ansatz and solution

The proper ansatz is given by

$$\mathcal{I}_z(t) = Df(\Omega t - \Phi|m). \tag{2.71}$$

Here f is a Jacobian elliptic function of amplitude D, frequency Ω, phase Φ and parameter m. Inserting this ansatz in eqn.(2.50) and using eqn.(2.24,2.25) one obtains three different types solutions, dependent on the parameter m.

- For $m < 0$ the solution is given by

$$\begin{aligned} \mathcal{I}_z &= Dnd(\sqrt{1+|m|}[\Omega t - \Phi_{nd}]|\frac{1}{1+|m|}), \\ \Phi_{nd} &= -\frac{1}{\sqrt{1+|m|}} F(\arcsin\sqrt{\frac{1-(\frac{D}{\mathcal{I}_z(t_0)})^2}{m}}|\frac{1}{1+|m|}). \end{aligned} \tag{2.72}$$

- For $0 < m < 1$ the solution is given by

$$\begin{aligned} \mathcal{I}_z &= Dcn(\Omega t - \Phi_{cn}|m), \\ \Phi_{cn} &= -F(\arccos\frac{\mathcal{I}_z(t_0)}{D}|m). \end{aligned} \tag{2.73}$$

- For $1 < m$ the solution is given by

$$\begin{aligned} \mathcal{I}_z &= Ddn(\sqrt{m}[\Omega t - \Phi_{dn}]|\frac{1}{m}), \\ \Phi_{dn} &= -\frac{1}{\sqrt{m}}F(\arcsin\sqrt{\frac{1-(\frac{\mathcal{I}_z(t_0)}{D})^2}{m}}|\frac{1}{m}). \end{aligned} \tag{2.74}$$

- The results for D, m and Ω are

$$D = \pm\frac{1}{I}\sqrt{-\frac{A}{B} + 2\kappa I\sqrt{I^2(1-\kappa^2)+\frac{A}{B}}}, \tag{2.75}$$

$$m = \frac{1}{2}(1 - \frac{\frac{A}{B}}{2\kappa I\sqrt{I^2(1-\kappa^2)+\frac{A}{B}}},) \tag{2.76}$$

$$\Omega = \frac{\zeta DI}{\kappa\sqrt{m}}. \tag{2.77}$$

Here cn, dn, nd are Jacobian elliptic functions and F an elliptic integral of the first kind.

There are several things to notice.

- First, for the different domains of the parameter m we get qualitatively differing results. Figure 2-13 shows the elliptic functions for different values of the parameter m.

  - The cn function oscillates between the upper bound D and lower bound $-D$. Thus the vibrational excitation is completely transferred after two quarterperiods, which are usually denoted by $K = F(\Omega t = \frac{\pi}{4}|m)$.
  - The dn function oscillates with the upper bound D (or lower bound $-D$) but does not change the sign of its range. Thus the vibrational excitation

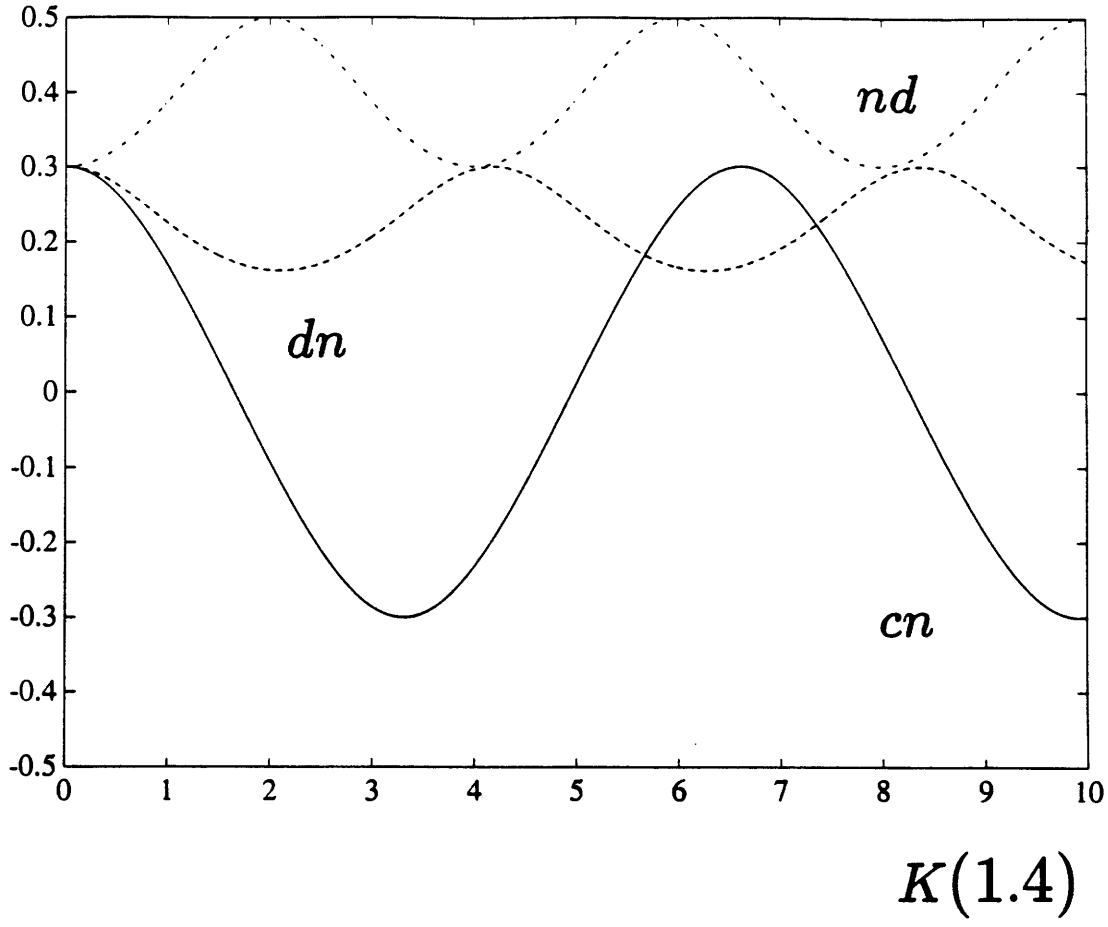

Figure 2-13: Jacobian elliptic functions. The abscissa is calibrated in units of the quarter periods $K(m = 1.4)$ of $dn(m = 1.4)$. The solid line (-) indicates $cn(m = 0.2)$, the dashed line(- -) $dn(m = 1.4)$ and the dashed-dotted line (-.) $nd(m = -0.5)$.

is never completely exchanged between the two bond oscillators, i.e. it is a local mode.

- The *nd* function oscillates with the lower bound D (or upper bound $-D$) and, like the *dn* function, does not change the sign of its range. Thus it describes a local mode as well. The difference to the *dn* solution is that the average of $\mathcal{I}_z$ over a period $4K$ is larger than for the evolution under the *nd* solution.

- Second, the frequency Ω depends on the initial amplitude D, in sharp contrast to linear dynamical systems.

- Third, let us consider limiting cases. Take an initially local state for large $I \approx n$, i.e. $\mathcal{I}_z(t_0) = 1$. From eqn.(2.75-2.77) we obtain $DI = 1, m = 1/4\kappa^2$ and $\Omega = 2\zeta$.

  - In the limit of vanishing anharmonicity $\chi \to 0$, $\kappa \to \infty$, the vibrational excitation oscillates unhinderedly between the local oscillators, as can be seen from

$$\lim_{m\to 0} \mathcal{I}_z = \lim_{m\to 0} cn(2\zeta t|m) = \cos(2\zeta t).$$

  - In the limit of vanishing coupling $\zeta \to 0$, $\kappa \to 0$, the initial distribution of vibrational excitation is maintained at all times, as can be seen from

$$\lim_{m\to \infty} \mathcal{I}_z = \lim_{m\to \infty} dn(2\zeta t|\frac{1}{m}) = 1.$$

Connection to the phase diagram

As we see, the transitions between these functions depend on the parameter m. Thus we should be able to recover the phase diagram from the expression for m as given by eqn.(2.76). This is indeed the case.

- The condition $m = \frac{1}{2}$ (appearance of additional points of inflection at half values of the quarter period K) yields $\mathcal{C} = \kappa$ and thus the bifurcation parabola is given by eqn.(2.67).

- The condition $m = 1$ (transition between cn and dn) yields $\mathcal{C} = 1$ and thus the localization parabola is given by eqn.(2.68).

Connection to the hindered rotor model

Let us briefly establish the connection to the hindered rotor model by Sibert et al. [6, 7]. Their analysis is carried out in action-angle coordinates, where the action of the hindered rotor is given by the action difference of the two bond oscillators, the angle of rotation by the difference in phase angles of the two bond oscillators. The potential of hindrance is periodic in 2π. Their analysis concludes that the regime of *local modes* coincides with *libration* of the rotor and *normal modes* coincides with *hindered rotation* of the rotor.

In order to recover their results from our analysis it is instructive to have a look at the normalized complex mode amplitudes $\tilde{a}_i = \frac{a_i}{\sqrt{I}}$ for an initially local state on oscillator one, which takes a particularly simple form for large I. Using eqn.(2.24,2.25,2.51) we obtain

- for $0 < m < 1$

$$\tilde{a}_1 = \cos[\frac{1}{2}am(2\zeta t|\frac{1}{4\kappa^2})] \tag{2.78}$$

$$\tilde{a}_2 = \sin[\frac{1}{2}am(2\zeta t|\frac{1}{4\kappa^2})]\exp[-i(\arccos dn(2\zeta t|\frac{1}{4\kappa^2}) + \frac{\pi}{2})], \tag{2.79}$$

- and for $1 < m$

$$\tilde{a}_1 = \pm\sqrt{\frac{1 + dn(2I\chi t|4\kappa^2)}{2}} \tag{2.80}$$

$$\tilde{a}_2 = \pm\sqrt{\frac{1 - dn(2I\chi t|4\kappa^2)}{2}}\exp[-\frac{i}{2}(am(2I\chi t|4\kappa^2) + \pi)]. \tag{2.81}$$

Here am is the elliptic amplitude and related to cn via $\cos[am(2\zeta t|m)] = cn(2\zeta t|m)$. For convenience we split the complex mode amplitudes in a real valued amplitude and a phase factor of modulus one that can take imaginary values.

Let us first discuss the case $0 < m < 1$. The argument of the trigonometric

functions is monotonically increasing with time. Therefore the amplitudes range from -1 to $+1$. After $t = K/\zeta$ the vibrational excitation is completely transferred from oscillator one to oscillator two. The phase factor has time dependence of the form $\arccos(dn)$. The range of dn is at most between 0 and $+1$. Thus the total phase $(\arccos dn(2\zeta t|\frac{1}{4\kappa^2}) + \frac{\pi}{2})$ can at most range between 0 and π. This amounts to a hindered rotation between the angles 0 and π. The case $1 < m$ can be discussed in complete analogy.

We conclude that a *trapped phase*, i.e. hindered rotation, implies *free transfer of vibrational excitation*, whereas a *free phase*, i.e. libration, implies *self-trapping of the vibrational excitation.* This result is identical to the hindered rotor model of Sibert et al. [6].

Polar representation of the mode amplitudes

It is customary to graph and analyse the dynamics of systems similar to the studied type in the polar representation of the complex mode amplitudes $\tilde{a}_i$ as obtained from numerical integration of the equations of motion. Although we consider this representation as not very instructive and somewhat esoteric let us view our results from this angle. In the following we compare the complex mode amplitude of oscillator two to the coordinate space trajectories of the oscillators and insert as "missing link" the real valued amplitude of the complex mode amplitudes. Again, we consider an excitation that is initially localized on oscillator one in the limit of large I. Figure 2-14 - Figure 2-17 shows

- the complex mode amplitude $\tilde{a}_2$ in polar representation (abscissa: real part of $\tilde{a}_2$; ordinate: imaginary part of $\tilde{a}_2$),
- the real valued amplitude $\sqrt{n_2}$ (abscissa: time in units of K; ordinate: $\sqrt{n_2}$) and
- the coordinate space trajectories in the harmonic approximation (abscissa: displacement from equilibrium of oscillator one; ordinate: displacement from equilibrium of oscillator two)

for different values of the parameter m.

We expect that as the vibrational excitation becomes trapped on oscillator one, the excitation will no longer be transferred completely to oscillator two and thus $\tilde{a}_2$ will undergo a transition towards decreased amplitudes.

The sequence shows, that as m gradually approaches 1, the complex mode amplitude exhibits a high density around the circle of radius $1/\sqrt{2}$ as can be calculated from eqn.(2.81). This high density region corresponds to the plateau in the amplitude forming at the same value and implies that for large periods of time the excitation becomes nearly equally distributed between the two oscillators. This amounts to a "blackening" of the diagonal for the normal coordinate space trajectory diagram. Thus the molecular oscillations appear as sudden kicks after some time of apparent standstill of dynamics. At $m = 1$ we observe that the complex mode amplitude of oscillator two collapses into the region within the circle of radius $1/\sqrt{2}$, i.e. the symmetry of the system is broken. A local coordinate space trajectory forms. Now, only oscillator one reaches full amplitude. As m increases further, the density of the complex mode amplitude of shifted back towards a uniform density with further increasing values of m. At this stage, oscillator two appears to have come to a standstill.

Technically, the transition occurs when the trajectory in the polar representation intersects itself before it passes the origin, i.e. the period of the phase factor becomes shorter than the period of the amplitude factor.

Let us close with a final aside. The trajectory around $m = 1$ looks "more complicated" than the trajectories in the limits $m = 0$ and $m \gg 1$. Suppose we couple the Darling-Dennison to another oscillator such that the excitation can be periodically transferred between that oscillator and the Darling-Dennison system. Then, the plot for the complex mode amplitude would "look like a mess" if the Darling-Dennison system is in the regime $m = 1$. One is then tempted to open the toolbox of chaotic dynamics and analyse the frequency spectrum of the trajectory to see whether the dynamics is periodic, quasiperiodic or chaotic. We demonstrate in Appendix A that the result will be ambiguous if, like in our case, the trajectory can be written in terms of elliptic functions.

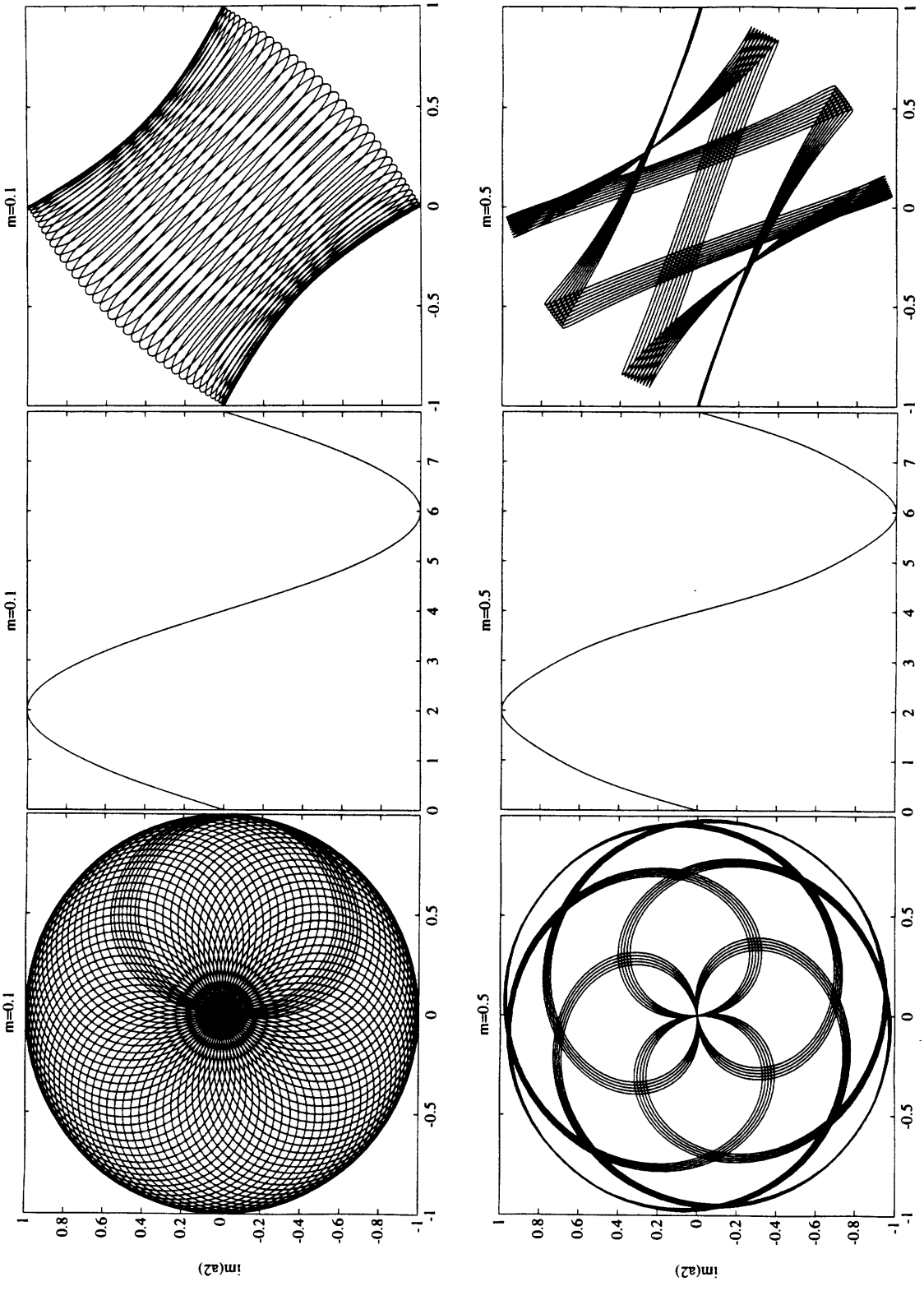

Figure 2-14: Comparative view of the complex mode amplitudes (1st column), the real amplitudes (2nd column) and the coordinate space trajectories (3rd column). See text for detailed explanation.

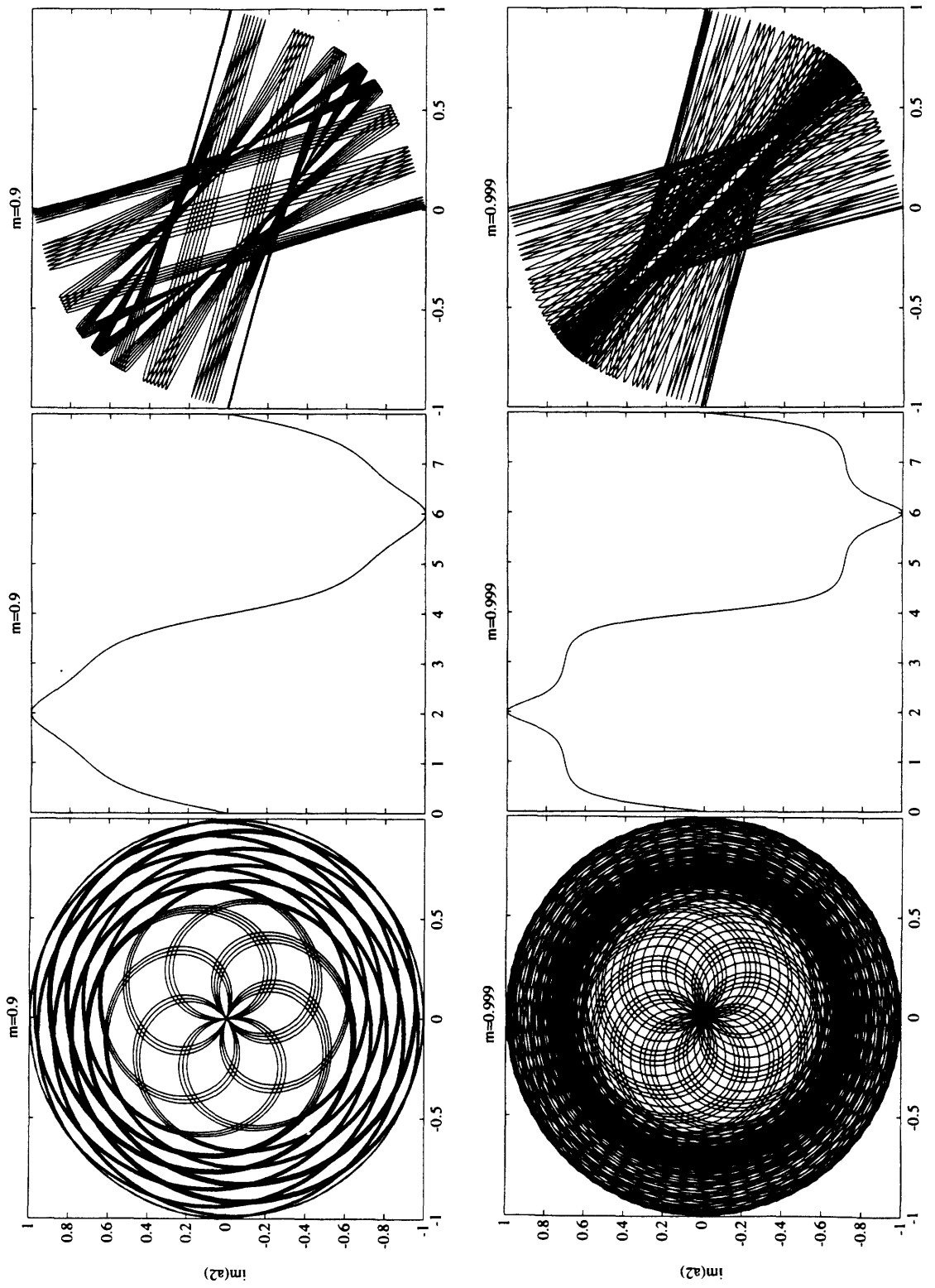

Figure 2-15: Comparative view of the complex mode amplitudes (1st column), the real amplitudes (2nd column) and the coordinate space trajectories (3rd column). See text for detailed explanation.

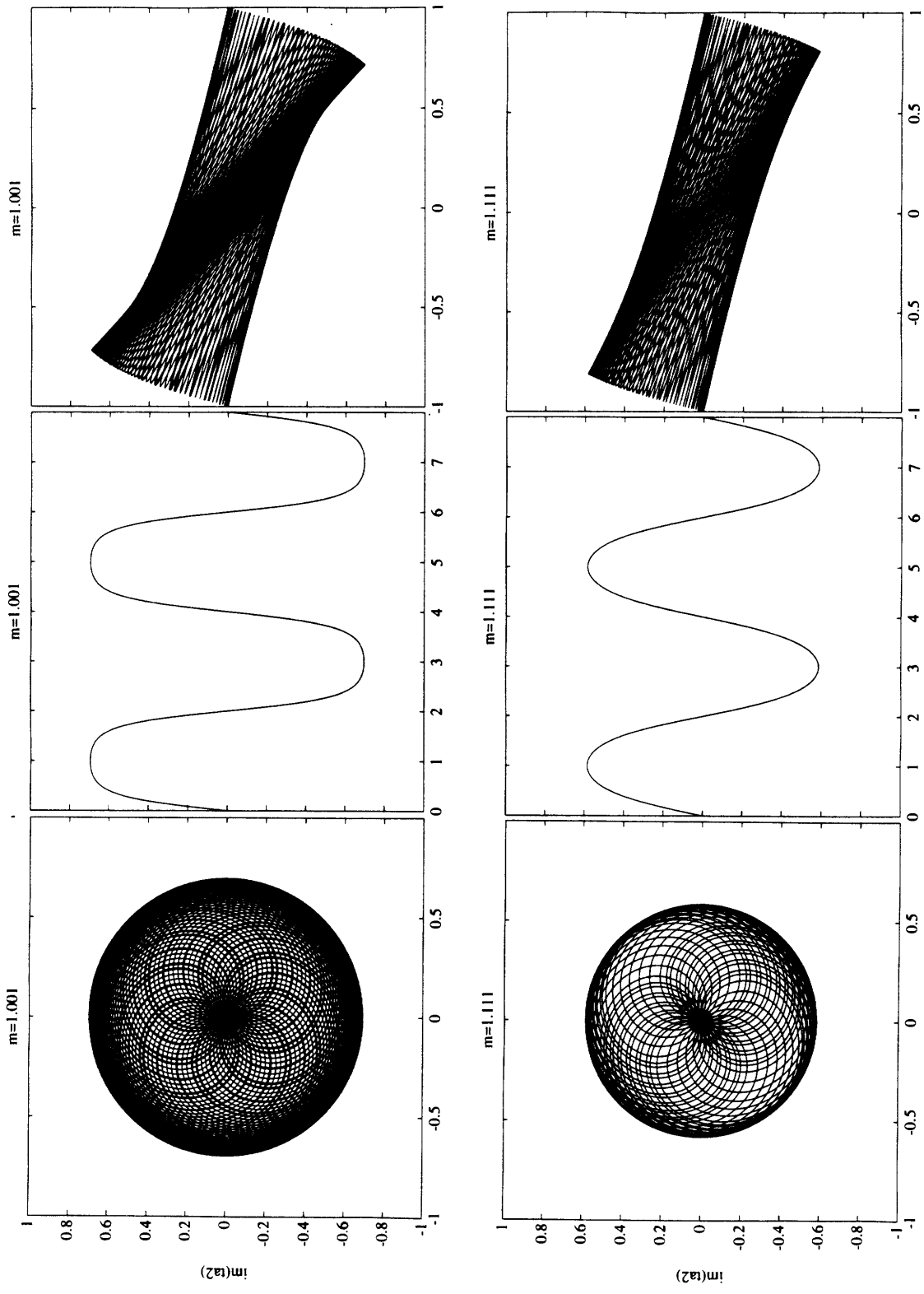

Figure 2-16: Comparative view of the complex mode amplitudes (1st column), the real amplitudes (2nd column) and the coordinate space trajectories (3rd column). See text for detailed explanation.

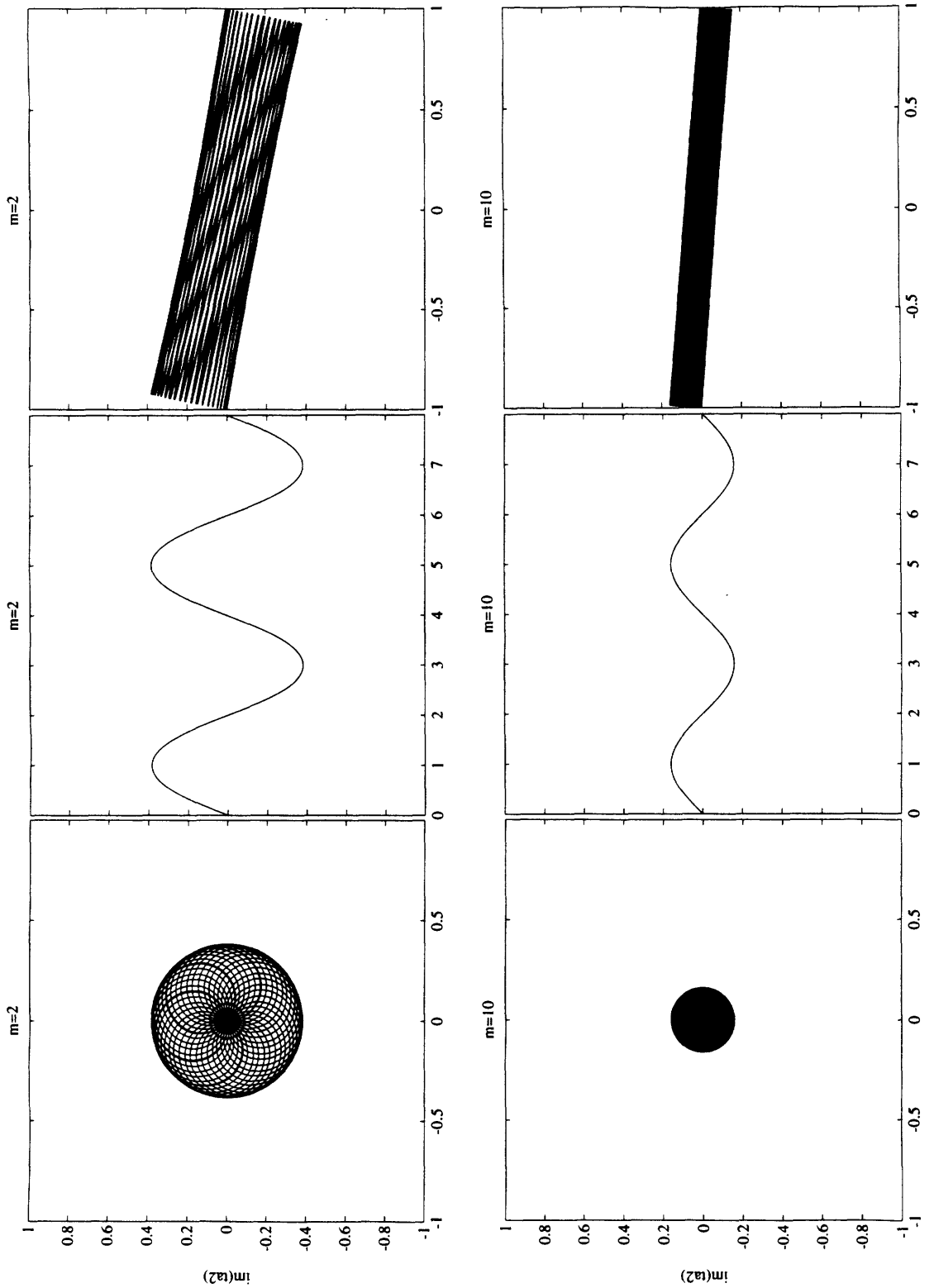

Figure 2-17: Comparative view of the complex mode amplitudes (1st column), the real amplitudes (2nd column) and the coordinate space trajectories (3rd column). See text for detailed explanation.

2.2.6 Panoptic view of different dynamic representations

We have seen in the last few sections that there is a variety of ways of looking at the dynamical properties of the molecular system. We pause a second in order to connect in Figure 2-18 the different representations used so far.

All features of the dynamical properties are contained in the motion of the vector I on the Poincaré sphere. The Poincaré sphere displays the phase portrait of all trajectories for a certain value of κ. The phase plane and the phase diagram are projections of the phase portraits onto perpendicular sections of the Poincaré sphere. The extrema of the potential $\mathcal{V}$ are identical to the foci of the motion in the phase plane, the kinetic contribution T specifies the direction of the flow in the phase plane and thus on the Poincaré sphere. All these geometric representations come to live as we implement the time dependence in terms of the explicit solutions for $\mathcal{I}_z$ or the complex mode amplitudes a_1 and a_2.

2.2.7 Extension to damped systems

So far we have treated only the dynamics of local or normal excitations and shown that the *process* of trapping of vibrational excitation can not be accounted for in the system in its current form.

The identification of the dynamics of $\mathcal{I}_z$ with that of an undriven Duffing oscillator without damping provokes the further exploitation for cases when $\mathcal{I}_z$ is subject to damping or to a driving force. Both cases have been carefully studied for the Duffing oscillator. In this section we qualitatively discuss the effect of damping on the system. We demonstrate that damping can change qualitatively the molecular dynamics and lead to localization of vibrational excitation. The physical situations for which damping becomes important range from dynamics of vibrational excitations in the high density gas phase to the liquid or solid phase.

Let us return to the original semiclassical Hamiltonian (2.23) and assume for simplicity that I stays invariant under damping, i.e. the trajectory remains on the polyad phase sphere. The consequence is that $\mathcal{C}$ is no longer invariant. Let us further

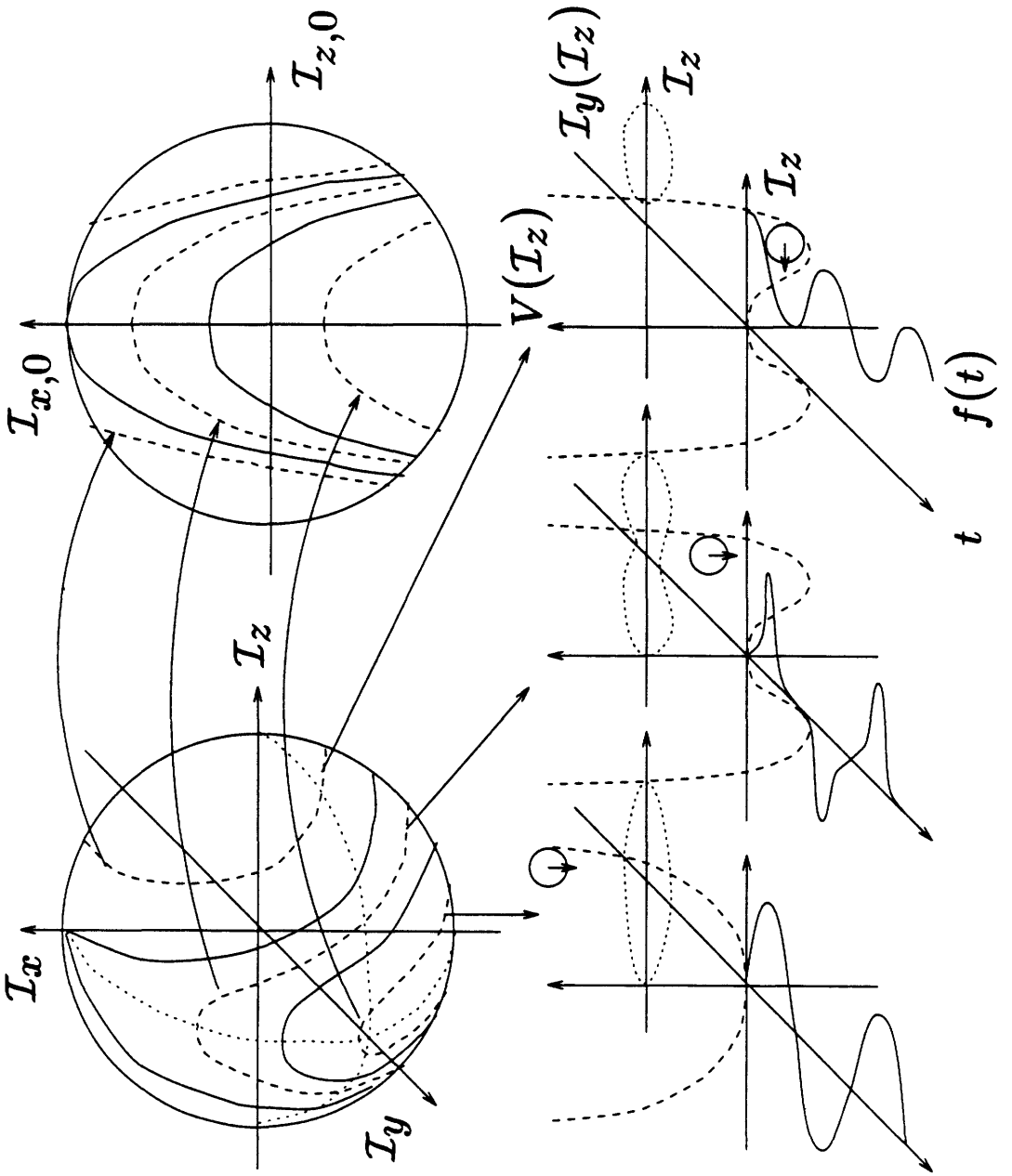

Figure 2-18: Panoptic view of different dynamic representations $0 < \kappa < 1$, containing the Poincaré sphere, the corresponding phase diagram, the phase planes, the Duffing potentials and the time dependent Jacobian elliptic functions. See text for explanation.

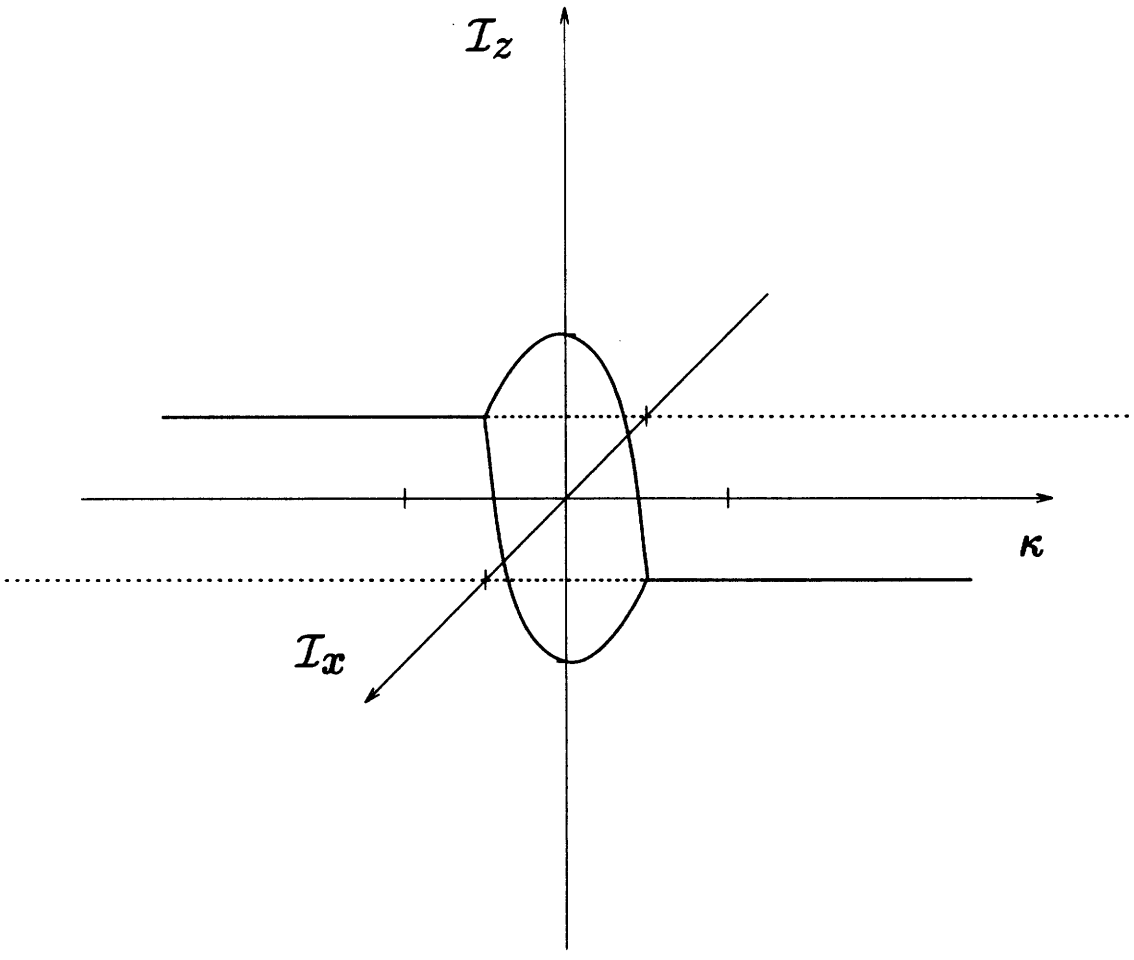

Figure 2-19: Bifurcation diagram for the damped Duffing oscillator without driving. Solid lines (-) indicate stable branches, dotted lines (...) unstable branches. At $|\kappa| = 1$ there occurs a pitchfork bifurcation and at $\kappa = 0$ there occurs a transcritical bifurcation.

assume that the loss of energy has the functional dependence $h(\dot{I}_z)$ and $h(\dot{I}_z = 0) = 0$. By construction the number and location of stationary points as well as the location of the bifurcations at $|\kappa| = 1$ and $\kappa = 0$ are identical to those in the undamped case.

Yet the stability of the stationary points and thus the phase portrait on the Poincaré sphere are different from the undamped case. The bifurcation diagram is displayed in Figure 2-19. The structure is similar to the undamped case. Again we find a combination of two pitchfork bifurcations occurring at $\kappa = \pm 1$. Two stable branches are bifurcating into a pair of stable and one unstable branch. In addition there is a transcritical bifurcation at $\kappa = 0$.

The assumptions made above can be motivated as follows. Consider a molecule embedded in a matrix of atoms. The vibrating molecule interacts with the matrix in two ways: first, by the oscillations along the bonds on a fast timescale, second, by transfer of excitation between the local bond oscillators on a slow timescale. The bond oscillations can persist damping especially if the difference in mass between the molecular oscillator and the atoms in the matrix is large. The transfer of excitation between the bond oscillators leads to considerable change in the relative amplitudes of the two local oscillators and forces rearrangement of the local environment. The damping of the periodic rearrangement is described by the model introduced above. It can be shown [19] that the total action I is an adiabatic invariant under the condition that the energy is dissipated slowly compared to a period of oscillation of the bond oscillators and therefore may be treated as a conserved quantity.

Now, let us have a look at the Poincaré sphere that shows the following features for the damped system.

The Poincaré sphere for $\kappa > 1$ is displayed in Figure 2-20. There are two stationary points:

- A stable spiral point at the north pole $(1, 0, 0)$ and
- an unstable spiral point at the south pole $(-1, 0, 0)$.

For all initial conditions but the unstable spiral point, the trajectory will converge to the north pole.

The Poincaré sphere for $\kappa < 1$ is displayed in Figure 2-21. There are four stationary points:

- A saddle at the north pole $(1, 0, 0)$,
- two stable spiral points at $(\kappa, 0, \pm\sqrt{1-\kappa^2})$ and
- an unstable spiral point at the south pole $(-1, 0, 0)$.

A separatrix originates at the unstable spiral point and leads to the saddle point. The sphere is split in two basins of attraction, one for each of the stable stationary points.

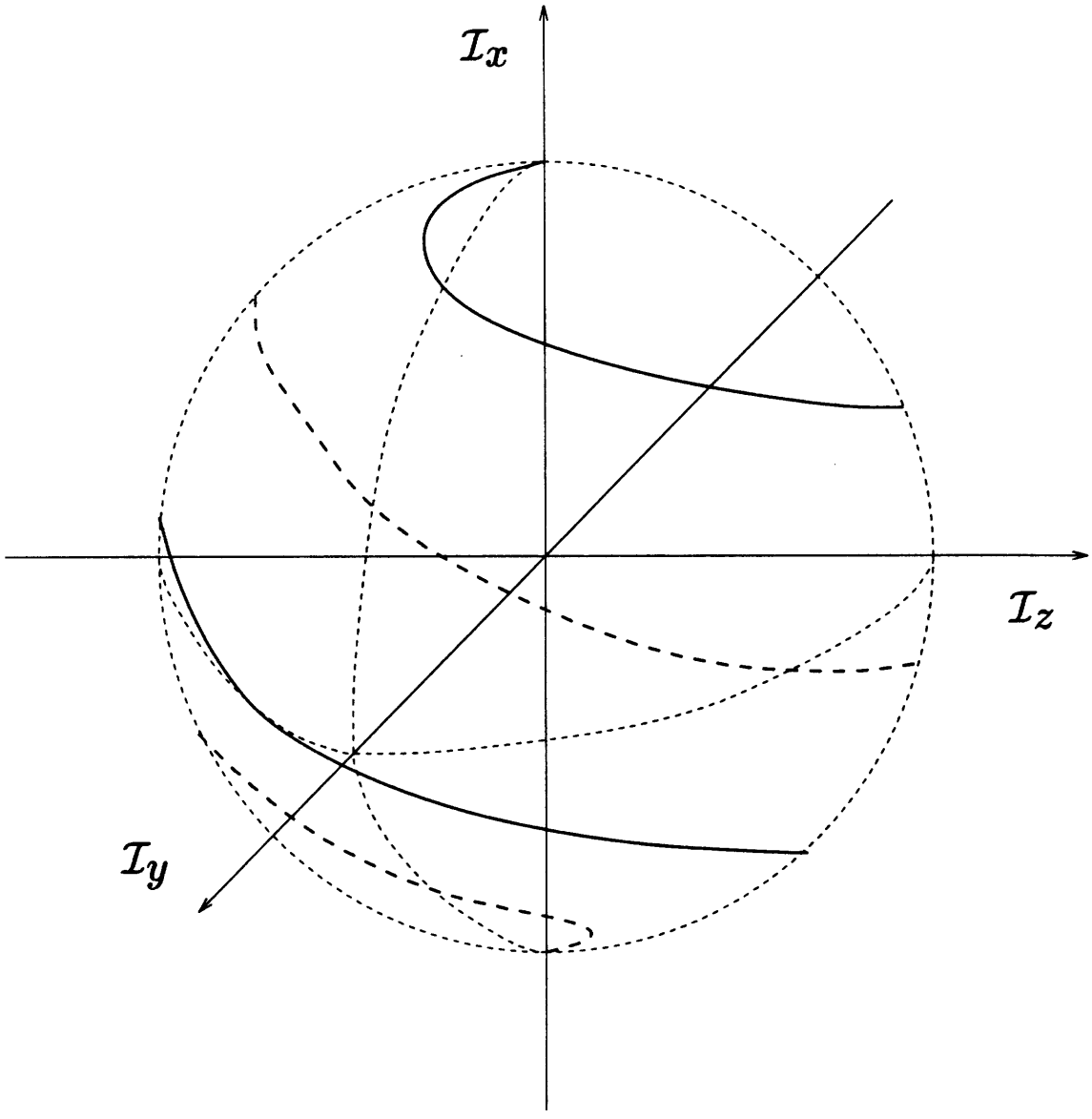

Figure 2-20: Poincaré sphere for the damped Duffing oscillator without driving, $\kappa > 1$. Solid (-) and dashed (- -) lines indicate flow from the south pole to the north pole of the sphere.

Thus for any initial condition but the unstable stationary points or the separatrix the behaviour of $\mathcal{I}_\ddagger$ at long times will be determined by the location of the stable stationary points.

Note the fundamental difference of the undamped and damped system in responding to a perturbation. This difference manifests itself in the magnitude of the perturbation necessary to induce a transition from normal to local behaviour. For the undamped system the perturbation necessary to induce a qualitative change in the dynamic behaviour depends on the distance of the trajectory on the Poincaré sphere to the separatrix, which has to be crossed in order to change from normal to local behaviour. In contrast the damped system directs under *any* infinitesimal perturbation

- for $\kappa > 1$ to the north pole (normal mode) and
- for $\kappa < 1$ to one of the stable stationary points on the northern hemisphere (local mode).

Typically perturbations are always present in the form of fluctuations in the surroundings the Darling-Dennison system interacts with. Thus the surroundings are in two ways responsible for the transition from normal to local modes. First, the symmetry is broken due to a fluctuation, then vibrational excitation is dissipated.

For molecules with more than two degrees of freedom the normal to local mode transition can occur under conservative conditions. The energy can be dissipated intramolecularly into the degrees of freedom that do not participate in the confinement of vibrational excitation. For the AB_2 type molecules this could be the bending mode, for more complex molecules any other vibrational mode.

2.2.8 Preliminary review of the classical results and conclusions

Before we begin with the discussion of quantum mechanical aspects of the normal to local mode transition let us follow up on the introductory questions. Up to this point we have investigated the classical correspondent to the quantum mechanical

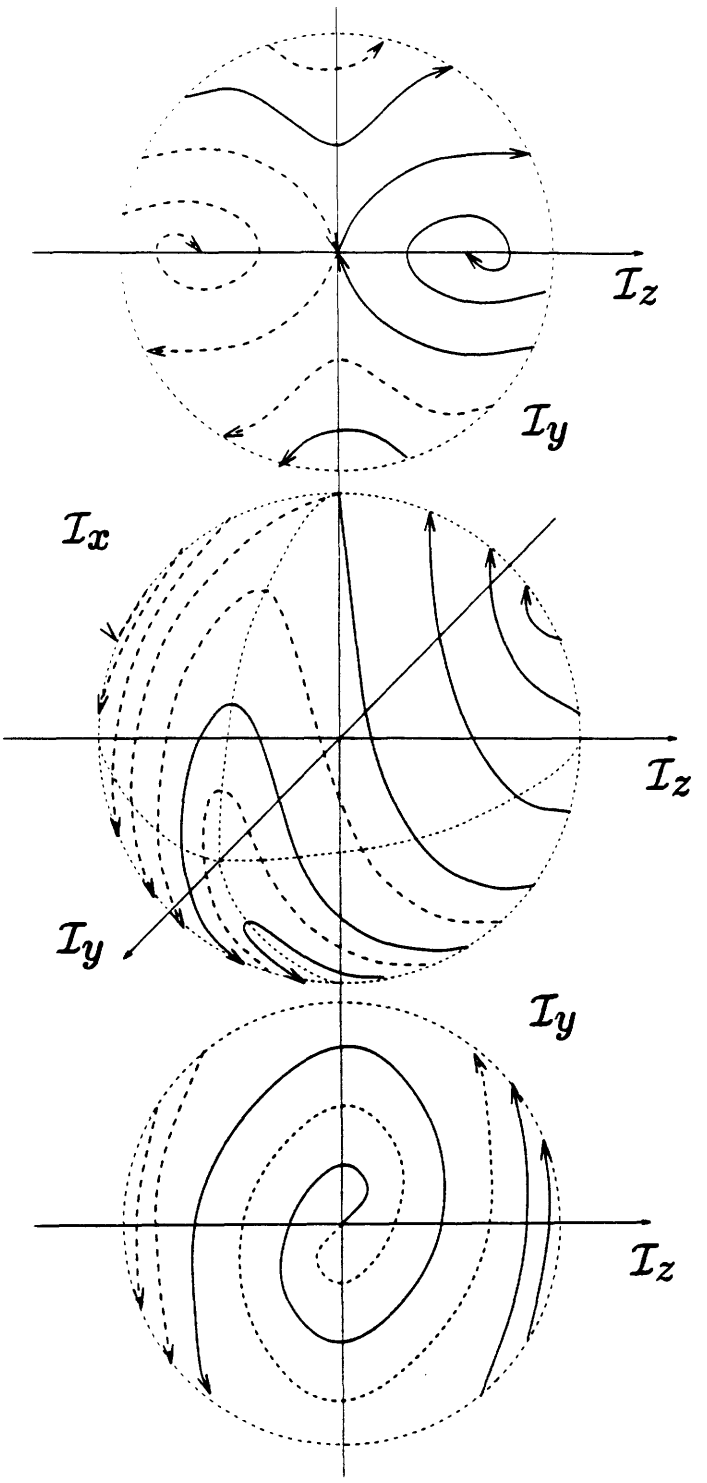

Figure 2-21: Poincaré sphere for the damped Duffing oscillator without driving, $1 > \kappa > 0$. Top: view from north, middle: view from(1,1,1) and bottom: view from south.

Darling-Dennison Hamiltonian which describes two identical harmonically-coupled Morse oscillators. Such a description is valid for moderately to highly exited systems. As a measure to detect localization of vibrational excitation under dynamical symmetry breaking we chose the occupational probability difference of the excitation on the two oscillators.

We found the analytical solution of the equations of motion of Darling-Dennison systems in terms of Jacobian elliptic functions and the associated elliptic parameter. Three qualitatively different solutions exist for different ranges of the elliptic parameter: one, allowing complete exchange of vibrational excitation as a normal mode and two others, confining the vibrational excitation as local modes. The normal to local mode transition occurs at a particular value of the elliptic parameter which depends on both the Hamiltonian parameters and the initial conditions. As a result, we can not only exactly state for any Darling-Dennison system the conditions under which the normal to local mode transition occurs, but also describe the dynamical details of the delocalized or localized excitation. However, the knowledge of the analytical solution to the problem is of little benefit from an intuitive point of view. The physical content of the normal to local mode transition can be better understood using geometrical methods from classical mechanics, i.e. phase plane analysis and potential analysis.

To begin with, we carried out a seemingly technical canonical transformation of the Darling-Dennison Hamiltonian into action-angle coordinates. The reason was to obtain the explicit dependence of the Hamiltonian on the the total action I that is a dynamic invariant. Thus it was possible to decompose the Hamiltonian into a sum of invariants. As an immediate consequence we could geometrically construct the trajectories of the system. They appeared as closed loops on a spherical surface called the Poincaré sphere spanned by the Euclidean components of the total action. The components of $\mathcal{I}$ could be interpreted in the following way.

- The $\mathcal{I}_z$ component of the total action is the occupational probability difference of the excitation on the two oscillators therefore indicating the position of the excitation. Large values of $\mathcal{I}_z$ imply that due to the form of the Morse potential

the molecule is in a distorted state. Vanishing values of $\mathcal{I}_z$ indicate that the molecule is in its undistorted equilibrium configuration. The energy lowering of the molecule due to the distortion by the anharmonic forces has a quadratic dependence on $\mathcal{I}_z$.

- The $\mathcal{I}_y$ component indicates the velocity of the excitation transfer between the bond oscillators and therefore the kinetic energy of the moving excitation. The transfer is the fastest for a phase difference of the bond oscillators close to $\pi/2$, i.e. one of the oscillators is fully stretched whereas the other is at its equilibrium position. The transfer is the slowest for a phase difference of the bond oscillators close to 0 or π, i.e. both bond oscillators are simultaneously stretched or one is stretched whereas the other one is compressed.

- The $\mathcal{I}_x$ component indicated the amount of energy contained in the coupling of the two bond oscillators. This energy can either be converted into kinetic energy of the excitation (increase in $\mathcal{I}_y$) or into distortion energy of the molecular equilibrium geometry. If the phase difference of the two bond oscillators is close to either 0 or π the coupling energy is frozen and cannot be converted.

There is only one time dependent degree of freedom to be solved for which we chose for convenience to be $\mathcal{I}_z$. The associated Hamiltonian turned out to be similar to the Hamiltonian for an undamped Duffing oscillator without driving, apart from dependence of the associated Duffing potential on the initial conditions. The Duffing potential appears either in single well or double well form, the exact shape depends on the Hamiltonian parameters and the initial conditions. The potential picture is intuitively appealing since now localization of vibrational excitation under dynamical symmetry breaking can be discussed treating the excitation as a quasiparticle with an associated kinetic and potential energy. A necessary but not sufficient condition for localization is the appearance of the Duffing potential as double well. The necessary and sufficient condition for the normal to local mode transition to occur is that the kinetic energy of the excitation vanishes at the top of the potential well.

The transition of the Duffing potential from single well to double well form ex-

clusively depends on the Hamiltonian parameters and the total action. Therefore it is characteristic of particular molecules and degrees of excitation. We introduced the bifurcation parameter κ relating the antagonistic tendencies of delocalization by coupling and localization by anharmonicity. Large moduli of κ favor delocalization, small moduli of κ favor localization. Since only the modulus appears to be of importance we came to the surprising conclusion that the particular physical mechanisms that lead to different signs in the Hamiltonian parameters are completely irrelevant.

In order to assign a trajectory of given energy to a normal or local mode we discussed the initial condition dependence of the dynamics in terms of a phase diagram. We found that specification of the energy alone is enough to assign unambiguously a given trajectory to a normal or local mode. This furthermore implied that the process of localization can only occur under dissipation of energy either within the system or into the surroundings.

Thus we were lead to classify the trajectories on the Poincaré sphere into three categories with increasing energy for given total action:

- local modes in a double well potential,
- normal modes in a double well potential and
- normal modes in a single well potential.

The dependence of the dynamics on the relative phase of the two oscillators can be directly read off the Poincaré sphere that therefore allows the straightforward refinement of the intuitive picture of a quasiparticle that we already developed in the introductory chapter.

2.3 Semiclassical interpretation

The technicality of mapping of the Darling-Dennison Hamiltonian onto the Duffing Hamiltonian goes far beyond the obvious benefit of obtaining an analytic solution for the classical trajectories.

In particular, the Duffing potential allows intuitive insight and provides an explanation for two observations in the quantum mechanical Darling-Dennison Hamiltonian. The number of states of local character and their locality increases with I. Using semiclassical ideas one can make the following predictions: for the case of a single well the spectrum consists of almost equidistant states of normal character. Upon excitation the potential barrier forms and grows. The spectrum splits into two regions. For energies above the barrier it contains almost equidistant states of normal character, while for energies below the barrier, there are nearly degenerate pairs of states of local character. Since the potential barrier grows like I^4, the limit of near degeneracy and thus high locality is attained for relatively small I. The time required for an initially localized state to pass over or to tunnel through the barrier is then approximated by the "inverse splitting".

Let us compare the time scales involved for the complete transfer of an initially localized wavepacket with energy below the barrier, and thus large components along the local character eigenstates, to an initially localized wavepacket with energy above the barrier, and thus large components along the normal character eigenstates. The wavepacket with energy below the barrier remains local during a period of transfer of the wavepacket above the barrier. Thus the distinction between states of local or normal character can be justified from the point of view of *dynamics*.

In order to define the significance of this argument for the *symmetric eigenstates* we must slightly change our point of view. Let us compare the dynamics of an eigenstate of local character to the dynamics of an eigenstate of normal character in the presence of a small symmetry breaking perturbation. The period of oscillation of a vibrational excitation between the two local oscillators is much longer for a former local character state than for a former normal character state. Within one period of transfer of a former normal character state, a former local character state *becomes more localized* whereas the symmetry of a former normal character state would be *on average* maintained. In terms of classical dynamics, a local character state is unstable whereas a normal character state is stable against a small symmetry breaking perturbation. This implies for the algebraic eigenvalue problem that the

local or normal character of eigenstates should become apparent in the presence of a symmetry breaking perturbation.

We will follow this line of thought in the discussion of the quantum mechanical aspects of the normal to local mode transition.

2.4 Quantum mechanical aspects of the normal to local mode transition

In this section, we demonstrate the difference in the physical properties between eigenstates of local and those of normal character. Quantum states that correspond to local modes in a classical description are extremely susceptible to symmetry-breaking perturbations. When a small symmetry breaking perturbation is added to the Hamiltonian these states become localized by mixing. States that correspond to normal modes in a classical description remain delocalized when the same perturbation is added to the Hamiltonian. Thus we can show that the susceptibility to symmetry breaking is very much larger in local character quantum states than in normal character quantum states. This allows us to formulate a quantitative measure for localization in these molecules.

Let us briefly sketch how to introduce the concept of stability for the eigenstates of $\hat{H}_{DD}$ and $\hat{H}$.

First, we discuss the eigenvalue problem of $\hat{H}_{DD}$ and $\hat{H}$. Where exact results are unavailable, we obtain estimates for eigenvalues and eigenvectors for large I. Then we recover the classical bifurcation parameter, κ, and discuss its relevance in the quantum mechanical context. We proceed examining the effect of a symmetry breaking perturbation on the eigenstates of $\hat{H}_{DD}$. The issue of instability under symmetry breaking perturbations is quantitatively addressed for each individual eigenstate using two measures to be defined later: (1) The effect is measured in terms of order parameters that indicate the mismatch in occupation numbers of the two local oscillators. (2) The sensitivity is measured in terms of susceptibilities. The usefulness of

the method is demonstrated by an application to experimental data.

2.4.1 The eigenvalue problem

In this section we solve the eigenvalue problem to $\hat{H}_{DD}$ and $\hat{H}$ which are familiar in the context of angular momentum. Since the exposition is essential to the further discussion we did not "ban" it into the Appendix.

From the commutation relations eqn.(2.19) we see that both $\hat{H}_{DD}$ and $\hat{H}$ are block diagonal in the representation of eigenstates to $\hat{I}$. Furthermore we note the invariance of both Hamiltonians under site exchange by the site exchange operator $\hat{P}_{12}$,

$$[\hat{P}_{12}, \hat{H}_{DD}] = 0 \tag{2.82}$$

$$[\hat{P}_{12}, \hat{H}] = 0. \tag{2.83}$$

Therefore each block of both Hamiltonian associated with a certain value of I can be further decomposed in two blocks in simultaneous eigenstates to both $\hat{I}$ and $\hat{P}_{12}$.

Thus it is of advantage to solve first the eigenvalue problem to $\hat{I}$ followed by that for $\hat{P}_{12}$. Then all that remains to be done is to diagonalize $\hat{C}$ in the basis of the simultaneous eigenstates to $\hat{P}_{12}, \hat{I}$. The eigenvalues of $\hat{H}_{DD}$ and $\hat{H}$ can easily be related using the eigenvalues λ_I and λ_C to $\hat{I}$ and $\hat{C}$.

Let us denote the nth eigenstate to one of the local oscillators by $|\Phi_n>$. The eigenstates $|\Phi_I, l>$ and eigenvalues λ_I to $\hat{I}$ are trivial to find and given by the outer product of the local oscillator states

$$\hat{I}|\Phi_I, l>=\hat{I}|\Phi_{n-l}>|\Phi_l>=I|\Phi_{n-l}>|\Phi_l>=I|\Phi_I, l>. \tag{2.84}$$

We use the normalization

$$<\Phi_I, l|\Phi_I, k>=\delta_{lk},$$

$$l, k = 0, 1, \ldots, n. \tag{2.85}$$

The action of the site exchange operator $\hat{P}_{12}$ onto the eigenstates to $\hat{I}$ is defined by

$$\hat{P}_{12}|\Phi_I, l>= \hat{P}_{12}|\Phi_{n-l}>|\Phi_l>= |\Phi_l>|\Phi_{n-l}>= |\Phi_I, n-l> . \tag{2.86}$$

Again, the eigenvalue problem is straightforward to solve. For given I we have to distinguish between the cases for which I is even or odd.

- For even I there are $(n+1)/2$ eigenstates associated with the eigenvalue $+1$ that are symmetric under site exchange. There are equally many eigenstates with eigenvalue -1 that are antisymmetric under site exchange.
- For odd I there are $(n+2)/2$ symmetric and $n/2$ antisymmetric eigenstates.

The symmetric and antisymmetric eigenstates $|\Phi_I, l, \pm>$ written in the basis of eigenstates to $\hat{I}$ are

$$\begin{aligned} \hat{P}_{12}|\Phi_I, l, \pm> &= \hat{P}_{12}\frac{1}{\sqrt{2}}(|\Phi_{n-l}>|\Phi_l> \pm|\Phi_l>|\Phi_{n-l}>) \\ &= \pm\frac{1}{\sqrt{2}}(|\Phi_{n-l}>|\Phi_l> \pm|\Phi_l>|\Phi_{n-l}>) = \pm|\Phi_I, l, \pm> . \end{aligned} \tag{2.87}$$

The states $|\Phi_I, l, \pm>$ are now simultaneously eigenstates to $\hat{I}$ and $\hat{P}_{12}$.

Let us denote $\hat{C}$ in the $|\Phi_I, l, \pm>$ basis by the matrix $\mathbf{C}$ and the Ith block of symmetry $\pm$ of $\mathbf{C}$ by $\mathbf{C}^{I,\pm}$ with the real matrix elements $c^{I,\pm}_{i,j}$. The matrix $\mathbf{C}$ is symmetric tridiagonal.

As before, we have to distinguish between the cases of even and odd I

- For even I the diagonal and off diagonal elements of $\mathbf{C}^{I,\pm}$ are given by

$$\begin{aligned} c^{I,\pm}_{l,l} &= \chi(n-2l)^2, \\ c^{I,\pm}_{l+1,l} &= \zeta\sqrt{(l+1)(n-l)}; \\ l &= 0, 1, \ldots, \frac{n-2}{2}. \\ c^{I,\pm}_{\frac{n-1}{2},\frac{n-1}{2}} &= \chi \pm \zeta\frac{n+1}{2}. \end{aligned} \tag{2.88}$$

- For odd I the diagonal and off diagonal elements of $\mathbf{C}^{I,\pm}$ are

$$\begin{aligned} c^{I,\pm}_{l,l} &= \chi(n-2l)^2; \\ l &= 0,1,\ldots,\frac{n-2}{2}. \\ c^{I,\pm}_{l+1,l} &= \zeta\sqrt{(l+1)(n-l)}; \\ l &= 0,1,\ldots,\frac{n-4}{2}. \\ c^{I,+}_{\frac{n}{2},\frac{n}{2}} &= 0. \\ c^{I,+}_{\frac{n}{2},\frac{n-2}{2}} &= \zeta\sqrt{n(\frac{n}{2}+1)}. \end{aligned} \tag{2.89}$$

The eigenvalue problem of $\hat{C}$ can be formulated in terms of the eigenvalue problems of the blocks $\mathbf{C}^{I,\pm}$ as

$$(\mathbf{C}^{I,\pm} - \lambda^{I,\pm}_{C,L}\mathbf{1})c = 0. \tag{2.90}$$

Thus the eigenvalues $\lambda^{I\pm}_{C}$ (for brevity denoted by λ) can be calculated

- for even I for the symmetric and antisymmetric eigenstates from the vanishing determinant $D^{I,\pm} =$

$$\begin{vmatrix} \chi n^2-\lambda & \zeta\sqrt{n} & 0 & \ldots & 0 \\ \zeta\sqrt{n} & \chi(n-2)^2-\lambda & \zeta\sqrt{2(n-1)} & \ldots & \vdots \\ 0 & \zeta\sqrt{2(n-1)} & \ldots & & 0 \\ \vdots & & \ldots & 9\chi-\lambda & \frac{\zeta}{2}\sqrt{(n-1)(n+3)} \\ 0 & \ldots & 0 & \frac{\zeta}{2}\sqrt{(n-1)(n+3)} & \chi\pm\zeta\frac{n+1}{2}-\lambda \end{vmatrix} \tag{2.91}$$

- for odd I for the symmetric eigenstates $D^{I,+} =$

$$\begin{vmatrix} \chi n^2-\lambda & \zeta\sqrt{n} & 0 & \dots & 0 \\ \zeta\sqrt{n} & \chi(n-2)^2-\lambda & \zeta\sqrt{2(n-1)} & \dots & \vdots \\ 0 & \zeta\sqrt{2(n-1)} & \dots & & 0 \\ \vdots & & \dots & 4\chi-\lambda & \zeta\sqrt{n(\frac{n}{2}+1)} \\ 0 & \dots & 0 & \zeta\sqrt{n(\frac{n}{2}+1)} & -\lambda \end{vmatrix} \tag{2.92}$$

and for the antisymmetric eigenstates $D^{I,-} =$

$$\begin{vmatrix} \chi n^2-\lambda & \zeta\sqrt{n} & 0 & \dots & 0 \\ \zeta\sqrt{n} & \chi(n-2)^2-\lambda & \zeta\sqrt{2(n-1)} & \dots & \vdots \\ 0 & \zeta\sqrt{2(n-1)} & \dots & & 0 \\ \vdots & & \dots & 16\chi-\lambda & \frac{\zeta}{2}\sqrt{(n-2)(n+4)} \\ 0 & \dots & 0 & \frac{\zeta}{2}\sqrt{(n-2)(n+4)} & 4\chi-\lambda \end{vmatrix} \tag{2.93}$$

The results up to I=4 can be obtained analytically.

$$\lambda_C^{2,\pm} = \chi \pm \zeta, \tag{2.94}$$

$$\lambda_{C,0,1}^{3,+} = 2(\chi \pm \sqrt{\chi^2+\zeta^2}), \tag{2.95}$$

$$\lambda_C^{3,-} = 4\chi, \tag{2.96}$$

$$\lambda_{C,0,1}^{4,+} = 5\chi+\zeta \pm 2\sqrt{4\chi^2-2\chi\zeta+\zeta^2}, \tag{2.97}$$

$$\lambda_{C,0,1}^{4,-} = 5\chi-\zeta \pm 2\sqrt{4\chi^2+2\chi\zeta+\zeta^2}. \tag{2.98}$$

The expectations of $\hat{H}_{DD}$ and $\hat{H}$ are then given by

$$E_{DD,L}^{I,\pm} = (\omega+\xi I)I + \lambda_{C,L}^{I,\pm}, \tag{2.99}$$

$$E_L^{I,\pm} = 2[\zeta^2(I^2-1) - (\lambda_{C,L}^{I,\pm})^2]. \tag{2.100}$$

Let us denote the corresponding eigenstates to $\hat{C}$ and thus to $\hat{H}_{DD}$ and $\hat{H}$ by $|\Psi_I, \pm, L>$ with the counting index $L = 0, 1, \dots$.

As an example, consider the eigenstate associated with $\lambda_C^{2,+} = \chi + \zeta$ which is now denoted by $|\Psi_2, +, 0 >= |\Phi_2, 0, + >= 1/\sqrt{2}(|1 > |0 > +|0 > |1 >)$.

The eigenstates to $\lambda_{C,l}^{I,\pm}$ reduce

- in the limit of vanishing coupling, i.e. $\zeta \to 0$ to degenerate pairs of the form $|\Phi_I, l >$
- and in the limit of vanishing anharmonicity, i.e. $\chi \to 0$ to nondegenerate $|\Phi_I, l, \pm >$.

2.4.2 The energetic splitting of eigenstates of the Darling-Dennison Hamiltonian

Since we are later on interested in the response of the system to perturbations, it is essential to have a look at the differences in energy between the eigenstates. For simplicity we focus on $\hat{H}_{DD}$ which is of practical relevance. The theoretically equally interesting discussion of $\hat{H}$ can be carried out in complete analogy.

Low excitation

It is instructive to begin with the weak coupling limit $\chi \gg \zeta$ and small I. For the differences in energy $\Delta\lambda_{C,0}^{I,\pm} = \lambda_{C,0}^{I,+} - \lambda_{C,0}^{I,-}$ between the lowest lying symmetric and antisymmetric eigenstates $|\Psi_I, \pm, 0 >$ we obtain from the analytical solutions in eqn.(2.98) to lowest non vanishing order in (ζ/χ):

$$\Delta\lambda_{C,0}^{2,\pm} = 2\zeta, \tag{2.101}$$

$$\Delta\lambda_{C,0}^{3,\pm} = \frac{\zeta^2}{\chi}, \tag{2.102}$$

$$\Delta\lambda_{C,0}^{4,\pm} = \frac{\zeta^3}{4\chi^2}. \tag{2.103}$$

We note that the energetic splitting of the two lowest lying eigenstates within a polyad decreases with increasing I and follows a power law of order $(n-1)$ in the small parameter (ζ/χ). A glance at the classical treatment indicates that the limit

$\chi \gg \zeta$ corresponds to the local mode limit $\kappa \ll 1$.

The eigenstate closest in energy to these pairs of states is given by the symmetric eigenstate with the next higher counting index, i.e. $|\Psi_I, +, 1>$. For the energy difference $\Delta\lambda^{I,+}_{C,0,1} = \lambda^{I,+}_{c,1} - \lambda^{I,+}_{c,0}$ between the lowest lying symmetric state $|\Psi_I, +, 0>$ and following symmetric state $|\Psi_I, +, 1>$ within the same polyad we obtain to $O(\zeta)$

$$\Delta\lambda^{3,+}_{C,0,1} = 4\chi, \tag{2.104}$$

$$\Delta\lambda^{4,+}_{C,0,1} = 8\chi - 2\zeta. \tag{2.105}$$

We conclude that in the weak coupling limit

- the two lowest lying eigenstates states form an almost degenerate pair
- and the separation between pairs of almost degenerate eigenstates is at least one order of magnitude larger in energy than the splitting of the degenerate pairs.

High excitation

We will now investigate under what conditions on χ and ζ this tendency of the two lowest lying states to form almost degenerate pairs of eigenstates is present for large I. In this limit the exact results are not accessible.

A first glance at the determinants $D^{I,\pm}$ in eqn.(2.91) shows that standard perturbation theory is not a good way to obtain an approximate result for the energy splitting of the two lowest lying states. The reason is that we have to compare the lowest lying eigenvalues and the corresponding eigenstates of two matrices that are tridiagonal and differ only in the lower right matrix element. For large I we expect the lowest lying eigenvalues to be in the vicinity of the largest diagonal element, i.e. the upper right matrix element which is identical for both matrices. In order to get a difference in the two necessary perturbative expansions we have to carry out the perturbative series to $(n-1)/2$ order since the matrices are tridiagonal and differ only by the lower right matrix element. This procedure becomes impractical with

increasing I.

We follow a different strategy that takes advantage of the fact that the Hamiltonian matrices are tridiagonal. The method we use is a continued fraction expansion of the secular determinant [20, 21] that appears to have been forgotten as an analytical method soon after its implementation on computers. The method is straightforward yet tedious to apply.

To begin, we recursively obtain the ratio of two consecutive components of an eigenvector as a function of the next ratio of two consecutive components, i.e.

$$\frac{c_l}{c_{l-1}} = \frac{-\zeta\sqrt{l(n-l+1)}}{\chi(n-2l)^2 - \lambda - \zeta\sqrt{(n-l)(l+1)}\frac{c_l}{c_{l-1}}}. \tag{2.106}$$

From now on, without loss of generality, let us consider even I. For $\zeta/\chi I < 1$ we obtain after some algebra an estimate for $\lambda_{C,0}^{I,\pm}$ as

$$\lambda_{C,0}^{I,\pm} \approx \chi n^2 + \frac{\zeta^2}{4\chi}\frac{n}{n-1}, \tag{2.107}$$

which in the limit stated above equals the energy of the classical stationary trajectories in the local mode limit $E_{DD}^{3,4}$ in eqn.(2.63) up to the contribution by the principal action I. Using this approximate result in eqn.(2.106) we can obtain an estimate for the ratio of the first component c_0 and last component $c_{\frac{n-1}{2}}$ of the eigenstates $|\Psi_I, \pm, 0>$ to $\lambda_{C,0}^{I,\pm}$

$$\frac{c_{\frac{n-1}{2}}}{c_0} \approx \sqrt{2}(\frac{\zeta}{4\chi})^{\frac{n-1}{2}}\frac{n}{\sqrt{(n+1)!}}. \tag{2.108}$$

We see, that in the stated limit successive components of the eigenstates $|\Psi_I, \pm, 0>$ decrease by an order of magnitude each. It is therefore possible to explicitly evaluate the difference in the expectation of the Hamiltonian for the two lowest lying eigenstates $|\Psi_I, \pm, 0>$. Since up to the component $c_{(n-3)/2}$ the contributions are identical it can be justified to consider for the difference in the eigenvalues contributions from the differing components $c_{\frac{n-1}{2}}$ only. To do so, let us assume that $|\Psi_I, \pm, 0>$ can be normalized and set c_0 to $O(1)$. Together with eqn.(2.91) we can then approximate

$\Delta\lambda_{C,0}^{I,\pm}$ by

$$\Delta\lambda_{C,0}^{I,\pm} \approx c^2_{\frac{n-1}{2}}(c^{I,+}_{\frac{n-1}{2},\frac{n-1}{2}} - c^{I,-}_{\frac{n-1}{2},\frac{n-1}{2}}) = 2\zeta(\frac{\zeta}{4\chi})^{n-1}\frac{n}{(n-1)!}. \tag{2.109}$$

As a preliminary check, let us evaluate this formula for even small values of I and compare to the results in the limit of small I and $\zeta \ll \chi$ in eqn.(2.103).

$$\Delta\lambda_{C,0}^{2,\pm} = 2\zeta, \tag{2.110}$$

$$\Delta\lambda_{C,0}^{3,\pm} = \frac{\zeta^2}{\chi}, \tag{2.111}$$

$$\Delta\lambda_{C,0}^{4,\pm} = \frac{3\zeta^3}{16\chi}. \tag{2.112}$$

We see that there is surprisingly good agreement to the splittings of eqn.(2.103). This might tell us that it is the ratio $\zeta/\chi I$ used to obtain eqn.(2.109), rather than χ/ζ or $1/I$ alone, that determines the order of magnitude of the splitting.

On second thought the result is not surprising since we had to expect exactly this from the crucial role of $\kappa = \zeta/2\chi I$ for the classical analysis in the previous chapters.

2.4.3 Recovery of the classical bifurcation parameter

The trajectories generated by the classical correspondent of the quantum mechanical Hamiltonian H_{DD} show parametric instability. In the following we *deduce* the stability properties of the *classical* trajectories from the properties of the *quantum mechanical* eigenstates and thus derive the classical bifurcation parameter κ from the quantum mechanical Darling-Dennison Hamiltonian. In the classical analysis the bifurcation parameter $\kappa = \zeta/2\chi I$ specifies the normal to local state transition. In the quantum mechanical model, this parameter arises once more, but the value of κ at which the transition occurs is shifted.

To show the analogy, we use the fact that if there are *any* states of local character within the block labelled by I, then the two states $|\Psi_I, \pm, 0>$ of lowest energy $\lambda_0^{I,\pm}$ are necessarily among them. Thus it is sufficient to identify the conditions where the $|\Psi_I, \pm, 0>$ undergo the normal to local character state transition.

Let us therefore further examine the ratio (2.108). We define

$$\tilde{\kappa} = \frac{e}{2}\kappa. \tag{2.113}$$

Using Stirling's formula and the definition of $\tilde{\kappa}$ we can approximate eqn.(2.108) as

$$\frac{c_{\frac{n-1}{2}}}{c_0} \approx (\tilde{\kappa})^{\frac{n-1}{2}} \frac{n}{(n+1)^{\frac{5}{4}}} \frac{2^{\frac{1}{4}} e}{\pi^{\frac{1}{4}}}. \tag{2.114}$$

For the ratio of the projections of the eigenstates lowest in energy $|\Psi_I, \pm, 0>$ onto the state of largest local character $|\Phi_I, 0, \pm>$, i.e. c_0, and onto the state of largest normal character $|\Phi_I, \frac{n-1}{2}, \pm>$, i.e. $c_{\frac{n-1}{2}}$, we can show under further neglect of non exponential factors in eqn.(2.114,2.109)

$$\ln\left(\frac{c_{\frac{n-1}{2}}}{c_0}\right) \approx \frac{n-1}{2} \ln\left(|\tilde{\kappa}|\right), \tag{2.115}$$

and for the difference in energy

$$\ln\left(\frac{\Delta\lambda_0^{I,\pm}}{2\zeta}\right) \approx (n-1) \ln\left(|\tilde{\kappa}|\right). \tag{2.116}$$

In the classical limit, $I \gg 1$, we obtain

- for $|\tilde{\kappa}| > 1$,

$$\lim_{I\to\infty} < \Psi_I, \pm, 0 | \phi_I, 0, \pm >= 0. \tag{2.117}$$

  Thus for large I and $|\tilde{\kappa}| > 1$ the eigenstates $|\Psi_I, \pm, 0>$ have a *vanishing local character* component and are thus of *normal character*. They become normal modes in the classical limit. The energy difference between these eigenstates increases with I according to eqn.(2.109).

- For $|\tilde{\kappa}| < 1$ we get

$$\lim_{I\to\infty} < \Psi_I, \pm, 0 | \phi_I, \frac{n-1}{2}, \pm >= 0. \tag{2.118}$$

For large I and $|\tilde{\kappa}| < 1$ the eigenstates $|\Psi_I, \pm, 0>$ have a *vanishing normal* character component and are thus of *local character.* They become truly local in the classical limit. The energy difference between these eigenstates decreases with I according to eqn.(2.116).

- The transition between the limiting forms occurs at $|\tilde{\kappa}| = 1$ which establishes the analogy to the classical bifurcation at $|\kappa| = 1$.

Note that $\tilde{\kappa}$ relates coupling and anharmonicity similar to the local mode indicator used in numerical studies by Child and Lawton [10]. At $|\tilde{\kappa}| = 1$ two qualitative *global* changes occur in the quantum system that are ultimately responsible for the change in the stability properties:

- The lowest lying eigenstates within a polyad change from *normal to local character or vice versa.*

- The first near degeneracy of eigenstates at lowest energy $\lambda_0^{\pm}$ *appears or disappears.*

Note that the quantum mechanical normal to local mode transition occurs at $|\tilde{\kappa}| = 1$, which is *later than* the classical transition at $|\kappa| = 1(|\tilde{\kappa}| = e/2)$. This may be interpreted, in terms of the classical dynamical potential V, using semiclassical ideas: the change from the single well to the double well form of V is *not sufficient* to lead to a localized quantum state. The barrier must be high enough so that at least one bound state lies at an energy below the barrier maximum.

Before we come to the perturbation analysis of the system, let us estimate the minimal energy difference $min(\Delta\lambda_{C,0,1}^{I,\pm})$ between the lowest lying antisymmetric state $|\Psi_I, -, 0>$ and the next higher symmetric state $|\Psi_I, +, 1>$ for large I. Using Gerschgorin's theorems from linear algebra we obtain for the difference of $min(\lambda_{C,0}^{I,-})$ and $max(\lambda_{C,1}^{I,+})$

$$min(\Delta\lambda_{C,0,1}^{I,\pm}) = 4\chi(n-1) - \zeta[\sqrt{n} + \sqrt{2(n-1)}] \approx 4\chi(n-1). \qquad (2.119)$$

Now the stage is set for more firmly establishing the connection between the stability of the classical stationary states and the eigenstates of the Darling-Dennison Hamiltonian. We are encouraged enough by the amazing recovery of the bifurcation parameter κ of the classical problem in the slightly different form $\tilde{\kappa}$ of the quantum mechanical problem.

2.4.4 Perturbative analysis and stability

For the symmetric Darling-Dennison Hamiltonian given in eqn.(2.15), the quantum eigenstates will always be delocalized in order to satisfy the symmetry condition, i.e. $< \hat{I}_z >= 0$. Note however, that in general $< \hat{I}_z^2 >$ takes large values for states of local character and small values for states of normal character. The standard deviation $\sigma = \sqrt{< \hat{I}_z^2 > - < \hat{I}_z >^2} = \sqrt{< \hat{I}_z^2 >}$ indicates the degree of local or normal character. But still, it does not give insight as to what the physical implications of this distinction are.

However, if a small symmetry breaking perturbation is added to the Hamiltonian, pairs of symmetrized states of local character and different parity will mix and become local while those of normal character will remain normal. In the following we will investigate the *stability properties* of eigenstates of $\hat{H}_{DD}$. The question of stability is decided by determining the magnitude of a symmetry breaking perturbation necessary to cause localization to a specified extent. We will show that eigenstates of local character become unstable against localization to a specified extent at smaller magnitudes of a symmetry breaking perturbation than occurs for eigenstates of normal character. A convenient choice for the perturbation is given by an energy mismatch between the two local oscillators. We will quantify the effect of the perturbations by determining the induced difference in vibrational excitation and the susceptibility of individual states by dependence of the induced difference in exitation on the energy mismatch. Other measures, such as the loss of initial eigenstate character, provide similar information and may be useful for different systems.

Before we get down to the details, let us begin with a brief aside.

Numerically unstable eigenvalue problems

It has been observed in the 1950's in a series of numerical investigations by Wilkinson [22], that the eigenvalue problem for matrices of same type as $\mathbf{C}$ is well posed, whereas the eigenvector problem is ill posed.

Miniscule deviations in the lowest lying approximate eigenvalues used to calculate the corresponding eigenvector can lead to dramatically differing results. Sometimes the erroneous eigenvector can be orthogonal to the actual eigenvector. For the higher lying eigenvalues the effect on the corresponding eigenvector is less dramatic.

Wilkinson identified two causes to be responsible which we discuss in some detail in Appendix B.

- First, eigenvalues appear in almost degenerate pairs, the splittings being particularly small for the lower lying eigenvalues.

- Second, the most dramatically responding eigenvectors have a large projection onto the basis states that are associated with diagonal element of $\mathbf{C}$ closest to the eigenvalue. For the lowest lying eigenvalues those basis states are the local character states.

The second cause is necessary and sufficient for the effect. It is completely independent of the first, that only amplifies the effect, and is present in even well posed eigenvalue problems.

This *numerical* instability of the computational problem gives us a hint that the physical system might be sensitive as well to small perturbations, especially for the lowest states within a polyad.

Before we close the aside, note however, that the condition number (see Appendix B), used to to quantify the sensitivity of an inversion problem to errors in the matrix elements, does not provide a satisfactory tool to identify instability in our problem. For matrices of the type $\mathbf{C}$ it is calculated to take the smallest possible value and therefore indicates that the problem is well conditioned.

Susceptibility and order parameter

Let us begin with the formal treatment of instability of the symmetrized eigenstates toward localization. Since we want to define stability towards *any* perturbation, let us assume the *most effective perturbation that breaks the symmetry of the system.* For that purpose let us introduce an energy mismatch between the two local oscillators. We will quantify the effect of that perturbation by determining the induced difference in vibrational excitation. The perturbed Hamiltonian, including an energy mismatch of magnitude 2ϵ, takes the form

$$\hat{H}_{DD,P} = \hat{H}_{DD} + \epsilon \hat{I}_z. \tag{2.120}$$

Let us denote the eigenstates to $\hat{H}_{DD,P}$ by $|\Psi_I, \pm, L >_P$. Note that these states are no longer symmetric in the strict sense. The induced difference between vibrational excitations of the two local oscillators is given by the expectation of the *order parameter* $\hat{I}_z$ for the *perturbed* state $|\Psi_I, \pm, L >_P$, which we will denote by

$$I_{z,I,\pm,L}(\epsilon) =< \hat{I}_z >_P . \tag{2.121}$$

Let us define the *susceptibility* of the unperturbed eigenstates $|\Psi_I, \pm, L >$ to the symmetry breaking perturbation $\hat{I}_z$ by

$$\gamma_{I,\pm,L} = [\frac{\partial I_{z,I,\pm,L}(\epsilon)}{\partial \epsilon}]_{\epsilon=0}. \tag{2.122}$$

The susceptibilities and order parameters are easily accessible by numerical calculation. An analytical expression for the susceptibilities can be obtained from time independent perturbation theory to first order in ϵ.

The shift in energy $\Delta_{I,\pm,L}$ is calculated to vanish according to

$$\Delta_{I,\pm,L} = \epsilon < \Psi_I, \pm, L|\hat{I}_z|\Psi_I, \pm, L >= 0. \tag{2.123}$$

The perturbed eigenstates $|\Psi_I, \pm, L>_P$ are

$$|\Psi_I, \pm, L>_P = |\Psi_I, \pm, L> + \epsilon \sum_K \frac{<\Psi_I, \mp, K|\hat{I}_z|\Psi_I, \pm, L>}{\lambda_{C,L}^{I,\pm} - \lambda_{C,K}^{I,\mp}} |\Psi_I, \mp, K> . \quad (2.124)$$

The expectation of the order parameter $I_{z,I,\pm,L}(\epsilon)$ is given by

$$I_{z,I,\pm,L}(\epsilon) = \epsilon \sum_K \frac{|<\Psi_I, \mp, K|\hat{I}_z|\Psi_I, \pm, L>|^2}{\lambda_{C,L}^{I,\pm} - \lambda_{C,K}^{I,\mp}}. \quad (2.125)$$

Finally, the susceptibility $\gamma_{I,\pm,L}$ of the eigenstate $|\Psi_I, \pm, L>$ to the symmetry breaking perturbation $\hat{I}_z$ turns out to be

$$\gamma_{I,\pm,L} = \sum_K \frac{|<\Psi_I, \mp, K|\hat{I}_z|\Psi_I, \pm, L>|^2}{\lambda_{C,L}^{I,\pm} - \lambda_{C,K}^{I,\mp}}. \quad (2.126)$$

We see that the susceptibility of an eigenstate contains both ingredients inferred by Wilkinson: the energetic distance to the other eigenstates and the magnitude of the components along basis states of large local character $|\Phi_I, 0, \pm> \approx |\Psi_I, \pm, 0>$.

Low excitation The following example will give us an idea how to interpret the susceptibilities. We evaluate the susceptibility for the first excited state $|\Psi_2, +, 0>$

$$\gamma_{2,+,0} = \frac{1}{2\zeta}. \quad (2.127)$$

We see that the susceptibility is given by the period of transfer for an initially localized excitation of the *unperturbed* system between the local oscillators. Equivalently, we can say that the susceptibility is proportional to the time an initially normal state of the *perturbed* system needs to evolve to a local state. This interpretation provides a nice analogy to the classical picture of stability: A local character excitation of the unperturbed system appears to become localized under perturbation if observed for times short compared to the period of transfer.

Note, that with the interpretation of the susceptibilities as periods of transfer the interpretation of the *inverse* susceptibilities as the perturbation necessary to induce

localization of the associated eigenstate follows immediately. These statements are further refined in the following.

High excitation Let us now establish the connection between the susceptibilities $\gamma_{I,\pm,L}$ and the notion of local and normal character from the semiclassical analysis. We have to derive an expression for $\gamma_{I,\pm,L}$ in the limit of large I. Let us make a two state approximation on the basis of the estimates eqn.(2.109,2.119). Note that this approximation becomes increasingly better with increasing I and decreasing κ.

For the lowest lying symmetric state $|\Psi_I, +, 0>$, the susceptibility can then be estimated from eqn.(2.126) as

$$\gamma_{I,+,0} \approx \frac{n!}{2\zeta(\frac{\zeta}{4\chi})^{n-1}}, \tag{2.128}$$

or, equivalently

$$\gamma_{I,+,0} \approx \frac{n^2}{\Delta\lambda_0^{I,\pm}}. \tag{2.129}$$

This result is satisfactory since it is a caricature of the susceptibility: the ratio of the square of the largest possible occupational difference and the smallest possible energetic splitting.

Let us investigate the limit of high excitation. Together with eqn.(2.109) we see, that,

- for $I \gg 1, |\tilde{\kappa}| > 1$ the susceptibility $\gamma_{I,+,0} \to 0$, whereas
- for $I \gg 1, |\tilde{\kappa}| < 1$ the susceptibility $\gamma_{I,+,0} \to \infty$.

This implies that the strength of the perturbation becomes irrelevant for the question of stability in the classical limit, which is well known from classical dynamics. Note the proportionality factor of n^2 which we missed in the interpretations in the limit of low excitations.

In order to compare this result with the *classical* analysis, let us calculate the susceptibility of a state $|\Psi_I, +, 0>$ whose associated classical trajectory may undergo

a bifurcation. We insert the definition of κ into eqn.(2.128) and set $|\kappa| = 1$ to obtain

$$\gamma_I^{crit} = \frac{2^{I-3} I}{2\zeta \exp(I)}. \tag{2.130}$$

Since all states of local character have larger and all states of normal character smaller susceptibilities than $\gamma_I^{crit}(I)$ we denote it the *critical susceptibility.*

For states of normal character the two state approximation is not applicable. But we can qualitatively predict that the susceptibilities for normal character states should be low for the following reasons:

- for each normal state there are at least two states that mix in under the perturbation by approximately the same amount. These states contribute with opposite signs to the susceptibility. Therefore the largest change in the probability amplitude of vibrational excitation will be around small values of $I_{z,I,\pm,L}$.

- The magnitude of change decreases with increasing energetic distance to the neighboring states and is therefore smaller for the wide split normal character states than for the almost degenerate states of local character.

For these two reasons, the susceptibility will be lower for states of normal character than for states of local character.

In the following sections we evaluate the susceptibility and the expectation of the order parameter for H_2O, O_3, SO_2, C_2H_2 and C_2D_2 and compare the result to the semiclassical phase diagram.

Evaluation of susceptibilities from experimental data

Let us begin with the susceptibilities for the eigenstates of H_2O up to $I = 10$ as given by eqn.(2.126). The results are displayed in Figure 2-22 and organized as follows. We plot the decadic logarithm of the absolute values of the susceptibility versus I. We distinguish between symmetric and antisymmetric eigenstates indicated as circles and crosses respectively. Furthermore, we compare the susceptibilities of the eigenstates $|\Psi_I, \pm, 0>$ to the estimates obtained in eqn.(2.128) which are indicated as stars. The

critical susceptibility is indicated as a dashed line.

The susceptibilities of H_2O change dramatically upon excitation. We delineate three trends:

- the individual susceptibilities increase with increasing energy and I;
- the number of states with susceptibilities higher than the critical susceptibilities increases;
- the eigenstates become unstable in pairs.

The susceptibility of all local character states is at least two orders of magnitude larger than that of a normal character state. The interpretation in terms of the semiclassical picture is straightforward.

Furthermore, the classical normal to local character transition is completely recovered quantum mechanically as can be seen from a comparison with the phase diagrams for the classical trajectories in Figure 2-5. Note however that without the knowledge of the critical susceptibility we could not draw a strict line between the local and normal character states. This is not a flaw of the treatment but its asset. Due to tunneling the quantum mechanical normal to local state transition cannot be as sharp as the classical normal to local mode transition, although we can unambiguously label each quantum state by the isoenergetic classical trajectories. This suggests that the proper way of thinking about the properties of the eigenstates to the Darling-Dennison Hamiltonian is in terms of the susceptibilities that constitute a physical property and not in terms of the classical normal/local mode distinction that is only a label.

In the last section we have interpreted the inverse susceptibilities as the magnitude of the perturbation necessary to induce localization of the associated state. For H_2O at $I = 10$ this means, that the perturbation necessary to localize the antisymmetric normal character state has to be 14 orders of magnitudes larger than the one that localizes the states of highest susceptibility. In absolute terms the perturbation necessary to localize the normal character state is two orders of magnitude larger than the coupling constant ζ which is of $O(10^2)cm^{-1}$.

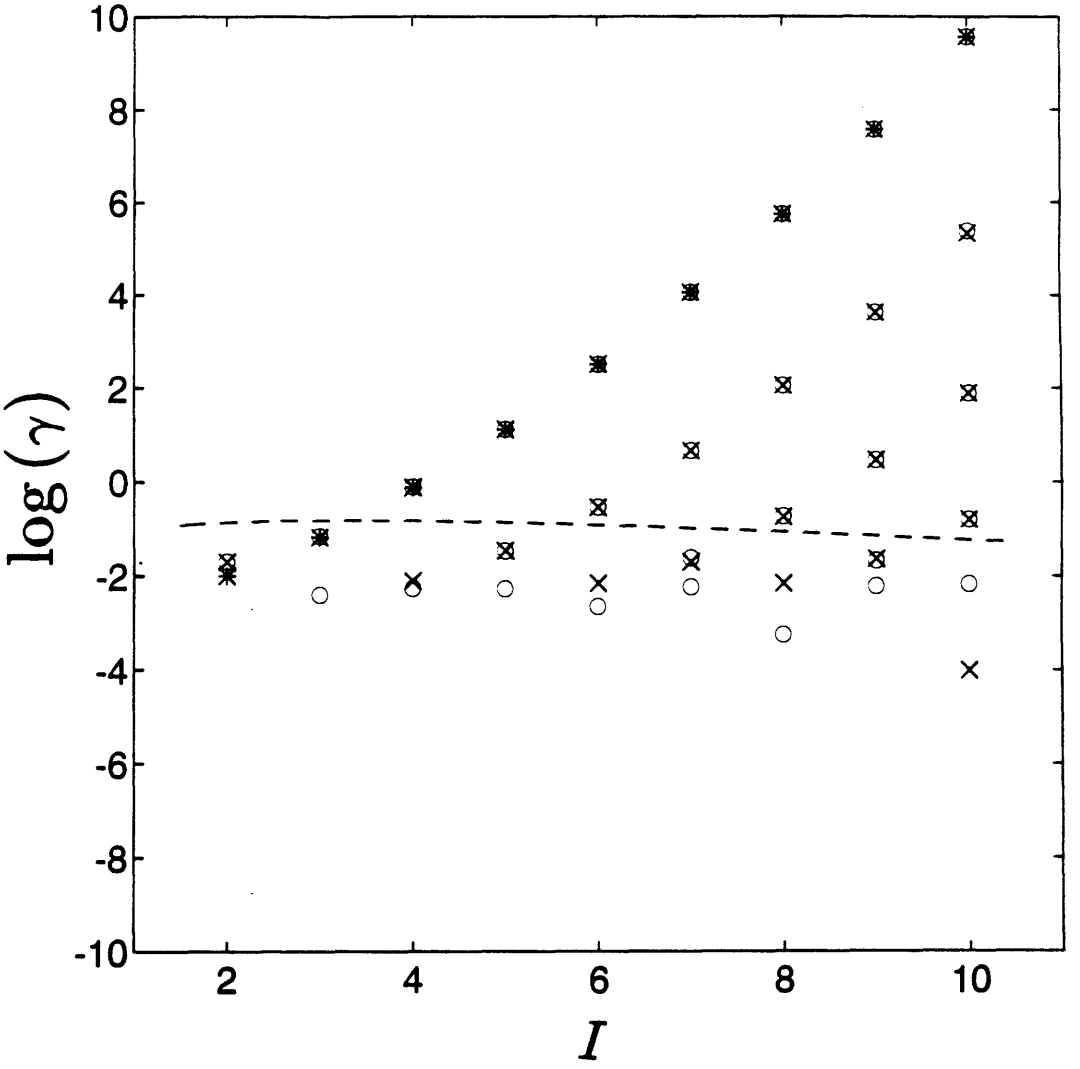

Figure 2-22: Susceptibility diagram for H_2O. The susceptibilities of symmetric eigenstates are indicated as circles (o), of antisymmetric eigenstates as crosses (x) and the estimated susceptibilities as stars (*). The critical susceptibilities are represented by the dashed line (- -).

The estimated susceptibilities are in excellent agreement with the calculated susceptibilities. From $I = 6$ the deviation from the calculated values are less than 1 %. This can be understood from the fact that the two state approximation is very good for H_2O since $\tilde{\kappa} < 1$.

As well in excellent agreement is the distinction of normal and local character states in the phase diagrams from the classical analysis. Note however, that whereas the pairing of states in the phase diagram can be solely explained from the near degeneracies in the eigenvalue spectrum, the pairing of the susceptibilities is caused by a combination of that near degeneracy *and* of the strong bias of the eigenstates along certain local character components. In the phase diagram the information concerning this bias is contained in the location of the focus of the motion, i.e. the point of intersection of the spectral parabolae with the abscissa.

Figure 2-23, Figure 2-24 show the susceptibilities for O_3, SO_2. Whereas O_3 displays high susceptibilities even for low values of I, SO_2 hardly shows significant susceptibilities up to $I = 10$. Note, that the estimate still gives the correct trend for large I. Yet it is not quite accurate, since the two state approximation is not good up to $I = 10$ since $\tilde{\kappa} > 1$. The agreement with the phase diagrams $I = 6$ is excellent.

Isotope effect Figure 2-25, Figure 2-26 compare the susceptibilities for C_2H_2 and C_2D_2. As we have already noticed earlier, there are dramatic quantitative and qualitative changes upon isotopic substitution of the hydrogen atoms in C_2H_2. Not only the frequencies of the modes, but also the stability against localization deviate dramatically. They differ up to four orders of magnitude for $I = 6$.

Evaluation of order parameters from experimental data

In order to further illustrate the relevance of the susceptibility, let us evaluate the change in the expectation of the order parameter upon variation of the strength of the perturbation ϵ over several orders of magnitude. In order to facilitate the collection of observations, let us anticipate here the notion of a bifurcation, which we will formally introduce in the following section. For reasons to become obvious then, we will call

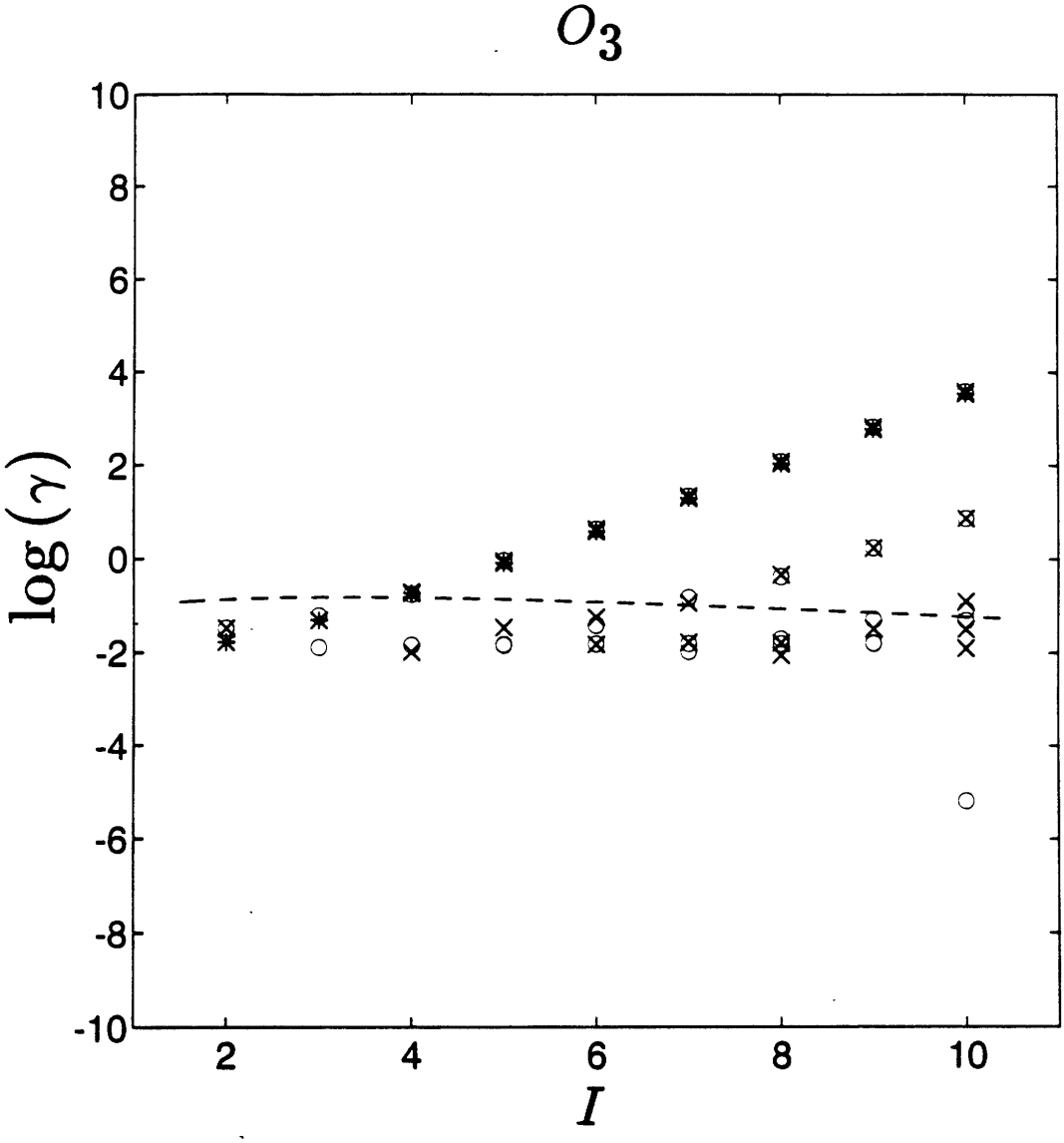

Figure 2-23: Susceptibility diagram for O_3.

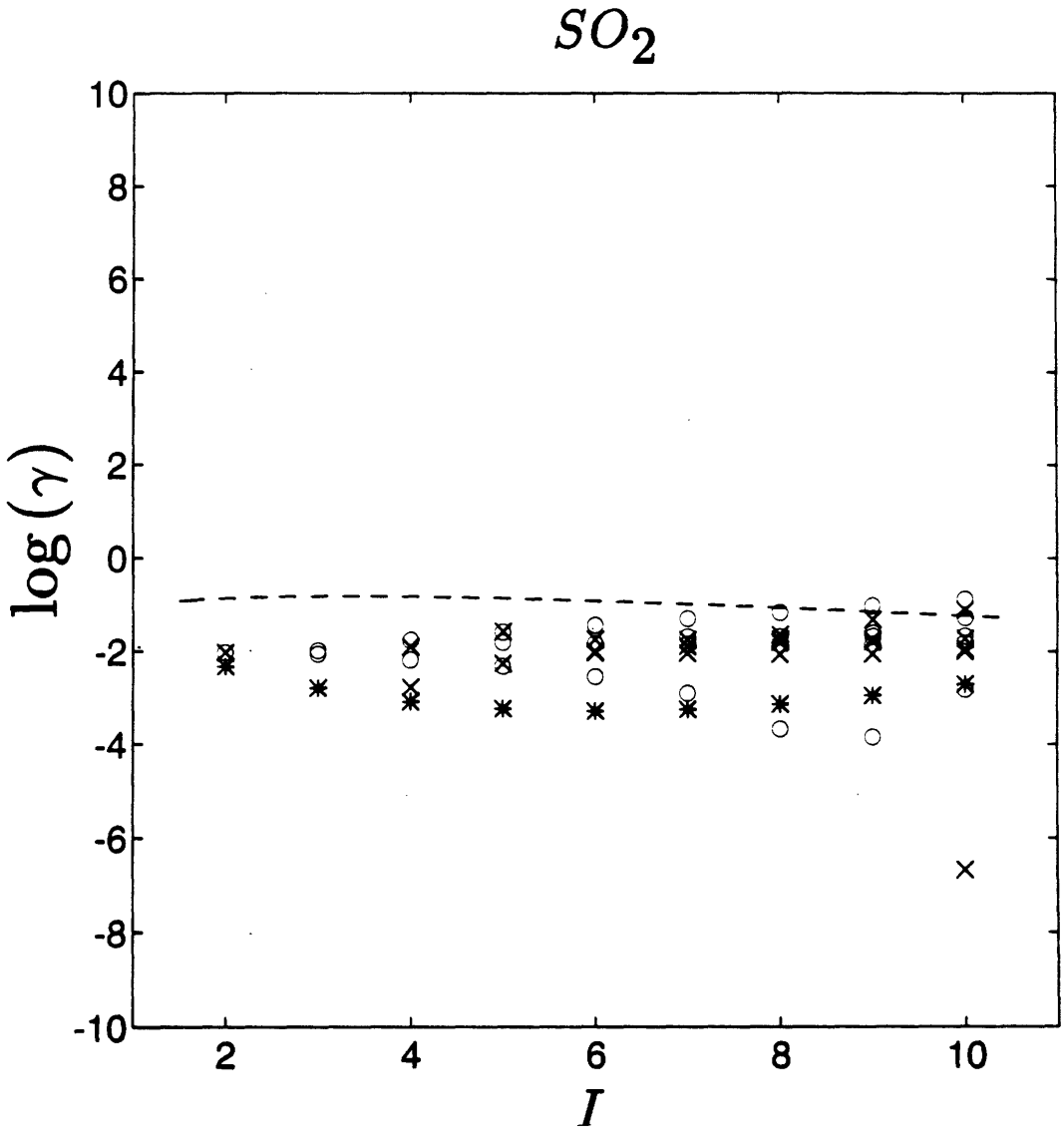

Figure 2-24: Susceptibility diagram for SO_2.

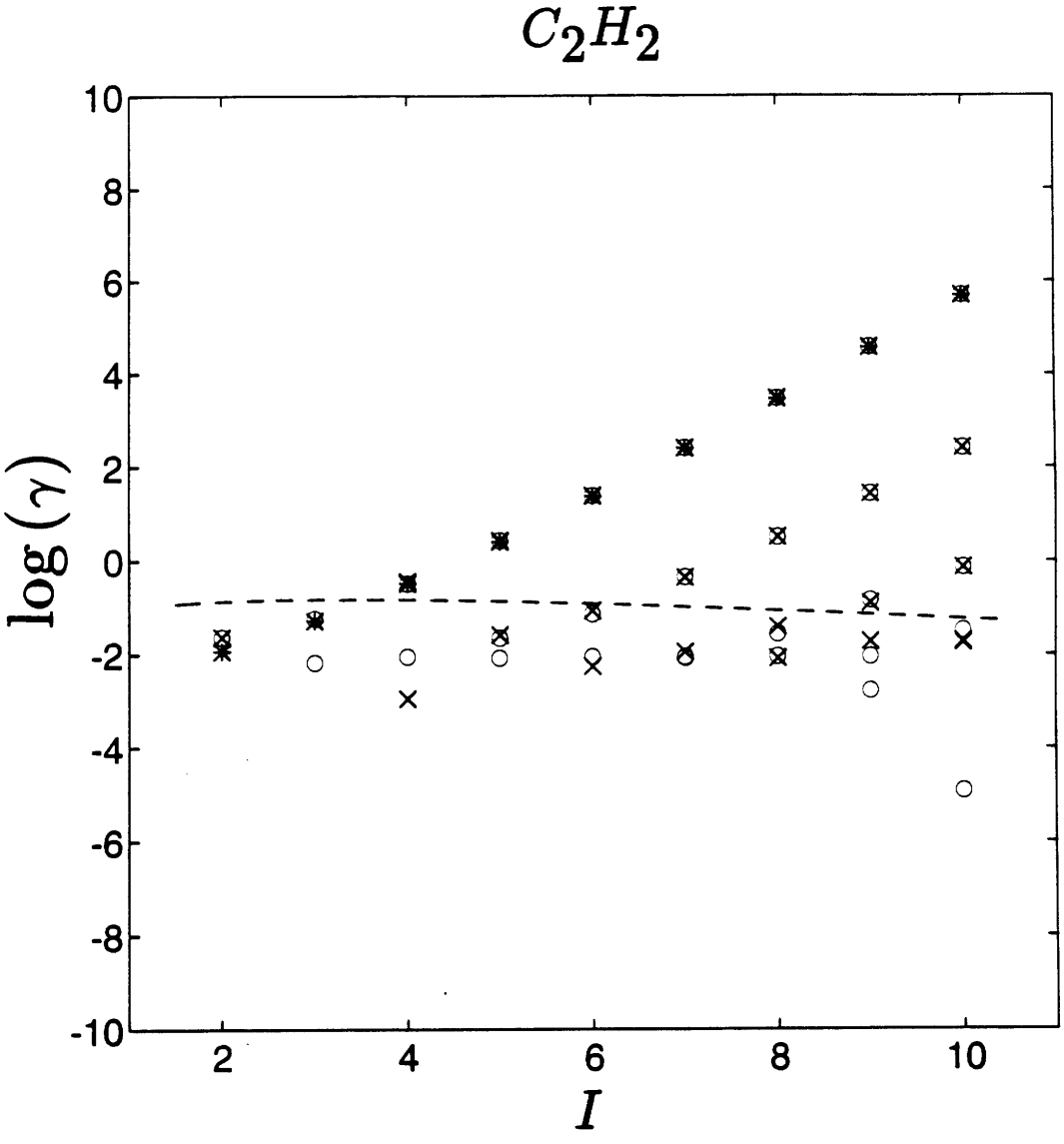

Figure 2-25: Isotope effect: Susceptibility diagram for C_2H_2.

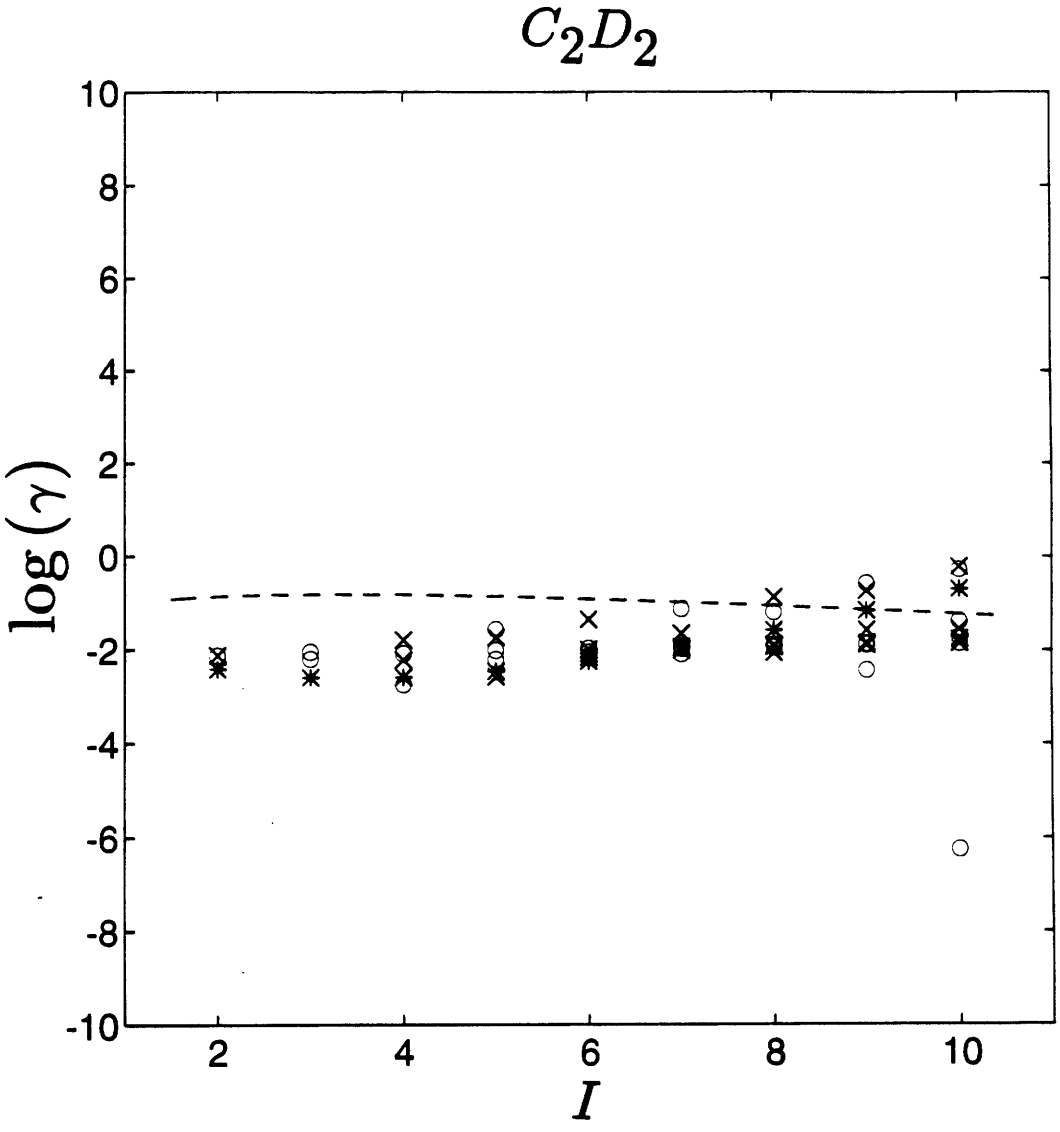

Figure 2-26: Isotope effect: Susceptibility diagram for C_2D_2.

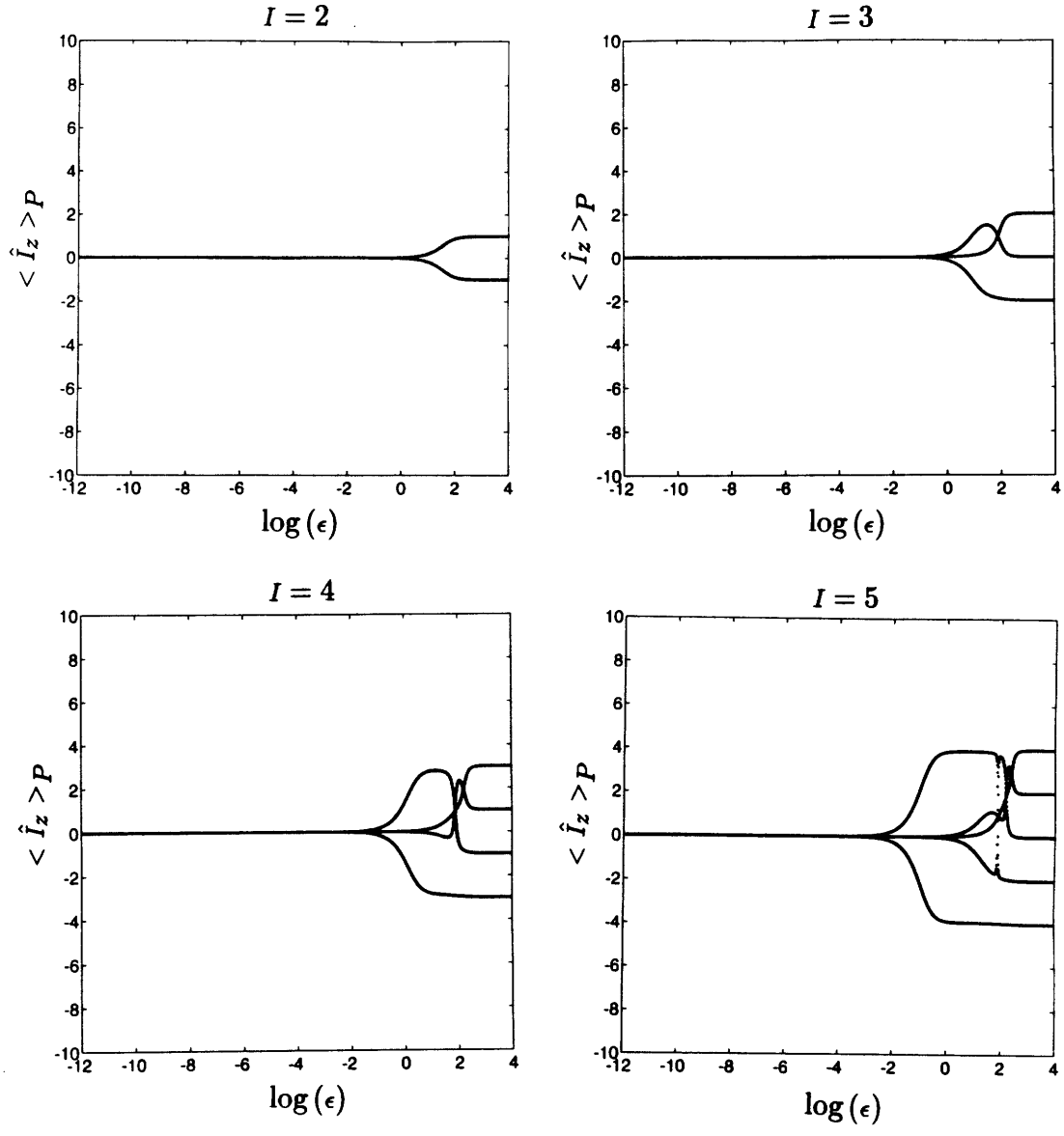

Figure 2-27: Order parameter diagrams for H_2O from $I = 2$ to $I = 5$.

the value of ϵ for which $I_{z,I,\pm,L}(\epsilon)$ has an infection point a *point of bifurcation* of the associated eigenstate.

Figure 2-27, Figure 2-28 and Figure 2-29 show the results of the exact calculation for H_2O from $I = 2$ to $I = 10$, where we plot $I_{z,I,\pm,L}$ versus the decadic logarithm of ϵ in wavenumbers.

There are four regimes to distinguish. We begin with the limiting cases.

- At perturbations $O(10^{-12})$ all states have order parameters close to zero.

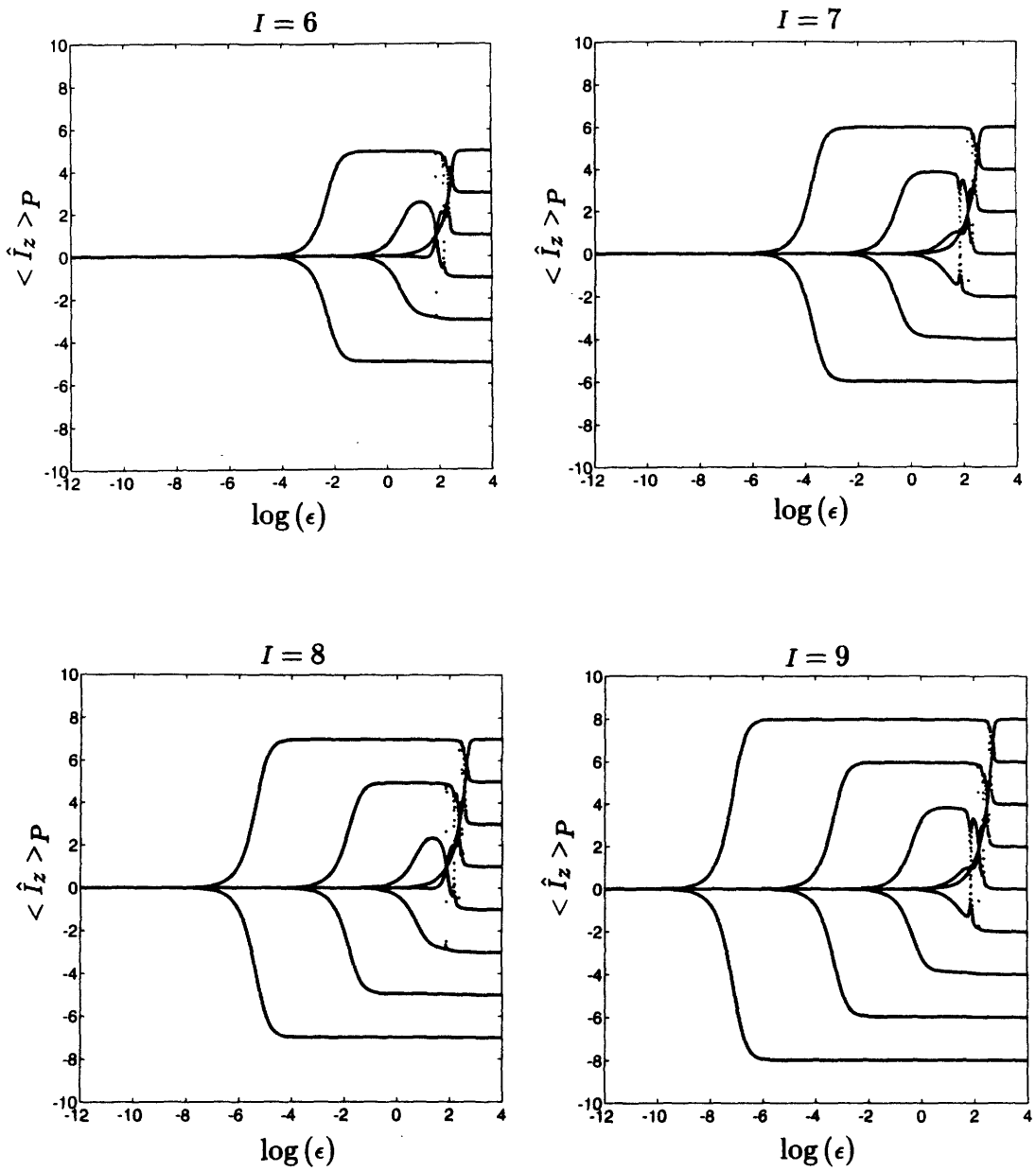

Figure 2-28: Order parameter diagrams for H_2O from $I = 6$ to $I = 9$.

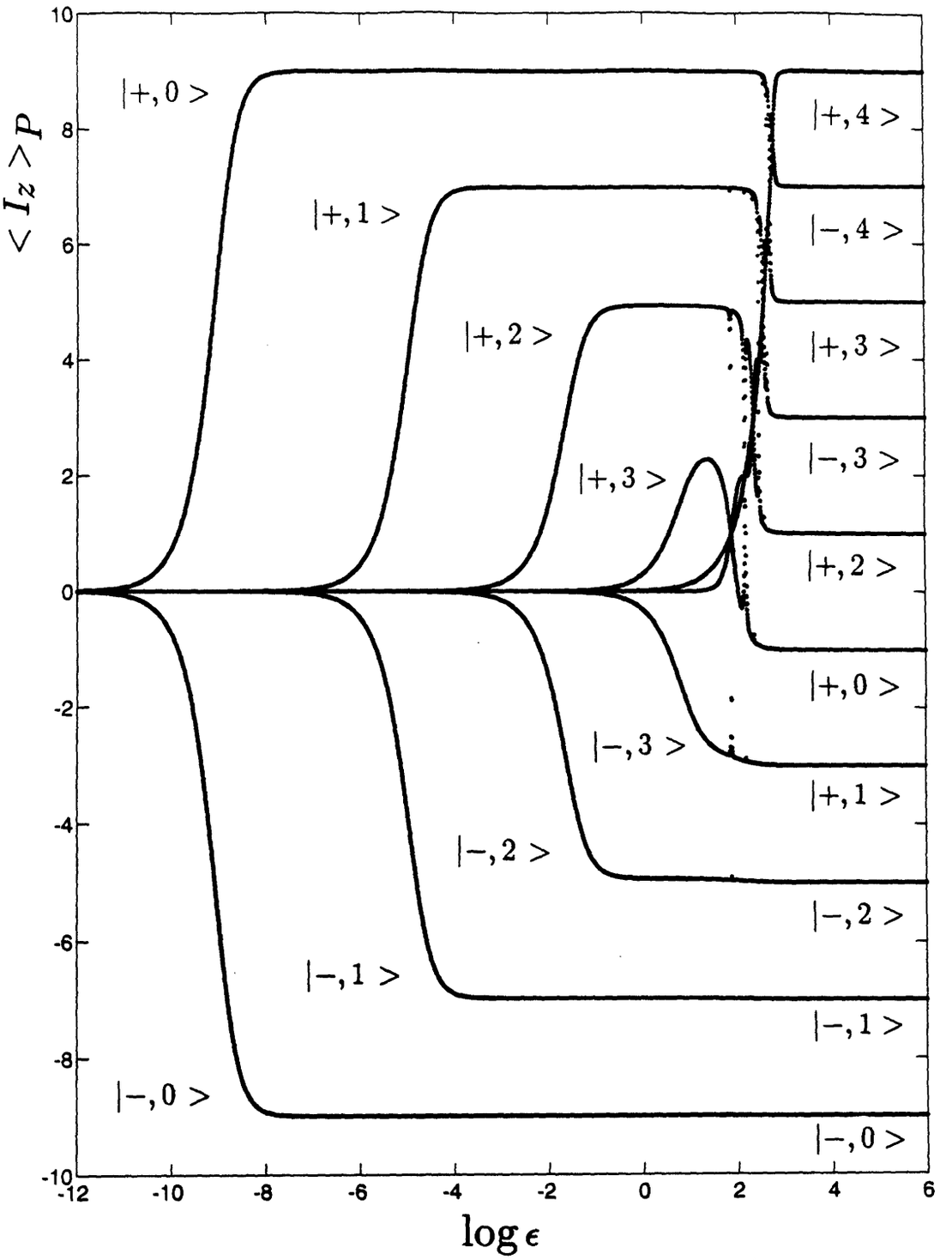

Figure 2-29: Order parameter diagram for H_2O, $I = 10$. The corresponding states $|\Psi_I, \pm, 1 >_P$ are assigned.

- At perturbations $O(10^4)$ the order parameters range from $I-1$ to $1-I$ in steps of two.

- At small intermediate values of $\log(\epsilon)$ there is a cascade of bifurcations, similar to a corn ear. The bifurcations occur in pairs. They begin with the pair $|\Psi_I, \pm, 0>$ for which $I_{z,I,\pm,0}$ is taking the maximum values $\pm(I-1)$, followed by $|\Psi_I, \pm, 1>$ yielding $\pm(I-3)$, and so on.

- At high intermediate values of $\log(\epsilon)$ several of the order parameters cross, mostly in the positive region. These crossings can be followed in detail. Figure 2-30 shows an example.

Most of the results can be directly deduced from the properties of the susceptibility plot, once the connection is established. According to the interpretation of the susceptibility being approximately the inverse of the perturbation necessary to form the associated localized eigenstate, the plot of the *negative* decadic logarithms of the susceptibilities versus I provides the approximate *bifurcation diagram.* By inspection we see that the agreement with the points of bifurcation in the order parameter plot is reasonable good. Better agreement can be achieved by considering the factor of n^2 from the estimate in eqn.(2.129).

As an example, take the bifurcation of the state $|\Psi_{10}, +, 0>$ at $\epsilon \approx 10^{-8} cm^{-1}$. From the order parameter diagram we read $\gamma_{10,+,0} \approx 10^{10} cm$. Then, according to the estimate in eqn.(2.129) the perturbation necessary to localize the excitation equals $9^2/10^{10} = 10^{-8} cm^{-1}$ which is the correct answer.

Figure 2-31 shows the order parameter for O_3 and SO_2 for $I = 6$. Whereas for O_3 there is a clear separation between the bifurcation points, for SO_2 the transition to the final values of the order parameter occurs over a broad range of ϵ almost simultaneously and without crossings. Figure reffig:14(m,n) shows the results for C_2H_2 and C_2D_2.

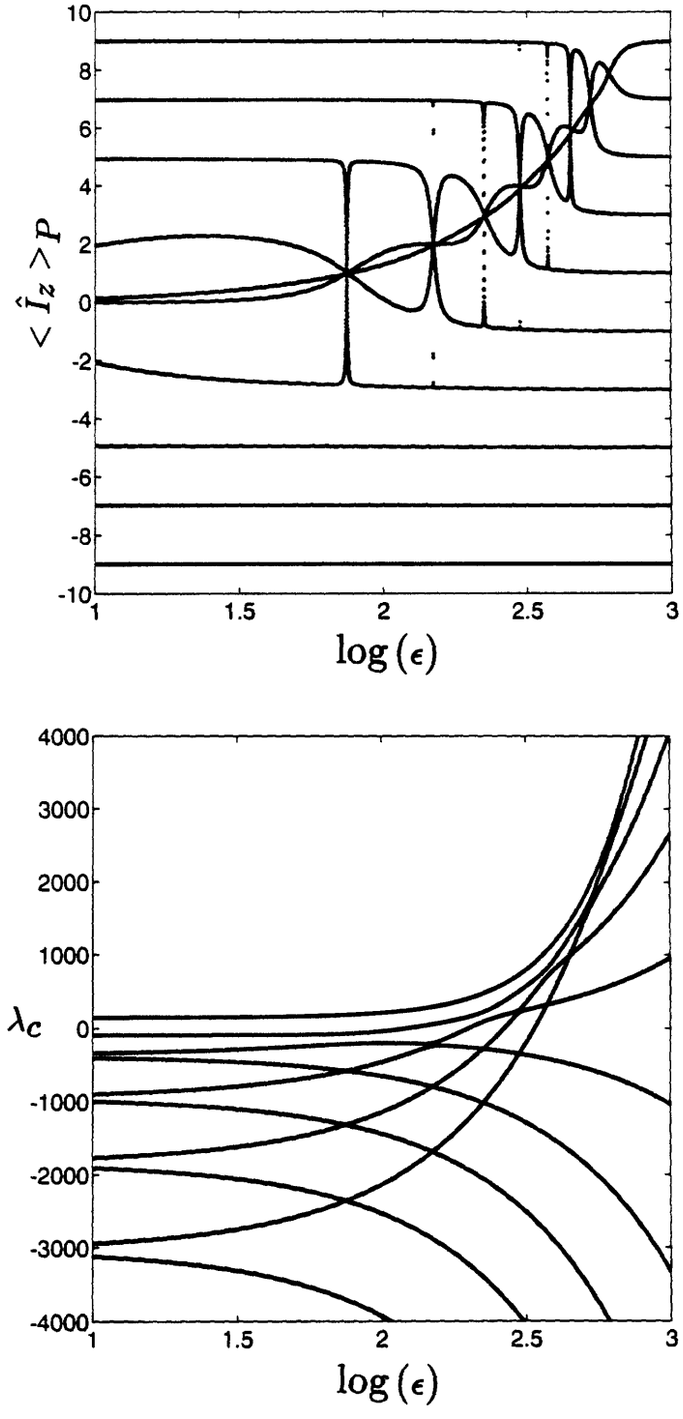

Figure 2-30: Window of order parameter diagram for H_2O, $I = 10$ and eigenvalues λ_C.

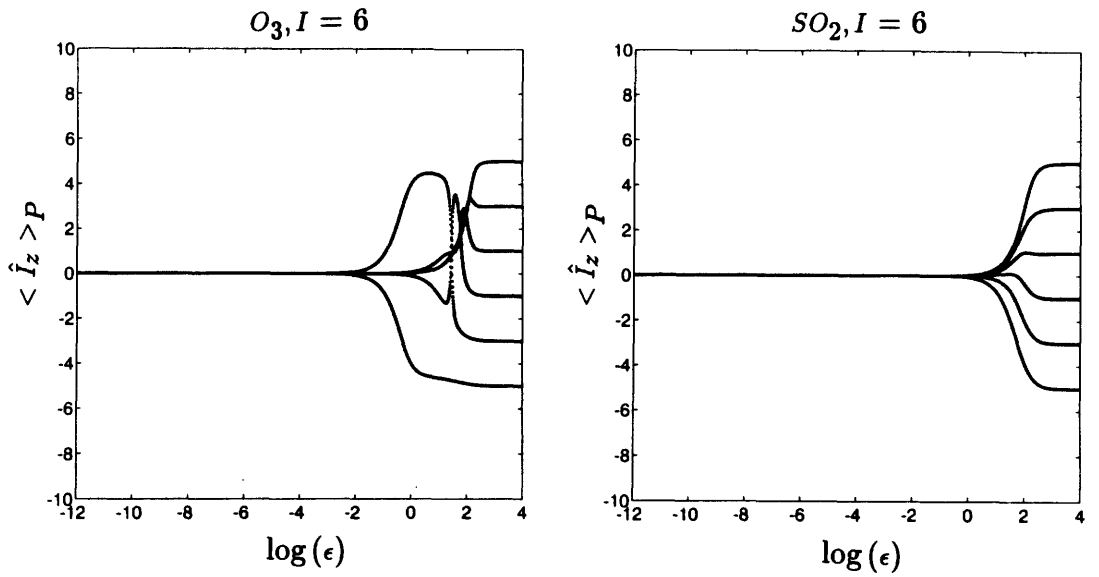

Figure 2-31: Order parameter diagrams for $O_3, SO_2,\ I = 6$.

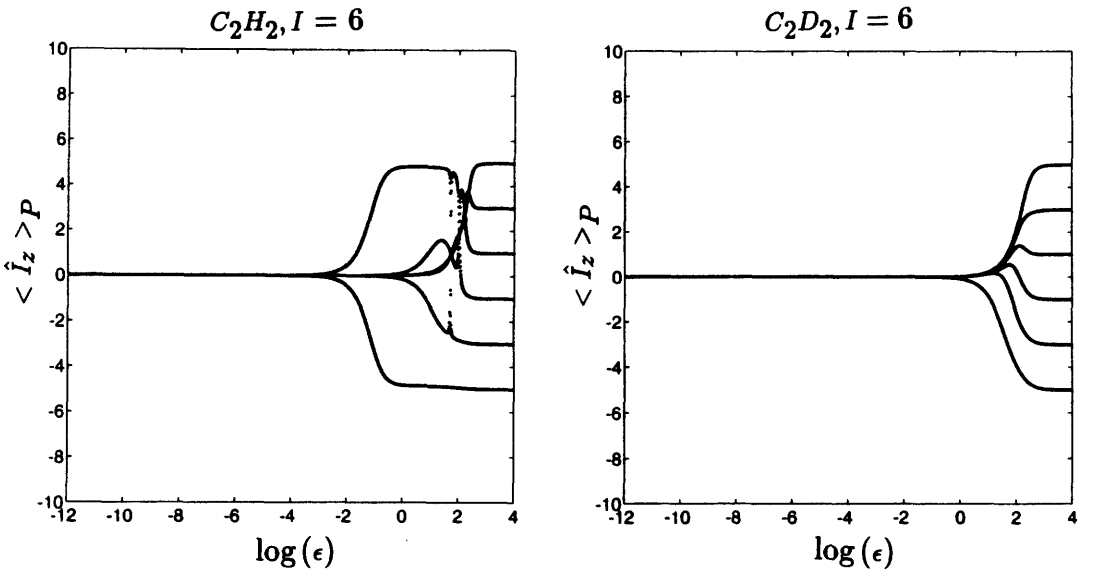

Figure 2-32: Isotope effect: order parameter diagrams for $C_2H_2, C_2D_2,\ I = 6$.

Crossing of order parameters

The crossing of order parameters can not be accounted for by the susceptibilities in the present definition.

Crossings occur when two perturbed eigenstates simultaneously undergo a bifurcation. As a result, they interchange their degree of locality.

We have investigated the crossing thoroughly and only report the results here. The crossing occurs at values of ϵ where two eigenvalues reach their minimum energetic distance. Note, that the eigenvalues repel and cannot cross.

Let us picture the effect of the slowly varying ϵ between the given limits as a rotation of the orthogonal system of eigenstates to $\hat{H}_{DD,P}$ onto the coordinate system spanned by the eigenstates to $\hat{I}_z$ with increasing magnitude of ϵ. Technically there are several possible ways to carry out successive rotations such that the two coordinate systems finally align. Yet in the studied case this path is set by the relative stabilities of the eigenstates for given ϵ. The more unstable eigenstates of local character are rotated first at small ϵ until at larger ϵ they are almost aligned with some eigenstates to $\hat{I}_z$. Then the more stable eigenstates of normal character rotate towards their final positions. However, this rotation makes it necessary for the almost aligned states to interchange their already aligned positions.

These crossings have physical relevance. In a range of ϵ, where they occur, a slight fluctuation in its value can lead to an interchange of the degree of locality of two or more eigenstates. Thus we expect a qualitative change in the dynamics of a state with nonvanishing components along one or both of these states. The order parameter can change significantly under a small variation of ϵ. This leads to a sensibility of the dynamics of one and the same state to small changes in the Hamiltonian parameter ϵ. The region of repelling eigenvalues coincides with the region of crossing order parameters. A perturbation in form of a time dependent field whose amplitude oscillates around one the values of ϵ where a crossing takes place would yield chaotic dynamics. Note that the Darling-Dennison Hamiltonian in a periodic driving field, e.g. for the periodically kicked Darling-Dennison system, is identical to

the kicked top, the epitome of quantum chaotic behavior.

2.4.5 Preliminary review of the quantum mechanical results and conclusions

The recovery of the classical bifurcation parameter κ in the modified form $\tilde{\kappa}$ implies that the classification of spectral states into states of normal and local character according to the properties of the associated classical trajectories is legitimate. The physical significance of this local/normal distinction can be understood by extending the concept of a classical bifurcation using semiclassical ideas. The same semiclassical picture hints at the intrinsic property of instability of eigenstates of the Darling-Dennison Hamiltonian under symmetry breaking perturbations. In the classical system, κ describes the global stability properties of the trajectories, while in the quantum mechanical system $\tilde{\kappa}$ describes the global stability properties of eigenstates. For each individual state the symptoms of instability can be quantified by the associated order parameter under perturbation, the extent of instability by the associated susceptibility. The susceptibilities are genuine properties of the unperturbed system. We conclude that the *classical bifurcation* can be understood as the classical correspondent of the *instability of the quantum mechanical eigenstates.*

The instability of eigenstates towards symmetry breaking perturbations is quite general and can be shown to be present in other classes of molecules, e.g. in AB_n or C_nH_n type molecules, that are also known to undergo the normal to local mode transition.

The breaking of the molecular symmetry can lead to significant changes in the physical properties. It should be possible to detect effects of dynamical symmetry breaking in condensed systems, such as for H_2O molecules in a solid matrix, where the duration and magnitude of perturbations in form of fluctuations, disorder or external stress may be sufficient. The distribution over localized eigenstates for given coupling between matrix and molecule can be determined on the basis of random matrix theory using a recently developed statistical stability criterion that will be

discussed elsewhere. Similar phenomena in molecular aggregates have been reported in other systems of coupled degrees of freedom such as Jahn-Teller systems, where the molecular distortion can be induced by mechanical stress [23].

The situation in the gas phase is delicate.

For *weakly* perturbed molecules in the gas phase we expect the effects of dynamical symmetry breaking to be insignificant since the transition rate into the states of broken symmetry decreases with increasing susceptibility. This can be seen from standard time dependent perturbation theory. Localization in the presence of a constant perturbation is significant only for times $t \sim 1/\Delta E_0^{I,\pm} = \gamma_{I,+,0}/n^2$ according to eqn.(2.129). Although a molecule could detect *miniscule* constant symmetry breaking perturbations, such as inhomogeneity in fields, by complete localization, the timescale involved would be experimentally inaccessible.

Nonetheless, a *strong* symmetry breaking perturbation, such as a large field inhomogeneity, might cause significant changes in the moment of inertia and the spin statistics of states with high susceptibility. Therefore the rotational structure of the vibrational transition changes. Similarly, in molecular collisions, interaction energies are frequently large enough, typically $O(cm^{-1})$, to allow transfer during the collision duration for the nearly degenerate susceptible states. The facile redistribution of vibrational energy during a collision should enhance the transfer rates of the highly susceptible local character levels compared to the normal character levels. To summarize the situation, a trade off between susceptibility, time of transfer and strength of applied perturbation could allow the observation of dynamical symmetry breaking in the gas phase.

2.4.6 A stability criterion for eigenstates

Three problems associated with the procedure in the previous sections remain:

- First, the choice of a specific symmetry breaking perturbation appears to be rather arbitrary and artificial. Since stability must prevail under any possible perturbation, the strategy to eliminate arbitrariness is to choose the most ef-

fective case. This requires that a chosen perturbation be shown most effective, even in cases where a particular choice seems intuitively clear. For example, in the water molecule, the most effective localizing perturbation is achieved by directly removing the symmetry through an imposed energy mismatch on the two local oscillators. Still, that most effective perturbation may be artificial in the sense that it is forbidden under the particular experimental conditions.

- Second, for more complex molecules the choice of the most effective perturbation may not be obvious, especially if there is a variety of symmetry restrictions or conservation laws for the states and processes.

- Third, even in unsymmetric systems one may observe susceptible states. This can easily be seen if one views the slightly perturbed symmetric system as the unsymmetric original to be perturbed. The most effective perturbation there will be the one that restores symmetry.

This leads directly to the issue of the stability of the eigenstates of the *perturbed* system whose susceptibilities in turn must be evaluated. If, for example, at the classical normal to local mode transition the normal modes become unstable when simultaneously the local modes become stable, does this imply that the symmetric eigenstates become unstable and simultaneously the local eigenstates become stable against any perturbation? In order to answer that question we are forced to repeat the procedure of adding a small arbitrary specific perturbation and evaluating the response Figure 2-33.

The response is going to depend on the specific choice of perturbation. In turn, it can be shown that the perturbed states are as susceptible to a symmetry restoring perturbation as the unperturbed states are to a symmetry breaking perturbation of the same magnitude. On the other hand, the perturbed states are insusceptible to the identical perturbation that produced them. Although we can define stability for the unperturbed states by the absence of instability towards any symmetry breaking perturbation we are confronted with the need to specify exactly the perturbation against which the perturbed state is unstable. The reason is that there is exactly

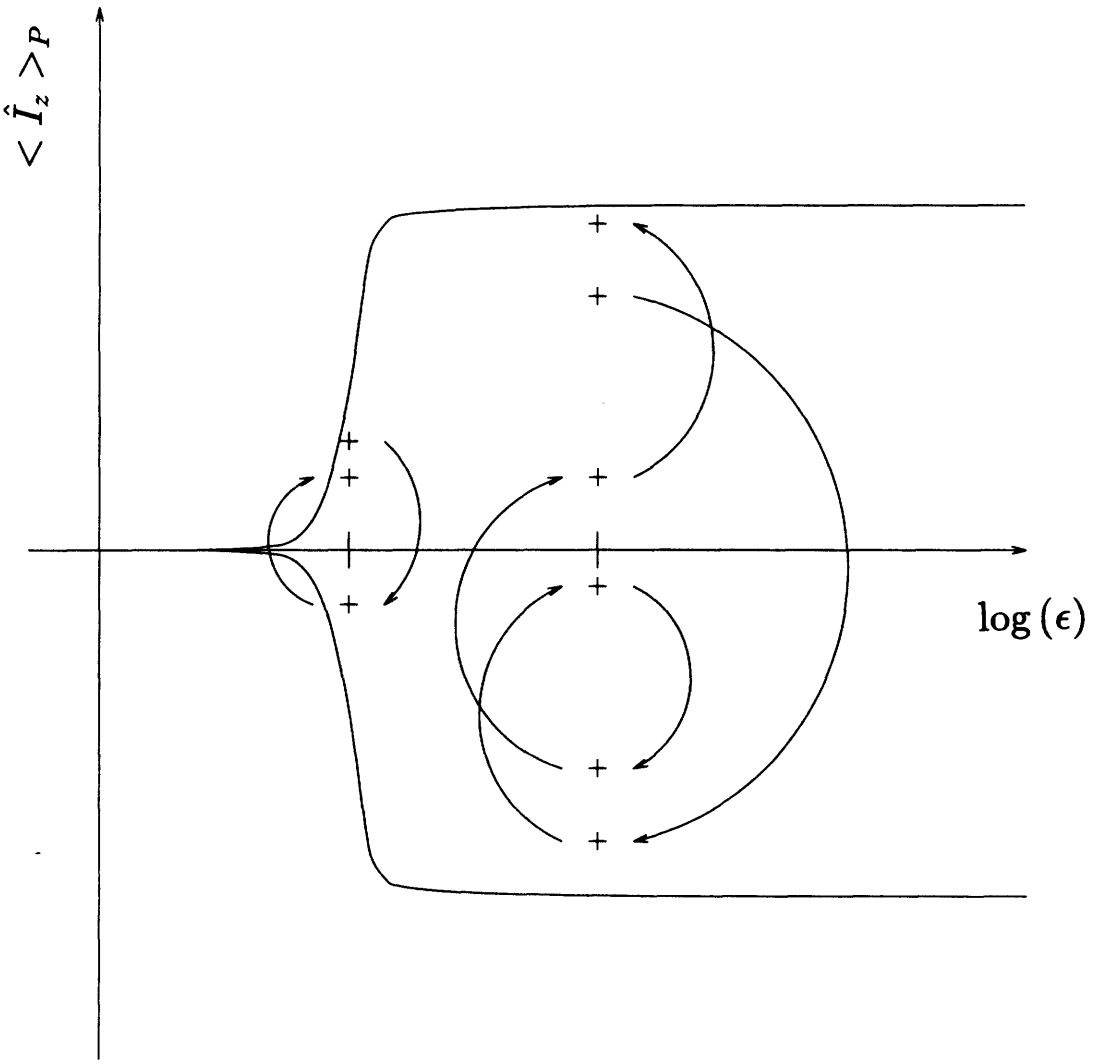

Figure 2-33: Instability of perturbed states under perturbations. Shown is an order parameter diagram. The solid line indicates the order parameter for a pair of eigenstates with respect to the $\hat{I}_z$ perturbation. The crosses (+) indicate the order parameter for one of those eigenstates under successive randomly chosen perturbations for the same magnitude of perturbation. For a large number of successive perturbations one can obtain by a simple counting scheme the distribution of the order parameters.

one type of perturbation that restores symmetry whereas there are many more that break symmetry originally. Therefore, though tempting, we cannot call a perturbed state stable when the unperturbed state becomes unstable in the same above defined sense. What is the proper way to define stability for quantum states? The following change in the point of view promises a solution. Instead of successively perturbing a particular state several times, we look for the ensemble of perturbations that generates the same individual results when directly applied to the unperturbed state. Thus we neglect the history of a particular perturbed state and obtain an ensemble of directly perturbed states that does not change under further perturbation.

In this section we propose a solution to the three problems by proceeding as follows. Beginning with a brief introduction to the eigenvalue problem of the Darling-Dennison Hamiltonian for triatomic AB_2 molecules of symmetry C_{2v}, we formally develop a local stability criterion for the normal to local character transition in those molecules on the basis of random matrix theory. According to the discussion above it seems cumbersome to define stability of a single state in terms of an individual response to a specific perturbation of given magnitude. In contrast, *we define stability of an ensemble of eigenstates in terms of the statistics of its response to an ensemble of random perturbations of given magnitude.* This definition is born from the physical picture of an ensemble of molecules interacting with an inhomogeneous environment. Then we carry out the stability analysis explicitly for triatomic molecules AB_2 of symmetry C_{2v} and show that in particular for the water molecule the individual response to the *most effective specific* perturbation almost coincides with the *most probable* response to an *ensemble of random* perturbations for the same magnitude of perturbation. For more complex molecules this suggests the use of an ensemble of random perturbations in order to *find* a very effective perturbation for detecting susceptible states. On the basis of the analytical and numerical results presented in this and previous sections we propose a generalization of the local stability criterion to other classes of symmetric and non-symmetric molecules. Stability properties are assigned to the *ensemble* of perturbed eigenstates that is *invariant* under an ensemble of random perturbations.

Stability under randomly occurring perturbations

We now turn to the construction of the local stability criterion for an ensemble of eigenstates to $\hat{H}_{DD}$ under an ensemble of random perturbations. Instead of the perturbation $\hat{I}_z$, we now impose an arbitrary perturbation to $\hat{H}_{DD}$ in the form of a random operator $\hat{G}$, which is an element of an ensemble of random operators to be determined in the following. In analogy to eqn.(2.120) we write for the perturbed Darling-Dennison Hamiltonian

$$\hat{H}_{DD,P} = \hat{H}_{DD} + \epsilon\hat{G}. \tag{2.131}$$

Let us choose as a basis for the representation of $\hat{G}$ the basis of eigenstates $|\Psi_I, \pm, L>$ of the unperturbed Hamiltonian $\hat{H}_{DD}$. This defines the square random matrix $\mathbf{G} = \{< \Psi'_I, \pm', L'|\hat{G}|\Psi_I, \pm, L >\}$. Let us assume the matrix elements of $\mathbf{G}$ to be independent identically distributed random variables subject to certain additional restrictions. These restrictions may arise from conservation laws or symmetry requirements.

The specific perturbation $\hat{I}_z$ is contained in the ensemble of random operators $\hat{G}$. Since we want to use the same magnitude ϵ for both the most effective and any other random perturbation, let us normalize $\mathbf{G}$ such that the largest matrix element is of magnitude $I-1$ which equals the magnitude of the largest matrix element in $\mathbf{I}_{z,I}$.

We are interested in the case of intermediate I and small $\epsilon \ll \zeta$, i.e. small perturbations at intermediate levels of excitation. In this region of parameters we do not expect significant changes in the spectrum due to $\mathbf{G}$. However, we do expect significant changes in the locality properties of the eigenstates.

Let us impose the following additional restrictions on the ensemble of random matrices $\mathbf{G}$. First, let us make the approximation that I is conserved, i.e. due to the large energy differences between different polyads for intermediate I only states within the same polyad are mixed appreciably by the weak perturbation. Therefore we may assume $\mathbf{G}$ to be diagonal in blocks $\mathbf{G}_I$ of size I. Second, let us impose the condition that the statistical properties of $\mathbf{G}_I$ are invariant under the similarity transformation that diagonalizes $\mathbf{H}^I_{DD}$. Since the blocks $\mathbf{H}^I_{DD}$ are real symmetric

matrices the transformation in question must be orthogonal. Therefore the ensemble of random matrices $\mathbf{G}$ is given by the Gaussian orthogonal ensemble (GOE) known from nuclear physics [25].

Let us recapitulate the properties of $\mathbf{G} \in$ GOE so far. The matrix representation consists of real symmetric blocks of size I with independent identically distributed matrix elements normalized such that the largest entry is of magnitude $I - 1$; they are similar under orthogonal transformations.

Note that the symmetry properties of a particular molecular system or physical process may cause these restrictions to be modified and that neither the perturbation $\hat{I}_z$ nor any single other member of the GOE is necessarily invariant under the orthogonal transformation that diagonalizes $\hat{H}_{DD}$.

Numerical evidence

Let us stop for a moment in the formal development in order to establish the connection between the effects of $\hat{I}_z$ and $\hat{G}$ on the eigenstates of $\hat{H}_{DD}$. Figure 2-34, Figure 2-35 and Figure 2-36 show the order parameter for H_2O evaluated at 3000 intermediate values of ϵ for randomly generated $\hat{G}$ from $I = 2$ to $I = 10$.

Instead of a continuous function $I_z(\epsilon)$ we have to deal now with a distribution over I_z at given ϵ. Yet, it is easy to see that the regions of high density of points coincide with the curves $I_z(\epsilon)$ calculated from eqn.(2.120). As claimed, they represent the worst effective case. They embrace regions of lower density of points at smaller I_z for low values of ϵ. At large values of ϵ they form a distribution concentrated around $I_z = 0$ which is identical to the distribution of order parameters for the GOE. The bifurcation cascade is also reproduced, whereas the crossing of order parameters can not be seen.

In popular terms we state that, once the magnitude of the perturbation exceeds the inverse susceptibility of an eigenstate, it ends up being more or less localized. We conclude, that it was in fact sufficient to use the perturbation $\hat{I}_z$ to demonstrate *instability* of eigenstates $|\Psi_I, \pm, L >$ to $\hat{H}_{DD}$ towards *any* perturbation. The numerical calculation also tells us how to understand the *stability* of the now localized eigenstates

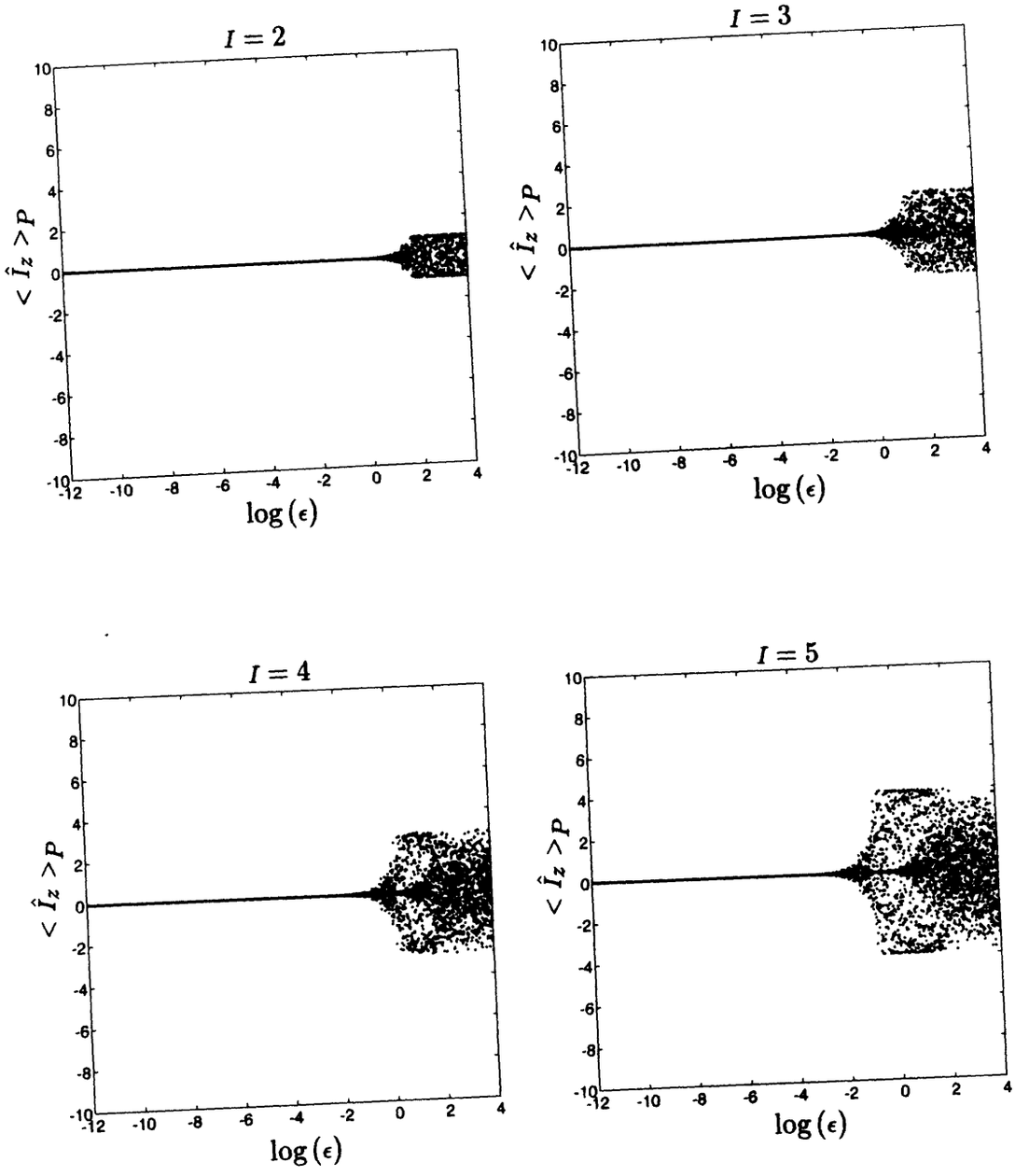

Figure 2-34: Order parameter diagrams for H_2O under random perturbations from $I = 2$ to $I = 5$. Each dot (.) indicates the response of an eigenstate to a randomly chosen perturbation of magnitude ϵ.

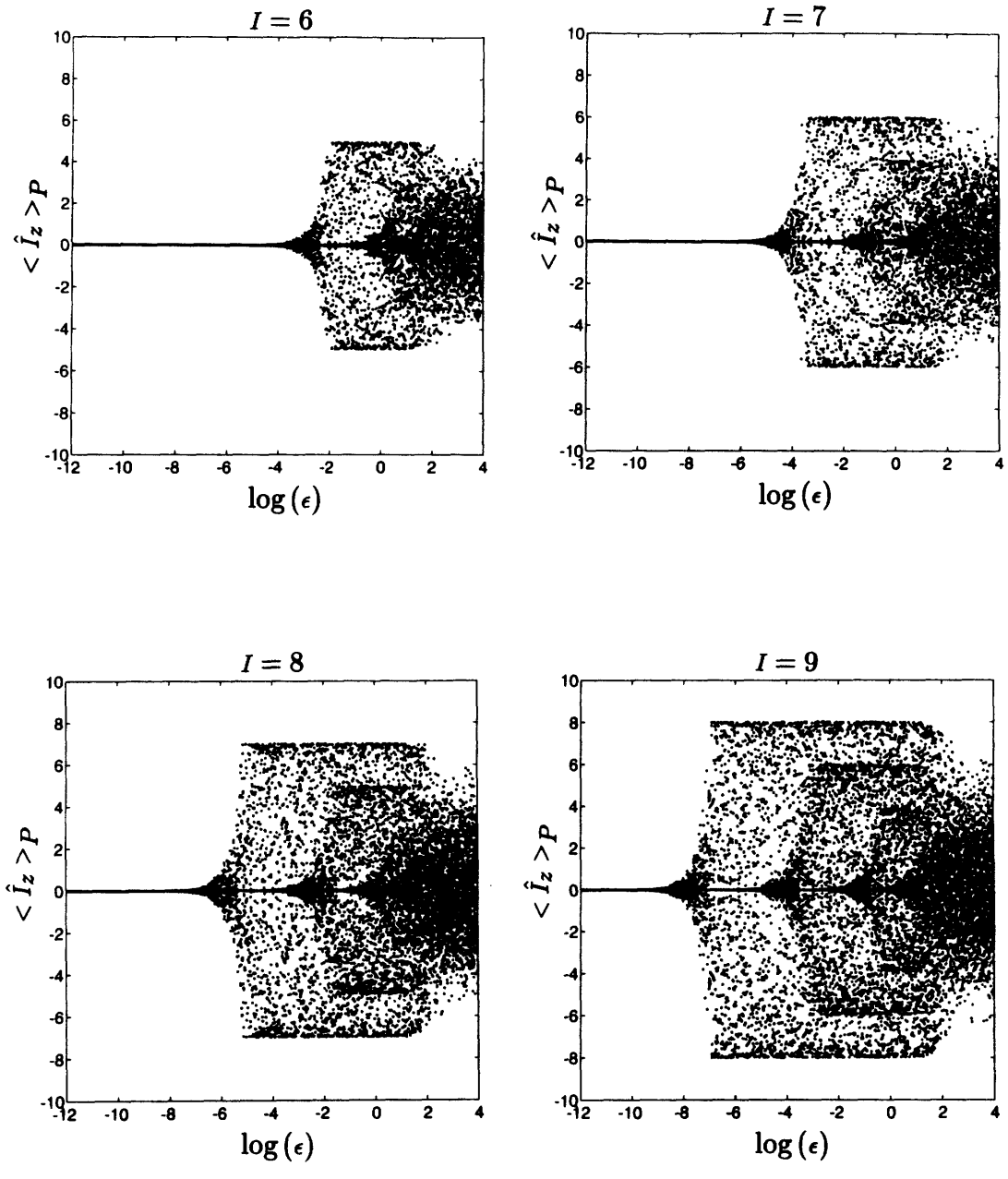

Figure 2-35: Order parameter diagrams for H_2O under random perturbations from $I = 6$ to $I = 9$. Each dot (.) indicates the response of an eigenstate to a randomly chosen perturbation of magnitude ϵ.

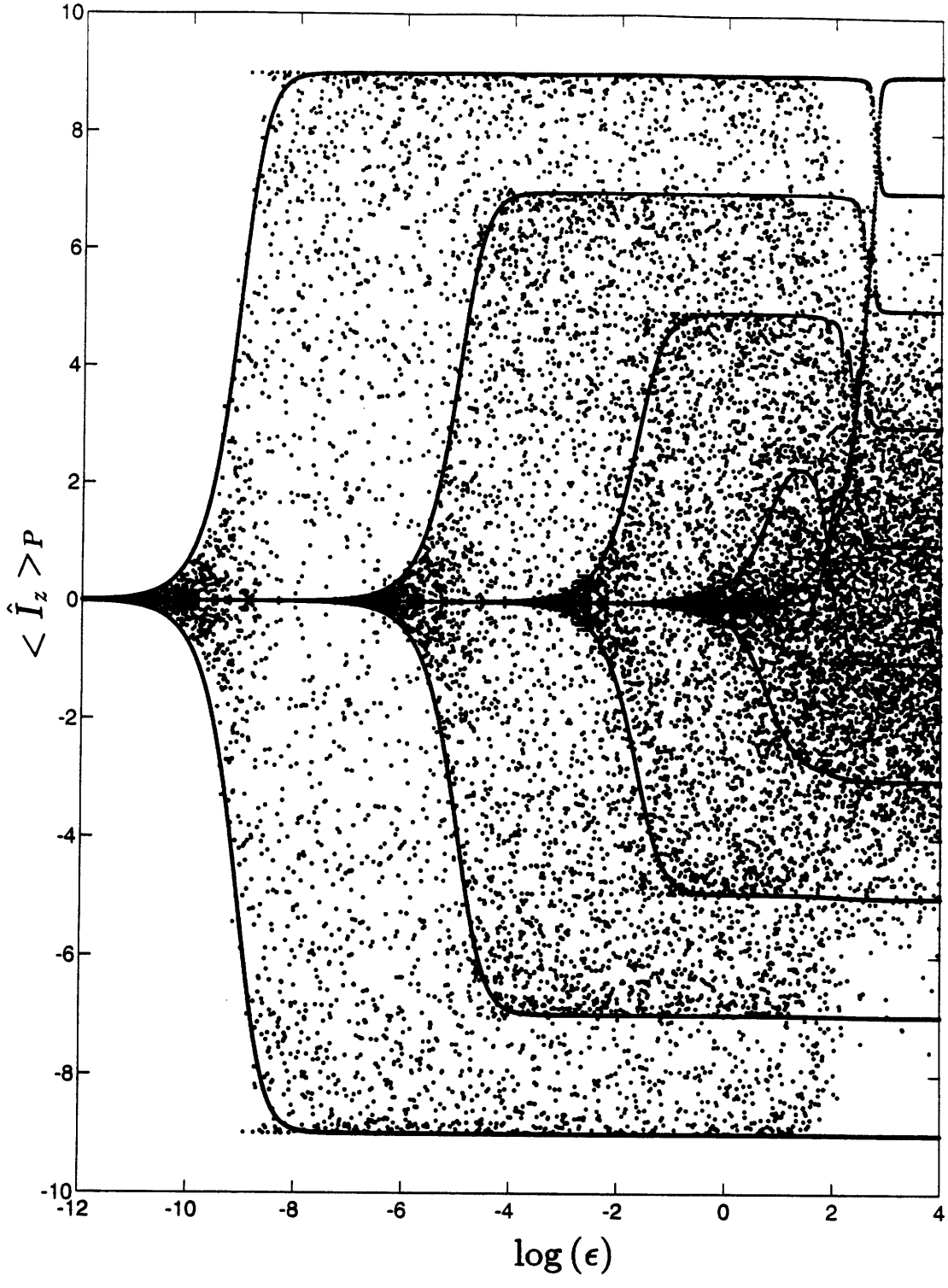

Figure 2-36: Order parameter diagrams for H_2O under random perturbations, $I = 10$. Each dot (.) indicates the response of an eigenstate to a randomly chosen perturbation of magnitude ϵ. Superimposed is the order parameter diagram under $\hat{I}_z$ perturbation.

$|\Psi_I, \pm, L >_P$ to $\hat{H}_{DD,P}$ just by quantifying the *more or less* of localization.

A stability criterion

Let us therefore return to the formal development.

We retain the definitions for the order parameter in eqn. (2.121) and for the susceptibility in eqn.(2.122) for the GOE perturbations. We are interested in reasonably small $\epsilon \ll \zeta$. For this region, only the eigenstates $|\Psi_I, \pm, 0 >_P$ can be completely localized to give $|I_{z,I,\pm,L}| = I - 1$, and the others only to a certain fraction of $I - 1$. Therefore we define the relative degree of locality $\Lambda_{I,\pm,L}$ of a state $|\Psi_I, \pm, L >_P$ by

$$\begin{aligned} \Lambda_{I,\pm,L} &= \frac{|I_{z,I,\pm,L}|}{I - (2L+1)}, \\ 1 &\geq \Lambda_{I,\pm,L} \geq 0, \end{aligned} \tag{2.132}$$

which takes the value $\Lambda_{I,\pm,L} = 1$ for maximum possible localization and $\Lambda_{I,\pm,L} = 0$ for maximum possible delocalization.

Now we can define a statistical measure of the relative degree of locality under an ensemble of random perturbations of given magnitude as follows.

Let $P_{\epsilon,I,\pm,L}(\Lambda|u \geq \Lambda \geq l)$ be the probability that, given a GOE perturbation of magnitude ϵ, the eigenstate $|\Psi_I, \pm, L >_P$ to $\hat{H}_{DD,P}$ has a relative degree of locality $\Lambda_{I,\pm,L}$ between the lower limit $\Lambda_{I,\pm,L} = l$ and the upper limit $\Lambda_{I,\pm,L} = u$, $1 \geq u \geq l \geq 0$.

The density function $P_{\epsilon,I,\pm,L}(\Lambda|u \geq \Lambda \geq l)$ is accessible through a simple numerical scheme. In this way we propose a local *stability criterion* for the transition from states of normal character to states of local character.

At given ϵ an ensemble of eigenstates $|\Psi_I, \pm, L >_P$ is stable local if $P_{\epsilon,I,\pm,L}(\Lambda|1 \geq \Lambda > 0.5) > 0.5$, stable normal if $P_{\epsilon,I,\pm,L}(\Lambda|1 \geq \Lambda > 0.5) < 0.5$ and neutrally stable if $P_{\epsilon,I,\pm,L}(\Lambda^{rel}|1 \geq \Lambda > 0.5) = 0.5$. A point of bifurcation for an eigenstate is given by the value of ϵ for which a change in stability occurs.

Discussion of the stability criterion

The construction given above appears to be rather technical. In the following we comment on it and explore its physical content.

The origin and action of the random operator $\hat{G}$ that perturbs the Hamiltonian $\hat{H}_{DD}$ can be justified and interpreted in many ways.

- For small (I, ϵ), $\hat{G}$ may reflect scattering processes between states mediated by weak coupling of the molecule to an inhomogeneous environment.

- For large (I, ϵ), the interaction between states of the isolated molecule may be so complex that the eigenvalues of $\hat{G}$ describe the spectrum to good approximation. That region is commonly referred to as the chaotic region of the spectrum.

- Similarly, $\hat{G}$ may also account in some way for the uncertainty in the Hamiltonian parameters that are obtained from fits to experimental spectra owing to perturbations by coupling mechanisms not explicitly included. From this point of view it seems reasonable to check the stability of any eigenstate calculation based on an approximate algebraic Hamiltonians.

The resulting ensemble of Hamiltonians $\hat{H}_{DD,P}$ generates for each given ϵ an ensemble of eigenstates $|\Psi_I, \pm, L >_P$ that is invariant under GOE perturbations. Therefore it is possible to assign to that ensemble of states properties that do not require further specification of the applied perturbation. A property of interest for the normal to local character transition in AB_2 molecules with C_{2v} symmetry is the degree of locality of a vibrational excitation defined by eqn.(2.132). The distribution of the degree of locality over the ensemble of perturbed states is obtained by equally weighting the response to each single $\hat{G}$. If more than half of the ensemble of perturbed eigenstates show localization of vibrational excitation to more than half of the possible degrees, it is reasonable to call that ensemble stable local. Whereas for the classical correspondent we are certain that the local modes become stable when the normal modes become unstable, for the underlying quantum system at that particular magnitude of perturbation we expect only that a particular state be more localized than delocal-

ized. Note that probabilistic concepts enter the picture in two ways. First, via the probabilistic interpretation of the quantum mechanical expectation value and second, via the expectation value over the response to an ensemble of random perturbations under some probability weight which we chose to be the same for all responses.

Let us establish by example the connection between the effects of the supposedly most effective perturbation $\hat{I}_z$ and the random perturbations $\hat{G}$ on the eigenstates of $\hat{H}_{DD}$. The calculation of the order parameter diagram for perturbation by $\hat{I}_z$ is straightforward. For GOE perturbations we implemented the following numerical scheme for $H_2O, I = 10, -12 \leq log(\epsilon) \leq 4$ to obtain the density function $P_{\epsilon,10,\pm,L}$. The logarithmic scale of ϵ is divided in 49 equal parts and the order parameter evaluated at each of the 50 points for 10^4 successively generated random perturbations $\mathbf{G}_{10} \in$ GOE. The range of the order parameter $|I_{z,10,\pm,L}| \leq 9$ is divided into 51 equal intervals and the number of calculated order parameters within each interval counted. The probabilities are obtained by normalization of those counts by the total number of counts for given ϵ. Using counting statistics as a rule of thumb we estimate the accuracy of the probabilities to be $1/\sqrt{10^4} = 0.01$. For the purpose of compact representation the results $P_{\epsilon,10,\pm,L}$ were combined into the distribution $P_{\epsilon,10}$ for all eigenstates $I = 10$ and further normalized to one. The result is shown in Figure 2-37.

Let us briefly summarize the main features.

- First of all, we notice for small ϵ the dominant peak in $P_{\epsilon,10}$ around $I_{z,10,\pm,L} = 0$. This peak represents all counts of states for which $I_{z,10,\pm,L} \leq 0.18$. Its value decreases from 1 for the unperturbed ensemble in discrete steps of approximately 0.2. This corresponds to successive pairs of eigenstates $|\Psi_1 0, \pm, 0 >_P$, $|\Psi_1 0, \pm, 1 >_P$, $|\Psi_1 0, \pm, 2 >_P$, ... becoming localized to more than 2% of the absolute possible value $I_{z,10,\pm,L} = 9$.

- Second, we see that at $\Lambda_{10,\pm,L} \approx 1$, for each state maxima in $P_{\epsilon,10}$ develop. After a cascade of four decreases in the center peak, the dominant peak and the outer maxima disappear and a broad distribution with a single maximum at $I_{z,10,\pm,L} = 0$ forms. For each state the contour line of maximal height has

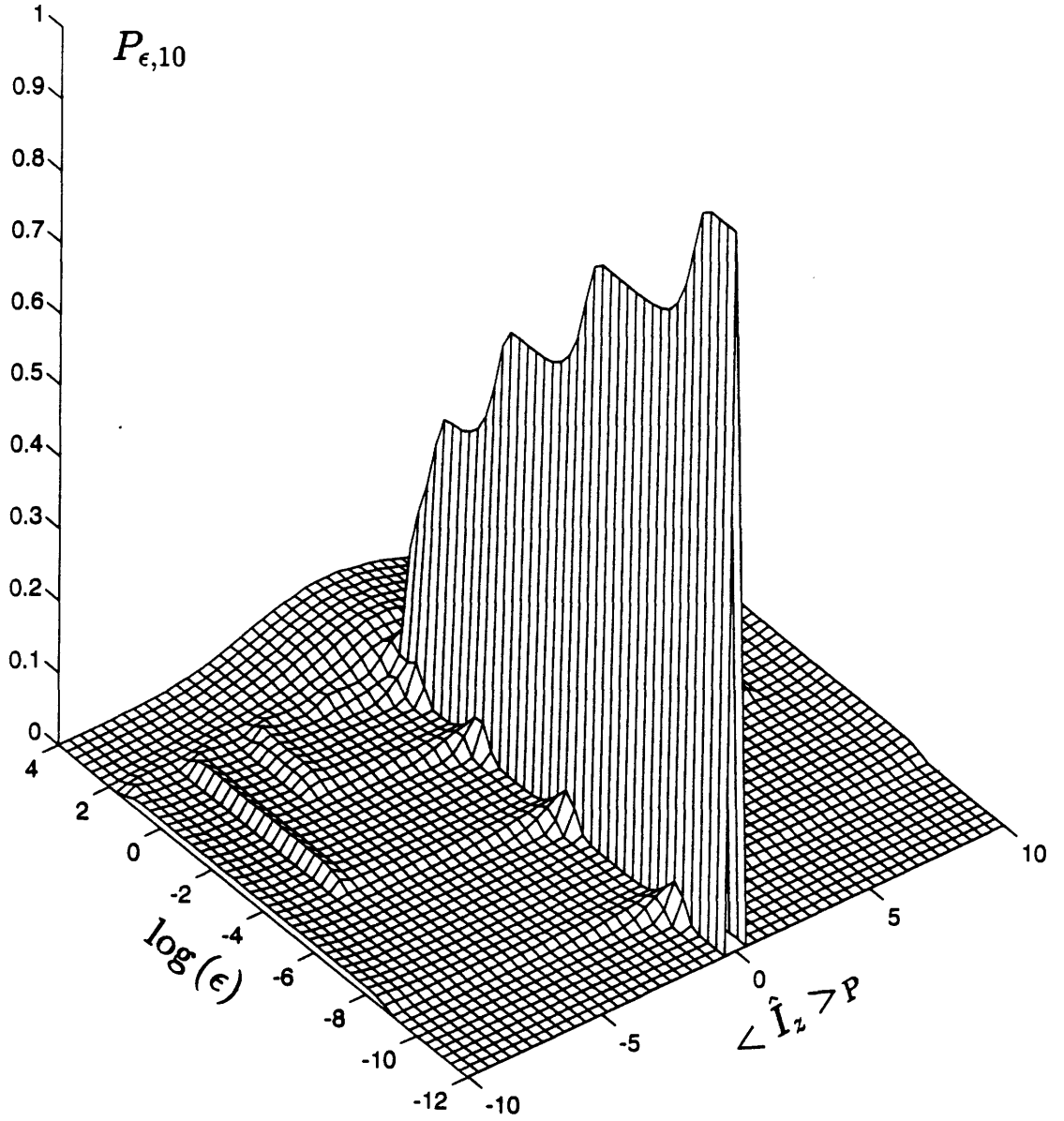

Figure 2-37: Probability distribution $P_{\epsilon,10}$ for H_2O. For explanation see text.

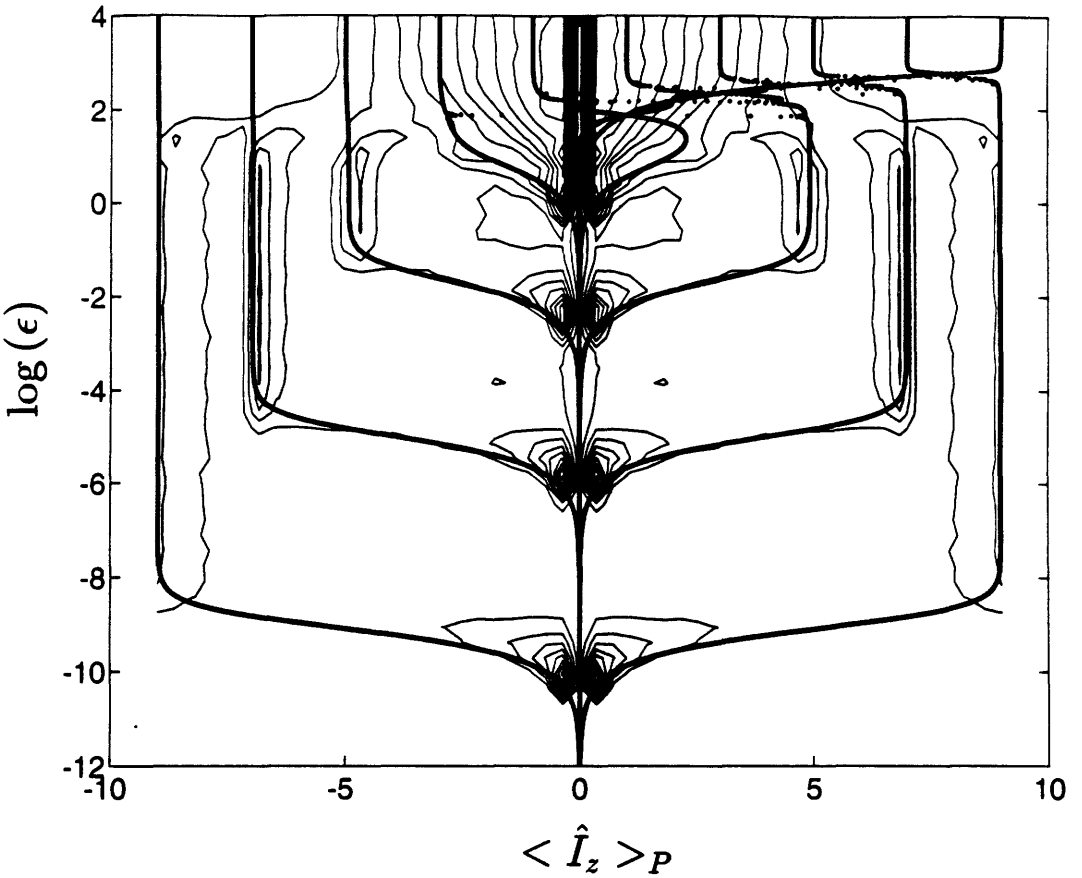

Figure 2-38: Contour of probability distribution $P_{\epsilon,10}$ for H_2O (indicated as thin lines), superimposed by the order parameters under $\hat{I}_z$ perturbation (indicated as thick line). For explanation see text.

a sigmoid shape and indicates the single most probable response to a random perturbation. This can be more clearly seen form the contour plot in Figure 2-38. Over a certain region of ϵ the single most probable response changes from almost no locality to almost total locality, i.e. a qualitative change in the stability properties occurs. The notion of a bifurcation point has been attached to the value of ϵ_{bif} where the expectation of locality is larger than one half.

Figure 2-38 shows the contour plot of $P_{\epsilon,10}$ on which is superimposed the order parameter plot for the $\hat{I}_z$ perturbation. We see that the contours of maximal height almost coincide with the the order parameter for the systematic perturbation after the bifurcation. From the graph we see that the bifurcation point coincides in good approximation with the point of inflection of the sigmoid given by the top contour.

Since the most probable single response lags behind the response to that particular single systematic perturbation, it is reasonable to call this perturbation more effective than the average perturbation. Since it causes the maximum possible localization at larger values of ϵ, we may call it the most effective perturbation.

The surprising aspect is that the most probable response and the largest possible response are so close. The reason can be outlined as follows. Consider the projection of any GOE perturbation onto the $\hat{I}_z$ perturbation. Let us assume for the sake of argument that the magnitude θ of the projection is uniformly distributed between 0 and 1, i.e. $\epsilon\hat{G} = \epsilon\theta\hat{I}_z + \epsilon(1-\theta)\hat{G}', 0 \leq \theta \leq 1$. Thus for any random perturbation for which $\epsilon\theta > \epsilon_{bif}$ we expect the maximum possible response. Under equidistribution of projections for values of $\epsilon \gg \epsilon_{bif}$ this will be most probable, i.e. almost any perturbation will be most effective.

This connection between the $\hat{I}_z$ perturbation and other GOE perturbations is vital from a practical point of view. For the $\hat{I}_z$ perturbation we can analytically predict for which range of Hamiltonian parameters and degree of excitation the molecular system will become unstable. In addition, as we have pointed out in a previous section, we can obtain the bifurcation points for individual states in good approximation by evaluation of the order parameter associated with eqn.(2.120) and in reasonable approximation from the inverse of the susceptibilities.

Therefore we can analytically predict the onset of instability of a vibrational excitation in the molecular system and of each individual state under an ensemble of randomly occurring perturbations.

The straightforward application of the normal to local character stability criterion to the water molecule shows that at a GOE perturbation $\epsilon \approx O(10^{-7})$ the eigenstates $|\Psi_{10}, \pm, 0>$ become unstable normal and the corresponding perturbed eigenstates $|\Psi_{10}, \pm, 0>_P$ become stable local. This coincides with the prediction from the analytical results $\tilde{\kappa}(I=10) < 1$ and $n^2/\gamma_{10,\pm,o} \approx O(10^{-8} cm^{-1})$.

Generalization of the stability criterion

In conclusion, let us summarize the answers to the questions posed at the beginning of this section and generalize the results.

First, the choice of a specific symmetry breaking perturbation to probe the instability against any symmetry breaking perturbation can be justified from the observation that the response to the *most effective* symmetry breaking perturbation almost coincides with the *most probable* response under an ensemble of random perturbations. Thus this response under the most effective perturbation is representative for the behavior under any perturbation.

Conversely, for complex symmetric molecules the instability against symmetry breaking perturbations can be investigated taking almost any random perturbation. Such a perturbation is easily found since the most probable response appears to be close to the maximum possible response.

Third, the statistics of the response of an ensemble of eigenstates to an ensemble of random perturbations of given magnitude defines their stability. The entire ensemble or a fraction of it is considered stable if in response to the perturbation at most half of the ensemble within previously specified limits is shifted outside those limits. The response can be described most simply by the overlap of the unperturbed and perturbed eigenstates or more sensible measures like order parameters that indicate reduction in symmetry. The ensemble of random perturbations can be chosen in a variety of ways. In the simplest case the proper random ensemble is chosen according to the transformation that diagonalizes the Hamiltonian and applied without further restrictions. By imposing restrictions such as conservation laws or symmetry requirements the perturbation can become of increasing selectivity in the sense that only a certain fraction of states will respond.

For the class of AB_2 molecules with C_{2v} symmetry these conclusions are based on analytical arguments that allow us to predict the onset of instability of vibrational excitations and the extent of instability for each individual state in terms of the Hamiltonian parameters and the degree of excitation.

Let us emphasize that the magnitudes of perturbation necessary to cause localization are extremely small compared to typical magnitudes of couplings between local oscillators. Therefore almost any small inhomogeneity in the surroundings of a molecule that contains an unstable normal excitation will cause localization of that excitation under reduction of the molecular symmetry.

It is straightforward to apply this procedure to polyatomic molecules of higher symmetry than C_{2v} or even to molecules without symmetry, where it may reveal a tendency towards localization beyond what must be expected from the mere absence of symmetry. The local to normal character stability criterion is then easily generalized:

At given ϵ, an ensemble of eigenstates is stable local if $P_{\epsilon,\Psi}(\Lambda|1 \geq \Lambda > 0.5) > 0.5$, stable normal if $P_{\epsilon,\Psi}(\Lambda|1 \geq \Lambda > 0.5) < 0.5$ and neutrally stable if $P_{\epsilon,\Psi}(\Lambda|1 \geq \Lambda > 0.5) = 0.5$. A point of bifurcation for an eigenstate is given by the value of ϵ for which a change in stability occurs.

$P_{\epsilon,\Psi}$ contains the statistics of the response of the ensemble of eigenstates $|\Psi>$ in terms of the random variable Λ that indicates the relative degree of locality of the perturbed eigenstates $|\Psi>_P$ under the ensemble of random perturbations. $P_{\epsilon,\Psi}$ and Λ can be defined for each particular case in analogy to the proposals made above. In the next section let us outline the practical relevance of our theoretical investigation for the control of intramolecular dynamics.

2.5 Relevance for control of intramolecular dynamics

Some twenty to thirty years ago, the first attempts were made to control molecular dynamics using lasers as a source of electromagnetic radiation [27]. In general, two different techniques of control were attempted:

- control by selective coupling of intramolecular degrees of freedom induced by a strong laser field, based on the idea of rerouting the pathways of energy flow;

- control by selective excitation of particular degrees of freedom, referred to as "mode-selective excitation", based on the idea of modifying the initial locus of excitation.

The degree of control turned out to be very poor for the following reasons. The effects of strong laser fields on molecules are too complex to be selectively used, and intramolecular distribution of excitation rapidly destroys initially prepared locality before significant progress in the reaction has taken place.

In awareness of these obstacles three different new techniques were proposed recently:

- Tannor and Rice put forward a more classically oriented scheme, based on wave packet dynamics [28]. An initially prepared wave packet is *continuously* guided through a particular reactive pathway to the desired product.

- Brumer and Shapiro advocate "coherent control" [29], based on quantum interference. A particular superposition of final states is targeted by *simultaneously* exciting several different reactive pathways under control of the relative phases.

- Nelson proposes a NMR-oriented control scheme based on wave packet dynamics [30]. The state of the system is directed by a series of *excitation-evolution steps* until the targeted product state is reached.

The differences between the three new schemes consist of the particular uses of the laser source as a tool

- to *continuously* drag the system through one particular pathway,

- to *simultaneously* feed several reactive pathways at fixed phase relations and

- to *successively* drive by "kick and wait" the system towards a particular product.

The advantages of each method are expected to be:

- continuous wave packet control renders selectivity for molecules with many reactive pathways since the wave packet is kept permanently under control;

- coherent control allows high selectivity for molecules with few reactive pathways, where the phase relations are easy to initiate and to maintain;

- pulsed wave packet control yields selectivity by adjustment of the successive pulses to the immediate response of the molecular dynamics and therefore is very flexible in applications.

Which of the schemes allows best selectivity and yield, if feasible at all, remains to be tested experimentally.

Common to all three schemes is the problem of optimal control, investigated early on by Rabitz [31]. Optimal control takes into account not only the physical properties of the reactive system but also technical constraints, such as available laser power, time resolution, wave lenghts, ... and constraints set by the particular scheme, such as phase, amplitude and delay parameters of the control field.

The optimal control procedure involves three steps. First, an immediate objective is set, usually "maximum yield" or "maximum yield and selectivity". Second, the constraints on the field are chosen and included into the immediate objective, now called the total objective. Finally, the parameters that optimize the total objective are obtained. The resulting field allows control closest to the immediate objective and is therefore called the optimal field. The following conceptual and practical problems are associated with this procedure.

The conceptual difficulty is that the complex numerical control process strips the scheme from insight and intuition. Therefore it appears to be difficult to actually learn from the results and consequently to improve the schemes themselves on a conceptual level. In addition, it may be difficult to detect occurring errors.

The practical problem is that as straightforward as this procedure seems, it is as difficult to implement. Mainly, the reason is that the optimization of the total objective typically involves *non linear* functionals, dependent on the particular functional form of the chosen field. Due to the non linearity the solution will in general not be unique. In addition, one has to expect an extraordinary sensitivity to both experimental and theoretical systematic and random errors. To be specific:

- the exact form of the system Hamiltonian is usually not known, in particular, the intramolecular couplings at high energies and the couplings to the field;
- the experimental setup allows control over the field only up to a certain accuracy, limited by practical restrictions, such as fluctuations of phase, amplitude and time delays and inherent restrictions, such as the time frequency uncertainty relation.

These problems are common to all three proposed schemes which therefore can be put reliably to work only by gaining far reaching insight and control over the effects of these uncertainties.

The susceptibility to almost any symmetry breaking perturbation may turn out to be extraordinarily high for some states that are intended for use in a control scheme. The susceptibility of local character states increases while the susceptibility for normal character states decreases with increasing excitation. The degree of excitation along reactive pathways is usually very high so that we have to expect extremely susceptible and extremely stable states in close energetic vicinity. Almost any inhomogeneity in the molecular environment, such as the medium of reaction or the controlling laser field, has a profound effect on the locality properties of highly susceptible states, whereas the nearby stable states remain essentially unaffected. In awareness of this problem we have defined a stability criterion for vibrational states of polyatomic molecules in an inhomogeneous environment.

The ensemble of random perturbations simulates the effect of both mentioned uncertainties in the optimal control schemes. The randomly perturbed model Hamiltonian now includes all possible sorts of constant couplings that were initially *omitted* either by accident or on purpose, or constant couplings that are *introduced* by an external field. In addition, the random perturbations mimic any uncertainties of amplitude, phase or frequency in the controlling field.

From our investigation we infer that control of selectivity and yield of a chemical reaction is limited by the ability to selectively excite states of large degree of locality which support the energizing or dissociation of one particular bond. Unfortunately,

it turns out that those states appear as almost degenerate pairs with increasing excitation. This sets a limit in principle on the time and frequency resolution of the controlling field and an experimental threshold of accuracy that has to be overcome. We conclude that in the case of static perturbations we already understand the inherent limitations of selectivity in single bond excitation.

The results reported in the previous section were obtained for *static* random perturbations. In order to demonstrate the practical relevance for the control of molecular dynamics we have to treat the more general case of *time dependent* randomly modulated perturbations. Similar numerical investigations have been carried out by Rabitz and co-worker, who were the first to look into the problem of stability of the control process [32]. In the future we wish to address

- the theoretical issue of inherent limitations of control due to fluctuating time dependent perturbations and
- the strategic issue of design of more intuitively oriented control schemes on the basis of stability information in terms of susceptibilities.

The susceptibilities hold the key to product selectivity and yield, to technical and operative efficiency and thus can be used as guidelines for new control schemes up to the theoretical limitations. The following scenarios may illustrate this.

- There is a trade-off between product selectivity and yield. High selectivity can be achieved by choosing reactive steps that involve stable states and thus are easy to control in their changes, yet lead only to a minor extent to localization of excitation. High yield can be achieved by choosing reactive steps that involve susceptible states which almost completely localize excitation, yet are difficult to control in their changes.
- Furthermore, susceptibilities specifically direct technological efforts. For example, susceptibilities towards phase fluctuations may be small, yet to frequency fluctuations may be large. Consequently, larger effort may have to be put in the development of sources with reliable frequencies.

- Finally, susceptibilities selectively direct operational efforts. For example, along a reactive path some states may require closer control than others. They can be distinguished on the basis of susceptibilities.

On the basis of the expected numerical and analytical results we intend to design in the future a variety of control schemes that are accessible to intuitive reasoning. We believe this approach to be intellectually more appealing and practically more promising than a recently proposed approach based on methods from artificial intelligence [35].

2.6 Review

In this chapter we have discussed in detail the phenomenon of dynamical symmetry breaking in the context of the normal to local mode transition of stretching vibrations in AB_2 molecules of C_{2v} symmetry. The model system studied consists of two identical Morse oscillators that are harmonically coupled and is referred to as the Darling-Dennison system. In particular, we stated the conditions of localization of vibrational excitation and determined its dynamical properties. Furthermore we discussed the purely theoretical aspects of the quantum-classical correspondence and practical implications for the control of localization of vibrational excitation in experiments. Let us briefly review the main results.

Conditions of localization The symmetry of Darling-Dennison systems allows no static potential that permits localization of vibrational excitation in a single bond oscillator. Therefore any localization that occurs must be due to the presence of a dynamical potential and the C_{2v} symmetry is dynamically broken. A convenient measure of localization is the time averaged difference in vibrational excitation of the single oscillators.

The classical Darling-Dennison system permits the description of a vibrational excitation as a quasiparticle that consists of a harmonic excitation and an induced distortion of the molecular equilibrium geometry. It moves under the influence of a

single well or double well potential, referred to as the Duffing potential. The particular topology and shape of the Duffing potential depends on the molecular species, i.e. Hamiltonian parameters, the amount of excitation, i.e. the number of vibrational quanta, and the total energy. The necessary condition for the double well form to develop is that for a given amount of excitation the maximum possible coupling energy be smaller than the sum of the maximum possible anharmonic distortion energies of the single oscillators. At this point a bifurcation occurs. The necessary and sufficient condition for the normal to local transition to occur is that the kinetic energy of the quasiparticle vanishes before it reaches the top of the potential well. This becomes more likely with increasing amounts of excitation. For a given amount of excitation, the localization tends to be the case for lowest possible energies. This picture applies to a variety of different molecules. For water, with its weakly coupled and strongly anharmonic bond oscillators, it indicates local modes already at moderate levels of excitation. For sulfur dioxide, with its strongly coupled and weakly anharmonic bond oscillators, it indicates exclusively normal modes up to high levels of excitation. The process of localization in Darling-Dennison systems cannot occur under conservation of energy.

The symmetry of the quantum mechanical Darling-Dennison does not permit localization of excitation in a single oscillator. However, each eigenstate can be associated with a corresponding isoenergetic trajectory of the classcial Darling-Dennsion system and therefore be unambiguously labelled as normal or local character state. A semiclassical interpretation of the Duffing potential hints at the physical content of this distinction: local character states are more susceptible to a symmetry breaking perturbation than normal character states under the same perturbation. The extent of localization under perturbation is conveniently measured in terms of an order parameter that specifies the mismatch in vibrational excitation of the single oscillators. Susceptibilities and order parameters indicate physical properties and make the labels of normal or local character superfluous.

Dynamical properties of the excitation The classical dynamical properties of the excitation can be summarized in the Poincaré sphere that displays in a single viewgraph several trajectories for a given amount of excitation. In particular, it facilitates the discussion of the initial condition and phase dependence of the dynamics. Furthermore, it allows a qualitative discussion of the change in dynamics under damping that yields an enhanced tendency to form local modes. For the quantum mechanical case the quasiparticle picture can be refined by incorporation of the possibility of tunneling between the wells of the Duffing potential.

Quantum-classical correspondence The correspondence between the bifurcation in the classical system and the onset of high susceptibilities in the quantum system is established by the recovery of the classical bifurcation parameter in the eigenvalue problem. A difference between classical instability and instability in the quantum system is that there the magnitude of perturbation to produce a significant effect has to be specified. Since the susceptibility of some eigenstates turns out to be extremely high under almost any perturbation, a statistical stability criterion for eigenstates under randomly occurring perturbations can be employed. It is particularly useful in cases where the molecule interacts with an inhomogeneous environment.

Practical implications The performance of several proposed control schemes for intramolecular vibrational excitation using laser fields can be investigated by the application of the statistical stability criterion for eigenstates.

Bibliography

[1] M.S. Child and L. Halonen, *Adv. Chem. Phys.* 57,1 (1984) and references therein.

[2] B. Podolsky, *Phys. Rev.* 32, 812 (1928).

[3] L.G. Bonner, *Phys. Rev.* 46,458 (1934).

[4] B.T. Darling and D. M. Dennison, *Phys. Rev.* 57, 128 (1940).

[5] B.R. Henry and W. Siebrand, *J. Chem. Phys.* 49,5369 (1968).

[6] E.L. Sibert III, W.P. Reinhardt and J.T. Hynes, *J. Chem. Phys.* 77,3583 (1982).

[7] E.L. Sibert III, W.P. Reinhardt and J.T. Hynes, *J. Chem. Phys.* 77,3595 (1982).

[8] P.R. Stannard, M.L. Elert and W.M. Gelbart, *J. Chem. Phys.* 74, 6050 (1981).

[9] O.S. Mortensen, B.R. Henry and Ali Mohamadi, *J. Chem. Phys.* 75, 4800 (1981).

[10] M.S. Child and R.T. Lawton, *Faraday Discuss. Chem. Soc.* 71, 273 (1981).

[11] K.K. Lehmann, *J. Chem. Phys.* 79, 1098 (1983).

[12] M. Kellman, *J. Chem. Phys.* 83, 3842 (1985).

[13] L. Xiao and M. Kellman, *J. Chem. Phys.* 90, 6086 (1989).

[14] A.C. Scott, P.S. Lohmdahl, J.C. Eilbeck, *Chem. Phys. Lett.* 113,29 (1985).

[15] V.I. Arnold, Mathematical Methods of Classical Mechanics, 2nd ed., New York: Springer (1991).

[16] G. Duffing, Erzwungene Schwingungen bei Veränderlicher Eigenfrequenz, I. Vieweg und Sohn (1918).

[17] J. Guckenheimer and P. Holmes, Nonlinear Oscillations, Dynamical Systems, and Bifurcations of Vector Fields, New York: Springer (1983).

[18] Z. Li, L. Xiao and M. Kellman, *J. Chem. Phys.* 92, 2251 (1990).

[19] L. D. Landau and E. M. Lifshitz, Mechanics, Course of Theoretical Physics I, Pergamon Press (1960).

[20] M.F. Manning, *Phys. Rev.* 48, 161 (1935).

[21] see, for example: P. M. Morse and H. Feshbach, Methods of Theoretical Physics, McGraw-Hill, Volume I 557ff (1953).

[22] J. H. Wilkinson, The Algebraic Eigenvalue Problem, Claredon Press, Oxford Science Publications (1965).

[23] R. Englman, The Jahn-Teller Effect in Molecules and Crystals, Wiley, 191ff (1972).

[24] F. Haake, Quantum signatures of Chaos, Springer (1991).

[25] M.L. Mehta, Ramdom Matrices, rev. and enl. 2nd ed., San Diego: Academic Press (1991).

[26] for reviews see: A. Ben-Shaul, Y. Haas, K. L. Kompa and R. D. Levine, *Lasers and Chemical Change*, Berlin: Springer (1981); J. Manz and C. S. Parmenter, eds., Mode Selectivity in Unimolecular Reactions, *Chem. Phys.*, 139, 1 (1989); R. D. Levine, A. H. Zewail and M. A. El-Sayed, eds., Berstein Memorial Issue on Molecular Dynamics, *J. Phys. Chem.*, 95, 7961 (1991).

[27] for reviews see: A. Zewail and R. Bernstein, *Chem. Eng. News*, 66, 24 (1988); A. Bandrauk, ed., Atomic and Molecular Processes with Short Intense Laser Pulses, New York: Plenum (1988). E. D. Potter, J. L. Herek, S. Pedersen, Q. Liu and A. H. Zewail, *Nature*, 355, 66 (1992).

[28] D. J. Tannor and S. A. Rice, *J. Chem. Phys.*, 83, 5013 (1985); D. J. Tannor and S. A. Rice, *Adv. Chem. Phys.*, 70, 441 (1988). See also N. F. Scherer, R. J. Carlson, A. Matro, M. Du, A. J. Ruggiero, V. Romero-Rochin, J. A. Cina, G. R. Fleming and S. A. Rice, *J. Chem. Phys.*, 95, 1487 (1991).

[29] P. Brumer and M. Shapiro, *Chem. Phys. Lett.*, 126, 541 (1986); for review see: P. Brumer and M. Shapiro, *Annu. Rev. Phys. Chem.*, 43, 257 (1992).

[30] A. M. Weiner, D. E. Leaird, G. P. Wiederecht and K. A. Nelson, *Science*, 247, 1317 (1990); M. M. Wefers and K. A. Nelson, *Science*, 262, 1381 (1993); for review see: L. Dhar, J. A. Rogers and K. A. Nelson, *Chem. Rev.* , 94, 157 (1994).

[31] A. Peirce, M. Dahleh and H. Rabitz, *Phys. Rev. A*, 37, 4950 (1988); for reviews see: W. S. Warren, H. Rabitz and M. Dahleh, *Science*, 259, 1581 (1993); D. Neuhauser and H. Rabitz, *Acc. Chem. Res.*, 26, 4996 (1993).

[32] P. Gross, D. Neuhauser and H. Rabitz, *J. Chem. Phys.*, 98, 9651 (1993).

[33] B. D. Cahn and C. C. Martens, *J. Chem. Phys.*, 99, 7440 (1993); B. Hartke, A. E. Janza, W. Karrlein, J. Manz and V. Mohan, *J. Chem. Phys.*, 96, 3569 (1992). W. Jakubetz, E. Kades and J. Manz, *J. Phys. Chem.*, 97, 12609 (1993).

[34] Y.-J. Yan, R. E. Gillilan, R. M. Whitnell, K. R. Wilson and S. Mukamel, *J. Phys. Chem.*, 97, 2320 (1993); A. D. Bandrauk, *Int. Rev. Phys. Chem.*, 13, 123 (1994).

[35] P. Gross, D. Neuhauser and H. Rabitz, *J. Chem. Phys.*, 98, 4557 (1993).

Chapter 3

Duffing's oscillator and the nonlinear dimer

3.1 Introduction

The object of our investigation is a Hamiltonian system with coupled classical and quantum mechanical degrees of freedom. This evergreen is of interest for both the pure and the applied theorist. On the pure side it has recently received some attention in connection with questions concerning the foundations of quantum mechanics [1, 2, 3]. On the applied side it has been developed to a standard model to explain a variety of experimental data ranging from charge transfer dynamics in mixed valence compounds [4], to neutron scattering in metals [5].

Our study is motivated by the phenomenon of self-trapping. Self-trapping is the process of localization of an excitation that interacts with itself by a feedback mechanism through the medium it is moving in. The most prominent examples are the formation of a polaron from an excess charge in a molecular crystal [6, 7], a solitary exciton from an electronic excitation in a molecular chain [8, 9, 10], or a local mode from a vibrational excitation in coupled normal modes [11]. The phenomenon arises from the interplay of two feedback mechanisms. Consider the polaron. A slow excess charge polarizes a molecular crystal. The resulting distortion provides a potential well for that charge to form a bound state which in turn enhances the polarization of its

immediate environment. The excess charge is self-trapped in the induced distortion. Charge and distortion can move as a unit, called a polaron. The emphasis on "self" is made to distinguish the phenomenon of self-trapping from others like radiative trapping in a defect or relaxation induced trapping due to coupling to a bath. In general, the self-trapped state does not have to be an eigenstate of the system.

If the number of sites the excitation can reside on is restricted to two, the situation is referred to as the "excitation on a dimer". The excitation is called to be "self-trapped on the dimer" if its motion does not extend over both sites. The minimal model that captures the phenomenon of self-trapping an excitation on a dimer can be derived from a Hamiltonian system with six degrees of freedom, two of which are coupled, which we declared to be the object of our investigation. Note however, that this model will not allow the description of the process of localization under conservative conditions.

Although the discussion could be carried out in general terms we will follow the physical picture of an excess charge on a pair of identical diatomic molecules, centers of mass residing on the sites and relative orientation fixed.

Before we get down to the details, a few more words about related investigations this study is partially built on, and how it differs. Let us introduce first some more notions. Taking the motion of the excitation as a reference one can distinguish between two limiting dynamic regimes. These are characterized by either a small or large ratio of timescales related to the dynamics of the excess charge and the molecular vibrational modes. In the first case one speaks of the molecular vibration enslaved to rapidly oscillate around the slowly moving excess charge density, thus providing a local potential for it. For reasons to become obvious later we will call this limiting regime the "Duffing limit". The second limiting regime displays the reversed situation and will be called the "standard adiabatic limit". If there are only two different timescales present, we shall call those quantities changing on the slow timescale "slow variables", the others "fast variables".

Aspects of the motion of self-trapped excitations in one dimension in the Duffing limit were described within the theoretical framework of a nonlinear Schrödinger

equation, the discrete self-trapping equation, which has been extensively studied [12, 13, 14, 15, 16, 17]. Partial analytical results were obtained for the dimer and trimer [18, 19, 20]. Numerical simulation [12] for larger systems suggests the existence of periodic, quasiperiodic and chaotic trajectories, extending over parts of or the entire system. The role of different symmetries for self-trapping were investigated using analytical and numerical methods [21, 22, 23].

Extensions to damped and driven systems were modeled by introduction of phenomenological damping [24, 25, 26] or Ohmic dissipation and a driving field [2, 3].

The objective is to demonstrate a straightforward method to analyse the dynamics associated with the system of consideration, which allows not only to readily rederive and reinterpret known results, but to line out how to transfer these to more complicated situations. The program to be carried out consists of two steps: first, derivation of the reduced dynamic equations for the excess charge and molecular vibrations, and second, their solution and interpretation.

We will derive the exact equations of motion by directly carrying out the variational procedure according to the principle of least action. We will single out two coupled dynamic variables, representing the excess charge and the molecular vibrations. The subsequent phase plane analysis will yield an extract of dynamical features that have to be matched by any approximation that claims to preserve the nonlinear core of the problem. This approximation will be carried out using perturbative methods to the order necessary.

As a result, we will reduce the equation of motion under different dynamic regimes to the Duffing equation which can be solved analytically in certain limits. We will provide a simple picture, i.e. the phase diagram from chapter 2, to interpret the analytical results and recent numerical studies [27, 25, 26, 28].

Immediate consequences from the equivalency of the system of consideration to Duffing's oscillator will be briefly lined out, without completely exploiting its physical and mathematical richness.

Many of the methods and tools employed are similar or identical to the ones used in the discussion of the normal to local mode transition in the previous chapter.

Therefore we will considerably abbreviate the current discussion in the overlapping sections and only briefly outline earlier results.

3.2 Derivation of the reduced dynamic equations

As outlined in the previous section, the focus of attention has been on those cases, where the dynamics associated with the degrees of freedom occur on timescales differing at least one order of magnitude. The standard approach to obtain the dynamic equations for the slow variables is to use the adiabatic approximation, which involves four steps:

- Neglect the contribution of the fast variables to the kinetic energy in the Hamiltonian.
- Find the values of the fast variables that minimize the total energy.
- Eliminate the fast variables from the Hamiltonian.
- Use Hamilton's equations to obtain the dynamic equations for the slow variables.

There are two difficulties associated with this procedure (which is carried out in Appendix C).

- One is to correctly identify the conjugate variables in the last step. It has been shown [29] that the equations of motion for the solitary exciton derived by Davydov using Hamilton's equations are not identical to those derived from the principle of least action. We will overcome this difficulty by using the time dependent variational principle of quantum mechanics [30]. The equations for the time evolution of the parameters in the ansatz for the wavefunction are obtained by directly carrying out the minimization of the differential of the total action.
- The other difficulty is to show that the obtained reduced dynamic equations for the slow variables are qualitatively correct and to obtain quantitative corrections. For example, if the complete equations of motion allow trapped motion of

the excess charge for a given set of parameters, so should the reduced dynamic equations for that same set of parameters. To show that this is the case we will use in analogy to classical mechanics phase plane analysis. We will compare the projection of the phase space of the complete system onto the surface spanned by the slow variables and the full phase plane of the reduced system by number, location and stability of stationary points. The reduced dynamic equations will be obtained by singular perturbation analysis [31] which will be carried out to the order at least necessary to reach qualitative agreement in the discussed sense. The method allows systematic generation of quantitative corrections to this result.

3.2.1 Variational procedure

The Lagrangian density for an excess charge on two identical diatomic molecules, centers of mass residing on two sites and fixed relative orientation can be approximated in the tight binding limit for the excess charge and the assumption of two classical uncoupled harmonic oscillators for the molecular vibrations and a linear coupling of excitation and oscillators as

$$\begin{aligned} L &= \frac{\mu}{2}[\dot{Q}_1^2 + \dot{Q}_2^2 - \omega^2(Q_1^2 + Q_2^2)] + \chi(Q_1|a_1|^2 + Q_2|a_2|^2) + \\ &\quad \frac{i}{2}(a_1^*\dot{a}_1 - \dot{a}_1^* a_1 + a_2^*\dot{a}_2 - \dot{a}_2^* a_2) + \zeta(a_1^* a_2 + a_2^* a_1). \end{aligned} \tag{3.1}$$

Here Q_1 and Q_2 are the displacements from equilibrium of oscillator one and two, a_1 and a_2 the probability amplitudes for the excess charge of residing on site one and two; μ is the reduced mass of the oscillators, ω the frequency of oscillation, χ the charge-molecular vibration coupling constant and ζ the electronic intersite coupling constant. χ, ζ are assumed to be positive. Note the symmetry with respect to site exchange. The number n is defined by

$$n = |a_1|^2 + |a_2|^2 \tag{3.2}$$

and takes the value $n = 1$ for the case of a single excess charge, which we will consider in the following. The action S is defined by

$$S = \int_{t_0}^{t_1} dt L(Q_i, \dot{Q}_i, a_i, \dot{a}_i, a_i^*, \dot{a}_i^*). \tag{3.3}$$

The equations for the time evolution of the variables $Q_1, Q_2, a_1, a_1^*, a_2, a_2^*$ can be derived using the principle of least action under the restriction that the number n is conserved, i.e.

$$\delta(S - \lambda n) = 0. \tag{3.4}$$

Here λ is the Lagrange multiplier associated with the differential of n. This tedious but nevertheless straightforward procedure leads to the exact equations of motion

$$\ddot{Q}_1 + \omega^2 Q_1 - \frac{\chi}{\mu}|a_1|^2 = 0, \tag{3.5}$$

$$\ddot{Q}_2 + \omega^2 Q_2 - \frac{\chi}{\mu}|a_2|^2 = 0, \tag{3.6}$$

$$i\dot{a}_1 - a_1(\lambda - \chi Q_1) + \zeta a_2 = 0, \tag{3.7}$$

$$i\dot{a}_2 - a_2(\lambda - \chi Q_2) + \zeta a_1 = 0. \tag{3.8}$$

From eqn. (3.5,3.6) we learn that the equilibrium displacement of each molecular oscillator is shifted proportionally to the probability of the excess charge being found on its site. This suggests a change of coordinates for the oscillators to the total and relative displacement coordinates Q_s and Q_a defined by

$$Q_{s,a} = Q_1 \pm Q_2. \tag{3.9}$$

They are by construction symmetric and antisymmetric with respect to exchange of sites. From eqn. (3.7,3.8) one can readily derive the discrete self-trapping equation. Again, site exchange symmetry suggests a change of coordinates for the excess charge to the real valued SU(2) coordinates

$$P_z = a_1^* a_1 - a_2^* a_2, \tag{3.10}$$

$$P_x = a_1^* a_2 + a_2^* a_1, \tag{3.11}$$

$$P_y = i(a_1^* a_2 - a_2^* a_1), \tag{3.12}$$

$$1 = P_x^2 + P_y^2 + P_z^2. \tag{3.13}$$

The polarization P_z can be interpreted as the probability difference for the excess charge of occupying sites one and two. In the new coordinates eqn.(3.5-3.8) take the form

$$\ddot{Q}_s + \omega^2 Q_s - \frac{\chi}{\mu} = 0, \tag{3.14}$$

$$\ddot{Q}_a + \omega^2 Q_a - \frac{\chi}{\mu} P_z = 0, \tag{3.15}$$

$$\ddot{P}_z + 4\zeta^2 P_z - 2\zeta\chi Q_a P_x = 0, \tag{3.16}$$

$$2\zeta\dot{P}_x + \chi Q_a \dot{P}_z = 0. \tag{3.17}$$

We see from eqn.(3.14), that Q_s is decoupled from Q_a, P_z and P_x and can be interpreted as a harmonic oscillator with fixed equilibrium displacement. Thus we will disregard Q_s in the following.

Eqn.(3.15-3.17) describe a system of two coupled oscillators with displacements Q_a and P_z and will be the starting point of subsequent approximations. The equilibrium value of Q_a is a linear function of P_z and vice versa. In terms of the original picture we can say that only the relative excess charge density P_z and the antisymmetric vibrational mode undergo coupled oscillations. Note that eqn.(3.17) is necessary to describe the time evolution of the relative phase of the original complex variables a_1 and a_2. For the reduced dynamic systems it will determine a dynamic invariant. In addition we note that

$$2\zeta P_y = \dot{P}_z \tag{3.18}$$

which will be of use later.

One can arrive at the same results using Hamilton's equations, starting with the

Hamiltonian density

$$H = \frac{1}{4\mu}(p_s^2 + p_a^2) + \frac{\mu\omega^2}{4}(Q_s^2 + Q_a^2) - \frac{\chi}{2}(Q_s + Q_a P_z) - \zeta P_x. \tag{3.19}$$

Then the knowledge that $p_{1,2}$ are the conjugate to $Q_{1,2}$ and $ia_{1,2}^*$ are conjugate to $a_{1,2}$ leads to eqn.(3.14-3.17) as well. Note that H and P are dynamic invariants, i.e.

$$\dot{H} = \dot{P} = 0, \tag{3.20}$$

which reduces the number of degrees of freedom by two and is ultimately responsible for the integrability of the reduced dynamic equations to be derived in the following sections.

3.2.2 Phase space analysis

Before we proceed with the elimination of variables in the Duffing and standard adiabatic limit, we will analyse the phase space associated with the complete set of dynamic equations.

A word about the different timescales in the system of consideration first. We will distinguish between two different timescales $1/\omega$ and $1/\zeta$ associated with the molecular vibration and the charge density motion, which define τ and θ

$$\tau = \omega t \tag{3.21}$$

$$\theta = 2\zeta t. \tag{3.22}$$

We will investigate two different cases, i.e. the Duffing limit $\tau \gg \theta$ and the standard adiabatic limit $\tau \ll \theta$.

Within the two limiting cases, the number of parameters can be reduced by one, so we expect the relative magnitudes of the two remaining parameters, i.e. (χ, ζ) or $(\chi, \mu\omega^2)$ to qualitatively determine the dynamics. Thus we define two new parameters

α, β by the following ratios

$$\alpha = \frac{\chi}{2\zeta} \tag{3.23}$$

$$\beta = -\frac{\chi}{\mu\omega^2}. \tag{3.24}$$

These definitions for α and β are motivated by the idea to compare two competing mechanisms. For example, α compares the tendency of charge density transfer via electronic coupling ζ versus the tendency of on site polarization via the coupling to molecular vibrations χ. The dimensionless constant

$$\kappa = -\frac{1}{\alpha\beta} \tag{3.25}$$

relates the polarization and both transfer tendencies, i.e. the transfer by electronic coupling and the transfer by coupling of excess charge and molecular vibrations. Note the difference to the bifurcation parameter from the normal to local mode transition in that here there are two competing transfer tendencies.

The phase space analysis will be carried out in the coordinates (P_x, P_y, P_z) and

$$Q_{a,1} = Q_a, \tag{3.26}$$

$$Q_{a,2} = \dot{Q}_{a,1}. \tag{3.27}$$

Substitution in eqn.(3.14-3.17) gives

$$\dot{Q}_{a,1} = Q_{a,2} \tag{3.28}$$

$$\dot{Q}_{a,2} = -\omega^2 Q_{a,1} + \frac{\chi}{\mu} P_z \tag{3.29}$$

$$\dot{P}_z = 2\zeta P_y \tag{3.30}$$

$$\dot{P}_y = -2\zeta P_z + \chi Q_{a,1} P_x \tag{3.31}$$

$$\dot{P}_x = -\chi Q_{a,1} P_y. \tag{3.32}$$

The stationary points of the system are given by the condition

$$\dot{Q}_{a,1} = \dot{Q}_{a,2} = \dot{P}_x = \dot{P}_y = \dot{P}_z = 0. \tag{3.33}$$

- For $\kappa > 1$ we find two stationary points $S_{Q_a,P} = (Q_{a,1}, Q_{a,2}, P_x, P_y, P_z)$ at

$$S^{(1,2)}_{Q_a,P} = (0, 0, \pm 1, 0, 0). \tag{3.34}$$

- For $\kappa < 1$ we find four stationary points at

$$S^{(1,2)}_{Q_a,P} = (0, 0, \pm 1, 0, 0), \tag{3.35}$$

$$S^{(3,4)}_{Q_a,P} = (\mp\beta\sqrt{1-\kappa^2}, 0, \kappa, 0, \pm\sqrt{1-\kappa^2}). \tag{3.36}$$

Linear stability analysis of eqn.(3.28-3.32) yield the following results

- For $\kappa < 1$, $S^{(1)}_{Q_a,P}$ is unstable (saddle point in both $Q_{a,1}, Q_{a,2}$ and $P_{z,1}, P_{z,2}$) and $S^{(2,3,4)}_{Q_a,P}$ are neutrally stable.

- For $\kappa > 1$, $S^{(1,2)}_{Q_a,P}$ are neutrally stable.

- At $\kappa = 1$ there occurs a pitchfork bifurcation in both $Q_{a,1}$ and P_z.

Note, that the bifurcation occurs *simultaneously* for both electronic and vibrational degrees of freedom which implies, that the *trapping of the excess charge forces the trapping of the molecular vibration and vice versa.* If we had not restricted the constants χ and ζ to be positive, we would have in analogy to the Darling-Dennison System a transcritical bifurcation at $\kappa = 0$.

Our scope now is to determine the conditions of existence of those trajectories in the phase space whose points of intersection with a surface section A_T of the phase space spanned by $T_1(Q_{a,1}, Q_{a,2}, P_x, P_y, P_z)$, $T_2(Q_{a,1}, Q_{a,2}, P_x, P_y, P_z)$ can be approximated by a continuous function in a properly scaled time θ or τ. We will determine the number, location and stability of stationary points in A_T for these trajectories. This will set the margin for the phase planes of the reduced equations in the the

Duffing limit, A_D, and in the standard adiabatic limit, A_L. To formulate the punch line: *We compare sections of the phase space of the complete system with the complete phase planes of the reduced systems.*

The following argument may help to understand the subsequent procedure. Let us place $Q_{a,1}, Q_{a,2}$ at their stationary state values, P_z, P_y be positive and $P_x = 0$. From eqn.(3.29,3.31,3.32) we see that P_y has negative slope and $Q_{a,2}$ after an instant positive slope, which forces an increase of $Q_{a,1}$. If $Q_{a,2}$ changes slope upon increase of $Q_{a,1}$, before P_z does, $Q_{a,1}$ will start oscillating around its equilibrium position $Q_{a,1}^{eq}$ given by eqn.(3.29)

$$Q_{a,1}^{eq} = -\beta P_z. \tag{3.37}$$

This will be the case for $\omega > 2\zeta$. The dynamics of the "equilibrium trajectory" $T(Q_{a,1}^{eq}, Q_{a,2}^{eq}, P_x, P_y, P_z)$ is confined to the section A_T of phase space spanned by $T_1(-\beta P_z, 0, P_x, 0, 0)$, $T_2(-\beta P_z, 0, 0, P_y, 0)$ and $T_3(-\beta P_z, 0, 0, 0, P_z)$. The invariant P allows to eliminate P_y. Let us go one step further. We evaluate the invariant C given by integration of eqn.(3.32) for $Q_{a,1}^{eq}$ and eliminate P_x. Thus the equilibrium trajectory $T = T(P_z)$ is parametrized in P_z and fixed in phase space by the constant C. We are interested in the case, where the points of intersections of the actual trajectory of the system and the equilibrium trajectory can be approximated as a continuous function of some time θ, i.e. $T[P_z(\theta)]$. This means that Q_a should carry out at least one cycle of characteristic time $1/\omega$ as $T[P_z(\theta)]$ changes to $T[P_z(\theta + \delta\theta)]$, i.e. it sweeps an infinitesimal section of one cycle of characteristic time $1/2\zeta$. This is the case for $\zeta \ll \omega$, i.e. the Duffing limit. As we will later reduce the equation of motion to the variables $P_z, \delta_\theta P_z$ the section A_T spanned by $T(Q_{a,1}^{eq}, Q_{a,2}^{eq}, 0, P_y, 0), T(Q_{a,1}^{eq}, Q_{a,2}^{eq}, 0, 0, P_z)$ has to be compared to A_D. We see, that by construction the stationary points contained in A_T coincide with those of the complete phase space.

We arrive by analogous argumentation at the standard adiabatic limit $\zeta \gg \omega$ where the dynamics can be approximated by the vibrational coordinates and the stationary state coordinates of the charge density motion. Here as well, the stationary points in A_T are identical with those of the complete system and have to be compared

to those in A_L in the reduced system.

We now have to confirm that in both limits the reduced equations of motion have to produce the same number, location and stability of stationary points as the complete phase space.

3.2.3 Elimination of fast variables in the Duffing limit

In the Duffing limit, the slow variable is P_z. It changes with the time $\theta = 2\zeta t$, which will be taken as the reference time now. The ratio of timescales of slow and fast variables is given by $\sqrt{\epsilon} = \frac{2\zeta}{\omega}$. Changing from variable t to θ and from differentiation with respect to t to differentiation with respect to θ, $\delta_t = 2\zeta\delta_\theta$, eqn.(3.15-3.17) take the form

$$\delta_\theta^2 Q_a = -\frac{1}{\epsilon}(Q_a + \beta P_z) \tag{3.38}$$

$$\delta_\theta^2 P_z = -P_z + \alpha Q_a P_x \tag{3.39}$$

$$\delta_\theta P_x = -\alpha Q_a \delta_\theta P_z. \tag{3.40}$$

We will solve eqn.(3.38-3.40) using perturbation expansions of Q_a, P_z and P_x in powers of ϵ, i.e.

$$Q_a = Q_a^{(0)} + \epsilon Q_a^{(1)} + \epsilon^2 Q_a^{(2)} + \ldots \tag{3.41}$$

$$P_z = P_z^{(0)} + \epsilon P_z^{(1)} + \epsilon^2 P_z^{(2)} + \ldots \tag{3.42}$$

$$P_x = P_x^{(0)} + \epsilon P_x^{(1)} + \epsilon^2 P_x^{(2)} + \ldots. \tag{3.43}$$

We substitute in eqn.(3.38-3.40) and collect terms of same order in ϵ.

To $O(\epsilon^{-1})$ we obtain

$$Q_a^{(0)} + \beta P_z^{(0)} = 0. \tag{3.44}$$

To $O(\epsilon^0)$ we obtain

$$\delta_\theta^2 Q_a^{(0)} = -(Q_a^{(1)} + \beta P_z^{(1)}) \tag{3.45}$$

$$\delta_\theta^2 P_z^{(0)} = -P_z^{(0)} + \alpha Q_a^{(0)} P_x^{(0)} \tag{3.46}$$

$$\delta_\theta P_x^{(0)} = -\alpha Q_a^{(0)} \delta_\theta P_z^{(0)}. \tag{3.47}$$

We use eqn.(3.44, 3.47) to eliminate $Q_a^{(0)}$ from eqn.(3.46) and arrive to lowest order at the differential equation that has to be satisfied by P_z in the Duffing limit:

$$\delta_\theta^2 P_z^{(0)} = -A P_z^{(0)} - B(P_z^{(0)})^3 \tag{3.48}$$

$$A = 1 - \frac{C}{\kappa} \tag{3.49}$$

$$B = \frac{1}{2\kappa^2} \tag{3.50}$$

$$C = P_x^{(0)}(\theta_0) + \frac{1}{2\kappa}[P_z^{(0)}(\theta_0)]^2. \tag{3.51}$$

Eqn.(3.48) is the dynamic equation for the undriven Duffing oscillator without damping, which explains why we called this regime the Duffing limit. Kenkre and Campbell derived eqn.(3.48) from the discrete self-trapping equation. As easily can be seen, the number, location and stability of the stationary points in the phase plane $A_D(P_z^{(0)}, \delta_\theta P_z^{(0)})$ associated with eqn.(3.48) are identical to those in A_T which we derived in the previous section. We conclude that eqn.(3.48) gives the correct *qualitative* behaviour and higher order terms $P_z^{(n)}$ achieve a *quantitative* correction. One can show that the dynamic equation for $P_z^{(1)}$ is linear (as it should be, since it should not add new stationary points) and describes oscillations of P_z in the neighborhood of $P_z^{(0)}$ which can be interpreted as the polarization of the charge density due to coupling to the molecular vibrations. Note that the zeroth order system has two invariants. One is $P^{(0)}$, the other C that can be obtained from eqn.(3.47).

3.2.4 Elimination of fast variables in the standard adiabatic limit

In the standard adiabatic limit, the slow variable is Q_a. It changes with the time $\tau = \omega t$, which will be taken as the reference time now. The ratio of slow and fast variables is given by $\sqrt{\tilde{\epsilon}} = \frac{\omega}{2\zeta}$. Changing from variable t to τ and from differentiation

with respect to t to differentiation with respect to τ, $\delta_t = \omega\delta_\tau$, eqn.(3.15-3.17) take the form

$$\delta_\tau^2 Q_a = -(Q_a - \beta P_z) \tag{3.52}$$

$$\delta_\tau^2 P_z = \frac{1}{\tilde{\epsilon}}(-P_z + \alpha Q_a P_x) \tag{3.53}$$

$$\delta_\tau P_x = -\alpha Q_a \delta_\tau P_z. \tag{3.54}$$

We will solve eqn.(3.52-3.54) using perturbation expansions of Q_a, P_z and P_x in powers of $\tilde{\epsilon}$, i.e.

$$Q_a = Q_a^{(0)} + \tilde{\epsilon} Q_a^{(1)} + \tilde{\epsilon}^2 Q_a^{(2)} + \ldots \tag{3.55}$$

$$P_z = P_z^{(0)} + \tilde{\epsilon} P_z^{(1)} + \tilde{\epsilon}^2 P_z^{(2)} + \ldots \tag{3.56}$$

$$P_x = P_x^{(0)} + \tilde{\epsilon} P_x^{(1)} + \tilde{\epsilon}^2 P_x^{(2)} + \ldots. \tag{3.57}$$

We substitute in eqn.(3.52-3.54) and collect terms of same order in $\tilde{\epsilon}$.

To $O(\tilde{\epsilon}^{-1})$ we obtain

$$-P_z^{(0)} + \alpha Q_a^{(0)} P_x^{(0)} = 0 \tag{3.58}$$

To $O(\tilde{\epsilon}^0)$ we obtain

$$\delta_\tau^2 Q_a^{(0)} = -(Q_a^{(0)} + \beta P_z^{(0)}) \tag{3.59}$$

$$\delta_\tau^2 P_z^{(0)} = -P_z^{(1)} + \alpha Q_a^{(1)} P_x^{(1)} \tag{3.60}$$

$$\delta_\tau P_x^{(0)} = -\alpha Q_a^{(0)} \delta_\tau P_z^{(0)}. \tag{3.61}$$

We use eqn.(3.58,3.61) to eliminate $P_z^{(0)}$ from eqn.(3.59) and arrive to lowest order at the differential equation that has to be satisfied by Q_a in the standard adiabatic limit:

$$\delta_\tau^2 Q_a^{(0)} = -Q_a^{(0)}[1 \mp \frac{1}{\kappa}\sqrt{\frac{G}{1 + (\alpha Q_a^{(0)})^2}}] \tag{3.62}$$

$$G = [P_z^{(0)}(\tau_0)]^2 + [P_x^{(0)}(\tau_0)]^2 = 1. \tag{3.63}$$

We recognize in eqn.(3.62) the equation for phonon dynamics as derived from the standard adiabatic potential. Again it can be easily checked that number, location and stability of stationary points of the phase plane associated with eqn.(3.62) are identical to those in $A_L(Q_a^{(0)}, \delta_\tau Q_a^{(0)})$ already discussed.

Note, that $G = 1$ as P_y is constant and has to be set tozero in order to guarantee conservation of $|P|$.

One final comment on the derivation of the reduced equation of motion is in place here. Our choice of the small parameters $\epsilon, \tilde{\epsilon}$ is *not unique*, yet turns out to be the *most convenient.* Other choices force the solution for higher order terms in the perturbation expansion, up to the order necessary to restore the features of the original phase space.

3.3 Solution and interpretation of the reduced dynamic equations

In this section we will solve and interpret the Duffing equation (3.48) and analytically approximate the standard adiabatic equation (3.62).

3.3.1 Charge density dynamics in the Duffing limit

Geometric methods from classical mechanics are the proper tools to extract the dynamical properties of the system in the Duffing limit. Although the analytic solutions to the Duffing equation in the above form are known and given in terms of Jacobian elliptic functions, we will show that the analytic solution is not necessary to predict the different dynamic regimes in the Duffing limit and to locate the transitions between them. A considerable amount of work has been done [5, 27, 18, 25, 26, 12] in the analysis of Duffing limit and we believe our analysis to be a supplement.

We will begin by defining a Hamiltonian density in terms of the invariants $P^{(0)}, C$, which allows a classical interpretation of the dynamics of $P_z^{(0)}$. The initial condition dependence will be summarized in a phase diagram. As a natural extension of that

phase diagram we will construct the trajectories $P(P_x, P_y, P_z)$ on the surface of the Poincaré sphere that was introduced in chapter 2. The analytical solution for the components of $P(P_x, P_y, P_z)$ as well as for the probability amplitudes a_1 and a_2 will be given. Numerical results for the damped Duffing oscillator [25, 26] will be interpreted.

Hamiltonian density in the Duffing limit

Let us simplify the notation by dropping the superscript (0) for all variables. Then eqn.(3.48-3.51) take the form

$$\delta_\theta^2 P_z = -AP_z - BP_z^3 \tag{3.64}$$

$$A = 1 - \frac{C}{\kappa} \tag{3.65}$$

$$B = \frac{1}{2\kappa^2}. \tag{3.66}$$

The invariants are

$$1 = P_x^2 + P_y^2 + P_z^2 \tag{3.67}$$

$$C = P_x + \frac{P_z^2}{2\kappa}. \tag{3.68}$$

From these two invariants and eqn.(3.18) we obtain the Hamiltonian density with conjugate variables $(P_z, \delta_\theta P_z)$ for the dynamics of P_z in the Duffing limit.

$$H_D = \frac{1}{2}\{1 - C^2\} = \frac{1}{2}P_y^2 + \frac{A}{2}P_z^2 + \frac{B}{4}P_z^4. \tag{3.69}$$

By construction the kinetic contribution T and potential contribution V to H_D are

$$T = \frac{P_y^2}{2} \tag{3.70}$$

$$V = \frac{A}{2}P_z^2 + \frac{B}{4}P_z^4. \tag{3.71}$$

Let us denote the corresponding energy by E_D. Thus we can visualize the dynamics of P_z by the motion of a classical particle in $V(P_z)$ with kinetic energy $T(\dot{P}_z)$ and

total energy E_D. The Hamiltonian density H_D and energy E_D defined in eqn.(3.69) are different from the Hamiltonian density $\tilde{H}_D$ and energy $\tilde{E}_D$ that can be derived directly from eqn.(3.19) in the Duffing limit,

$$\frac{\tilde{H}_D}{\zeta} = -(\frac{1}{2\kappa} + C) \tag{3.72}$$

and will allow us to determine the dependence of the dynamics on the energy of the original system. For both the trajectory given by the motion of the polarization vector $P(P_x, P_y, P_z)$ is restricted by the invariant P to a sphere of radius $|P| = 1$ and determined on that sphere by the invariant C given by eqn.(3.68). The sphere is called the "Poincaré sphere" and is in extensive use in molecular mechanics under the notion "polyad phase-sphere" [32]. It allows us to display the phase space trajectories of eqn.(3.64) for given κ. The initial condition dependence is absorbed in the invariant C.

From here on we will proceed in three steps. First, we will discuss the initial condition dependence of the dynamics of P_z in terms of the Hamiltonian density H_D and summarize the results in a phase diagram. Second, we will connect that phase diagram to the phase plane A_D. As a result we will arrive at the Poincaré sphere. Third, the parametric forms of the trajectories as functions of θ will be given.

Phase diagram in the Duffing limit

In this section we lay out briefly the construction of the phase diagram. A more detailed discussion can be found in chapter 2.

The potential parameters A, B in V depend on the original Hamiltonian parameters $\mu\omega^2, \chi$ and ζ; in addition, A depends on the initial conditions $(P_x(\theta_0), P_z(\theta_0))$. Since $B > 0$, $V(P_z)$ can either have one minimum or one maximum and two minima, dependent on the sign of A. The transition between these two forms occurs at $A = 0$ and indicates a possible bifurcation in P_z, where the center point $S_D^{(1)}$ at the origin of A_D changes to a saddle point and two new center points $S_D^{(3,4)}$ appear. The following dynamic regimes are possible.

- For all extrema of $V(P_z)$, P_z is stationary.

- For the case of a single minimum P_z oscillates around $P_z = 0$, i.e. the charge density undergoes complete exchange between the two sites within half a period P_z.

- For the case of two minima we distinguish between two situations.

  - First, if $E_D > 0$, P_z again oscillates around $P_z = 0$, yet due to the potential well with reduced velocity at its equilibrium position.

  - Second, if $E_D < 0$, P_z oscillates around one of values for which $V(P_z)$ has a minimum, i.e. the charge density is not completely exchanged between the two sites and is trapped on one of the sites.

- Transitions between regimes occur for certain values of κ and the initial conditions $(P_z(\theta_0), P_x(\theta_0))$, which we will discuss first.

The dependence on initial conditions is best displayed in a phase diagram spanned by $(P_z(\theta_0), P_x(\theta_0))$ similar to the one used in the previous chapter. Let us briefly reintroduce the construction. First, note that $(P_x(\theta_0))^2 + (P_z(\theta_0))^2 \leq 1$ which restricts the accessible area of the phase diagram to the unit circle. There are two lines that separate three different dynamic regimes.

- The regions of single minimum and double minima potentials are separated by the bifurcation parabola

$$P_x^b(\theta_0) = \kappa - \frac{P_z^2(\theta_0)}{2\kappa}, \tag{3.73}$$

  which we readily we obtain from the condition $A = 0, C = \kappa$ in eqn.(3.65) .

- The regions for which $E_D > 0$ and $E_D < 0$ are separated by self-trapping parabola

$$P_x^s(\theta_0) = 1 - \frac{P_z^2(\theta_0)}{2\kappa}, \tag{3.74}$$

  which we readily we obtain from the condition $E_D = 0, C = 1$ in eqn.(3.69).

- In order to locate a state of given energy $\tilde{E}_D$ in the phase diagram, we solve eqn.(3.72) for $P_x(\theta_0)$, to obtain the spectral parabola

$$P_x^{\lambda}(\theta_0) = C - \frac{P_z^2(\theta_0)}{2\kappa}, \tag{3.75}$$

$$C = -(\frac{\tilde{E}_D}{\zeta} + \frac{1}{2\kappa}). \tag{3.76}$$

- For the case that the system is found in one of its stationary states we obtain from eqn.(3.64), $S_D[P_z(\theta_0), P_x(\theta_0)]$

$$S_D^{(1,2)} = (0, \pm 1), S_D^{(3,4)} = (\pm\sqrt{1-\kappa^2}, \kappa). \tag{3.77}$$

The stationary states lie on the unit circle. Their location depends only on the parameter κ, which was also found by [12].

Figure 3-1 displays several possible states in the phase diagram for given κ.

We see that the area of the phase diagram within the unit circle is divided into three regions by two parabolae of slope $-1/\kappa$, one, whose ordinate is fixed at $P_x(\theta_0) = 1$, the other variable at $P_x(\theta_0) = \kappa$.

- For $C > 1$ the corresponding state lies in the region of trapped motion,
- for $1 > C > \kappa$ the corresponding state lies in the region of free motion, yet is subjected to a double minimum potential and
- for $\kappa > C$ the corresponding state lies in the region of free motion in a single minimum potential.

The parametric dependence on κ of these transitions can be immediately read from the phase diagram. Remember, that small values of κ imply a dominance of the on site polarization mediated by χ over the transfer of charge density between the sites mediated by ζ, resulting in a high tendency of the excess charge to be trapped on one of the sites. This translates into the phase diagram as follows. For small absolute values of κ the area of trapped motion is large compared to the area of free motion.

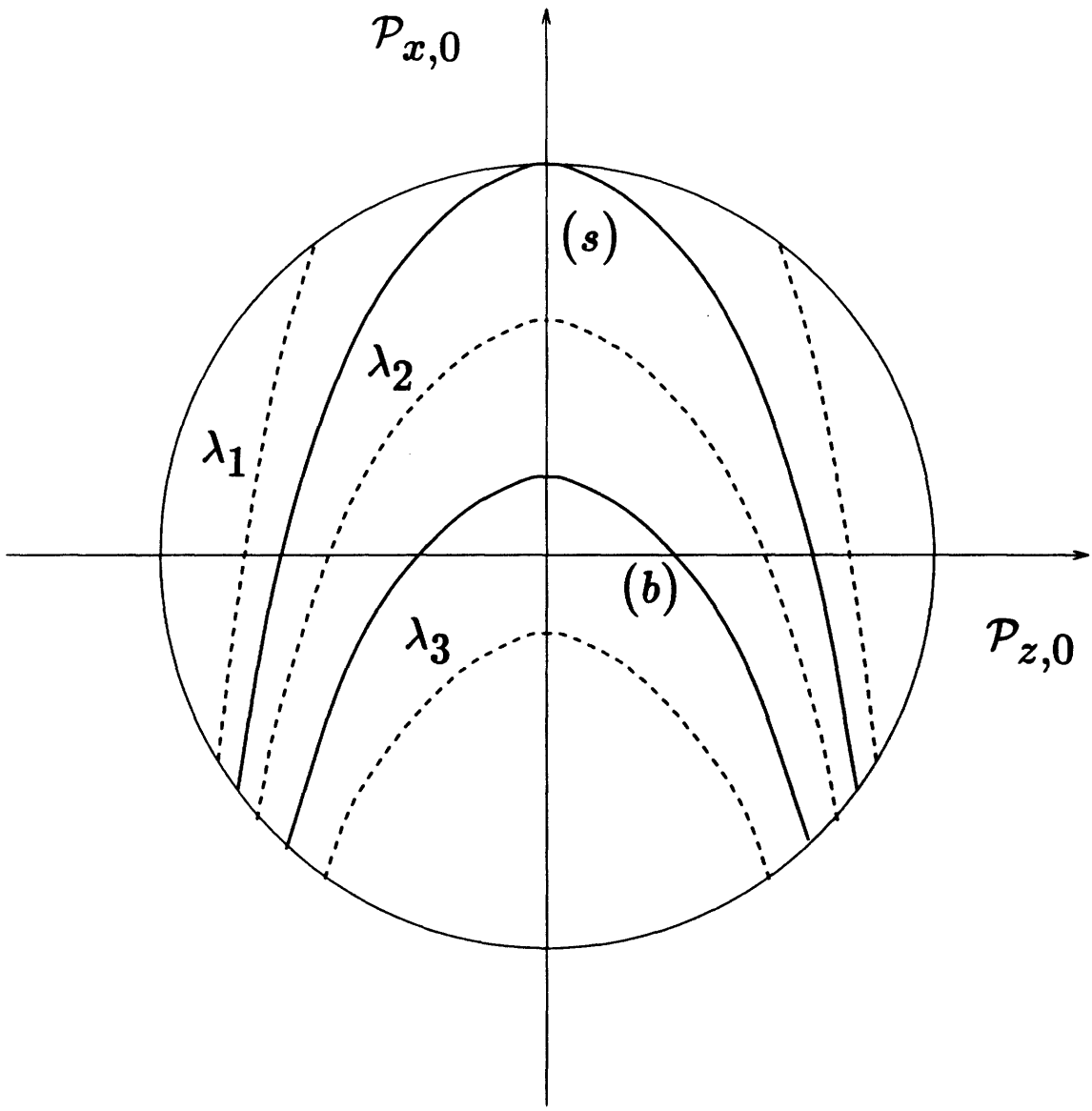

Figure 3-1: Phase diagram for $0 < \kappa < 1$. The solid circle (-) restricts the accessible area of the phase diagram. The solid parabolae (-) are the localization parabola (s) and the bifurcation parabola (b). The dashed parabolae (- -) are in the local mode region (λ_1), in the normal mode region in a double well potential (λ_2) and in the normal mode region in a single well potential (λ_3)

Thus there exists a wide range of initial conditions for which the excess charge is undergoing trapped motion. For large values of κ the situation is reversed.

In agreement with the phase space analysis we see that a *necessary condition for self-trapping is that* $\kappa < 1$, since for $\kappa > 1$ the self-trapping line and the unit circle includes no area within the circle. Then self-trapping is impossible for any initial condition.

In addition, since all the parabolae in the phase diagram have the same curvature, a change in dynamical properties is only possible by shifting the spectral parabolae horizontally, i.e. by a change in energy. Therefore the process of trapping cannot be described by the model in its current form.

The amplitude transition In addition to the two discussed transitions, a third transition was reported, called the "amplitude transition" [27]. It was observed, that for given initial conditions $P_z(\theta_0) \leq 1, P_y(\theta_0) = 0$ the amplitude of oscillation is either upper or lower bounded by $P_z(\theta_0)$, depending on κ. We will argue that the amplitude transition is not a well defined concept. First, let us consider the potential V and its minimum at $P_{z,min} > 0$. Suppose that $P_z(\theta_0) > 0$. The kinetic contribution $T = 0$. Thus if $P_z(\theta_0) < P_{z,min}$ the amplitude of oscillation will increase initially and have the lower bound $P_z(\theta_0)$. If $P_z(\theta_0) > P_{z,min}$ the amplitude of oscillation will decrease initially and have the upper bound $P_z(\theta_0)$. In the phase diagram this transition is located at the point $(\sqrt{1-\kappa^2}, \kappa)$ on the unit circle, thus being different from the other two transitions occurring along lines and separating regions in the diagram. Second, let us drop the condition $P_y(\theta_0) = 0$ and consider the phase plane A_D. Let us divide the area around the focal point, given by the intersection of the spectral line and the $P_z(\theta_0)$ at $P_{z,foc}$ in quadrants. Now we have to distinguish four cases. If we place the system initially in one of these quadrants, we would observe that $P_z(\theta_0)$ would neither be the upper nor the lower bound of the amplitude of P_z. Thus, the notion of the amplitude transition has lost its meaning.

A brief comment on the eigenstates of the system is in order: site exchange symmetry forces the eigenstates to $P_z = 0$. For $\kappa < 1$ the symmetry of the eigenstates

is parametrically unstable against a symmetry breaking perturbation. The effect of symmetry breaking perturbations was numerically investigated for the eigenstates of the Peierls-Hubbard dimer [33] and is extensively discussed in chapter 2 in the context of the Darling-Dennison System.

Geometrical representation of the trajectories on the Poincaré sphere

Difficulties in the interpretation of the effects of change in the initial condition can be avoided by combining the information contained in the phase plane $A_D(P_z, P_y)$ and the phase diagram (P_z, P_x) on the surface of the Poincaré sphere in the right handed coordinate system (P_x, P_y, P_z). The invariant P gives the radius of the Poincaré sphere by $|P| = 1$. The invariant C determines the trajectory on the sphere. The phase plane A_D can be obtained from the Poincaré sphere as the projection of a trajectory specified by C, κ onto the (P_y, P_z) plane, and the phase diagram as the projection onto the (P_z, P_x) plane. We will call the points $(1, 0, 0), (-1, 0, 0)$ the north pole and the south pole, the lines $P_x = 0, (P_z)^2 + (P_y)^2 = 1; P_z = 0, (P_x)^2 + (P_y)^2 = 1$ the equator and the zeroth meridian, separating the northern and southern or western and eastern hemispheres.

- For $\kappa < 1$ the north pole is occupied by a saddle, the south pole by a center as stationary points. Two additional centers as stationary points specified by the coordinates $(\kappa, 0, \pm\sqrt{1-\kappa^2})$ lie on the stationary meridian in the northern hemisphere parametrized by $P_y = 0, P_x \leq 0, (P_z)^2 + (P_x)^2 = 1$. The self-trapping line appears as a separatrix on the sphere, originating at the north pole, embracing regions of trapped motion on the western and eastern hemispheres, largely extended over the northern hemisphere. Around the south pole we find the region of free motion. The bifurcation line appears as a bifurcation loop south from the separatrix. The picture is in complete analogy to Figure 2-3.

- For $\kappa > 1$ we find centers on the poles as stationary points. The area of free motion extends over the complete Poincaré sphere.

The charge density dynamics can be interpreted as motion in the harmonic potential C under the constraint that the trajectory has to lie on a sphere.

For a given trajectory in the phase diagram, we can identify the points of intersection of the spectral line and the unit circle with the turning points of the motion. The points of intersection with the P_z axis constitute foci of the motion in A_D. At these points the trajectory on the sphere arrives at the maximum value of P_y.

It is straightforward to show, that trajectories in the areas of free motion circulate counterclockwise around the P_x axis and trajectories in the trapped region counterclockwise for positive P_z, clockwise for negative P_z around the P_z axis.

In summary, the excitation of the nonlinear dimer behaves in the limit of slow charge density motion and instantaneous adjustment of the vibrational equilibrium configuration like a quasiparticle in a single or double well potential. The quasiparticle consists of the excess charge and the induced distortion of the molecular equilibrium configuration that it drags around. They become simultaneously trapped if the kinetic energy of the quasiparticle vanishes before it reaches the top of the potential barrier of the double well form of the Duffing potential. The details of this process can be directly read off the Poincaré sphere and interpreted in complete analogy to the discussion of the Darling-Dennison system in chapter 2.

Analytic solution of the Duffing equation

The analytical form of $P(P_x, P_y, P_z)$ are obtained in a straightforward manner. P_z can be solved for in terms of Jacobian elliptic functions. Most of the results for P_z were obtained by Kenkre and co-workers [5, 27, 18, 25, 26]. The solutions for P_x, P_y follow immediately from eqn.(3.67,3.68). From the definitions of P_x, P_y, P_z in eqn.(3.10-3.13) one can then easily solve for the wavefunction of the excess charge in terms of a_1, a_2.

The proper ansatz is given by

$$P_z(\theta) = Df(\Omega\theta - \Phi|m). \tag{3.78}$$

Here f is a Jacobian elliptic function with frequency Ω, phase Φ and parameter m.

Inserting in eqn.(3.64) and using eqn.(3.67,3.68) one obtains three different solutions, dependent on the parameter m.

- For $m < 0$ the solution is given by

$$\begin{aligned} P_z &= Dnd(\sqrt{1+|m|}[\Omega\theta - \Phi_{nd}]|\frac{1}{1+|m|}) \\ \Phi_{nd} &= -\frac{1}{\sqrt{1+|m|}}F(\arcsin\sqrt{\frac{1-(\frac{D}{P_z(\theta_0)})^2}{m}}|\frac{1}{1+|m|}). \end{aligned} \tag{3.79}$$

- For $0 < m < 1$ the solution is given by

$$\begin{aligned} P_z &= Dcn(\Omega\theta - \Phi_{cn}|m) \\ \Phi_{cn} &= -F(\arccos\frac{P_z(\theta_0)}{D}|m). \end{aligned} \tag{3.80}$$

- For $1 < m$ the solution is given by

$$\begin{aligned} P_z &= Ddn(\sqrt{m}[\Omega\theta - \Phi_{dn}]|\frac{1}{m}) \\ \Phi_{dn} &= -\frac{1}{\sqrt{m}}F(\arcsin\sqrt{\frac{1-(\frac{P_z(\theta_0)}{D})^2}{m}}|\frac{1}{m}). \end{aligned} \tag{3.81}$$

- The results for D, m and Ω are

$$D = \pm\sqrt{-2\kappa(\kappa - C) + 2\kappa\sqrt{1+\kappa(\kappa-2C)}} \tag{3.82}$$

$$m = \frac{1}{2}(1 - \frac{\kappa - C}{\sqrt{1+\kappa(\kappa-2C)}})] \tag{3.83}$$

$$\Omega = \frac{D}{2\kappa\sqrt{m}}. \tag{3.84}$$

Here cn, dn, nd are Jacobian elliptic functions, F an elliptic integral of the first kind. There are several things to notice.

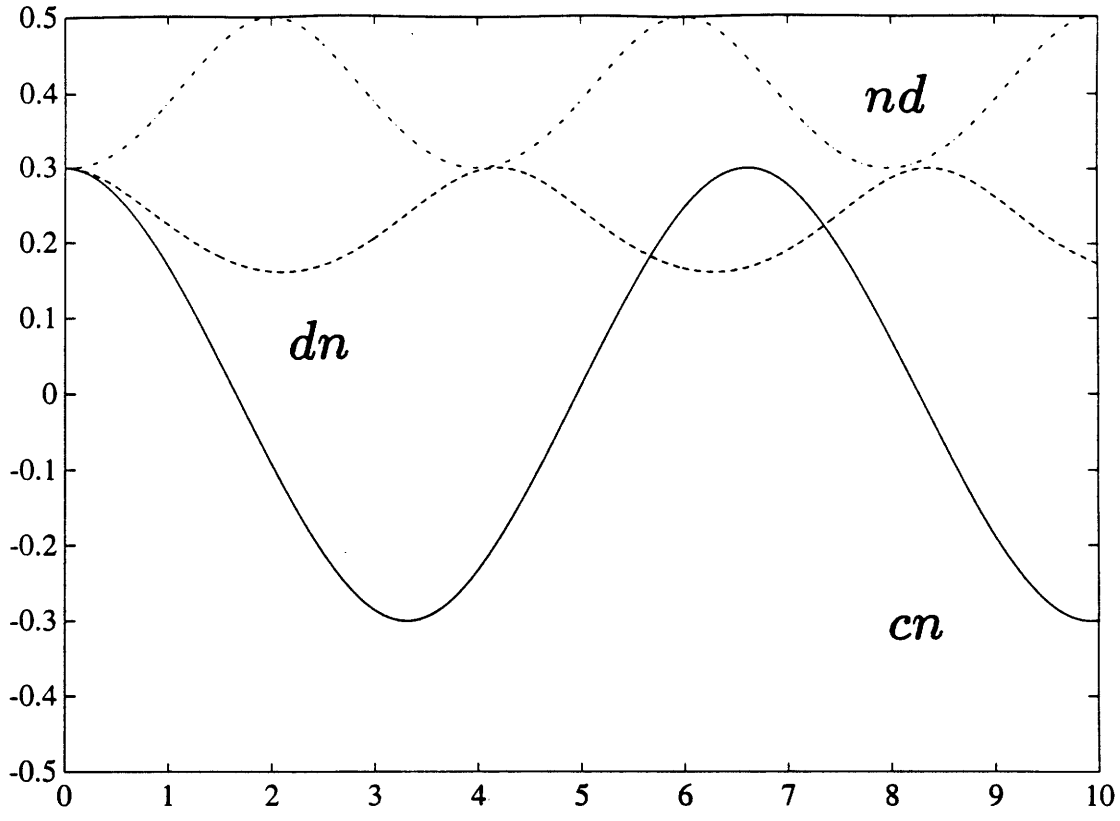

Figure 3-2: Jacobian elliptic functions. The abscissa is calibrated in units of the quarter periods $K(m = 1.4)$ of $dn(m = 1.4)$. The solid line (-) indicates $cn(m = 0.2)$, the dashed line(- -) $dn(m = 1.4)$ and the dashed-dotted line (-.) $nd(m = -0.5)$.

- First, for the different domains of the parameter m we get qualitatively differing results as displayed in Figure 3-2.
  - The cn function oscillates between the upper bound D and lower bound $-D$. Thus the excess charge density is completely transferred after two quarterperiods, which are usually denoted by K.
  - The dn function oscillates with the upper bound D (or lower bound $-D$) but does never change the sign of its range. Thus the excess charge density is never completely transferred and has to be considered trapped.
  - The nd function oscillates with the lower bound D (or upper bound $-D$) and thus describes trapped motion as well.

The transitions between these functions depend on the parameter m. Thus we

should be able to recover the phase diagram of the foregoing section from the expression for m as given by eqn.(3.83). This is indeed the case. The condition $m = 1/2$ yields $C = \kappa$ and thus the bifurcation line as given by eqn.(3.73). The condition $m = 1$ yields $C = 1$ and thus the self-trapping line as given by eqn.(3.74). For the discussion of the transition from dn to nd which formally occurs as m changes sign, see the last section.

- Second, the frequency Ω depends on the initial amplitude D, in sharp contrast to linear dynamical systems.

- Third, let us consider the case of a pure state, i.e. $P_z(\theta_0) = 1$. From eqn.(3.82-3.84) we obtain $D = 1, m = 1/4\kappa^2, \Omega = 1$.

  - In the limit of no coupling between excess charge and molecular vibration, $\kappa \to \infty$, the excess charge density oscillates unhinderedly between the sites, as can be seen from

$$\lim_{m\to 0} P_z = \lim_{m\to 0} cn(\theta|m) = \cos(\theta). \tag{3.85}$$

  - In the limit of no electronic intersite coupling, $\kappa \to 0$, the initial excess charge distribution is maintained at all times, as can be seen from

$$\lim_{m\to \infty} P_z = \lim_{m\to \infty} dn(\theta|\frac{1}{m}) = 1. \tag{3.86}$$

To see how the wavefunction of the nonlinear dimer compares to the linear case, $\kappa \to \infty$, let us have a look at the analytic expression for the wavefunction for the pure state. Using eqn.(3.67,3.68,3.10-3.13) we obtain for $0 < m < 1$

$$a_1 = \cos[\frac{1}{2} am(\theta|\frac{1}{4\kappa^2})] \tag{3.87}$$

$$a_2 = \sin[\frac{1}{2} am(\theta|\frac{1}{4\kappa^2})] \exp[-i(\arccos dn(\theta|\frac{1}{4\kappa^2}) + \frac{\pi}{2})], \tag{3.88}$$

and for $1 < m$

$$a_1 = \pm\sqrt{\frac{1 + dn(\frac{\theta}{2\kappa}|4\kappa^2)}{2}} \tag{3.89}$$

$$a_2 = \pm\sqrt{\frac{1 - dn(\frac{\theta}{2\kappa}|4\kappa^2)}{2}} \exp\left[-\frac{i}{2}(am(\frac{\theta}{2\kappa}|4\kappa^2) + \pi)\right]. \tag{3.90}$$

Here am is called the elliptic amplitude and related to cn via $\cos\left[am(\theta|m)\right] = cn(\theta|m)$. For $0 < m < 1$ we see, that the phase difference of a_1, a_2 oscillates around $\frac{\pi}{2}$ but does not complete cycles of 2π, whereas the argument of the trigonometric functions does. For $1 < m$ the situation is reversed. Note that neither the phase nor the argument show linear time dependence but are periodic functions in time. An interpretation of the charge density motion in term of a hindered rotation is possible in analogy to the hindered rotor model for the Darling-Dennison system.

Extension to damped and driven systems and comparison to numerical results

The identification of the dynamics of P_z with that of an undriven Duffing oscillator without damping suggests further exploitation for cases when P_z is subject to damping or to a driving force. Both cases have been carefully studied for the Duffing oscillator.

Damping of P_z can be introduced in the equations of motion in various ways, e.g. on the level of the reduced dynamic equations by a phenomenological damping term of the form $f(\delta_\theta P_z)$, or on the level of the complete dynamic equations by a damping term of the form $f(\dot{Q}_a, \dot{P}_z)$. In any case, C is no longer an invariant.

The phenomenological damping term of the reduced dynamic equations brings the advantage of simple mathematical treatment, yet has the disadvantage of being an ad hoc correction lacking physical meaning. The damping of P_z mediated by the damping of the molecular vibrations introduced on the level of the complete dynamic equations correctly reflects the physical situation. The nonlinear dimer loses energy due to the coupling of the molecular vibrations to a bath of phonons. The disadvantage is, that after the elimination of the vibrational coordinates the dynamic equation for P_z

is a nontrivial extension of the Duffing equation, making additional approximations necessary. Similar difficulties appear upon introduction of a driving force term in the dynamic equations. The topic is still under investigation.

In this section we will only qualitatively discuss extensions to the damped Duffing oscillator without driving force and thus prepare the way for the interpretation of numerical studies by Kenkre and Wu [25, 26]. The model under investigation includes a phenomenological damping term for the vibrational mode Q_a in the complete dynamic equations. Eqn.(3.15) reads now

$$\ddot{Q}_a + \gamma\dot{Q} + \omega^2 Q_a - \frac{\chi}{\mu} P_z = 0. \tag{3.91}$$

Under the assumption $\gamma \gg \omega \gg \zeta$ it was shown that the number and location of the stationary points in the Duffing limit are the same for both the damped and undamped system. Q_a reaches the equilibrium position $-\beta P_z$ on a timescale γ . The numerical studies were carried out beyond this limit.

It is easy to see from eqn.(3.28,3.29) that number and location of the stationary points as well as the value $\kappa = 1$ of the bifurcation of the complete system do not change. Yet the stability of the stationary points and thus the phase portrait on the Poincaré sphere is different from the undamped case. Let us assume, for simplicity, that the Poincaré sphere is still the proper representation for the charge density dynamics in the Duffing limit. This assumption is justified if the characteristic time $1/\gamma$ is short compared to $1/\zeta$.

The Poincaré sphere shows the following features for the damped system, already described in the last chapter in Figure 2-19 and Figure 2-20. Since they are crucial for the following discussion of numerical data let us briefly review the features. For $\kappa > 1$ there are two stationary points: a stable spiral point at the north pole $(1, 0, 0)$ and an unstable spiral point at the south pole $(-1, 0, 0)$. For all initial conditions but the unstable spiral point, the trajectory will converge to the north pole. For $\kappa < 1$ there are four stationary points: the saddle at the north pole $(1, 0, 0)$, two stable spiral points at $(\kappa, 0, \pm\sqrt{1-\kappa^2})$ and an unstable spiral point at the south pole $(-1, 0, 0)$. A

separatrix originates at the unstable spiral point and leads to the saddle point. The sphere is split in two basins of attraction, one for each of the stable stationary points. Thus for any initial condition but the unstable stationary points or the separatrix the stationary state of P_z will be determined by the location of the stable stationary points.

We will now list the findings of the two numerical studies in terms of our conventions and definitions and interpret these with the help of the Poincaré spheres.

The first study [25] was concerned with the changes in the propagation of a pure state, $P_z(\theta_0) = 1$ for different values of m.

- At $m = \frac{1}{2}$ a "static transition" was observed: For $m < \frac{1}{2}$ the stationary state is located at the north pole $(1, 0, 0)$, for $m > \frac{1}{2}$ at $(-\kappa, 0, \pm\sqrt{1-\kappa^2})$.

  This transition is the bifurcation in P_z discussed in the previous section.

- At $m = 1$ a "dynamic transition" was observed: For $m < 1$ the short time behaviour of P_z is given by the *cn* evolution, for $m > 1$ by the *dn* evolution.

  This transition is the self-trapping transition discussed in the previous section. In the first case, the trajectory has to pass the region embraced by the separatrix which is wrapped around the south pole of the Poincaré sphere, in the second it just circulates in the hemisphere of one of the stable stationary points.

- For $\frac{1}{2} < m < 1$ there appeared to be a "potentially misleading evolution": After being initially damped to the value $P_z \approx 0$ the following evolution led to one of the stable stationary points.

  After having passed the separatrix wrapped around the south pole, the trajectory approaches the north pole and is then further directed in the corresponding basin of one of the stable stationary points.

- For $m > \frac{1}{2}$ the location of the stationary state depends on the damping rate γ.

  Different damping rates correspond to different phase portraits, the separatrix embraces different regions on the Poincaré sphere as basins of attraction. Thus

for fixed initial conditions of P we have to expect a switching back and forth of the stationary states between the stationary points as we vary γ.

The second study [26] was concerned with the changes of the propagation of states $P_z \approx 0$ with varying initial phase differences.

- For initial phase difference 0, i.e. $P_x(\theta_0) = 1$, it was found, that P_z rapidly converges against one of the stable stationary points. For initial phase difference π, i.e. $P_x(\theta_0) = -1$, it was observed, that P_z starts oscillating around $P_z = 0$ with increasing amplitude ("antidamping"), until it eventually shows bias towards positive or negative values and finally approaches one of the stable stationary points.

  In the first case the trajectory starts near the north pole of the Poincarè sphere and consequently circulates towards one of the stable stationary points. In the second case it starts nearby the south pole. Since the stable stationary points lie on the northern hemisphere, the trajectory has to overcome the equator. Depending on the slope of the separatrix along the equator, P_z has to oscillate with increasing amplitude upon crossing the equator until it will finally converge to one of the stable stationary points.

- For intermediate values of the initial phase difference and $P_z(\theta_0) = 0.6$ two phenomena have been observed. First, the location of the stationary state switches back and forth between the two stable stationary points, second the "undamping" becomes less explicit as the initial phase difference approaches π.

  Changing the initial phase difference for fixed $P_z(\theta_0)$ sweeps the initial point of the trajectory over the two alternating basins of attraction embraced by the separatrix, thus causing the switching between the stable stationary points as stationary states. The loss of "undamping" has already been discussed.

3.3.2 Remarks on the dynamics of molecular vibrations in the standard adiabatic limit

The standard adiabatic equation eqn.(3.62) has been extensively studied, yet the analytical solution is not known to our knowledge. We will only briefly line out how to approximate analytically the solution in the regime of weak coupling of the excess charge and the molecular vibrations for small amplitudes.

Let us first simplify the notation by dropping the superscript (0). Eqn.(3.62,3.63) read now

$$\delta_\tau^2 Q_a = -Q_a[1 \pm \frac{1}{\kappa\sqrt{1+(\alpha Q_a)^2}}]. \tag{3.92}$$

We will now connect eqn.(3.92) to the result from standard adiabatic theory. Here one solves for the dynamics of the molecular vibrations under the assumption that the excess charge occupies an eigenstate for each value of the parameter Q_a. Technically, the Hamiltonian density eqn.(3.19) is brought into diagonal form by a real valued wavefunction for the excess charge. The two eigenvalues are calculated as functions of Q_a. One can then obtain the lower and upper adiabatic potential by plotting separately the lower and the upper of the two eigenvalues versus the vibrational coordinate Q_a. This translates in our derivation into the condition $P_y(\tau_0) = 0$. We see, that for this condition the timescale analysis and the standard adiabatic theory yield the same result, which explains, why we called eqn.(3.62) the standard adiabatic equation.

Yet there is one important difference. If one is interested in the phonon dynamics for the case that the charge density contains states of the upper and lower adiabatic potential surface, the potential obtained from standard adiabatic theory is no longer correct. As easily can be checked, a modification as to forming a coherent superposition of the two adiabatic eigenstates does *not* give the factor $\sqrt{G}$ in eqn.(3.63). The perturbative result eqn.(3.92) is valid only if on the timescale of the phonon motion the kinetic energy of the charge density motion is *on average* vanishing, i.e.

$P_y^{(0)}(\tau_0) = P_y^{(0)}(\tau) = 0.$

The adiabatic potential is not static but *dynamic* in the sense that it depends on the initial momentum of the charge density motion. Thus placing a wavepacket in one potential well at some energy above the ground state not only reduces the difference to the top of the barrier by that amount, but also lowers the barrier, so that in effect the distance to the top of the barrier is further reduced. The zeroth order perturbative result is no longer sufficient to correctly describe the dynamics.

Let us continue with a discussion of the phonon dynamics. In analogy to the procedure in the Duffing limit we define the Hamiltonian H_L for the molecular vibration in the standard adiabatic limit by

$$H_L = \frac{1}{2}\dot{Q_a}^2 + \frac{1}{2}Q_a^2 \mp \frac{\beta}{\alpha}\sqrt{1+(\alpha Q_a)^2}. \tag{3.93}$$

We identify the kinetic contribution T and the potential contribution $V(Q_a)$ to the total energy E_L as

$$T = \frac{1}{2}\dot{Q_a}^2 \tag{3.94}$$

$$V_{\mp} = \frac{1}{2}Q_a^2 \mp \frac{\beta}{\alpha}\sqrt{[1+(\alpha Q_a)^2]}. \tag{3.95}$$

For the lower potential V_- we observe a change from one to three extrema at $\kappa = 1$. Self-trapping occurs at $E_L = 0$. Now let us consider the limit of weak coupling between the excess charge and the molecular vibrations for small amplitudes, i.e. $\sigma = (\alpha Q_a)^2 \ll 1$. V_- can be approximated to order σ^2 by

$$V_- \approx -\frac{\beta}{\alpha} + \frac{1}{2}(1-\frac{1}{\kappa})Q_a^2 + \frac{\alpha^2}{8\kappa}Q_a^4. \tag{3.96}$$

Within this approximation, the dynamics of Q_a is governed by the Duffing equation

$$\delta_\tau^2 Q_a = -(1-\frac{1}{\kappa})Q_a - \frac{\alpha^2}{2\kappa}Q_a^3, \tag{3.97}$$

which can be solved exactly in terms of Jacobian elliptic functions. Note that number

and stability of the stationary points as well as the value of κ for the bifurcation coincide with those of the complete phase space, yet the location is different.

3.4 Conclusion

We have shown a systematic way to explore the dynamical properties of the nonlinear dimer. The exact dynamic equations were directly obtained from the principle of least action. Phase plane analysis led us to approximations based on time scale arguments. The bifurcation parameter κ plays a prominent role in several ways. It shows that charge density motion and molecular vibrations become simultaneously unstable against localization and indicates the onset of instability *regardless* of any assumption about the involved timescales. We conclude that localization is possible not only in the two limiting cases where the timescales of charge density motion and molecular vibration can be separated, but also in the intermediate regime. Furthermore, κ can be used as a guide to assure the qualitative correctness of the analytic results obtained in the limiting cases. These limiting cases are instructive from a physical point of view, since the actual mechanism of localization can be understood.

In the Duffing limit the charge density dynamics can be mapped on the dynamics on a classical Duffing oscillator, yet with the difference that the potential is not static but dynamic since in the electronic coordinates it depends on the electronic momentum. In particular, it can change upon decrease of initial kinetic energy from a single well potential to a double well potential. Localization can then occur in one of the wells. We have devised two graphical representations of the charge density dynamics that allow the complete overview of all possible dynamical behaviors in the Duffing limit and proved to be especially useful in the interpretation of numerical results for the damped dimer. There, the kinetic energy of the charge density motion is decreasing, a potential barrier is forming, and the final extent of charge density localization is decreased with increasing coupling χ.

In the standard adiabatic limit the dynamical analysis showed, that the adiabatic procedure is valid only for stationary charge densities. With increasing initial kinetic

energy of the charge density motion the adiabatic potential barrier becomes more and more transparent. In the weak coupling limit, the dynamics of molecular vibrations can be approximated by a Duffing oscillator.

In terms of the quasiparticle language, the Duffing limit produces an electronic excitation that is accompanied by an instantaneously adjusting distortion of the molecular equilibrium configuration and the standard adiabatic limit produces a vibrational excitation that is accompanied by an instantaneously adjusting charge density configuration. If the quasiparticle excitation of the nonlinear dimer becomes localized in one potential well of the double well forms of the dynamical potentials, the system takes a ground state that does not carry the site exchange symmetry of the Lagrangian. Then dynamical symmetry breaking occurs in the nonlinear dimer.

Let us finish with a brief comment on the relevance for the phenomenon of *collapse of a wave packet.* It has been argued [2, 3], that the localization of the charge density is due to the classical nature of the associated phonon coordinate. Our own numerical calculations show, that for the quantum mechanical phonon, localization occurs as well, yet the transition is shifted to smaller values of $|\kappa|$. This can be explained from the fact that the potential barrier has to be high enough to allow a bound state of the phonon. If this is the case, then it can be shown in analogy to the treatment of the quantum mechanical Darling-Dennison system, that the system is susceptible to fluctuations in form of symmetry breaking perturbations that lead to largely localized eigenstates.

Bibliography

[1] L. J. Bernstein, *Physica D* 53 240 (1991).

[2] L. L. Bonilla, F. Guinea, *Phys. Lett. B* 271 196 (1991).

[3] L. L. Bonilla, F. Guinea, *Phys. Rev. A* 45 (11) 7719 (1992).

[4] P. N. Schatz, in: Mixed Valence Compounds, ed D. B. Brown, D. Reidl Publ. Comp. (1980).

[5] V. M. Kenkre, G. P. Tsironis, *Phys. Rev. B* 35 (4) 1473 (1987).

[6] T. Holstein, *Ann. Phys.* 8 325 (1959).

[7] T. Holstein, *Ann. Phys.* 8 343 (1959).

[8] A. S. Davydov, *J. theor. Biol.* 38 559 (1973).

[9] A. S. Davydov, N. I. Kilukha, *Phys. Stat. Sol. B* 59 465 (1973).

[10] A. S. Davydov, *Sov. Phys. Usp.* 25 (1982) 898.

[11] A. C. Scott, P. S. Lohmdahl, J. C. Eilbeck, *Chem. Phys. Lett.* 113 (1) 29 (1985)

[12] J. C. Eilbeck, P. S. Lohmdahl, A. C. Scott, *Physica D* 16 318 (1985).

[13] J. Carr, J. C. Eilbeck, *Phys. Lett. A* 109 (5) 201 (1985).

[14] I. Nussbaum, *Phys. Lett. A* 118 (3) 127 (1986).

[15] S. De Filippo, M. Salerno, *Phys. Lett. A.* 142 (8,9) 479 (1989).

[16] V. Z. Enol'skii, M. Salerno, N. A. Kostov, A. C. Scott, *Physica Scripta* 43 229 (1991).

[17] V. Z. Enol'skii, M. Salerno, A. C. Scott, J. C. Eilbeck, *Physica D* 59 1 (1991).

[18] V. M. Kenkre, D. K. Campbell, *Phys. Rev. B* 34 (7) 4959 (1987).

[19] L. Cruzeiro-Hansson, P. L. Christiansen, J. N. Elgin, *Phys. Rev. B* 37 (13) 7896 (1988).

[20] D. Hennig, *Physica D* 64 121 (1993).

[21] P. X. Tran, L. E. Reichl, *Phys. Lett. A* 121(3) 135 (1987).

[22] P. X. Tran, *Phys. Lett. A* 123(5) 231 (1987).

[23] P. X. Tran, T. Tamura, *Phys. Rev. B* 37 (4) 2270 (1988).

[24] A. C. Scott, *Philos. Trans. R. Soc. London*, Ser A 315 423 (1985).

[25] V. M. Kenkre, H. -L. Wu *Phys. Rev. B.* 39 (10) 6907 (1989).

[26] V. M. Kenkre, H. -L. Wu *Phys. Lett. A* 135 (2) 120 (1989).

[27] G. P. Tsironis, V. M. Kenkre, *Phys. Lett. A* 127 (4) 209 (1988).

[28] K. W. DeLong, J. Yumoto, N. Finlayson, *Physica D* 54 36 (1991).

[29] Q. Zhang, V. Romero-Rochin, R. Silbey, *Phys. Rev. A* 38 (12) 6409 (1988).

[30] P. Kramer, M. Saraceno, Geometry of the time dependent variational principle in quantum mechanics, (1981) Springer.

[31] N. G. Van Kampen, *Phys. Rev.* 124 (2) 69 (1985).

[32] L. Xiao, M. Kellman, *J. Chem. Phys.*, 90 6086 (1989).

[33] Q. Zhang, R. Silbey, *J. Chem. Phys.* 92 (8) 4899 (1990).

Appendix A

Discrete fourier analysis of dynamical systems

The dynamical systems studied in this thesis are non-chaotic. However, it is instructive to apply some of the diagnostic tools that are commonly used to detect chaotic dynamics and to extrapolate to their performance for more complex systems. There are three major categories of such tools: Fourier transform methods, Lyapunov exponents and entropy measures [1]. Here we will deal only with the Fourier transform method and demonstrate that results obtained from it are quite ambiguous for the studied systems.

We begin with a brief account of the method. Fourier analysis of a time dependent real valued function $f(t)$ reveals its frequency components and associated power spectrum. It became practically relevant after the implementation as the fast Fourier transform algorithm on computers. Since the fast Fourier transform is a discrete method, let us denote the value of $f(t_k)$ at the instant $t_k = k\Delta t$ by f_k where Δt is a uniform time interval.

We expand each element $f_k, k = 1, 2, \ldots, n$ of the set of points $\{f_k\}$ as

$$f_k = \frac{1}{n} \sum_{l=1}^{n} \hat{f}_l \exp(-2\pi i k l/n). \tag{A.1}$$

$\hat{f}_l$ is then called the discrete Fourier transform of the set $\{f_k\}$. It is straightforward

to show that

$$\hat{f}_k = \sum_{l=1}^{n} f_l \exp(2\pi ikl/n), \tag{A.2}$$

i.e. f_k and $\hat{f}_l$ form a discrete Fourier transform pair. In order to extract the desired frequencies $\omega_l = 2\pi l/n\Delta t$ and associated powers $|\hat{f}_l|^2$ that constitute the power spectrum of the set $\{f_k\}$, we define the autocorrelation function

$$G_m = \sum_{k=1}^{n} f_k f_{k+m}, \tag{A.3}$$

which after some calculation can be shown to form a discrete Fourier transform pair with the powers $|\hat{f}_l|^2$, i.e.

$$G_m = \frac{1}{n} \sum_{l=1}^{n} |\hat{f}_l|^2 \exp(-2\pi iml/n), \tag{A.4}$$

$$|\hat{f}_l|^2 = \sum_{m=1}^{n} G_m \exp(2\pi iml/n). \tag{A.5}$$

This result is know as the Wiener-Kintchin theorem. It states that one can obtain the power spectrum of the set $\{f_k\}$ from its autocorrelation function and vice versa.

The time interval Δt and number of elements n influence the shape of the power spectrum. According to the sampling theorem, the Nyquist critical frequency $\omega_c = \pi/\Delta t$ must be larger than the bandwidth of $f(t)$ in order to allow the accurate determination of power spectrum. If this is not the case there results a distortion, called aliasing, that gives too large weight to the low frequency components. In addition, frequency components whose periods become comparable to $n\Delta t$ tend to distort the power spectrum towards the low frequency components.

Different dynamic regimes of the sets $\{f_k\}$ are to be distinguished on the basis of the corresponding power spectra:

- periodic motion results in power spectra that show distinct peaks at commensurate frequencies,
- quasiperiodic motion results in power spectra that show distinct peaks at non-commensurate frequencies and

- chaotic motion results in continuous noisy power spectra with bias towards low frequencies. This bias is due to the appearance of periods comparable of the size of the analysed set.

However, due to the discreteness of the computational transform the distinction between quasiperiodic and chaotic motion is academic, i.e. they can produce essentially the same characteristic discrete power spectra. Nevertheless, a large number of contributing frequencies often serves as an indicator of chaotic motion and was used in the context of the discrete self-trapping equation [2].

We will now show that this indicator is misleading for the systems discussed in this thesis and related systems. The analytic solutions for the complex mode amplitudes involve elliptic functions and are dependent on the frame of reference trigonometric functions (see e.g. eqn.(2.79,2.81)). The elliptic functions can be expanded in terms of trigonometric functions as [3]

$$cn(u|m) = \frac{2\pi}{\sqrt{m}K}\sum_{n=0}^{\infty}\frac{q^{n+1/2}}{1+q^{2n+1}}\cos(2n+1)v, \tag{A.6}$$

$$dn(u|m) = \frac{\pi}{2K}+\frac{2\pi}{K}\sum_{n=1}^{\infty}\frac{q^{n}}{1+q^{2n}}\cos 2nv, \tag{A.7}$$

$$nd(u|m) = \frac{\pi}{2\sqrt{1-m}K}+\frac{2\pi}{\sqrt{1-m}K}\sum_{n=1}^{\infty}(-1)^{n}\frac{q^{n}}{1+q^{2n}}\cos 2nv, \tag{A.8}$$

with the nome $q = \exp(\pi K'/K)$, the argument $v = \pi u/2K$, the quarter periods $K(m) = K'(1-m)$ and the parameter m. Now, it can be shown that as $m \to 1$, i.e. where the normal to local mode transition or trapping transition occur, $K \to \infty, q \to 1$ and $v \to 0$. This implies for the cn function that close to $m = 1$ many low frequency components begin to contribute with an exponential bias towards the lowest frequencies, and the power spectrum becomes very dense in that region. The discrete Fourier transform with its additional distortions discussed above will therefore not be able to distinguish the perfectly periodic behaviour of the elliptic functions from quasiperiodic or chaotic dynamics, especially if non-commensurate trigonometric functions are additionally involved due to different reference frames.

Obviously the situation becomes worse for more complex systems, such as higher

dimensional discrete self-trapping equations [2]. Here discrete Fourier transforms have been applied to study different dynamical regimes. The observed changes in the power spectra may result from the effect described above and are most probably not due to chaotic dynamics.

Bibliography

[1] S. N. Rasband, Chaotic Dynamics of Nonlinear Systems, John Wiley & Sons, Chapter 9, (1990).

[2] J. C. Eilbeck, P. S. Lohmdahl and A. C. Scott, *Physica D*, 16, 318 (1985).

[3] M. Abramowitz and I.A. Stegun, Handbook of Mathematical Functions, Dover, Chapter 16, (1965).

Appendix B

The spectroscopic condition number

The eigenvalue problem of the Darling-Dennison Hamiltonian H_{DD} exhibits the peculiarity that some eigenstates are extremely sensitive to symmetry breaking perturbations whereas others are not. The eigenvalues however do not show this sensitivity. One is tempted to state that somehow the problem of finding the eigenstates is "ill-conditioned" whereas the one of finding the eigenvalues is "well-conditioned".

Computational problems are called *ill-conditioned* if the values to be computed are very sensitive to small changes in the data. In algebraic eigenvalue problems the degree to which an eigenvalue problem is ill-conditioned is quantified in terms of a single parameter, called the *spectral condition number*. Although in general this number labels the behaviour of a particular matrix under diagonalization it does not indicate the particularly sensitive eigenvalues or their number. Neither does it imply that eigenvectors corresponding to sensitive eigenvalues are sensitive or that insensitive eigenvalues correspond to insensitive eigenvalues.

Let us briefly introduce the concept of the spectral condition number and then show why this number does not help us to detect the encountered instability in the Darling-Dennison Hamiltonian. This should make ultimately clear that the susceptibilities are not "just a trivial consequence of the near degeneracy of the eigenvalues" as a critic put it. We follow an exposition by Wilkinson [1].

The spectroscopic condition number

Consider the matrix R that under the similarity transformation by the matrix of its eigenvectors T takes the diagonal normal form

$$T^{-1}RT = diag(\lambda_i). \tag{B.1}$$

We introduce some erratic elements ϵS, ϵ being a parameter, into R according to

$$\tilde{R} = R + \epsilon S, \tag{B.2}$$

such that $\tilde{R}$ is diagonalizable and has an eigenvalue $\lambda \neq \lambda_i$. Then we may write

$$T^{-1}(\tilde{R} - \lambda I)T = diag(\lambda_i - \lambda)[I + \epsilon diag(\lambda_i - \lambda)^{-1}T^{-1}ST]. \tag{B.3}$$

Since by construction the matrix on the left is singular, the matrix on the right must be singular also and therefore have a vanishing determinant.

In order to proceed from here let us define the spectral norm $\| X \|_s$ of a matrix X as its largest possible eigenvalue. If $I + X$ is singular, $\| X \|_s \geq 1$ must be true; otherwise the determinant of $I + X$ cannot vanish. Therefore we may write

$$\epsilon \| diag(\lambda_i - \lambda)^{-1}T^{-1}ST \|_s \geq 1, \tag{B.4}$$

and after some manipulation

$$\epsilon \| T^{-1} \|_s \| T \|_s \| S \|_s \geq min|\lambda_i - \lambda|. \tag{B.5}$$

Thus there is at least one eigenvalue λ_i of R for which

$$|\lambda_i - \lambda| \leq \epsilon\rho(T) \| S \|_s, \tag{B.6}$$

$$\rho(T) = \| T^{-1} \|_s \| T \|_s . \tag{B.7}$$

ρ is called the spectral condition number. The larger ρ is the larger the upper bound on the deviation of the erroneous λ from the actual λ turns out to be. Note that for normal R

$$\rho(T) = \| T^{-1} \|_s \| T \|_s \geq \| T^{-1} T \|_s = 1. \tag{B.8}$$

This is certainly true for unitary or orthonormal T, i.e. hermitian or symmetric R. In those cases the condition number takes its smallest possible value $\rho = 1$. This implies that all quantum mechanical eigenvalue problems are well conditioned due to the hermiticity of the Hamiltonian.

Still, that seems surprising considering the Darling-Dennison system with its miniscule splittings between successive eigenvalues within a polyad. However, we have to bear in mind that each of those eigenvalues of a split pair can be obtained from a different block of the Hamiltonian in a symmetry adapted representation. Within those blocks all eigenvalues appear well separated. Therefore, in principle, we may separately determine those eigenvalues to any accuracy.

Instability of the eigenvector calculation for well-conditioned problems

Even if the eigenvalue problem is well conditioned the eigenvector problem may not be. This phenomenon appears in many algebraic eigenvalue problems. Wilkinson identifies as the most notorious case tridiagonal matrices with varying diagonal elements which appear in almost every field of physics. He offers an explanation which requires to go into some detail without trying to be pretentious.

Consider a real symmetric tridiagonal matrix R with diagonal elements $d_1, d_2, \ldots, d_n$ and off-diagonal elements $o_2, o_3, \ldots, o_n$. The eigenvalue problem is readily formulated for the components $a_1, a_2, \ldots, a_n$ of the eigenvector a and the eigenvalue λ as follows

$$(d_1 - \lambda)a_1 + o_2 a_2 = 0, \tag{B.9}$$

$$o_i a_i + (d_i - \lambda)a_i + o_{i+1} a_{i+1} = 0, i = 2, 3, \ldots, n-1 \tag{B.10}$$

$$o_n a_{n-1} + (d_n - \lambda)a_n = 0. \tag{B.11}$$

Let us suppose that we possess knowledge only of an approximate eigenvalue $\tilde{\lambda}$ close to λ and try to solve for the components a_i. This is equivalent to having small errors in all the diagonal elements d_i and solving for the components a_i using the correct eigenvalue λ of R. Now we use $\tilde{\lambda}$ to solve the system of eqn.(B.9,B.10,B.11) except one equation, say the $rth, 1 \leq r \leq n$, that by assumption cannot obey eqn.(B.10). Without loss of generality we set the error to 1 and write in matrix notation

$$(R - \tilde{\lambda}I)a = u_r, \tag{B.12}$$

where u_r is the rth unit vector. Since $(R - \tilde{\lambda}I)$ is by assumption regular we can solve for a by inversion

$$a = (R - \tilde{\lambda}I)^{-1}u_r. \tag{B.13}$$

Since R is symmetric its eigenvalue problem is well conditioned and in order to make clear that the instability we are about to encounter is not due to degeneracies in the eigenvalue spectrum we assume all eigenvalues $\lambda_1, \lambda_2, \ldots, \lambda_n$ to be well separated. We chose $\tilde{\lambda}$ close to λ_k and therefore well separated from all other eigenvalues.

Now we expand u_r in the basis of normalized eigenvectors $t_1, t_2, \ldots, t_r$ to R

$$u_r = \sum_{i=1}^{n} \alpha_i t_i. \tag{B.14}$$

Together with eqn.(B.13) we find that

$$a = \frac{\alpha_k t_k}{\lambda_k - \tilde{\lambda}} + \sum_{i \neq k} \frac{\alpha_i t_i}{\lambda_i - \tilde{\lambda}}. \tag{B.15}$$

We conclude that a is a good approximation to t_k only if $\alpha_k/(\lambda_k - \tilde{\lambda})$ is much larger than the sum of all other terms $\alpha_i/(\lambda_i - \tilde{\lambda}), i \neq k$. By assumption the denominator $(\lambda_k - \tilde{\lambda})$ is much smaller than any other denominator $(\lambda_i - \tilde{\lambda})$. However, we have no guarantee that α_k is not much smaller than $(\lambda_k - \tilde{\lambda})$ and therefore much smaller than the sum of all other $\alpha_i, i \neq k$. If this is the case the approximate eigenvector a will

be nearly orthogonal to u_k. This is the case when

$$\alpha_k = t_k^T u_r, \tag{B.16}$$

i.e. the rth component of the true eigenvector t_k is almost vanishing. Surprisingly, this appears to be very common and is the case for the Darling-Dennison Hamiltonian with its eigenstates that show strong bias towards particular components.

Let us briefly illustrate how the eigenstates to the lowest lying eigenvalues of Darling-Dennison Hamiltonian for the water molecules, $I = 10$, react onto a perturbation of a single element far off the diagonal. To be specific, we chose the element $c_{1,9}^{10}$. The order parameter diagram is shown in Figure B-1. The perturbation appears to have no effect up to magnitudes comparable to the size of the harmonic couplings as can be seen from (a). Note however the two dots at $\log(\epsilon) \approx -7$, i.e. a possible instability as predicted from the susceptibilities in chapter 2. We magnify the interval $-7.770735 \leq \log(\epsilon) \leq -7.770715$ and see in (b) that the order parameter shows full response for the eigenstates $|\Psi_{10}, \pm, 0>$, as we expected from the discussion in chapter 2. Further magnification of the positive ordinate region (c) shows a quite complicated pattern of response [1]. A look at the lowest lying eigenvalues (d) shows that they scatter statistically over the last digit available for computation, i.e. the round off error causes fluctuations ($O(10^{-12} cm^{-1})$ in the energy eigenvalues ($O(10^3 cm^{-1})$). These tiny fluctuations are responsible for the observed pattern in the order parameter. Physically, we can interpret these tiny fluctuations as arising from the coupling of the molecule to its environment.

Near degeneracy of eigenvalues of tridiagonal matrices

As a final aside let us show that if the eigenvector t_k has a pronounced minimum around $1 \ll r \ll n$, then there are at least two nearly degenerate eigenvalues. Note

[1] This pattern was independently exposed to some test persons that unanimously identified it as an angel. Upon exposure several times the statement "God is in the details" was heard. However, no agreement could be reached on one of the tantalizing questions of scholastics: what is the sex of an angel ?

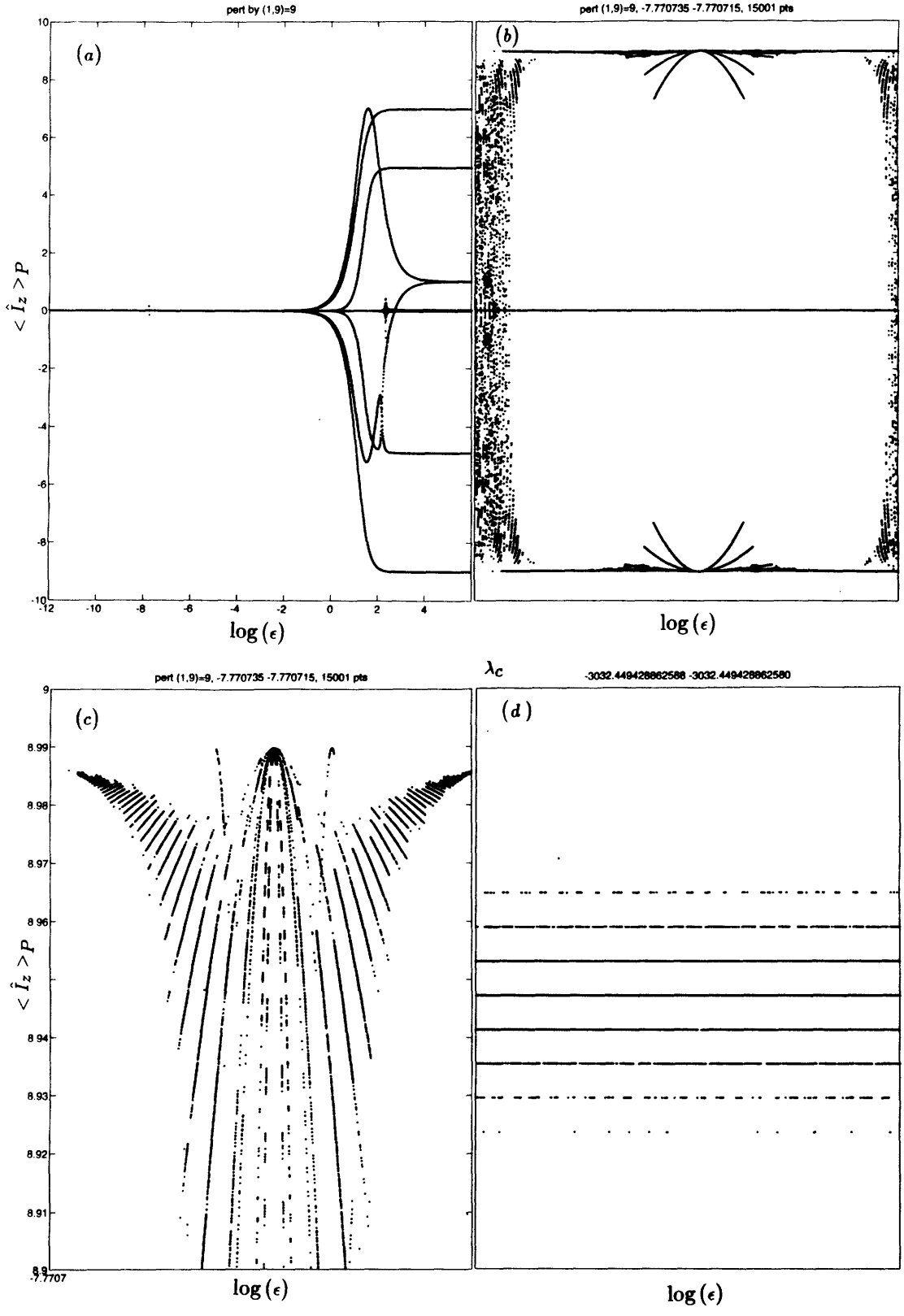

Figure B-1: Sensitivity of the $|\Psi_{10}, \pm, 0>$ states for water to a symmetry breaking perturbation.

that the Darling-Dennison Hamiltonian in the local representation tends to have eigenvectors like this in the low energy end of each polyad. This can be explained from the quadratic regression followed by quadratic progression of the diagonal elements. The idea is to show that if three consecutive components of an eigenvector to a tridiagonal matrix are small, then there are at least two almost degenerate eigenvalues. This is obviously true if those elements are zero and consequently the eigenvalues are exactly degenerate.

It is straightforward to quantify this as follows. Assume that the components of the eigenvector are minimal around $1 \ll r \ll n$, i.e.

$$t_k = t = (t_1, t_2, \ldots, t_{r-1}, t_r, t_{r+1}, \ldots, t_{n-1}, t_n)^T, \tag{B.17}$$

and the components $t_r, t_{r\pm1}$ are much smaller than any other component. The eigenvalue equation

$$Rt_k - \lambda_k t_k = o \tag{B.18}$$

is exactly obeyed. Now we seek only approximate solutions $s_1, s_2, \ldots, s_n$ of eqn.(B.18). By inspection we try

$$s_1 = (t_1, t_2, \ldots, t_{r-2}, 0, \ldots, 0)^T, \tag{B.19}$$

$$s_2 = (0, \ldots, 0, t_{r+2}, \ldots, t_{n-1}, t_n)^T. \tag{B.20}$$

The approximate eigenvalue equations then read

$$(\lambda_k I - R)s_1 = (0, \ldots, 0, o_{r-1}t_{r-1}, (d_{r-1} - \lambda_k)t_{r-1} + o_r t_r, 0, \ldots, 0)^T, \tag{B.21}$$

$$(\lambda_k I - R)s_2 = (0, \ldots, 0, o_{r+1}t_r + (d_{r+1} - \lambda_k)t_{r+1}, o_{r+2}t_{r+1}, 0, \ldots, 0)^T. \tag{B.22}$$

Based on the assumption on the magnitude of $t_r, t_{r\pm1}$ we conclude that λ_k is close to a pair of nearly degenerate eigenvalues, because s_1, s_2 fulfill the eigenvalue equation (B.18) to $O(t_r, t_{r\pm1})$. The approximate eigenvectors s_1, s_2 are orthogonal. From s_1, s_2 we can construct t_k and the almost degenerate $t_{l\neq k}$ to $O(t_r, t_{r\pm1})$ that are deficient in

their components $r-1, r, r+1$.

Bibliography

[1] J. H. Wilkinson, The Algebraic Eigenvalue Problem, Claredon Press, Oxford Science Publications (1965).

Appendix C

The discrete self-trapping equation

The dynamics of the two model systems studied in this thesis, i.e. the Darling-Dennison system and the nonlinear dimer in the Duffing limit, have as common mathematical root a particular type of nonlinear Schrödinger equation: the discrete self-trapping equation (DSE). The equations of motion for a variety of quasiparticles in condensed systems like a polaron, soliton, conformon or local mode can be brought into into the form of the DSE. All those systems have the common physical feature that an excitation moves in a medium that responds to the presence of the excitation. In turn, the excitation responds to the induced change in physical properties of the medium. To wit, the medium mediates the interaction of the excitation with itself. Therefore the formation of those quasiparticles is sometimes referred to as *self-trapping*. The particular mechanisms for a local mode and a small polaron are explained in this thesis. In this appendix we will discuss the DSE and show how it can be derived from the Hamiltonians of the model systems under study. Furthermore, we will establish the connection of localization on a microscopic scale to localization of excitation on a macroscopic scale in form of solitary waves.

Formal introduction

This formal introduction of the DSE follows essentially an exposition by Eilbeck et al. [1]. First, let us have a look at the explicit form of the DSE and then show some possible derivations.

The dynamics of an excitation in a medium with the specified loci $1 \leq j \leq l$ that responds instantaneously to its presence can be approximated by the following set of ordinary differential equations with modular quadratic nonlinearities

$$(id_t - \eta)a + \delta diag(|a_1|^2, |a_2|^2, \ldots, |a_l|^2)a + \epsilon Ma = 0. \tag{C.1}$$

Here

$$a = (a_1, a_2, \ldots, a_l) \tag{C.2}$$

contains the probability amplitudes a_j of finding the excitation at the locus j in the medium.

The connectivity of the loci is recorded in the real symmetric connectivity $l \times l$ matrix $M = m_{jk}$, the coupling strength between those loci is ϵ.

The time evolution of the probability amplitude a_j is linear in $a_k, k \neq j$, i.e. the excitation can be periodically transferred between the loci j and k.

The time evolution is also linear in the probability densities $|a_j|^2$ (to be explicit, bilinear in the probability amplitudes and densities), i.e. the transfer of the excitation from locus j is either retarded or accelerated, dependent on whether the proportionality factor δ is positive or negative. This can be seen if we view $\eta - \delta|a_j|^2$ as the resonance frequency at locus j that depends on the amount of excitation being present there.

Therefore the constant δ reflects the tendency of localization, whereas the constant ϵ reflects the tendency of transfer.

Formally the DSE can be derived from the Lagrangian density L and the varia-

tional principle.

$$L = \sum_{j=1}^{l}\{\frac{1}{2}[ia_j^*\dot{a}_j + (ia_j^*\dot{a}_j)^*] - \eta|a_j|^2\frac{\delta}{2}|a_j|^4 + \epsilon\sum_{k\neq j}^{l} m_{jk}a_j^*a_k\}, \tag{C.3}$$

$$0 = d_t\frac{\partial L}{\partial \dot{a}_j^*} - \frac{\partial L}{\partial a_j^*}, \tag{C.4}$$

$$0 = d_t\frac{\partial L}{\partial \dot{a}_j} - \frac{\partial L}{\partial a_j}. \tag{C.5}$$

Note the gauge invariance under the transformation $a_j \rightarrow a_j \exp(i\eta t)$ that allows the elimination of the corresponding term $-\eta a_j$ from the DSE.

It may be more convenient to consider the Hamiltonian density H defined by

$$H = \sum_{j=1}^{l}\frac{1}{2}[ia_j^*\dot{a}_j + (ia_j^*\dot{a}_j)^*] - L, \tag{C.6}$$

$$H = \sum_{j=1}^{l}(\eta\ |a_j|^2 - \frac{\delta}{2}|a_j|^4 - \epsilon\sum_{k\neq j}^{l} m_{jk}a_j^*a_k). \tag{C.7}$$

Then the DSE follows directly from Hamilton's canonical equations where a_j and ia_j^* are conjugate

$$\begin{aligned} \dot{a}_j &= \frac{\partial H}{\partial i a_j^*}, \\ i\dot{a}_j^* &= -\frac{\partial H}{\partial a_j}. \end{aligned} \tag{C.8}$$

Furthermore, let us define the numbers

$$n_j = |a_j|^2, \tag{C.9}$$

$$n = \sum_{j=1}^{l} n_j. \tag{C.10}$$

Then it is is straightforward to show that H and n are dynamic invariants, i.e.

$$\dot{H} = \dot{N} = 0, \tag{C.11}$$

which implies that the DSE conserves energy and the total amount of excitation.

In the following, we will briefly connect to the studied model systems and then show an interesting implication of the DSE for the behavior of a highly excited chain of coupled Morse oscillators.

Dynamics of the Darling-Dennison system

We begin with the classical Darling-Dennison Hamiltonian that can be written in the form

$$H_{DD} = \omega n + \frac{\alpha}{2}(n_1^2 + n_2^2) + \alpha_{12} n_1 n_2 + \zeta(a_1^* a_2 + a_1 a_2^*), \tag{C.12}$$

using the notation introduced in the second chapter. A straightforward application of Hamilton's equations (C.8) together with eqn.(C.10) and $4\chi = \alpha - \alpha_{12}$ yields

$$\begin{aligned} [id_t - (\omega + N\alpha_{12})]a_1 - 4\chi|a_1|^2 a_1 - \zeta a_2 &= 0, & \text{(C.13)} \\ [id_t - (\omega + N\alpha_{12})]a_2 - 4\chi|a_2|^2 a_2 - \zeta a_1 &= 0. & \text{(C.14)} \end{aligned}$$

Comparing with the DSE (C.1), $l = 2, m_{11} = m_{22} = 0, m_{12} = m_{21} = 1$, we see that $\eta = \omega + N\alpha_{12}, \delta = -4\chi, \epsilon = -\zeta$. We conclude that the tendency to localize a vibrational excitation δ is related to the sum of the anharmonic contributions $4\chi = \alpha - \alpha_{12}$. The transfer tendency ϵ is given by the coupling ζ.

Dynamics of the nonlinear dimer in the Duffing limit

Next, let us consider the nonlinear dimer. The Hamiltonian can be written as

$$H = \frac{\mu}{2}[\dot{Q}_1^2 + \dot{Q}_2^2 + \omega^2(Q_1^2 + Q_2^2)] - \chi(Q_1|a_1|^2 + Q_2|a_2|^2) - \zeta(a_1^* a_2 + a_1 a_2^*), \tag{C.15}$$

using the notation introduced in the third chapter. Note that here χ is the electron-phonon coupling constant. Assuming that $\omega \gg \zeta$ we employ the adiabatic approximation in the Duffing limit, i.e. we neglect the kinetic energy of the oscillators and minimize H over the coordinates (Q_1, Q_2). The result is

$$Q_i^{ad} = \frac{\chi}{\mu\omega^2}|a_i|^2, i = 1, 2. \tag{C.16}$$

Then we eliminate the oscillator coordinates from H to obtain the adiabatic Hamiltonian

$$H^{ad} = -\frac{\chi^2}{2\mu\omega^2}(|a_1|^4 + |a_2|^4) - \zeta(a_1^* a_2 + a_1 a_2^*). \tag{C.17}$$

In order to obtain the equations of motion for the amplitudes a_1, a_2 we use Hamilton's equations (C.8). The result is

$$id_t a_1 + \frac{\chi^2}{\mu\omega^2}|a_1|^2 a_1 + \zeta a_2 = 0, \tag{C.18}$$

$$id_t a_2 + \frac{\chi^2}{\mu\omega^2}|a_2|^2 a_2 + \zeta a_1 = 0. \tag{C.19}$$

Comparing with the DSE (C.1), $l = 2, m_{11} = m_{22} = 0, m_{12} = m_{21} = 1$, we see that $\eta = 0, \delta = \chi^2/\mu\omega^2, \epsilon = \zeta$. We conclude that the tendency to localize the electron is given by the ratio of the square of the electron-phonon coupling constant χ and the force constant of the oscillators $k = \mu\omega^2$. The tendency to transfer the electron is given by the electronic coupling ζ.

Localization on a macroscopic scale: solitary waves

It it interesting to see that the tendency to localize excitation in the discussed systems is not only present on the microscopic scale of two sites but prevails over larger scales. We will demonstrate this by sketching the behaviour of an infinite chain of harmonically coupled Morse oscillators in a highly excited state. The mathematical aspects are discussed along the lines of Davidov's work [2] on solitary excitons in proteins and Holstein's work [3] on polaron motion.

The Hamiltonian can be written as a generalization of the classical Darling-Dennison Hamiltonian.

$$H = \omega n + \sum_{k=1}^{\infty}[\frac{\alpha}{2}n_k^2 + \zeta(a_k a_{k+1}^* + a_k^* a_{k+1})]. \tag{C.20}$$

Here we assume nearest neighbour coupling and can neglect the diagonal couplings of the form $n_k n_{k+1}$ without loss of generality since they lead only to a modification of the parameters in the DSE. The equation of motion for the kth component can be

obtained from Hamilton's equations (C.8)

$$(id_t - \omega)a_k - \alpha|a_k|^2 a_k - \zeta(a_{k-1} + a_{k+1}) = 0. \tag{C.21}$$

We introduce the dimensionless distance coordinate $\rho = r/(r_{k+1} - r_k)$, where r is a distance coordinate along the chain and $r_{k+1} - r_k$ is the distance of the equilibrium points kth and $(k+1)th$ unexcited oscillators. Now we take the continuum limit, i.e.

$$a_k \rightarrow a(\rho), \tag{C.22}$$

$$a_{k+1} - 2a_k + a_{k-1} \rightarrow \frac{\partial^2 a(\rho)}{\partial \rho^2}. \tag{C.23}$$

Then eqn.(C.21) takes the form

$$i\dot{a}(\rho,t) - \zeta\frac{\partial^2 a(\rho,t)}{\partial\rho^2} - \tilde{\omega}a(\rho,t) - \alpha|a(\rho,t)|^2 a(\rho,t) = 0, \tag{C.24}$$

where $\tilde{\omega} = \omega - 2\zeta$. This is type of equation has been extensively studied and its solution is called a solitary wave, i.e. a wave that moves without loosing coherence.

We try as ansatz the normalized function

$$a = \sqrt{\frac{nC}{2}} \exp i[A(\rho - \rho_o) - Bt] sech[C(\rho - \rho_o) - Dt], \tag{C.25}$$

such that

$$\int (a^* a) d\rho = n \tag{C.26}$$

and find

$$A = -\frac{2D}{\alpha n}, \tag{C.27}$$

$$B = \omega - 2\zeta + \frac{(\alpha n)^2}{16\zeta} - \frac{4D^2\zeta}{(\alpha n)^2}, \tag{C.28}$$

$$C = -\frac{\alpha n}{4\zeta}. \tag{C.29}$$

Let us have a look at the energy B of the moving excitation where we introduce the

velocity v of the excitation as $v = D/C = 4\zeta D/\alpha n$ and find

$$B = \omega - 2\zeta + \frac{1}{2}\frac{(\frac{\alpha n}{2})^2}{2\zeta} - \frac{1}{2}\frac{1}{2\zeta}v^2. \tag{C.30}$$

Typically the coupling between oscillators lowers the total energy of the chain. Therefore, we may assume ζ to be negative. Then we may interpret the last term in eqn.(C.30) as an increase in the energy of the solitary wave due to the kinetic energy of the excitation with the inertia 2ζ and the term before the last as decrease in energy due to the distortion of the chain according to the anharmonicity of the single oscillators. The excitation becomes "heavier" by distorting the chain. This is in complete agreement with the intuitive picture outlined in the introductory chapter of this thesis.

What is particularly surprising is that the particle like excitation is not due to the presence of a non vibrational degree of freedom like an electron, hole, spin, dots, but arises from the *anharmonicity of the single oscillators*, i.e. a property of the medium itself.

However, we can save the picture of an excitation that distorts the medium it is moving in by interpreting the Morse oscillator as a harmonic oscillator whose resonance frequency is a linear function of the amount of excitation being present.

What remains is to state the conditions for the formation of such an excitation. We estimate the density of solitary excitation to be significant if the width $\Delta\rho$ around the center obeys the condition $\Delta\rho C \approx O(1)$. The continuum limit can be justified if $\Delta\rho > O(1)$ and thus $C < 1$, i.e. $\zeta > \alpha n$. Comparing this to the condition for localization on the Darling-Dennison dimer, $\kappa = \zeta/2\chi I < 1, \chi = (\alpha - \alpha_{12})/4$ we see that the conditions for formation of a "small" localized excitation and a "large" localized excitation are complementary, i.e. if the localization does not occur on the microscopic scale it still can happen on a macroscopic scale. Then the halfwidth should certainly not extend over the entire system, i.e. $\Delta\rho \ll L/(r_{k+1} - r_k)$ must be true, where L is the length of the chain. Therefore the lower limit on α to allow localization on a macroscopic scale is given by $1/C \ll L/(r_{k+1} - r_k)$, i.e. $\alpha n \gg$

$\zeta(r_{k+1} - r_k)/L$. Therefore we can state the following approximate conditions: the macroscopic solitary excitation is forming if $\zeta(r_{k+1} - r_k)/L \ll \alpha n < \zeta$ and a local mode on a single oscillator is forming if $\alpha n > \zeta$.

Bibliography

[1] J. C. Eilbeck, P.S. Lohmdahl and A. C. Scott, *Physica D*, 16 318 (1985).

[2] A. S. Davydov, *J. theor. Biol.* 38 559 (1973). A. S. Davydov, N. I. Kilukha, *Phys. Stat. Sol. B* 59 465 (1973). A. S. Davydov, *Sov. Phys. Usp.* 25 898 (1982).

[3] T. Holstein, *Ann. Phys.* 8 325 (1959). T. Holstein, *Ann. Phys.* 8 343 (1959).